

AD-A038 247 MISSOURI UNIV-ROLLA DEPT OF ELECTRICAL ENGINEERING F/G 17/7
RANGE-LIMITED HORIZON CORRELATION FOR NAVIGATION CHECKPOINTING.(U)
MAR 77 G E CARLSON, C M BENOIT, P W SAPP N00014-75-C-0639

UNCLASSIFIED

CSR-77-1

NL

1 OF 2
AD A038247



AD A 038247

UNCLASSIFIED

SECURITY CLASSIFICATION OF THIS PAGE (When Data Entered)

REPORT DOCUMENTATION PAGE		READ INSTRUCTIONS BEFORE COMPLETING FORM
1. REPORT NUMBER 14 CSR-77-1	2. GOVT ACCESSION NO.	3. RECIPIENT'S CATALOG NUMBER
4. TITLE (and Subtitle) 6 Range-Limited Horizon Correlation for Navigation Checkpointing.	5. TYPE OF REPORT & PERIOD COVERED 9 Technical <i>rept.</i> 1 Mar 1976 - 28 Feb 1977	6. PERFORMING ORG. REPORT NUMBER
7. AUTHOR(s) 10 Gordon E. Carlson, Charles M. Benoit Paul W. Sapp	8. CONTRACT OR GRANT NUMBER(s) 15 N00014-75-C-0639	10. PROGRAM ELEMENT, PROJECT, TASK AREA & WORK UNIT NUMBERS NR 387-076
9. PERFORMING ORGANIZATION NAME AND ADDRESS University of Missouri-Rolla Rolla, Missouri 65401	11. CONTROLLING OFFICE NAME AND ADDRESS Geography Programs Branch (Code 462) Office of Naval Research Arlington, Virginia 22217	12. REPORT DATE 11 Mar 1977
14. MONITORING AGENCY NAME & ADDRESS (if different from Controlling Office) 12 167P.		13. NUMBER OF PAGES 164
16. DISTRIBUTION STATEMENT (of this Report) This document has been approved for public release and sale; its distribution is unlimited.	15. SECURITY CLASS. (of this report) Unclassified	15a. DECLASSIFICATION/DOWNGRADING SCHEDULE
17. DISTRIBUTION STATEMENT (of the abstract entered in Block 20, if different from Report)	<i>D D C</i> <i>REAPPLIABLE</i> <i>APR 14 1977</i> <i>C</i>	
18. SUPPLEMENTARY NOTES		
19. KEY WORDS (Continue on reverse side if necessary and identify by block number) Navigation Checkpointing Profile Matching Profile Correlation		
20. ABSTRACT (Continue on reverse side if necessary and identify by block number) A performance study for a system which uses range-limited horizons as navigation checkpoints for an airborne vehicle is presented. This is a continuation of performance studies previously reported for systems using actual horizons and fixed-range terrain profiles. The use of range-limited horizons permits a single system concept to be used at all vehicle altitudes. Digital topographic data and computer simulations used for system performance analyses are described. → OVER		

408389

(P)
UNCLASSIFIED

SECURITY CLASSIFICATION OF THIS PAGE(When Data Entered)

Analysis results are presented for flights at various altitudes. Different terrain roughnesses and a range of random profile errors and vehicle altitude errors are considered. System error limits are selected to give suitable checkpoint detection performance and position and heading determination errors are analyzed. The results indicate that system operation is feasible if sufficient terrain roughness is available at the checkpoint location. The results of an analysis of the effects of vehicle motion during sensor scan and sensor azimuth beamwidth are presented.

↑

UNCLASSIFIED

SECURITY CLASSIFICATION OF THIS PAGE(When Data Entered)

RANGE-LIMITED HORIZON CORRELATION

FOR NAVIGATION CHECKPOINTING

This document contains material which may be subject to copyright or other legal protection. It is the property of the University of Missouri-Rolla and is loaned to you; it is to be used only for research purposes and must not be reproduced without permission of the University. It is to be returned to the University when no longer needed. It is the responsibility of the borrower to ensure that all rights in the document are retained by the University.

Gordon E. Carlson
Charles M. Benoit
Paul W. Sapp

Department of Electrical Engineering
University of Missouri-Rolla
Rolla, Missouri 65401

Technical Report CSR-77-1
March 1977

ONR Contract #N00014-75-C-0639
Project #NR387-076

This document has been approved for public release and sale; its distribution is unlimited

"Reproduction in whole or in part is permitted for any purpose of the United States Government"

A

ACCESSION for	White Section	Buff Section	<input type="checkbox"/>	<input type="checkbox"/>
NTIS				
DDC				
UNANNOUNCED				
JUSTIFICATION				
DISTRIBUTION AVAILABILITY CODES				
Dist.	Acq.	Ref.	SP	DM

ABSTRACT

A performance study for a system which uses range-limited horizons as navigation checkpoints for an airborne vehicle is presented. This is a continuation of performance studies previously reported for systems using actual horizons and fixed-range terrain profiles. The use of range-limited horizons permits a single system concept to be used at all vehicle altitudes. Digital topographic data and computer simulations used for system performance analyses are described. Analysis results are presented for flights at various altitudes. Different terrain roughnesses and a range of random profile errors and vehicle altitude errors are considered. System error limits are selected to give suitable checkpoint detection performance and position and heading determination errors are analyzed. The results indicate that system operation is feasible if sufficient terrain roughness is available at the checkpoint location. The results of an analysis of the effects of vehicle motion during sensor scan and sensor azimuth beamwidth are presented.

FOREWORD

This technical report covers a portion of the work performed from March 1, 1976 to February 28, 1977 under contract number N00014-75-C-0639, project number NR387-076, entitled "Geographic Orientation". The work was performed by Dr. Gordon E. Carlson, Principal Investigator and Charles M. Benoit and Paul W. Sapp, Graduate Students in Electrical Engineering at the University of Missouri-Rolla, Rolla, Missouri under the supervision of Dr. James S. Bailey, Director of the Geography Programs Branch, Earth Sciences Division, Office of Naval Research.

TABLE OF CONTENTS

	Page
ABSTRACT	ii
FOREWORD	iii
LIST OF ILLUSTRATIONS	vii
LIST OF TABLES	xii
I. INTRODUCTION	1
II. SYSTEM CONCEPT AND PARAMETERS	3
A. RANGE-LIMITED HORIZON PROFILES	3
B. SYSTEM CONCEPT	6
C. HORIZON COMPARISON AND IDENTIFICATION	9
D. SYSTEM AND PERFORMANCE PARAMETERS	12
III. SYSTEM PERFORMANCE ANALYSIS	15
A. SELECTION OF TERRAIN DATA AND FLIGHT PATHS	15
B. ANALYSIS TECHNIQUES	25
1. RANGE-LIMITED HORIZON GENERATION	25
2. ANALYSIS APPROACH	28
C. HORIZON DATA	31
D. HORIZON COMPARISON FUNCTION DATA	38
E. SYSTEM PERFORMANCE	44
1. DETECTION THRESHOLD AND HORIZON ERROR LIMIT . .	44
2. POSITION DETERMINATION ACCURACY	54
3. PERFORMANCE COMPARISON OF RANGE-LIMITED HORIZON AND FIXED-RANGE PROFILE SYSTEMS	59
F. EFFECT OF ERRONEOUS VEHICLE ALTITUDE	63

TABLE OF CONTENTS (cont.)

	Page
IV. EFFECT OF PRACTICAL SENSOR CHARACTERISTICS	77
A. VEHICLE MOTION DURING SENSOR SCAN	77
1. SYSTEM MODEL AND ANALYSIS METHOD	77
2. PERFORMANCE EFFECTS	79
B. FINITE SENSOR BEAMWIDTH	89
1. SYSTEM MODEL AND ANALYSIS METHOD	91
2. PERFORMANCE EFFECTS	96
V. SUMMARY AND CONCLUSIONS	109
REFERENCES	113
APPENDIX A. TABULATED POSITION AND HEADING ERROR RESULTS FOR ZERO ALTITUDE ERROR	115
APPENDIX B. DETECTION THRESHOLD NEEDED TO GIVE $P_D = 0.99$ FOR VARIOUS VEHICLE ALTITUDE ERRORS	119
APPENDIX C. TABULATED POSITION AND HEADING ERROR RESULTS FOR NON-ZERO ALTITUDE ERROR	129
APPENDIX D. ALONG-TRACK AND CROSS-TRACK POSITION ERRORS AS A FUNCTION OF ALTITUDE ERROR	139
APPENDIX E. ADDITIONAL DATA FOR FINITE BEAMWIDTH ANALYSES	145

LIST OF ILLUSTRATIONS

	Page
1. Terrain Contributing to a Range-Limited Horizon Profile	4
2. Single Pulse Output Signal for an Off-Boresight Angle Measuring Radar	5
3. Horizon Comparison System Concept	7
4. Example Horizon Profiles	8
5. Along-Track Position Identification	10
6. Map Data Used for Analyses	16
7. Terrain and Flight Path Used to Analyze Case 1	17
8. Terrain and Flight Path Used to Analyze Case 2	18
9. Terrain and Flight Path Used to Analyze Case 3	19
10. Terrain and Flight Path Used to Analyze Case 4	20
11. Terrain and Flight Path Used to Analyze Case 5	21
12. Terrain and Flight Path Used to Analyze Case 6	22
13. Terrain and Flight Path Used to Analyze Case 7	23
14. Terrain Points Used to Evaluate One Horizon Elevation Data Point	26
15. Determination of One Horizon Elevation Data Point	27
16. Required Flight Path Position Variations for Statistical Analysis of System Performance	29
17. Horizon Viewing Location Geometry for Performance Analysis	30
18. Sensed Horizons for Cases 1, 2, and 3 (Valley flights) . .	32
19. Sensed Horizons for Case 4 (Relatively Smooth Terrain) . .	33
20. Sensed Horizons for Case 5 (Moderately Rough Terrain) . .	34
21. Sensed Horizons for Case 6 (Rough Terrain)	35

LIST OF ILLUSTRATIONS (cont.)

	Page
22. Sensed Horizons for Case 7 (Very Rough Terrain)	36
23. Horizon Comparison Functions for Cases 1, 2, and 3 (Valley Flights)	39
24. Horizon Comparison Functions for Case 4 (Relatively Smooth Terrain)	40
25. Horizon Comparison Functions for Case 5 (Moderately Rough Terrain)	41
26. Horizon Comparison Functions for Case 6 (Rough Terrain) . .	42
27. Horizon Comparison Functions for Case 7 (Very Rough Terrain)	43
28. Required Detection Threshold for $P_F < 0.001$ at Distances Greater than 1 Km from Line Array	46
29. Required Detection Threshold for $P_F < 0.001$ at Distances Greater than 2 Km from Line Array	47
30. Detection Threshold Needed to Give $P_D = 0.99$ (Valley Flights)	49
31. Detection Threshold Needed to Give $P_D = 0.99$ (Flights at 100m Above Max. Terrain Height)	50
32. Detection Threshold Needed to Give $P_D = 0.99$ (Flights at 500m Above Max. Terrain Height)	51
33. Maximum Allowable Random Horizon Error with Threshold Set for $P_F < 0.001$ at Distances Greater than 1 Km from Line Array	52
34. Maximum Allowable Random Horizon Error with Threshold Set for $P_F < 0.001$ at Distances Greater than 2 Km from Line Array	53
35. Position and Heading Determination Accuracy (Valley Flights)	55
36. Position and Heading Determination Accuracy (Flights at 100m Above Maximum Terrain Height)	56

LIST OF ILLUSTRATIONS (cont.)

	Page
37. Position and Heading Determination Accuracy (Flights at 500m Above Maximum Terrain Height)	57
38. Sensed Profiles for Case 6 (Range-Limit = Fixed-Range = 5 Km, H_A = 500m Above Max. Terrain Height)	60
39. Horizon Comparison Functions for Case 6 (Range-Limit = Fixed-Range = 5 Km, H_A = 500m Above Max. Terrain Height)	61
40. Maximum Allowable Random Profile Error for Systems Using Range-Limited Horizons and Fixed-Range Profiles (Flights at 500m Above Max. Terrain Height)	62
41. Position and Heading Determination Accuracy for System Using Fixed-Range Profiles (Flights at 500m Above Max. Terrain Height)	64
42. Detection Threshold Needed to Give $P_D = 0.99$ (Case 6 Flight at 100m Above Max. Terrain Height)	66
43. Maximum Allowable Random Horizon Error as a Function of Altitude Error for Valley Flights	68
44. Maximum Allowable Random Horizon Error as a Function of Altitude Error for Flights at 100m Above Max. Terrain Height	69
45. Maximum Allowable Random Horizon Error as a Function of Altitude Error for Flights at 500m Above Max. Terrain Height	70
46. Position and Heading Determination Accuracy as a Function of Altitude Error for Valley Flights	72
47. Position and Heading Determination Accuracy as a Function of Altitude Error for Case 5	73
48. Position and Heading Determination Accuracy as a Function of Altitude Error for Case 6	74
49. Position and Heading Determination Accuracy as a Function of Altitude Error for Case 7	75
50. Geometry for Stationary and Moving Horizon Viewing Locations	78

LIST OF ILLUSTRATIONS (cont.)

	Page
51. Sensed Horizons for Case 6 with Stationary and Moving Viewing Locations	80
52. Horizon Comparison Functions for Case 6 with Stationary and Moving Viewing Locations	81
53. Geometry for Moving Horizon Viewing Locations with Flight Direction Mismatch	83
54. Sensed Horizons for Case 6 with Moving Viewing Locations on Flight Path to Right of Planned	85
55. Horizon Comparison Functions for Case 6 with Moving Viewing Locations on Flight Paths at Different Azimuth Angles	86
56. Detection Threshold Needed to Give $P_D = 0.99$ for Moving Horizon Viewing Location Variations of Case 6	87
57. Elevation Angle Measurement with Finite Azimuth Beamwidth	92
58. Geometry for Radar Return Determination for Finite Beamwidth Analysis	94
59. Diagram Illustrating Terrain Return Data Processing for a Single Range	95
60. Sensed Horizons for Case 6 with Sensor Beamwidths of 0° and 1°	97
61. Sensed Horizons for Case 6 with Sensor Beamwidths of 2° and 4°	98
62. Horizon Comparison Function for Case 6 with Various Sensor Beamwidths	99
63. Required Detection Threshold, T_1 , as a Function of Sensor Beamwidth when Sensed and Reference Horizons are Generated with the Same Beamwidth	101
64. Required Detection Threshold, T_1 , as a Function of Sensor Beamwidth when Reference Horizons are Generated with a 0° Beamwidth	102
65. Detection Threshold Needed to Give $P_D = 0.99$ for Various Sensor Beamwidths, θ_B , for Case 6	103

LIST OF ILLUSTRATIONS (cont.)

	Page
66. Maximum Allowable Random Horizon Error as a Function of Sensor Beamwidth when Sensed and Reference Horizons are Generated with the Same Beamwidth	104
67. Maximum Allowable Random Horizon Error as a Function of Sensor Beamwidth when Reference Horizons are Generated with a 0° Beamwidth	105
68. Position and Heading Determination Accuracy when Sensed and Reference Horizons are Generated with the Same Beamwidth, θ_B (Case 6)	107
69. Position and Heading Determination Accuracy when Reference Horizons are Generated with a 0° Beamwidth (Case 6)	108

LIST OF TABLES

	Page
I. Standard Deviation of Sensed Horizons for All Analysis Cases	37
II. Required Detection Threshold for a Probability of False Alarm Less Than 0.001	45
III. Maximum Allowable Random Horizon Error Standard Deviation and Associated Maximum Allowable Altitude Error	67
IV. Required Detection Threshold, T_1 , for Moving Horizon Viewing Location Variations of Analysis Case 6	88
V. Maximum Allowable Random Horizon Error, σ_{NM} , for Moving Horizon Viewing Location Variations of Analysis Case 6	88
VI. Position and Heading Determination Errors for Moving Viewing Location Variations of Analysis Case 6	90

RANGE-LIMITED HORIZON CORRELATION FOR NAVIGATION CHECKPOINTING

I. INTRODUCTION

Horizon profiles are different for different viewing locations. Therefore, they contain information which should be useful in determining an airborne vehicle's location. It has been proposed that horizon profiles be sensed by an on-bound sensor and compared with reference horizon profiles generated for viewing locations in the neighborhood of the desired flight path to provide navigation checkpoint information. The horizon profiles used could be obtained from any azimuth angle with respect to the aircraft for which a sensor mounting position is available. Only a forward looking sensor has been considered in system analyses. However, similar system performance should be available with a sensor looking in any other direction.

One advantage of the proposed horizon profile comparison system is that sensed profiles covering a long horizontal dimension can be obtained rapidly with an azimuth scanning sensor. This eliminates the need for a long flight path increment to obtain a profile with significant data content. A second advantage is that automatic computer generation of reference profiles is possible and requires only topographic data. A third advantage occurs since reference profiles can cover a wider azimuth angular dimension than the sensed profiles. This means that profile identification is possible even if the aircraft heading is incorrectly known if the sensed profile is within the limits of the reference profile angular extent and the reference profile contains significant data over its extent.

The feasibility of the proposed technique for obtaining navigation checkpoints is under study. Earlier technical reports^{1,2} have reported on work done in analyzing the use of horizon profiles and fixed-range, forward-sensed profiles. Horizon profiles proved to be satisfactory for flights designed to maximize terrain masking by being very low altitude between ridges (valley flights). Horizon profiles did not prove to be very satisfactory at aircraft altitudes above the majority of the surrounding terrain since they result from terrain which is at very long ranges from the aircraft and thus have small profile variations and are highly susceptible to radar profile errors. To circumvent this problem, a system which used profiles generated for a fixed range was analyzed. This system gives satisfactory performance if the vehicle altitude is high enough so radar shadows do not constitute more than 40% of the desired checkpoint profile.

It was recognized that a better system concept would be one for which the profile generated by the maximum elevation angle to the terrain within a fixed range limit (range-limited horizon) is used.

At higher altitudes, such a profile is essentially a fixed-range profile since terrain at the range limit is not shadowed for almost all azimuth angles. At very low altitudes the resulting range-limited horizon profile is essentially the actual horizon profile since almost all terrain points contributing to it are at a range which is less than the range limit. The use of range-limited horizon profiles thus should provide similar performance to that previously obtained with horizon and fixed-range profiles. However, the system is applicable to all altitudes and radar shadows do not cause a problem. This report presents the results of an analysis of the navigation checkpointing system which uses range-limited horizon profiles. Also included are the results of studies of some practical system constraints.

Analyses have been performed by using actual terrain topographic data and computer simulations. The terrain data used for the analyses reported here was a set of the cases previously considered which span a range of different terrain roughness. The basic data used was digitized topographic data generated by the Defense Mapping Agency (DMA) from standard 1:250000 scale United States Geological Survey (USGS) maps. As before, linear interpolation between every third data point (190.5m spacing) was used to generate the terrain model to provide system simulations in reasonable computation time. The basic parameters and philosophy used for the analyses is the same as that reported in the previous report.¹ However, some changes were made in the results format used to more clearly indicate system performance.

This report consists of three parts. The first part briefly reviews and discusses the system concepts, techniques, and parameters for the range-limited horizon correlation checkpointing system. The second part defines the terrain data and profiles used in the analysis, briefly reviews the analysis techniques, and presents performance results. Performance is considered with no system errors, with radar profile errors, and with vehicle altitude errors. Part three considers the effect on system performance of two practical sensor constraints. The first of these is the effect of motion of the vehicle while the sensed profile is being obtained and the second is the effect of finite sensor beamwidth. The final section in the report presents a summary and conclusions.

II. SYSTEM CONCEPT AND PARAMETERS

This section briefly reviews the concept on which the range-limited horizon profile comparison checkpoint system is based. The locations from which the profiles are to be generated, the method of comparison, and various system and performance parameters are defined.

A. RANGE-LIMITED HORIZON PROFILES

A range-limited horizon profile results when the maximum elevation angle to the terrain is determined as a function of azimuth angle for terrain within a fixed range limit. All terrain at greater ranges is ignored. The terrain which is utilized in generating a range-limited horizon profile is illustrated in plan view in Fig. 1. The range-limited horizon profile generation is easily accomplished with an off-boresight radar mechanization for measuring elevation angle (uses phase or amplitude monopulse) since the return from each radar pulse gives the elevation angle of the terrain with respect to the antenna boresight (center of beam) as a function of range. A peak angle detection and knowledge of the antenna boresight elevation angles are all that are then required to determine the maximum elevation angle to the terrain over the limited range considered. This is illustrated in Fig. 2 where missing data indicates that the terrain at that range is shadowed by terrain at a shorter range. The maximum elevation angle data is obtained for each pulse as the radar scans in azimuth and gives the desired range-limited horizon profile.

The range to most of the actual horizon profile points for many low-altitude valley flights is less than the range limit for a reasonable range-limited horizon profile and thus the resulting range-limited horizon profile is essentially the actual horizon profile. For flights above the majority of the surrounding terrain, profile points would be obtained for terrain points at the range limit except when it is shadowed by intervening terrain. When the range limit is shadowed by intervening terrain, then profile points are obtained from this intervening terrain. It is obvious that the portion of the terrain at the range limit which is unshadowed increases as the vehicle altitude increases. Thus, the range-limited horizon profile approaches a fixed-range profile as vehicle altitude increases.

Range-limited horizon profiles are referred to simply as on horizons in the remainder of this report. This simplifies the text. Horizons obtained without a range limit are called actual horizons to distinguish them from the range-limited horizon profiles.

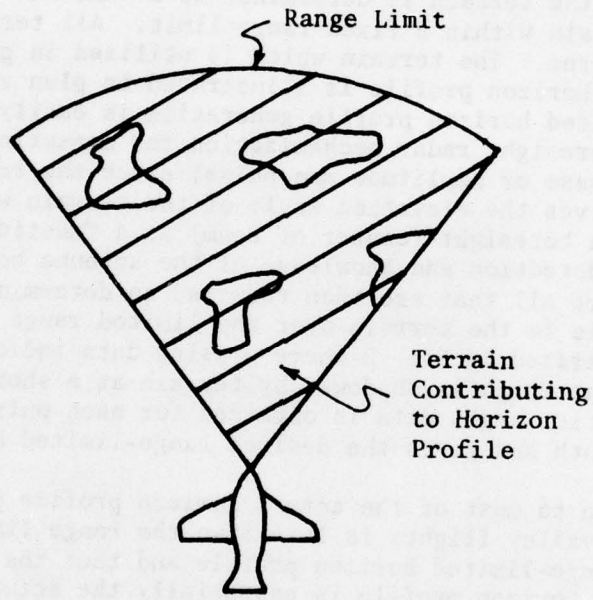
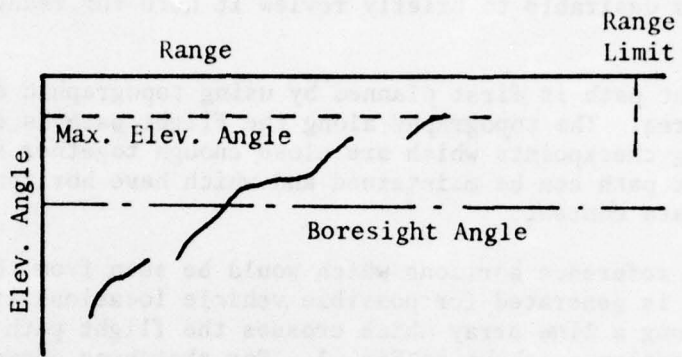
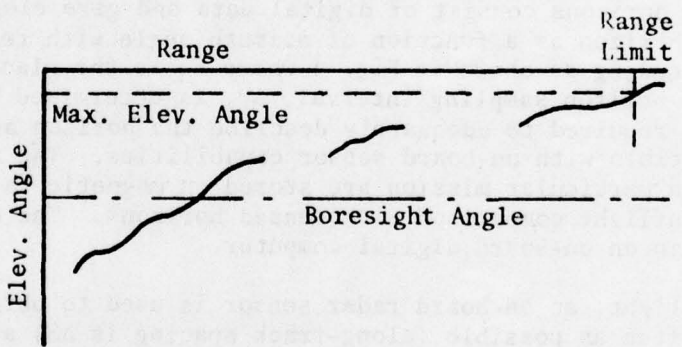


Fig. 1. Terrain Contributing to a Range-Limited Horizon Profile.



(a) Terrain at Range Limit
Shadowed



(b) Terrain at Range Limit
Not Shadowed

Fig. 2. Single Pulse Output Signal for an Off-Boresight Angle Measuring Radar.

B. SYSTEM CONCEPT

The system concept has been presented in previous reports. However, it is desirable to briefly review it here for ready reference.

The flight path is first planned by using topographic data for the mission area. The topography along the flight path is considered in identifying checkpoints which are close enough together so the desired flight path can be maintained and which have horizons with significant data content.

A set of reference horizons which would be seen from the airborne vehicle is generated for possible vehicle locations with spacing ΔR along a line array which crosses the flight path at each checkpoint location as shown in Fig. 3. For sketching convenience, the profiles are indicated as coming from a fixed range even though this would not be true in an actual case. The length of the line array required is established by expected vehicle cross-track position errors when it arrives at the checkpoint. This depends on vehicle dynamics and checkpoint separations and has not been analyzed. The reference horizons are generated with a digital computer from topographic data and correspond to the planned vehicle altitude and heading. The horizons consist of digital data and give elevation angle to the horizon as a function of azimuth angle with respect to flight path heading as shown in Fig. 4 where θ_H is the planned vehicle heading. The horizon sampling interval, $\Delta\theta$, is determined by the sampling rate required to adequately describe the horizon and must also be compatible with on-board sensor capabilities. The reference horizons for a particular mission are stored on magnetic tape in the vehicle for inflight comparison with sensed horizons. The comparison is performed in an on-board digital computer.

During flight, an on-board radar sensor is used to obtain sensed horizons as often as possible (along-track spacing is ΔS) along the flight path as also shown in Fig. 3. As the sensed horizons are obtained, they are compared with all the reference horizons in the upcoming line array until identification is achieved with one of the reference horizons in that line array (the identification criteria are discussed in the following section). The identification specifies the time at which the array is crossed (along-track position) and the location along the array at which it is crossed (cross-track position) as shown in Fig. 3. Actually, it may be desirable to make comparisons with several upcoming line arrays to avoid the possibility of mission abort due to a single erroneous line array mismatch.

A sensed horizon is generated with a narrower azimuth angular extent, θ_S , than the angular extent of the reference horizons, θ_R , as shown in Figs. 3 and 4. It is compared with horizon segments along the extent of the reference horizon to find the segment which

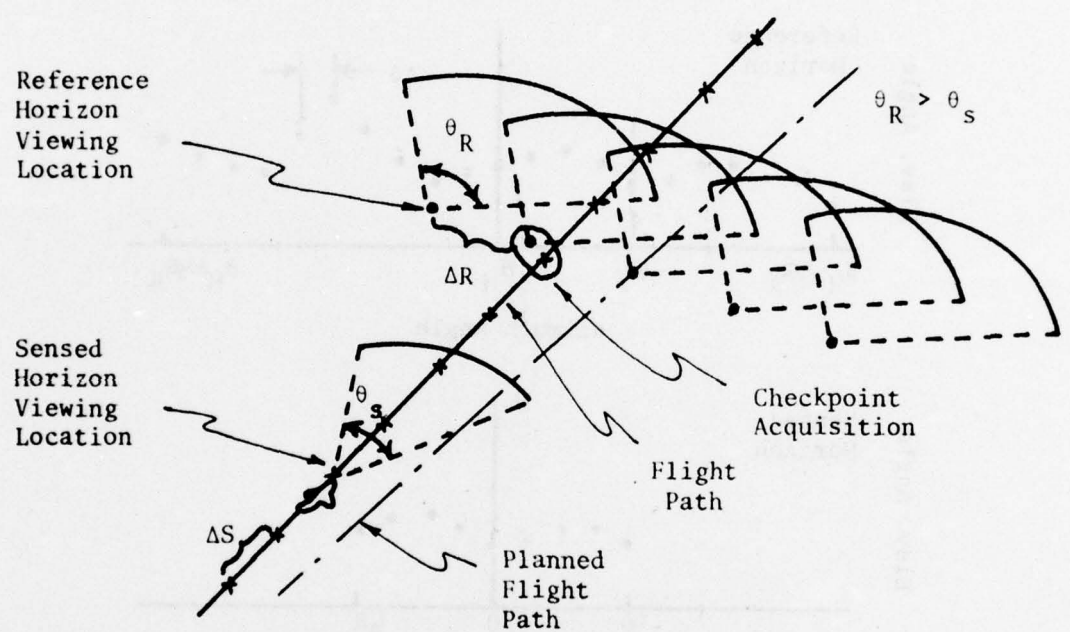


Fig. 3. Horizon Comparison System Concept.

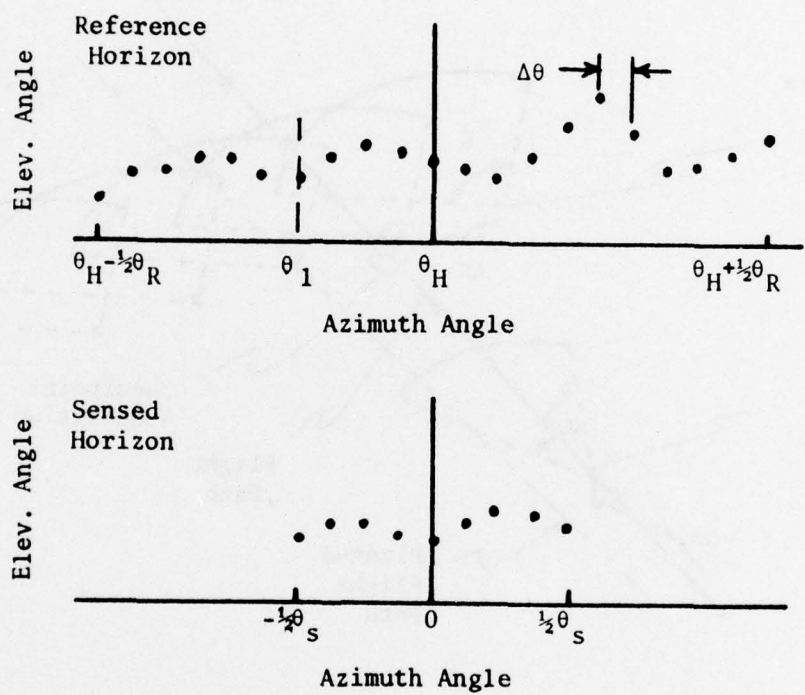


Fig. 4. Example Horizon Profiles.

it best matches. Thus horizon identification for position determination is achieved even if the airborne vehicle heading is incorrectly known provided the sensed horizon is within the limits of the reference horizon angular extent. The angular offset along the reference horizon at which identification occurs (θ_1 for the example shown in Fig. 4) determines the vehicle heading. Actual flight path heading can be determined if the vehicle "crab" angle is known.

C. HORIZON COMPARISON AND IDENTIFICATION

The horizon comparisons indicated above are to be performed by the computer on-board the aircraft and must produce output values which are measures of how well sensed horizons and segments of reference horizons match. The comparison technique must be as simple as possible, consistent with good horizon selectivity, so that horizon comparisons can be made quickly. Various comparison techniques have been studied and reported previously.² Based on simplicity and performance, it was determined that comparison of a sensed horizon and a reference horizon segment is best performed by computing the integral absolute difference (IAD) between the sensed horizon with its mean value removed and the reference horizon segment with its mean value removed. Mean values are removed to eliminate sensitivity to sensed horizon mean value errors. A brief description of this comparison technique follows.

If $s(n)$ are the sensed horizon data points for a horizon of length N and $r_i(m)$ are the reference horizon data points for the i^{th} reference horizon of length M , then the IAD expression for the k^{th} segment of the i^{th} reference horizon is

$$\text{IAD}_i(k) = \sum_{n=1}^{N} |[s(n) - \mu_s] - [r_i(n+k-1) - \mu_i(k)]| \quad (1)$$

where μ_s is the sensed horizon mean value, $\mu_i(k)$ is the mean value of the k^{th} segment of length N of the i^{th} reference horizon, and $1 \leq k \leq M-N+1$. The value of k for which $\text{IAD}_i(k)$ is minimum identifies the angular location along the i^{th} reference horizon at which the best match occurs between the sensed horizon and the reference horizon.

The minimum IAD value (I_m) computed for one sensed horizon and all segments of all reference horizons in one line array is used to determine if the sensed horizon was obtained from the neighborhood of the line array of reference horizons. Fig. 5 shows an example variation of I_m for sensed horizons taken from points along the flight path on both sides of the reference array. The value of I_m as a function of the along-track distance from the line array of reference horizons at a checkpoint location is referred to as the horizon comparison function. As indicated a detection threshold is set and a sensed horizon is determined to be from the neighborhood of the line

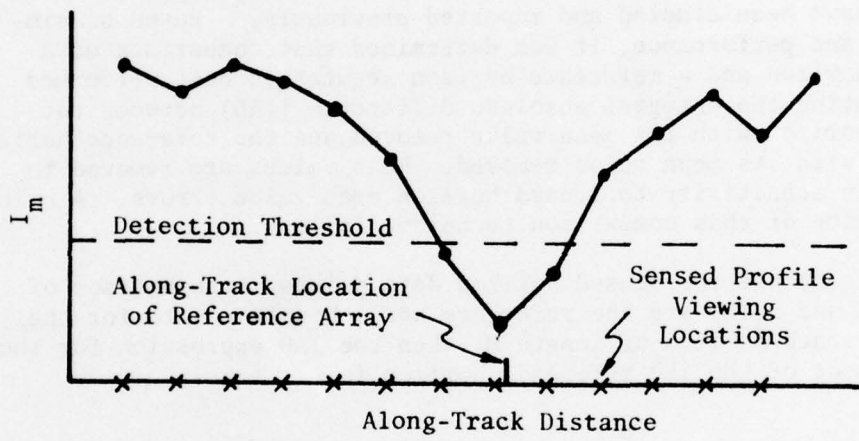


Fig. 5. Along-Track Position Identification.

array when I_m is less than this threshold. Thus, as sensed horizons are obtained, they are compared with the upcoming line array of reference horizons by determining I_m . When I_m becomes less than the detection threshold, then it is determined that the sensed horizon is from the neighborhood of the reference line array. The minimum value of I_m which is also less than the detection threshold identifies the sensed horizon which was obtained closest to the reference line array and thus identifies the aircraft crossing time for the line array, that is, the along-track aircraft position. The particular reference horizon in the array and the azimuth heading angle along it at which the minimum I_m occurs identifies the aircraft cross-track position and heading at the array crossing.

The detection threshold indicated in Fig. 5 must be established for any particular horizon comparison so it can be determined if the sensed horizon was obtained from the neighborhood of the reference horizon array. The threshold must be high enough to permit check-point identification even if there are system errors but low enough so false identifications will not occur. The value of this threshold depends on the particular system parameters used, on the terrain roughness and on the magnitude of horizon and system errors expected.

The detection threshold could be established for each flight based on the system parameters used and the roughness of the terrain to be encountered. However, previous analyses indicated that a problem exists when a single threshold is used for even a relatively short flight path (20km). The required threshold is too large which results in difficulty in rejecting false identifications. The problem results from the non-homogeneity of the terrain which means that if the threshold is set to be satisfactory for all line arrays over an extended flight path, then it is set too high for the line arrays which produce the smaller values of I_m (line arrays from regions with smaller terrain variation). The result is that it is difficult to reject false identifications for these line arrays and sensed horizons from other regions with small terrain variation since the resulting I_m will be small.

Based on the above result, it is apparent that an adaptive detection threshold should be used. In other words, the value of threshold used should depend on the line array being considered. This can be easily established before the flight and appropriate threshold values stored for each line array of reference horizons. Equivalently, the threshold dependence on the sensed horizon standard deviation could be established and stored for use with each sensed horizon obtained. The value of the threshold required is considered in the performance analyses and curves presented of threshold required as a function of horizon standard deviation.

D. SYSTEM AND PERFORMANCE PARAMETERS

Both valley flights and flights above the majority of the surrounding terrain have been previously considered using actual horizons and fixed-range profiles respectively. Performance results are presented in this report for a subset of the previous analysis cases with a system using range-limited horizon profiles (horizons).

Previous analyses have considered the system parameters of reference profile viewing location separation, ΔR , and sensed profile length, θ_S , parametrically for tradeoff purposes. The performance of a system using horizons should be similar to that using fixed-range profiles on actual horizons in the cases considered; therefore, the compromise parameters selected in the previous report (i.e. $\Delta R = 400m$, $\theta_S = 90^\circ$) are used for the analyses reported here. The same sensed horizon viewing location separation, $\Delta S = 200m$, as used previously is also used here. It is felt that it is probably a lower limit on the spacing possible due to the antenna scan time required. The required sample spacing for horizons is the same as that previously established for actual horizons and fixed-range profiles since they will be of similar form. The sample spacing established was 1° based on an analysis of profile frequency content.

Tradeoffs for vehicle altitude, H_A , and the range to a fixed-range profile, R_F , were also established when flights above the majority of the surrounding terrain were considered. These are not applicable here since they were based on shadow considerations which don't effect horizons. However, most of the cases selected for analyses here used $R_F = 5Km$ when performance for a fixed-range profile comparison system was analyzed. Therefore, the range limit, R_L , chosen for the performance analyses reported here has been set to $R_L = 5Km$ so comparisons can be made with the fixed-range profile comparison system.

Vehicle altitudes, H_A , chosen for the analyses here include the altitudes previously used for the individual cases as well as an additional altitude for flights above the majority of the surrounding terrain. The altitudes selected will be specified in a later section when the flight paths used for the analyses are defined.

System performance results presented in this report include the effect of random profile error (error standard deviation = σ_N) and vehicle altitude error, ΔH (difference between actual and planned vehicle altitude).

In order to specify system performance, several performance indicators are defined. These include: (1) the standard deviation of the along-track position determination error, σ_x ; (2) the standard deviation of the cross-track position determination error, σ_y ;

(3) the circular error probable*, CEP, for the position determination error, and (4) the standard deviation of the heading error, σ_θ . The probability of detection, P_D , (probability of correct sensed profile identification) and the probability of false alarm, P_F , (probability of incorrect sensed profile identification) are used to establish the required selection threshold value and the maximum allowable random profile error and vehicle altitude error.

* Circular error probable is defined to be the radius of the circle centered on the correct position in which 50% of the erroneously determined positions lie. If the errors are Gaussian, then $CEP \approx 0.5887 (\sigma_x + \sigma_y)$ as long as σ_x and σ_y are similar in magnitude.³

III. SYSTEM PERFORMANCE ANALYSIS

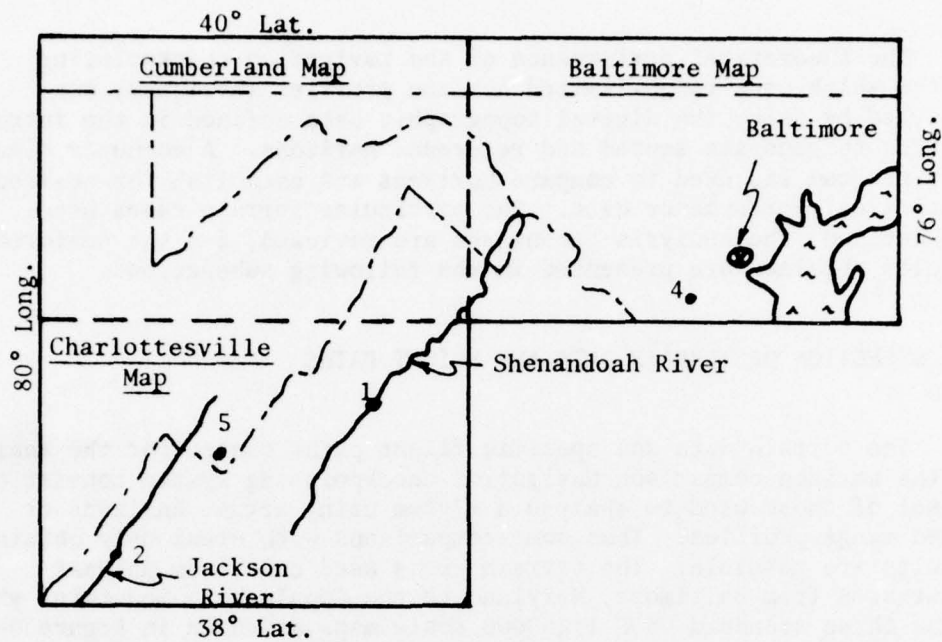
The theoretical performance of the navigation checkpointing system which uses range-limited horizon profiles (horizons) was analyzed by using the digital topographic data defined in the Introduction to generate sensed and reference horizons. A computer simulation program was used to compare horizons and establish the desired statistical performance data. The particular terrain cases used are defined, the analysis techniques are reviewed, and the performance results obtained are presented in the following subsections.

A. SELECTION OF TERRAIN DATA AND FLIGHT PATHS

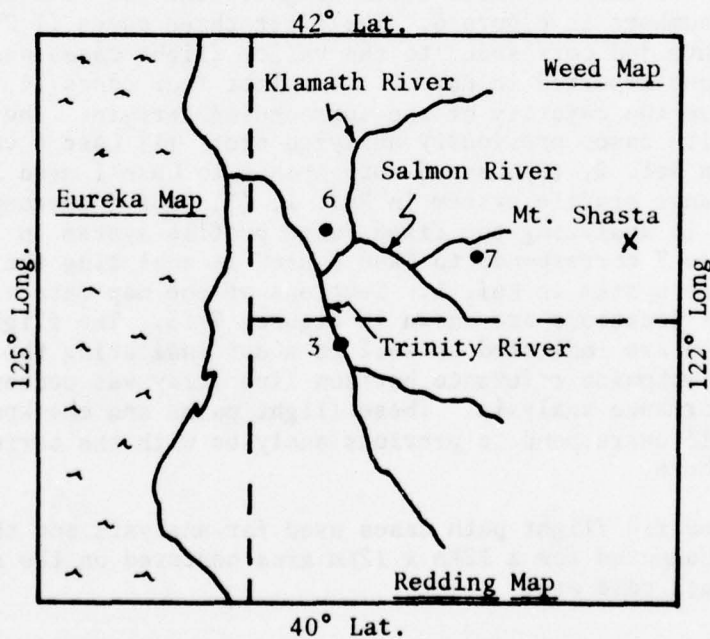
The terrain data and specific flight paths chosen for the analysis of the horizon comparison navigation checkpointing system consist of a subset of those used to analyze a system using actual horizons or fixed range profiles. Thus some comparisons with previously obtained results are possible. The terrain areas used came from an East coast area from Baltimore, Maryland to the Appalachian Mountains which spans three standard USGS 1:250000 scale maps as shown in Figure 6a and a Northern California area which spans three standard USGS 1:250000 scale maps as shown in Figure 6b.

A total of seven different flight paths were chosen for analysis. The general location of these seven flight paths are indicated and given case numbers in Figure 6. The first three cases (1,2,3) are valley flights and correspond to the valley flight cases analyzed previously and reported in Ref. 2. The last four cases (4,5,6,7) are flights above the majority of the surrounding terrain. The correspondence with cases previously analyzed are: (1) Case 4 corresponds to Case 4 in Ref. 2, (2) Case 5 corresponds to Case 1 used in analyzing the fixed-range profile system in Ref. 1, (3) Case 6 corresponds to Case 4 used in analyzing the fixed-range profile system in Ref. 1 and, (3) Case 7 corresponds to Case 6 used in analyzing the fixed-range profile system in Ref. 1. Sections of the map data at each of the analysis locations are shown in Figures 7-13. The flight path and direction are indicated as well as a dot indicating the location where the checkpoint reference horizon line array was centered for system performance analysis. These flight paths and checkpoint locations all correspond to previous analyses with the correspondences indicated above.

The specific flight path cases used for analysis and the terrain statistics computed for a 12Km x 12Km area centered on the analysis point for each case are:



(a) East Cost Area



(b) West Coast Area

Fig. 6. Map Data Used for Analyses.

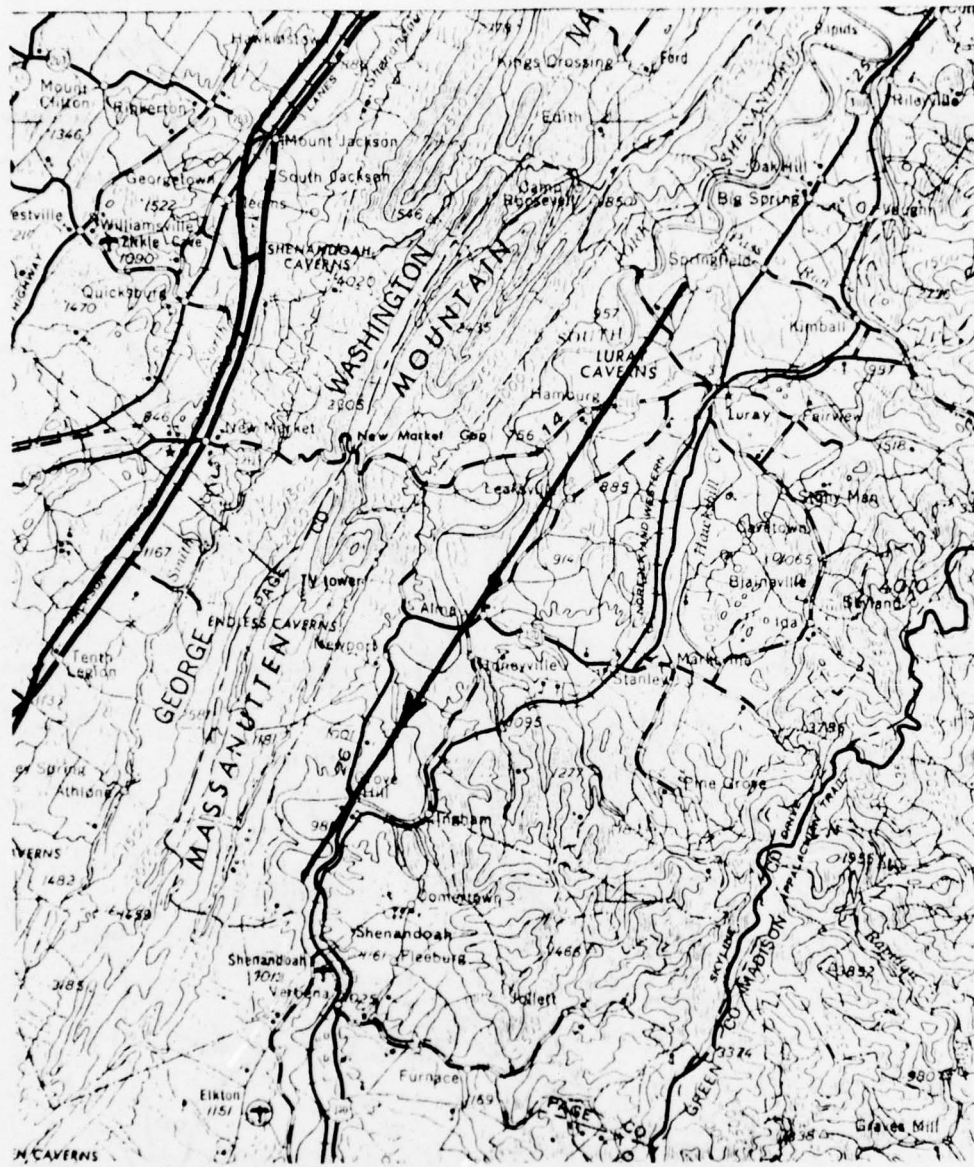
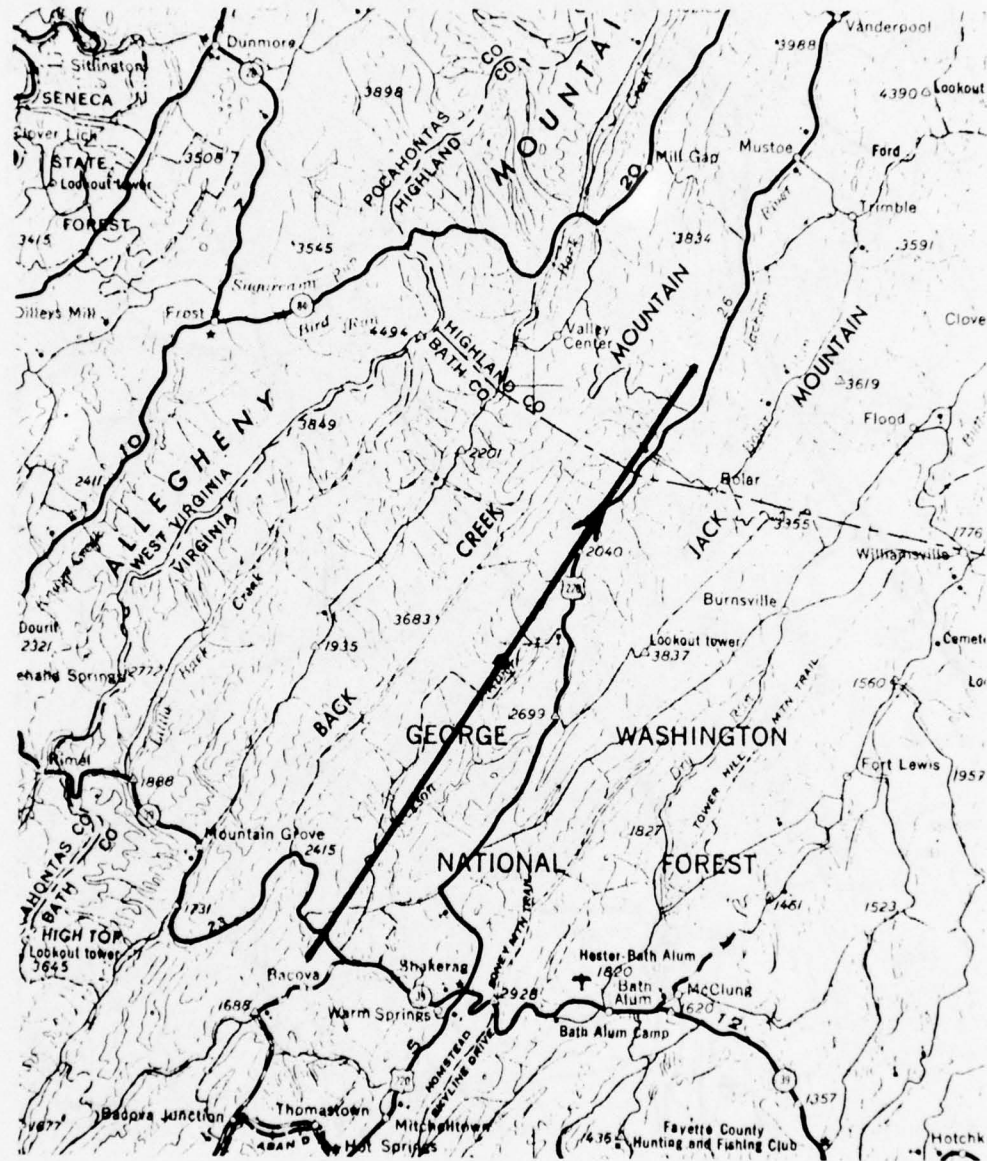


Fig. 7. Terrain and Flight Path Used to Analyze Case 1.

BEST AVAILABLE COPY

BEST AVAILABLE COPY



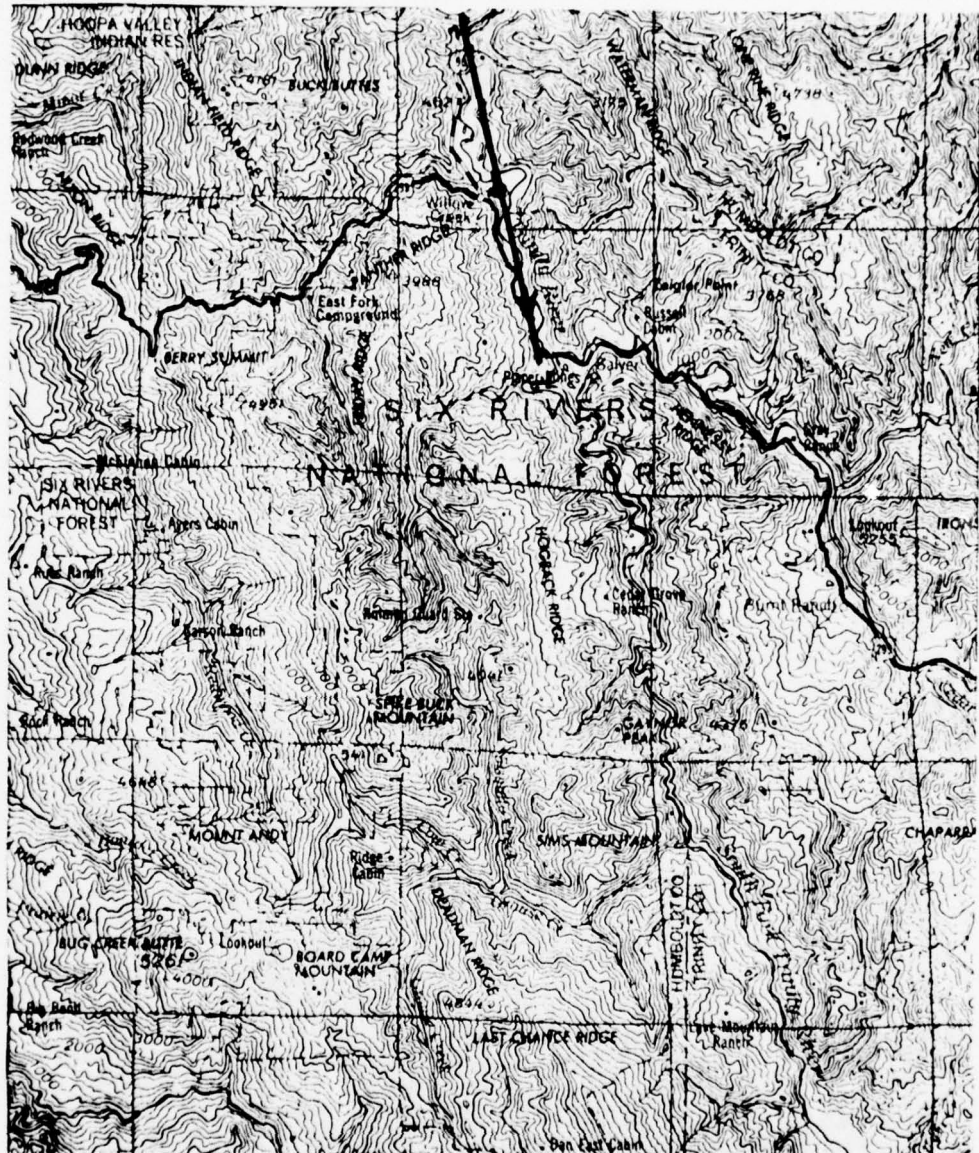


Fig. 9. Terrain and Flight Path
Used to Analyze Case 3.

BEST AVAILABLE COPY

BEST AVAILABLE COPY



Fig. 10. Terrain and Flight Path
Used to Analyze Case 4.

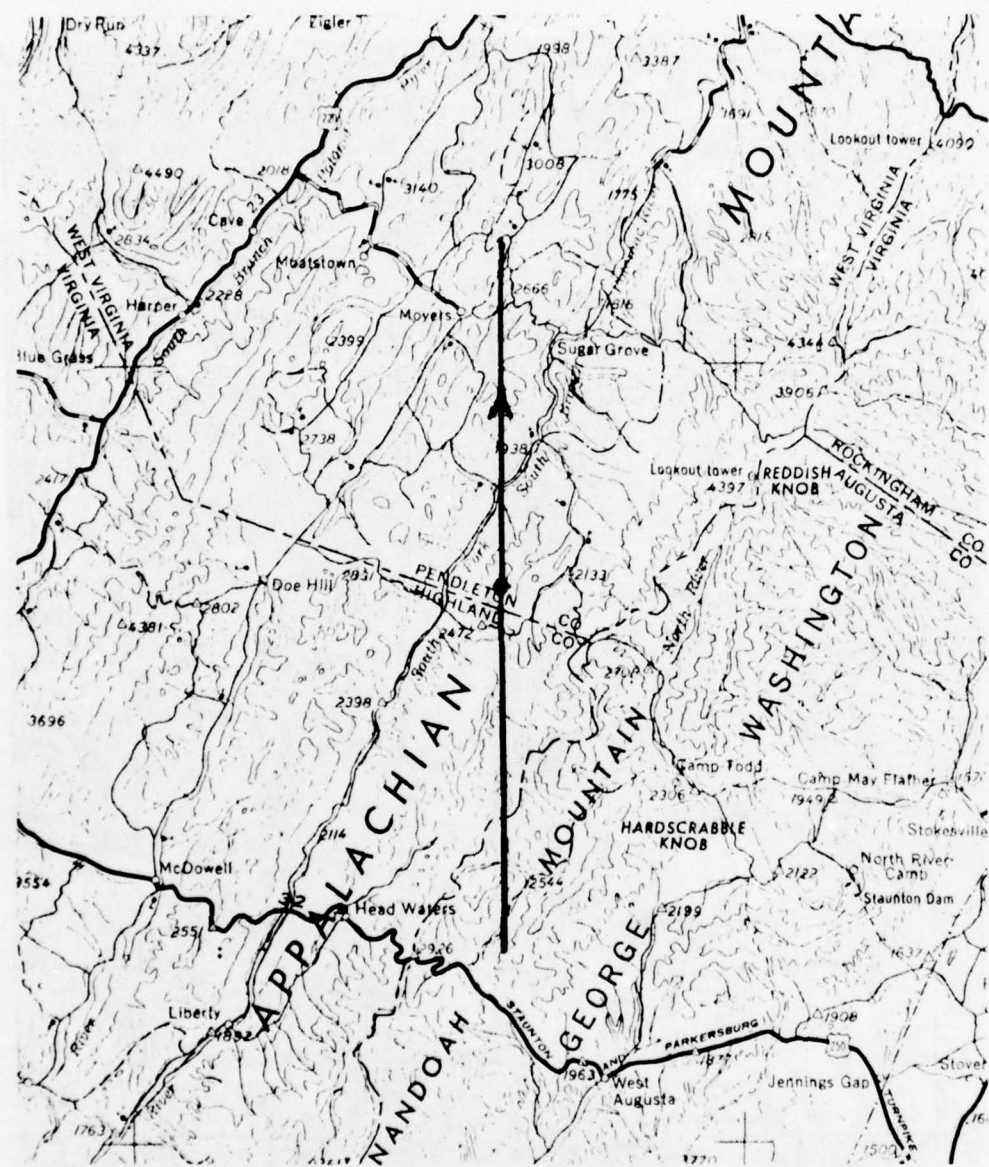


Fig. 11. Terrain and Flight Path
Used to Analyze Case 5.

BEST AVAILABLE COPY

BEST AVAILABLE COPY



Fig. 12. Terrain and Flight Path
Used to Analyze Case 6.

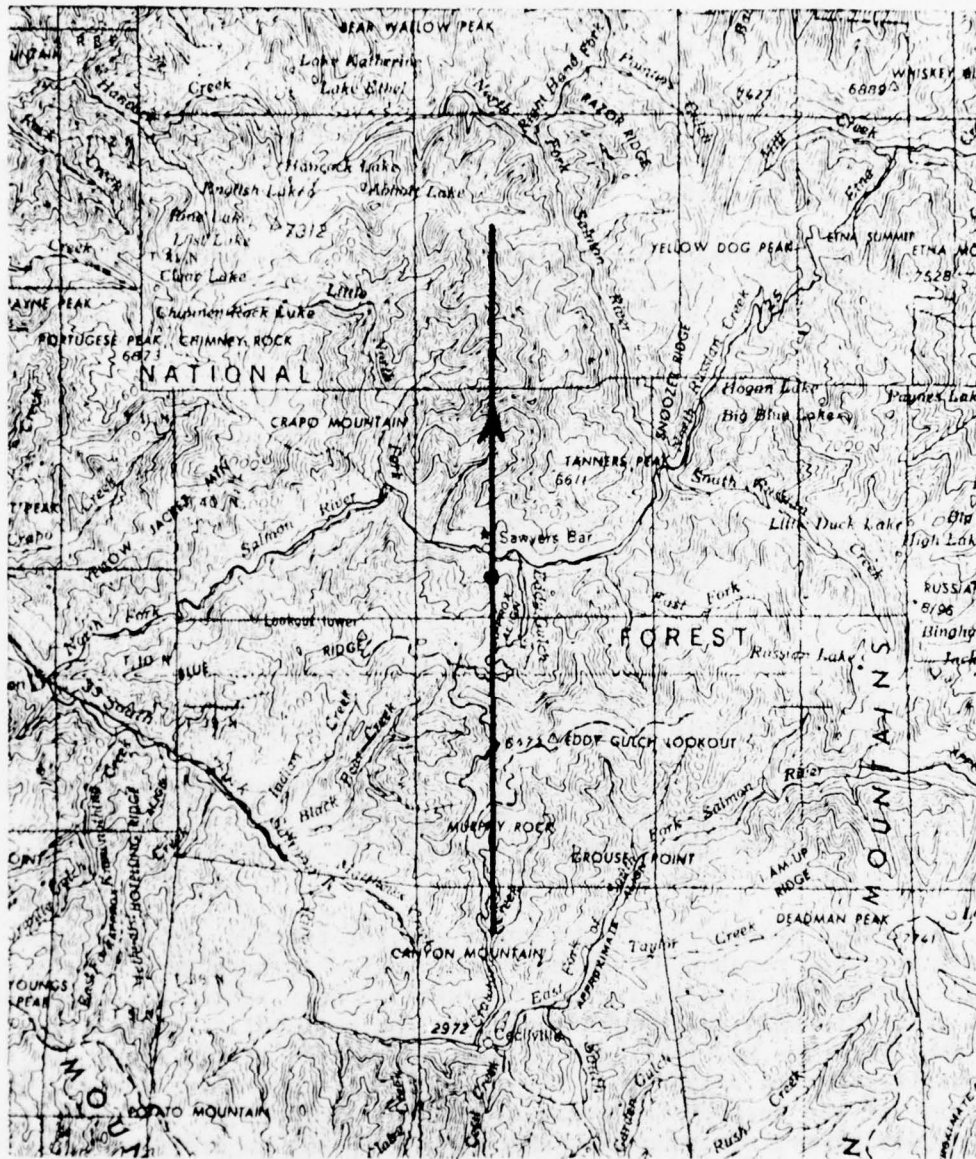


Fig. 13. Terrain and Flight Path
Used to Analyze Case 7.

BEST AVAILABLE COPY

Case 1 - Flight through the wide Shenandoah River Valley in moderately rough terrain in Virginia. The terrain height standard deviation is 122m and the terrain height average correlation length is 2667m.

Case 2 - Flight through the narrow Jackson River Valley in moderately rough terrain in Virginia. The terrain height standard deviation is 135m and the terrain height average correlation length is 1548m.

Case 3 - Flight through the narrow Trinity River Valley in rough terrain in northern California. The terrain height standard deviation is 268m and the terrain height average correlation length is 2460m.

Case 4 - Flight over relatively smooth terrain north of Silver Spring, Maryland. The terrain height standard deviation is 21m and the terrain height average correlation length is 2476m.

Case 5 - Flight over moderately rough terrain on the West Virginia - Virginia border. The terrain height standard deviation is 95m and the terrain height average correlation length is 1937m.

Case 6 - Flight over rough terrain near the Klamath River in northern California. The terrain height standard deviation is 226m and the terrain height average correlation length is 2300m.

Case 7 - Flight over very rough terrain in the Salmon Mountains in northern California. The terrain height standard deviation is 328m and the average terrain height correlation length is 2271m.

The first two valley flight cases are for terrain with approximately the same roughness. However, the valley is narrower for the second case which results in horizons with greater variation since much of the terrain which contributes to the horizon is closer to the vehicle. The valley flight cases are numbered in the order of increasing terrain roughness. The cases for flights above the majority of the surrounding terrain are also numbered in the order of increasing terrain roughness and span more than an order of magnitude change in terrain roughness.

The vehicle flying altitudes above the valley floor used for the valley flights were: 100m for Case 1, 200m for Case 2, and 300m for Case 3. These are the same as those used for previous analyses with actual horizons as reported in Ref. 2. Higher flying altitudes were required for the narrower valleys to provide reasonable space for likely lateral flight path variations on an actual flight.

Two vehicle flying altitudes were used for all cases involving flights above the majority of the surrounding terrain (Cases 4, 5, 6, and 7). The altitudes chosen were 100m and 500m above the maximum terrain height beneath the aircraft flight path. The 500m altitude corresponds to the altitude used in analyzing the fixed-range profile system as reported in Ref. 2; therefore, it was included here so system comparisons are possible. Lower altitudes could not be considered with fixed-range profiles due to their excessive shadow content. It was felt that the lower altitude of 100m is of practical interest; therefore, it was also considered when analyzing the system using horizons for navigation checkpointing.

B. ANALYSIS TECHNIQUES

Except for the method used to generate profiles, the techniques used to obtain performance data for the navigation checkpointing system using horizons were identical to those used in obtaining performance data to analyze the system using fixed-range profiles as recorded in Ref. 2. Some of the methods used to analyze and present the performance data were changed slightly to permit a clearer and more concise presentation of performance results. It is appropriate to review the analysis techniques here to provide background for the performance results to be presented in later sections.

1. RANGE-LIMITED HORIZON GENERATION

Horizons required for performing the system analyses were obtained from the DMA digital topographic data defined in the introduction. Each reference on sensed horizon needed was generated in the same manner as described in Ref. 2 except for an additional interpolation which is required if the horizon point results from terrain at the range limit. Thus, for each horizon data point, the elevation angle to the terrain was computed for points at regularly spaced intervals along a radial line emanating from the vehicle horizontal position by using the first order terrain model (linear interpolation between terrain data points). The points considered included one beyond the defined range limit, R_L , as shown in Fig. 14. The maximum elevation angle to the terrain was computed and was the horizon elevation angle if it did not occur at the point beyond the maximum range limit as shown in Fig. 15a. If the maximum elevation angle occurred at the point beyond the range limit, then the elevation angle to the terrain was computed by first using linear interpolation between the terrain height at this point and the terrain height at the point preceding it in range to determine the terrain height at the range limit. The terrain height at the range limit was then used to compute the horizon elevation angle as shown in Fig. 15b.

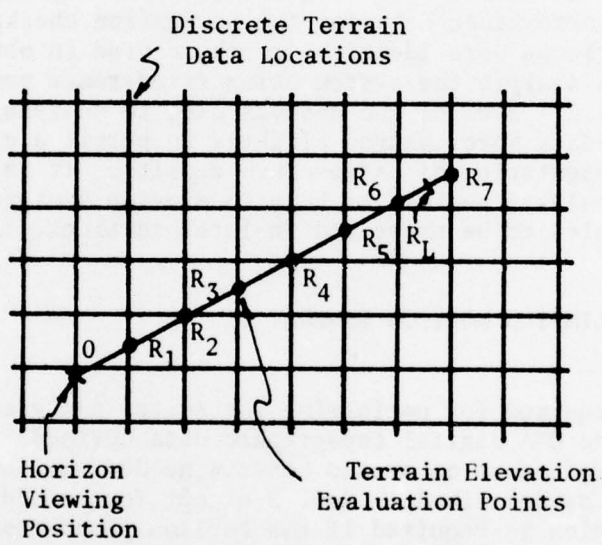
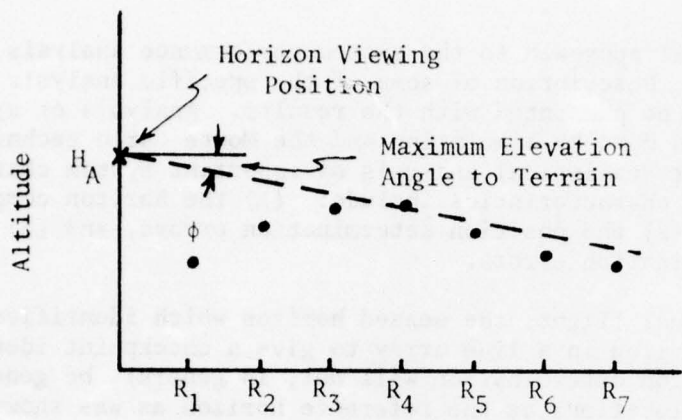
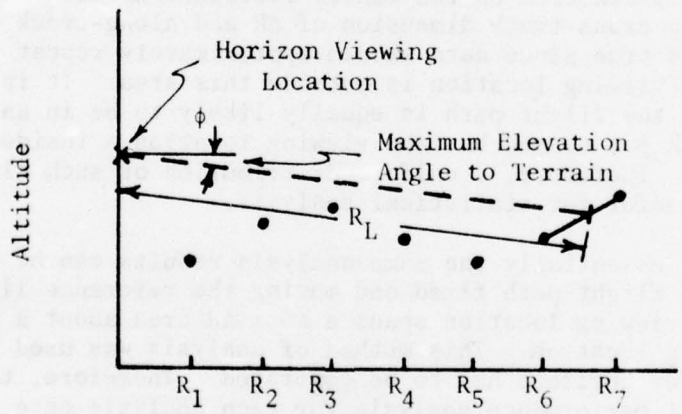


Fig. 14. Terrain Points Used to Evaluate One Horizon Elevation Data Point.



(a) Determination of Horizon Elevation Angle when not from Terrain at Range Limit



(b) Determination of Horizon Elevation Angle when from Terrain at Range Limit

Fig. 15. Determination of One Horizon Elevation Data Point.

2. ANALYSIS APPROACH

The overall approach to the system performance analysis is reviewed here. Description of some of the specific analysis detail is deferred to be presented with the results. Analysis of system performance was done by simulation and the Monte Carlo technique to obtain data for statistical analysis of important system characteristics. These characteristics include: (1) the horizon comparison function, I_m , (2) the position determination errors, and (3) the heading determination errors.

On an actual flight, the sensed horizon which identifies with a reference horizon in a line array to give a checkpoint identification and position determination will not, in general, be generated from the same locations as the reference horizon as was shown in Fig. 3. Therefore, the flight path must be moved to various positions with respect to the reference array so the statistics of the horizon comparison function and position and heading determination errors can be computed. If it is assumed that the terrain is approximately homogeneous over the reference array area, then, as shown in Fig. 16, it is only necessary to analyze flight path positions such that the sensed horizon which should identify with the array (from viewing location A in Fig. 16) is obtained from viewing locations spanning an area which is centered on the center reference horizon in the array and has a cross-track dimension of ΔR and along-track dimension of ΔS . This is true since data should approximately repeat if the sensed horizon viewing location is outside this area. It is reasonable to assume that the flight path is equally likely to be in any of the positions which put sensed horizon viewing location A inside the analysis area. Therefore, a uniform distribution of such flight path locations is useful for statistical analysis.

Actually, essentially the same analysis results can be obtained by holding the flight path fixed and moving the reference line array so its center viewing location spans a $\Delta S \times \Delta R$ area about a sensed horizon viewing location. This method of analysis was used to minimize cost since fewer horizons had to be generated. Therefore, to perform the statistical performance analysis for each analysis case, 52 sensed horizons were generated for vehicle locations at the desired vehicle altitude and separated by 200m along the flight path defined for that case. This is illustrated in Fig. 17. The center of the resulting 10.2Km flight path segment was located at the defined analysis location. Reference horizons were generated for 32 line arrays of viewing location with 5 reference horizons in each line array. The line arrays were chosen so the center viewing locations in the arrays were uniformly distributed about the center two sensed horizon viewing locations as shown in Fig. 17. Therefore, a group of 16 line arrays were closest to each of the center two sensed horizon viewing locations.

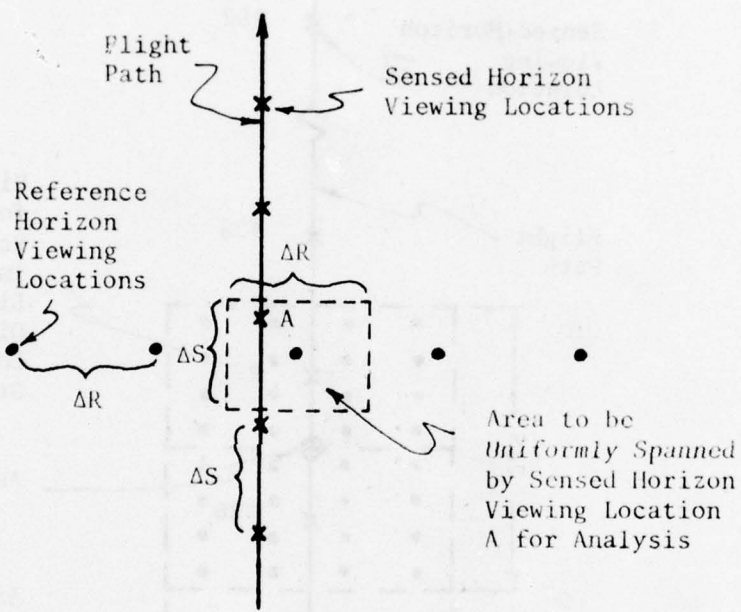


Fig. 16. Required Flight Path Position Variations for Statistical Analysis of System Performance.

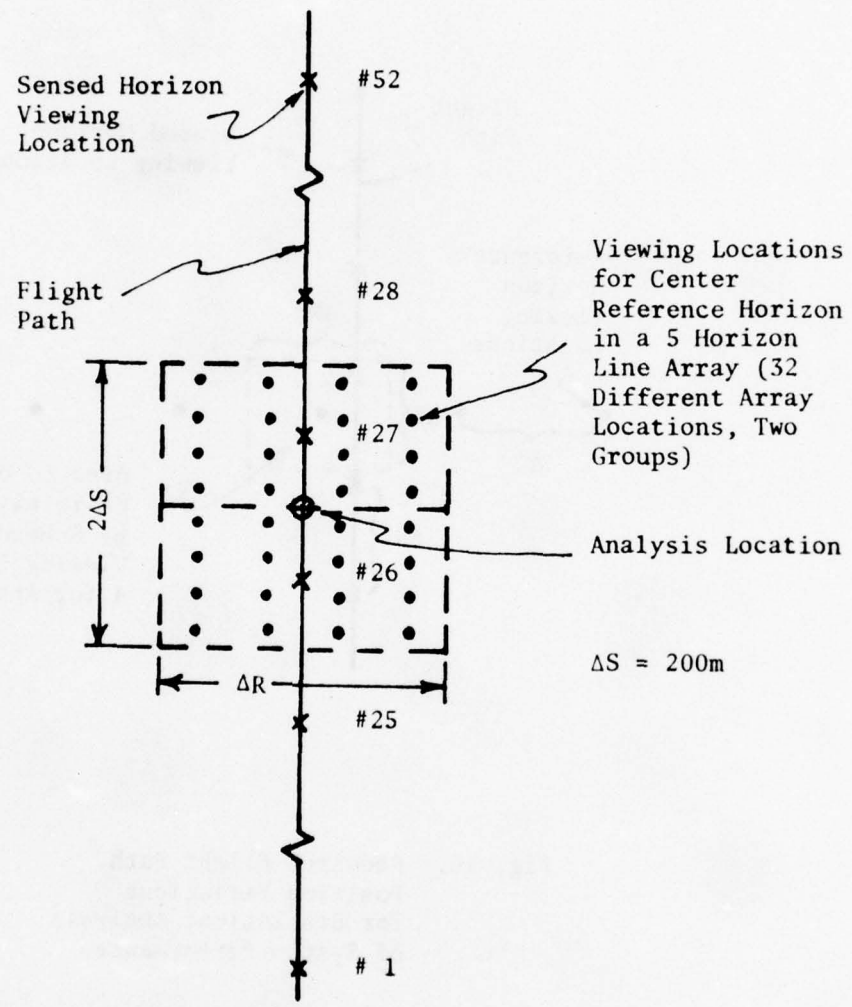


Fig. 17. Horizon Viewing Location Geometry for Performance Analysis.

The reference line arrays were chosen to span two sensed profile viewing locations rather than one to provide better statistical averaging by avoiding anomalies which might result because of the particular characteristics of a single sensed horizon.

Horizons generated from the locations just defined were compared in a computer simulation by computing the horizon comparison function, I_m . The position and heading differences between the sensed horizon viewing location and the reference horizon segment viewing location and heading which gave the minimum value for the horizon comparison function were computed to obtain the position and heading determination errors. The first 16 reference horizon arrays were compared with sensed horizons 1 through 51 (see Fig. 17) and the second group of 16 reference horizon arrays were compared with sensed horizons 2 through 52 to obtain performance data for flight path intervals of $\pm 5\text{Km}$ with respect to the two groups. These data were averaged to provide mean values and standard deviations of the performance data (e.g. horizon comparison function, position errors, heading error).

It should be noted that no variations of flight path heading were used. This should not greatly affect the results obtained since reference horizons are generated to be 20° wider than the sensed horizons so similar performance should result as long as the flight path heading is within $\pm 10^\circ$ of the planned flight path heading.

C. HORIZON DATA

Sensed horizons (elevation angle, ϕ , as a function of azimuth angle) for one of the center two viewing locations along the flight path (location #26 in Fig. 17) are shown in Figs. 18-22 for each of the analysis cases and vehicle altitudes. To facilitate direct comparison, the same scale has been used for all plots even though this results in plots for relatively smooth horizons which are poorly scaled for illustrating the detailed horizon shape.

Fig. 18 shows the sensed horizons for the three valley flights (i.e. Cases 1, 2, and 3). The valley is apparent in each case. It can be seen that the valley is quite broad for Case 1. The flight path is not very near the center of the valley horizon in Case 2. This resulted from curvature in the valley being considered so the valley seen 5Km ahead of the vehicle was to the right of center.

Figures 19, 20, 21, and 22 show the sensed horizons for vehicle altitudes of 100m and 500m above the highest terrain point beneath the flight path for Cases 4, 5, 6, and 7 respectively. The horizons obtained for an altitude of 100m have basically the same shape as horizons obtained at an altitude of 500m. Their mean values are different as expected. Differences in shape result primarily from the fact that more of the terrain profile at the range limit is

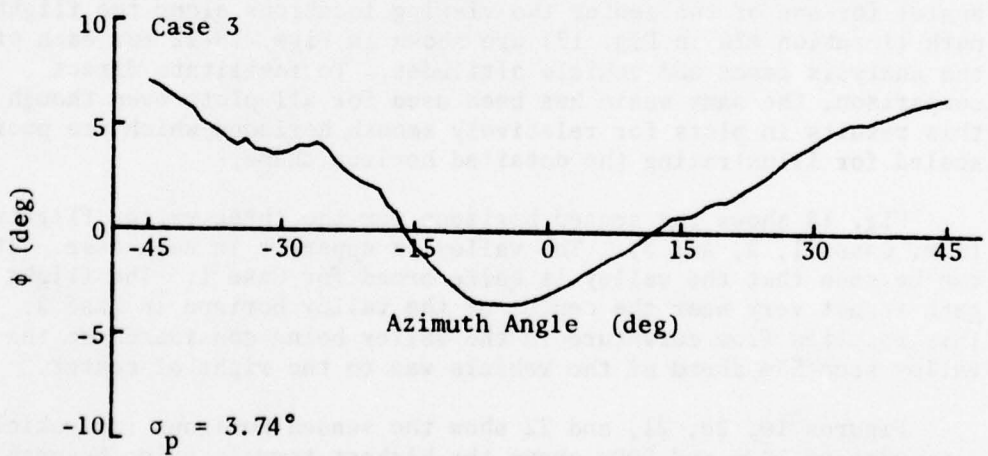
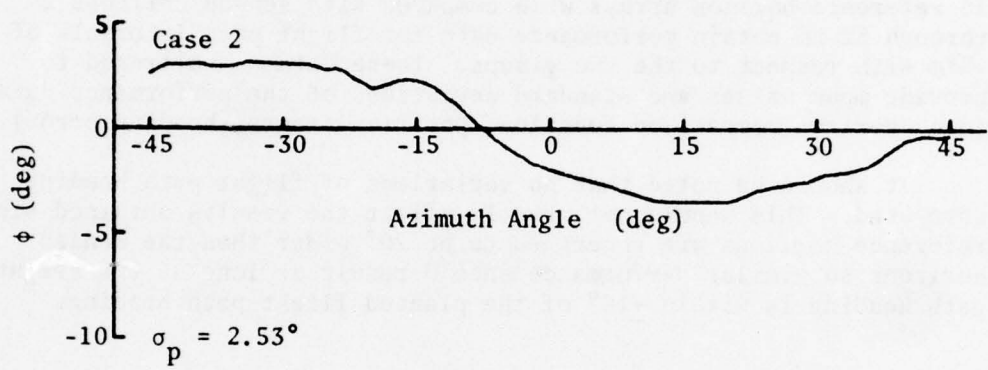
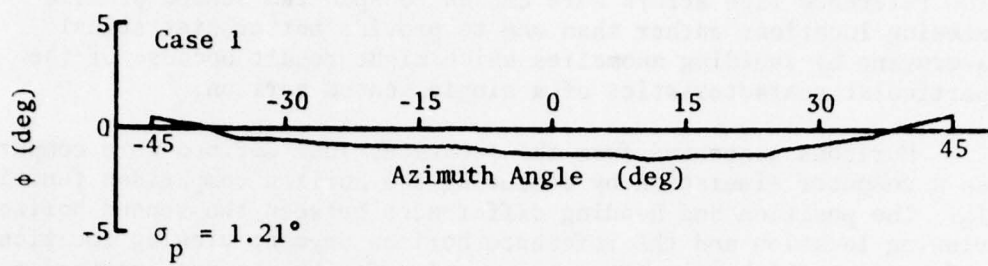


Fig. 18. Sensed Horizons for Cases 1, 2, and 3 (Valley flights).

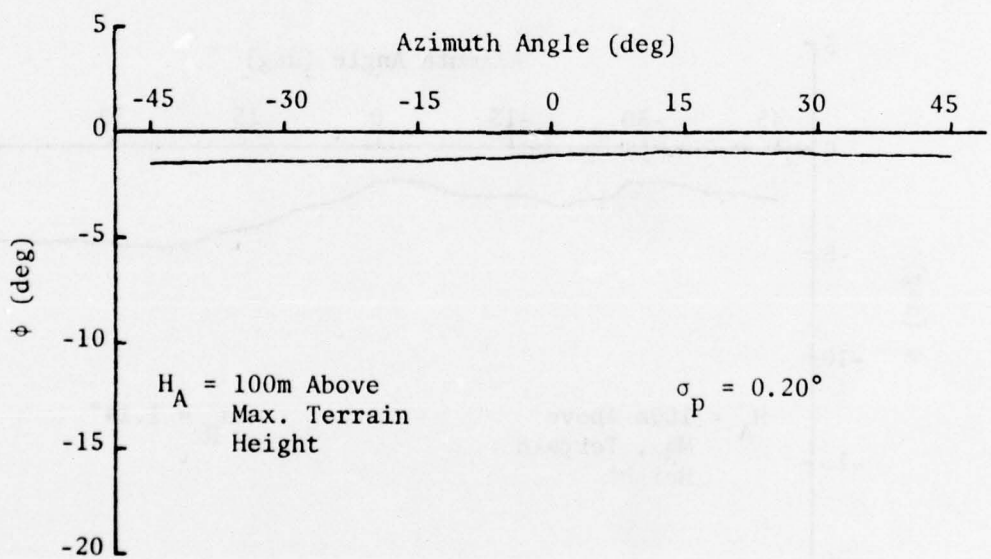
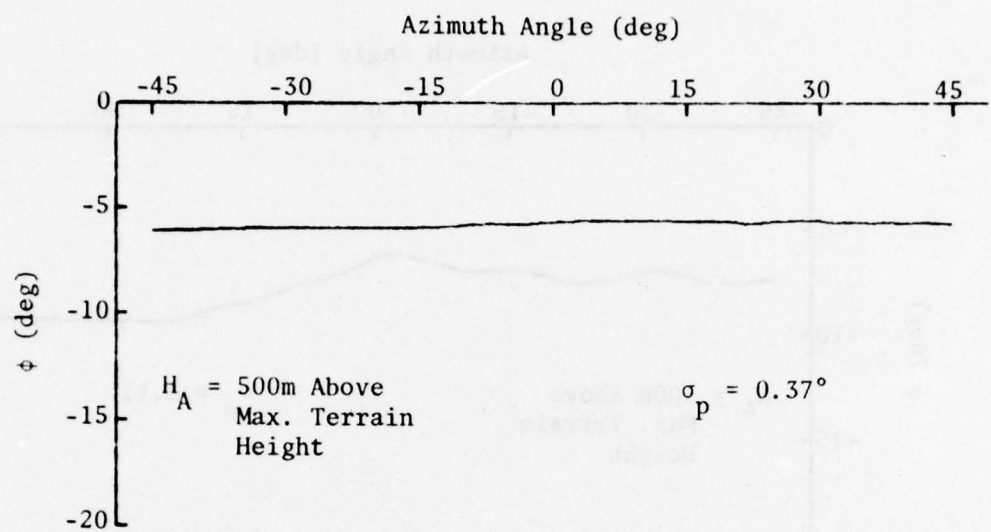


Fig. 19. Sensed Horizons for Case 4
(Relatively Smooth Terrain).

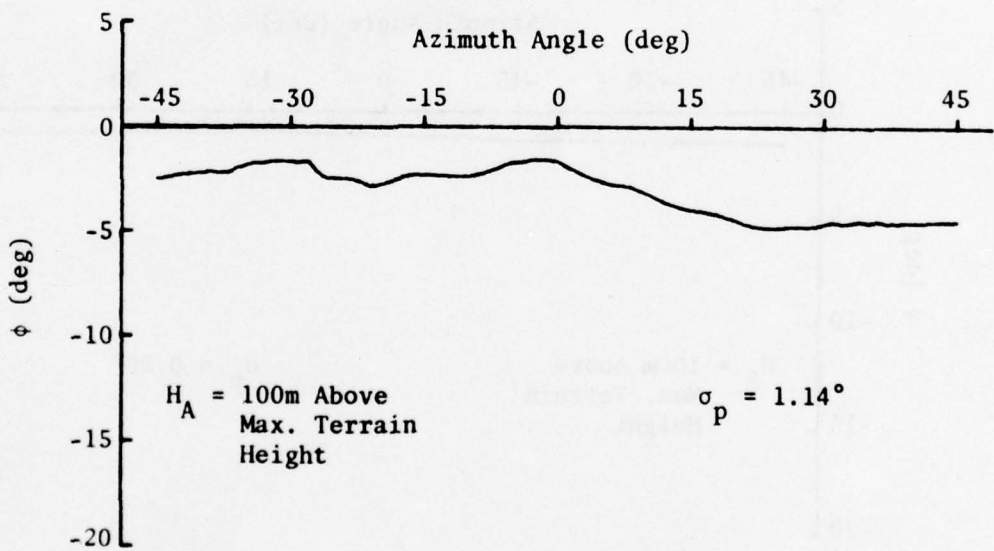
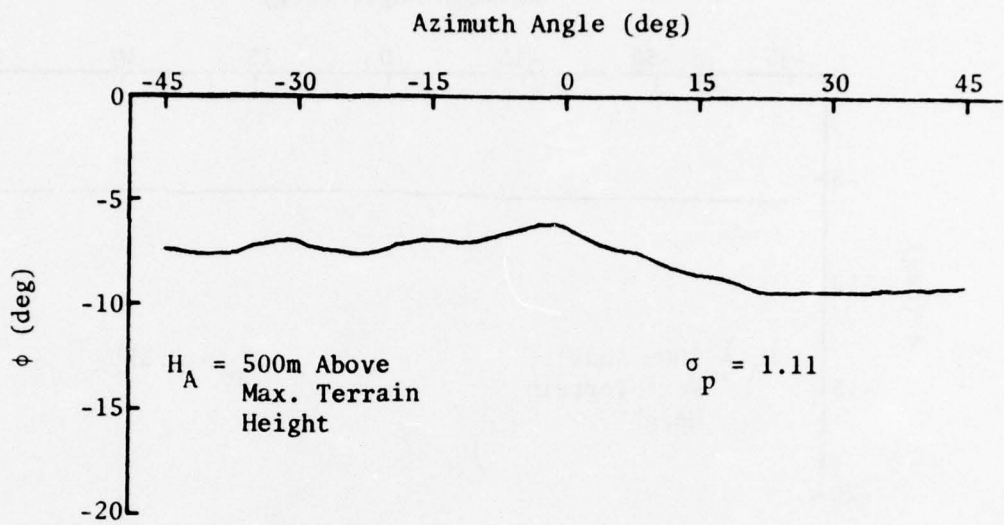


Fig. 20. Sensed Horizons for Case 5
(Moderately Rough Terrain).

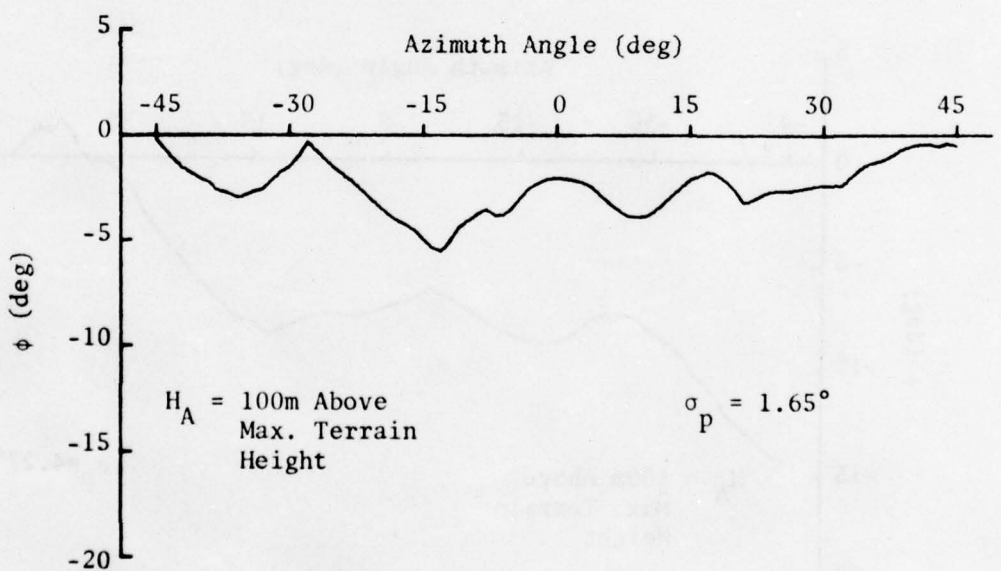
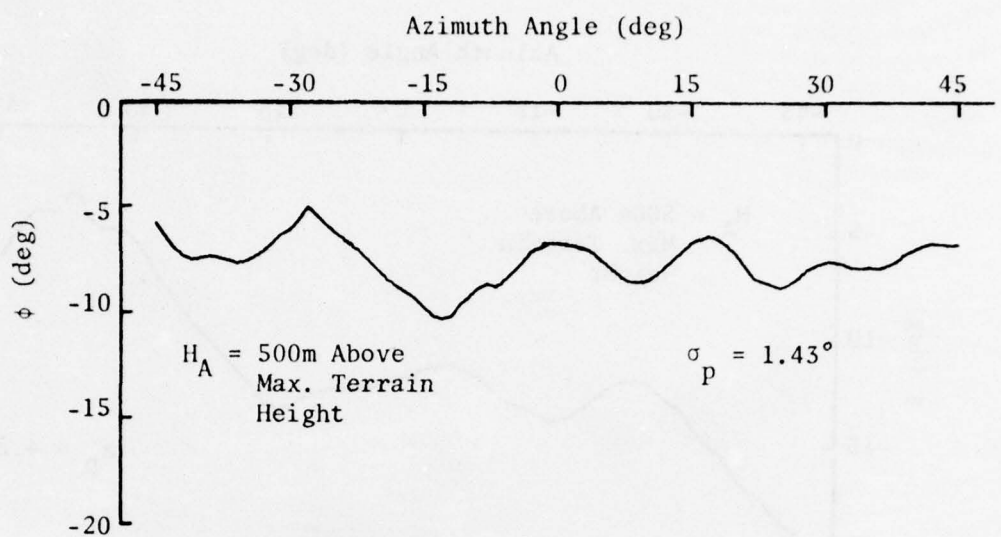


Fig. 21. Sensed Horizons for Case 6
(Rough Terrain).

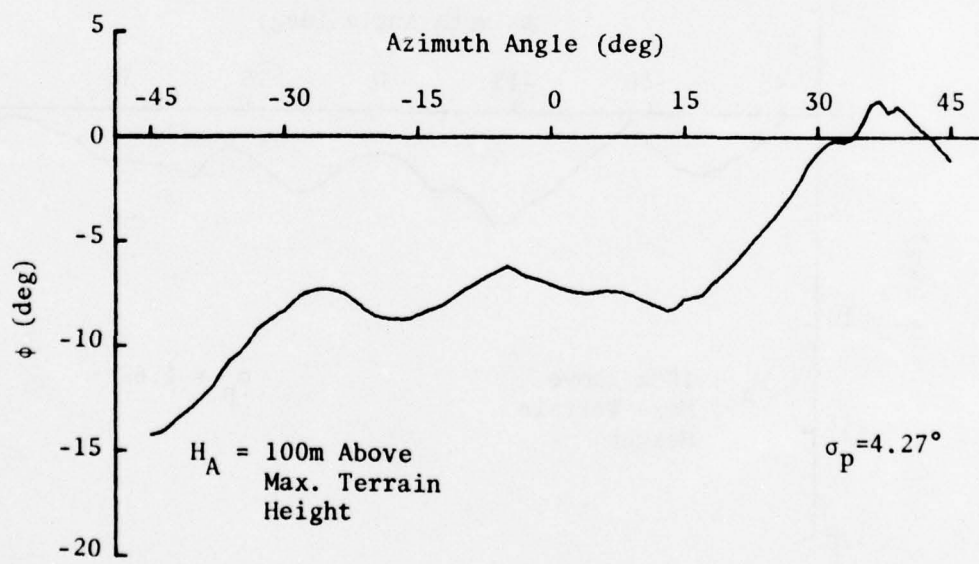
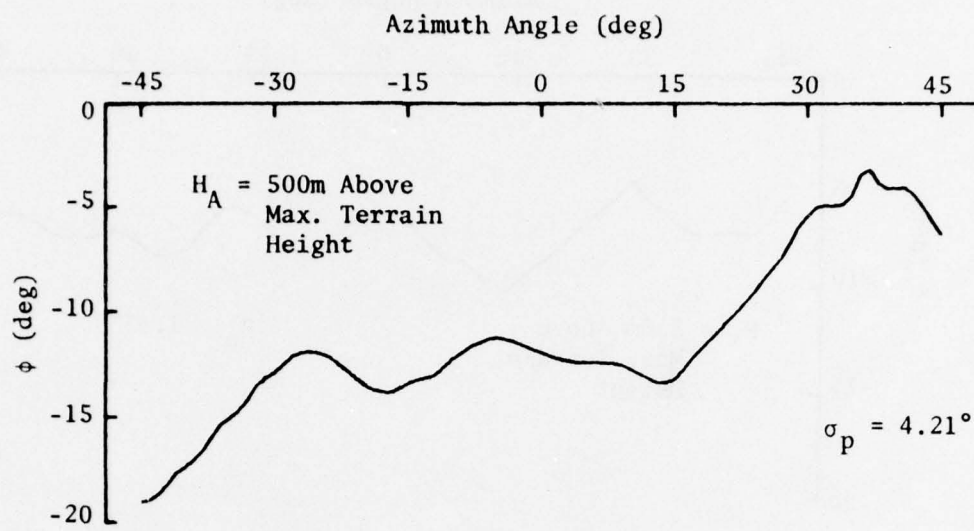


Fig. 22. Sensed Horizons for Case 7
(Very Rough Terrain).

shadowed at the lower altitude so the terrain contributing to the horizon is located at a different (shorter) range from the vehicle.

A numerical indication of the roughness of the horizons obtained in each case was obtained by computing their standard deviations, σ_p . In order to provide averaging over the analysis region, the mean and standard deviation were computed by utilizing the horizon data for the center segment (segment length equal to sensed horizon length) of all reference horizons. The values obtained are shown on the sensed horizons plotted in Figs. 18-22 and also in Table I. Table I also contains the terrain height standard deviations.

TABLE I. Standard Deviation of
Sensed Horizons for All
Analysis Cases.

Case	Flight Type	σ_T (m)	σ_p (deg)		
			$H_A = \text{Neg.}$	$H_A = 100\text{m}$	$H_A = 500\text{m}$
1		122	1.21	--	--
2	Valley	135	2.53	--	--
3		268	3.74	--	--
4		21	--	0.20	0.37
5	Above	95	--	1.14	1.11
6	Terrain	226	--	1.65	1.43
7		328	--	4.27	4.21

It can be seen from Table I that the horizon variation increases with increasing terrain height standard deviation as expected. For the valley cases, another factor enters in the increase of the horizon variation. This factor is the narrowness of the valley being considered and is apparent in the relation between Case 1 and Case 2 since these cases are for approximately equally rough terrain but Case 2 uses a narrower valley. For flights above the majority of the surrounding terrain, it can be seen that horizon variation increases with terrain roughness as expected. The rate of increase is not always the same since the terrain data is not really homogeneous and thus the horizon variation obtained depends somewhat on the location from which the horizon is obtained. In general, the horizon variation is slightly larger at the lower altitude. This also is as expected since more of the terrain contributors to the horizon are at shorter ranges for the lower altitude.

System performance should be closely related to the horizon variation available. Therefore, the values of horizon standard

deviation are used in the following performance analysis rather than values of terrain height standard deviation for presentation of results as a function of terrain roughness.

D. HORIZON COMPARISON FUNCTION DATA

For each analysis case, all of the sensed horizons defined previously were compared with the 5 reference horizons in all of the 32 reference horizon arrays defined. The comparison was performed by computing the integral absolute difference (IAD) for all sensed horizons and segments of reference horizons to obtain data for the previously defined horizon comparison function, I_m . The data for the 32 reference horizon arrays was averaged as previously indicated to determine the mean and standard deviation of the horizon comparison function as a function of distance from the line array. Data averaged for each point on the horizon comparison function is from an increment of flight path distance equal to ΔS surrounding that point. Initial computations of the horizon comparison function were performed with no system errors introduced.

Figs. 23-27 show the horizon comparison functions for each of the analysis cases and vehicle altitudes. Curves are shown for the mean value, μ_I , of I_m and for the upper and lower one standard deviation variations from this mean value, $\mu_I + \sigma_I$ and $\mu_I - \sigma_I$. Once again, to facilitate direct comparison, the same scale has been used for all plots even though this results in plots for the smoother horizons which are poorly scaled for good determination of specific values.

Fig. 23 shows the horizon comparison functions for the three valley flights (Cases 1, 2, and 3). The values of the horizon standard deviations for each case are also shown on the curves for a ready indication of the horizon variations which produced the horizon comparison functions. It can be seen that the horizon comparison function increases in magnitude and that its selection notch deepens as terrain roughness increases. Thus it should be possible to tolerate more random horizon errors for rougher terrain since the detection threshold can be set higher.

Figs. 24, 25, 26, and 27 show the horizon comparison functions for vehicle altitudes of 100m and 500m above the highest terrain point beneath the flight path for Cases 4, 5, 6, and 7 respectively. As for the valley cases, horizon standard deviations are included on the curves and it can be seen that the horizon comparison function increases in magnitude and that its selection notch deepens as terrain roughness increases which should provide greater immunity to random horizon errors. It appears as if the selection notch width does not change greatly with increased terrain roughness. It is felt that this is true as long as the reference horizons are selected

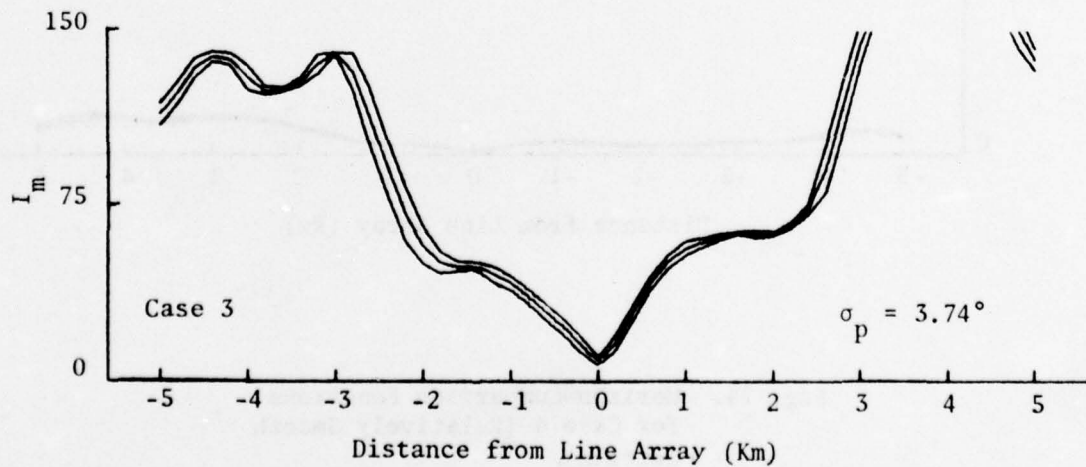
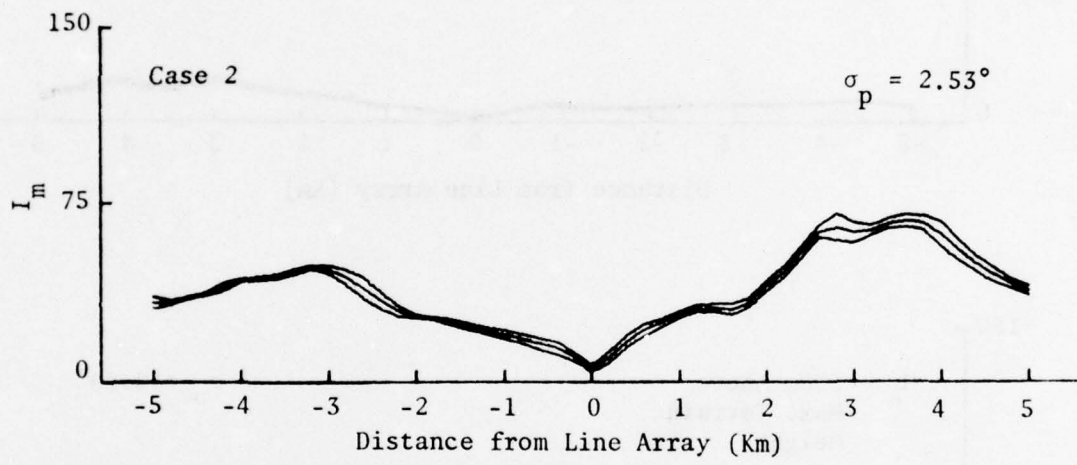
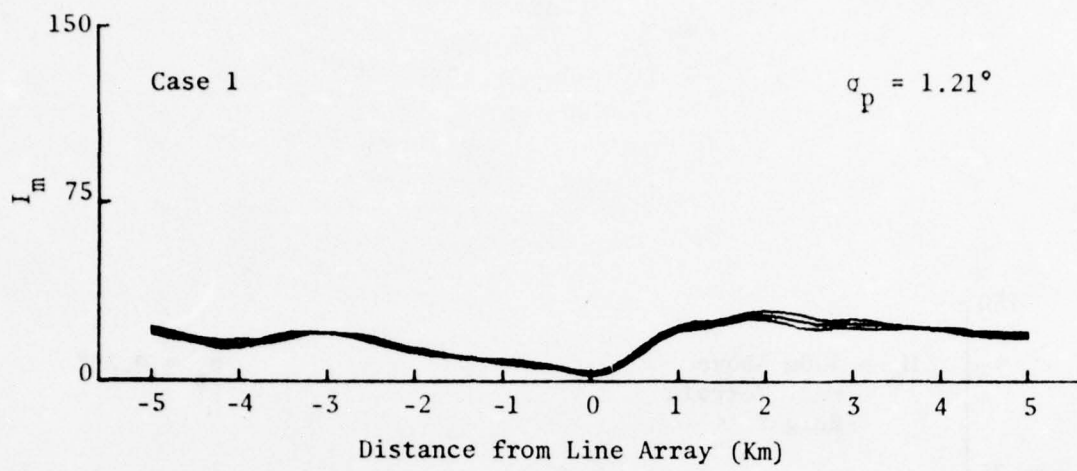


Fig. 23. Horizon Comparison Functions
for Cases 1, 2, and 3 (Valley Flights).

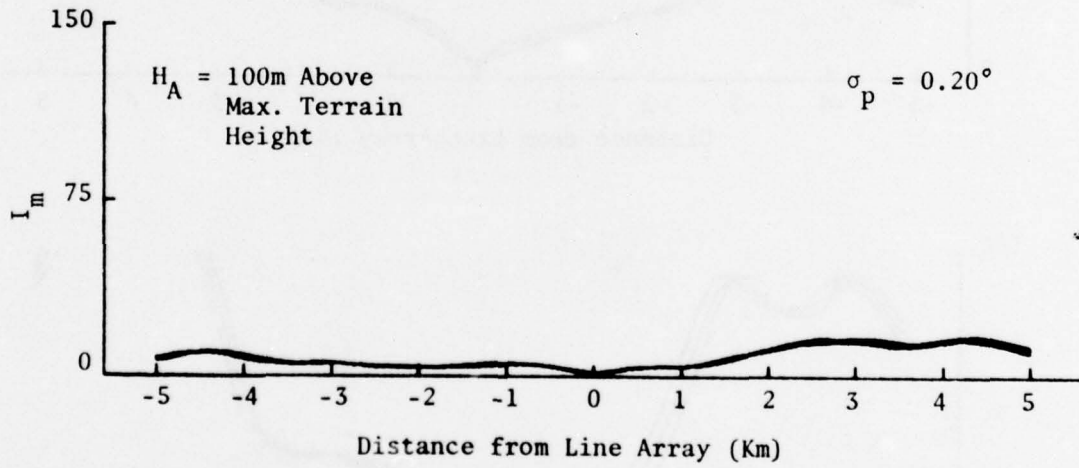
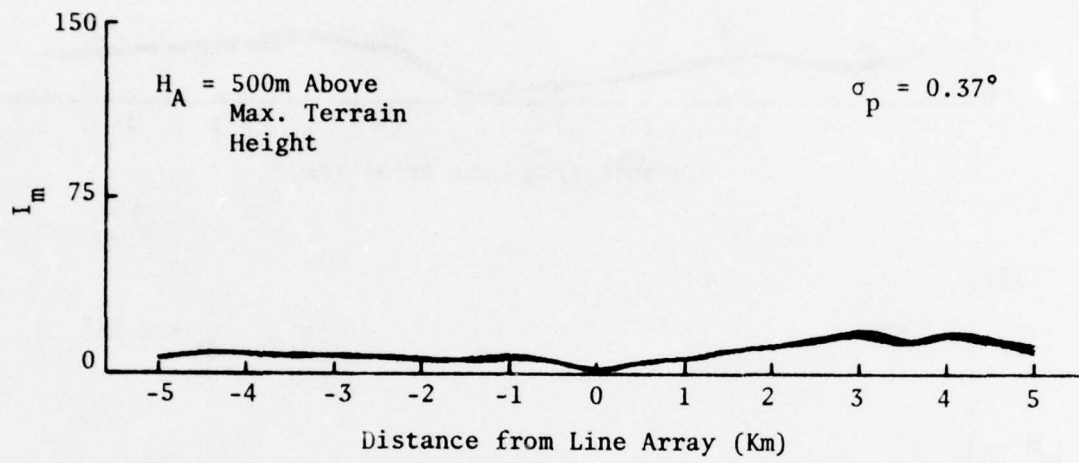


Fig. 24. Horizon Comparison Functions for Case 4 (Relatively Smooth Terrain).

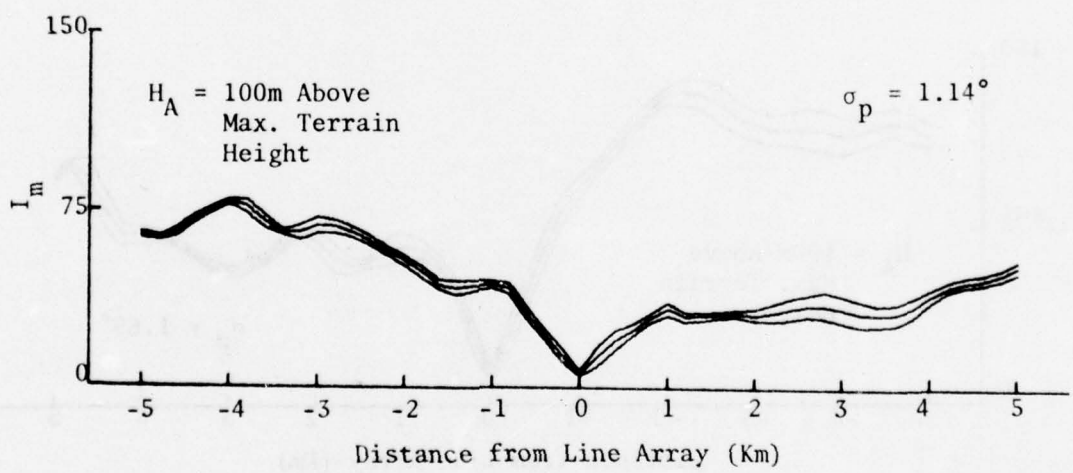
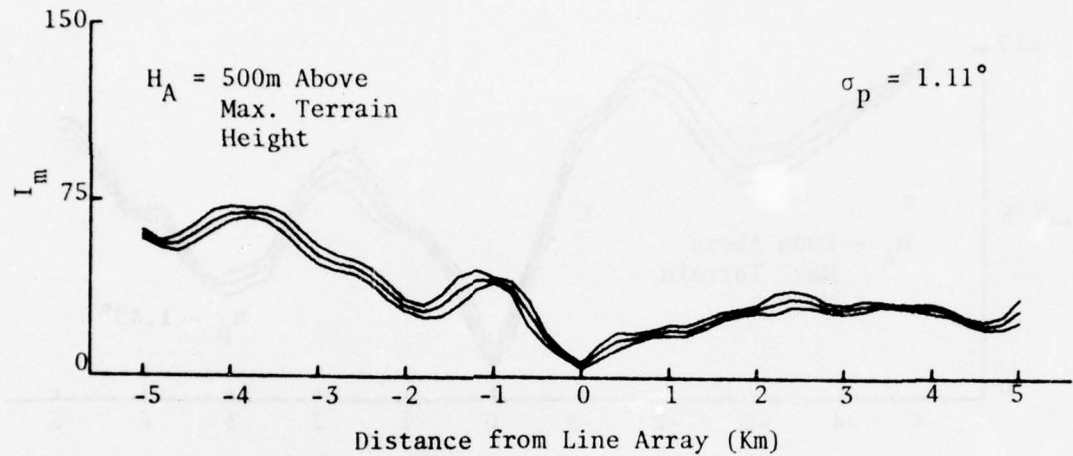


Fig. 25. Horizon Comparison Functions for Case 5 (Moderately Rough Terrain).

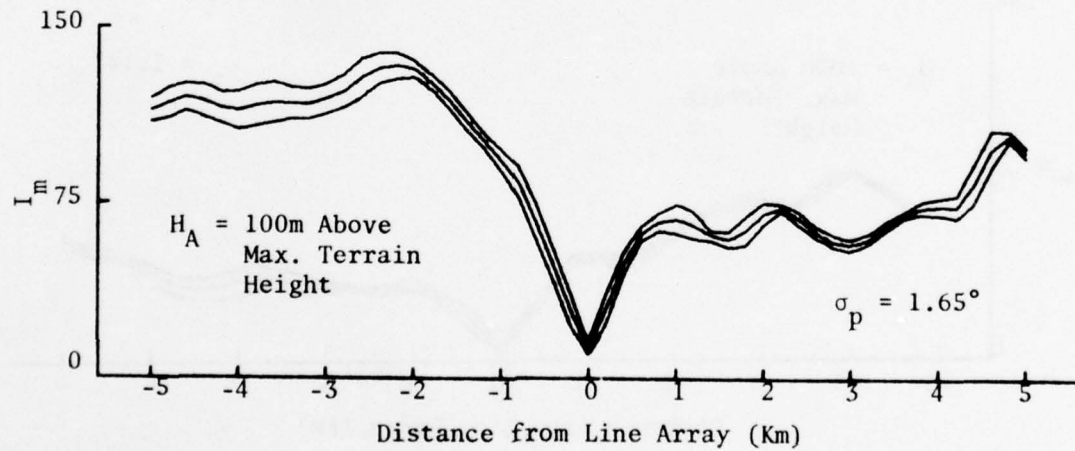
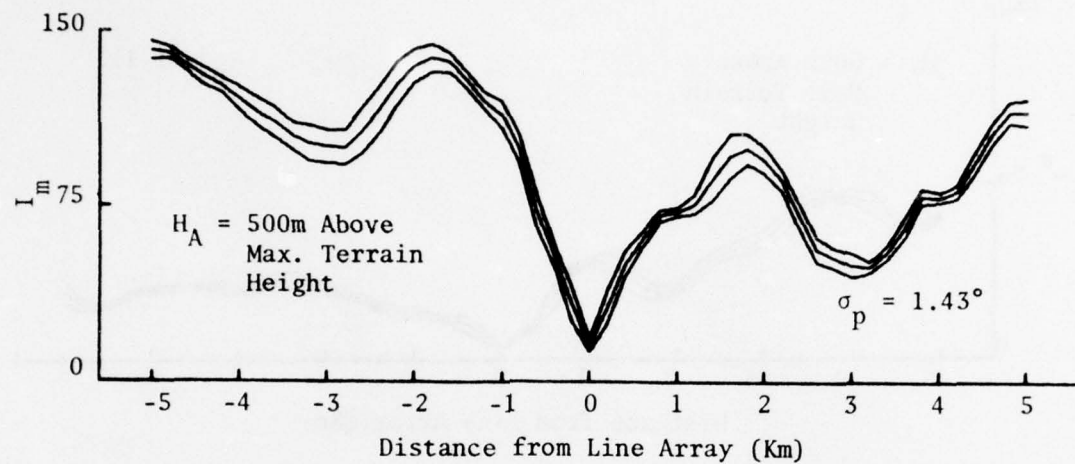


Fig. 26. Horizon Comparison Functions
for Case 6 (Rough Terrain).

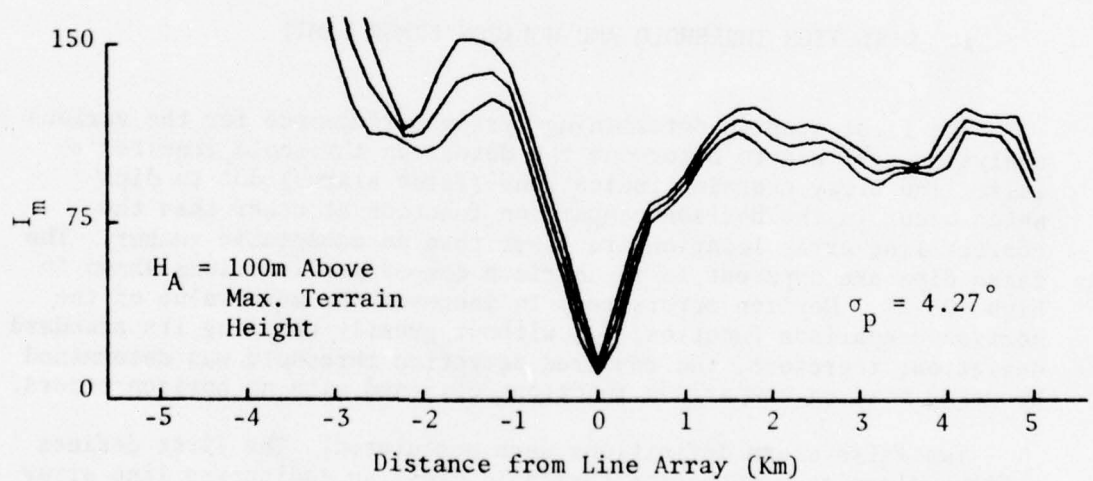
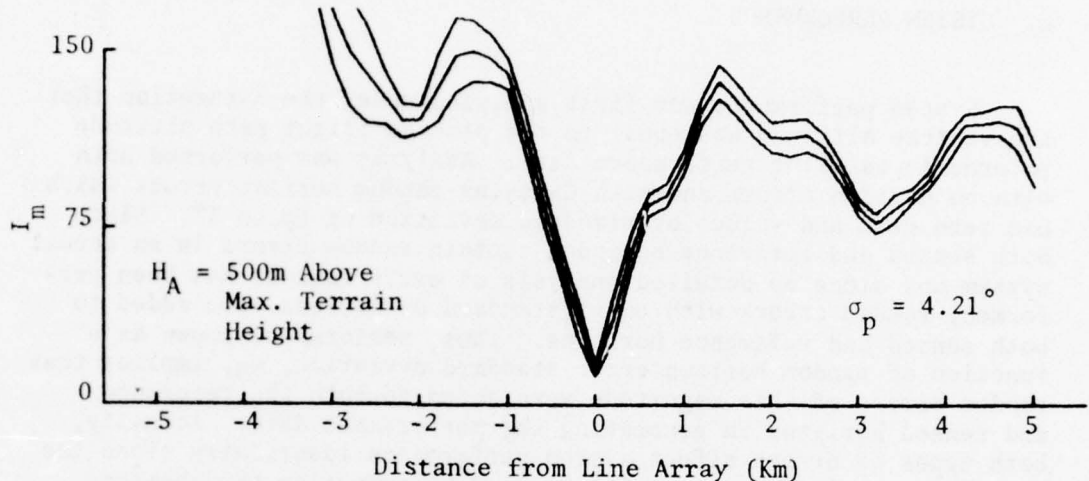


Fig. 27. Horizon Comparison Functions
for Case 7 (Very Rough Terrain).

from areas which supply sufficient horizon data content to make them good checkpoints since terrain height correlation lengths do not vary widely for the cases analyzed.

E. SYSTEM PERFORMANCE

System performance was first analyzed under the assumption that the vehicle altitude was equal to the planned flight path altitude to provide baseline performance data. Analysis was performed both with no horizon errors and with Gaussian random horizon errors which had zero mean and values of standard deviation of up to 1° . Since both sensed and reference horizons contain random errors in an actual system and since no detailed analysis of error sources has been performed, random errors with equal standard deviations were added to both sensed and reference horizons. Thus, performance shown as a function of random horizon error standard deviation, σ_N , implies that random errors of this magnitude were added to both the reference and sensed horizons in generating the performance data. Actually, both types of errors affect system performance identically since the horizon comparison function is obtained by computing the absolute value of the difference between sensed and reference horizons.

1. DETECTION THRESHOLD AND HORIZON ERROR LIMIT

The first step in determining system performance for the various analysis cases was to determine the detection threshold required so false line array crossing indications (false alarms) due to dips which occur in the horizon comparison function at other than the correct line array location are fewer than an acceptable number. The false dips are apparent in the horizon comparison functions shown in Figs. 23-27. Horizon errors tend to increase the mean value of the horizon comparison function, I_m , without greatly changing its standard deviation; therefore, the required detection threshold was determined by using horizon comparison functions obtained with no horizon errors.

Two false alarm definitions were postulated. The first defines a false alarm as a detection threshold crossing indicating line array identification when the vehicle is more than 1Km from the line array location. The second definition is the same except that the distance is increased to 2Km. It can be seen from Figs. 23-27 that the primary identification dip in I_m covers approximately this along-track distance so no false identification should occur if I_m crosses the detection threshold at distances of less than 1Km or 2Km from the correct line array location.

The required detection threshold was determined as follows. The value of I_m at any point along the flight path was assumed to have an approximately Gaussian distribution. This approximation was verified in Ref. 2 for actual horizons as long as the standard deviation was a small fraction of the mean value and the region of interest on the distribution was not too close to zero. It should be noted that I_m values cannot have an exact Gaussian distribution since they cannot be negative. The detection threshold required to obtain a probability of false alarm of $P_F = 0.001$ was then computed as $\mu_I - 3.08\sigma_I$ for all points of I_m at distances greater than 1Km or 2Km from the line array location. The minimum threshold value obtained for a distance greater than 1Km from the line array location was defined as T_1 corresponding to the first false alarm definition. The minimum threshold value obtained for a distance greater than 2Km from the line array location was defined as T_2 corresponding to the second false alarm definition. The results obtained are shown in Table II.

TABLE II. Required Detection Threshold
For a Probability of False
Alarm Less than 0.001.

Case	Below Max. Terrain Height (Valley Flights)		100m Above Max. Terrain Height		500m Above Max. Terrain Height	
	T_1	T_2	T_1	T_2	T_1	T_2
1	4.8	9.5	--	--	--	--
2	14.1	22.2	--	--	--	--
3	31.8	32.9	--	--	--	--
4	--	--	2.8	2.8	3.4	4.6
5	--	--	14.9	14.9	13.7	13.8
6	--	--	45.6	49.4	33.6	33.6
7	--	--	69.4	69.4	63.8	63.8

Table II shows that there is little difference between the two false alarm definitions for flights above the majority of the surrounding terrain. This could be anticipated by observing, from Figs. 24-27, that dips which contribute the false alarms are in general outside the 2Km distance for these cases. The same is not true for the valley flights since the horizon shape changes much more rapidly. The data shown in Table II are plotted as a function of the horizon standard deviation in Figs. 28 and 29. The curves show that the

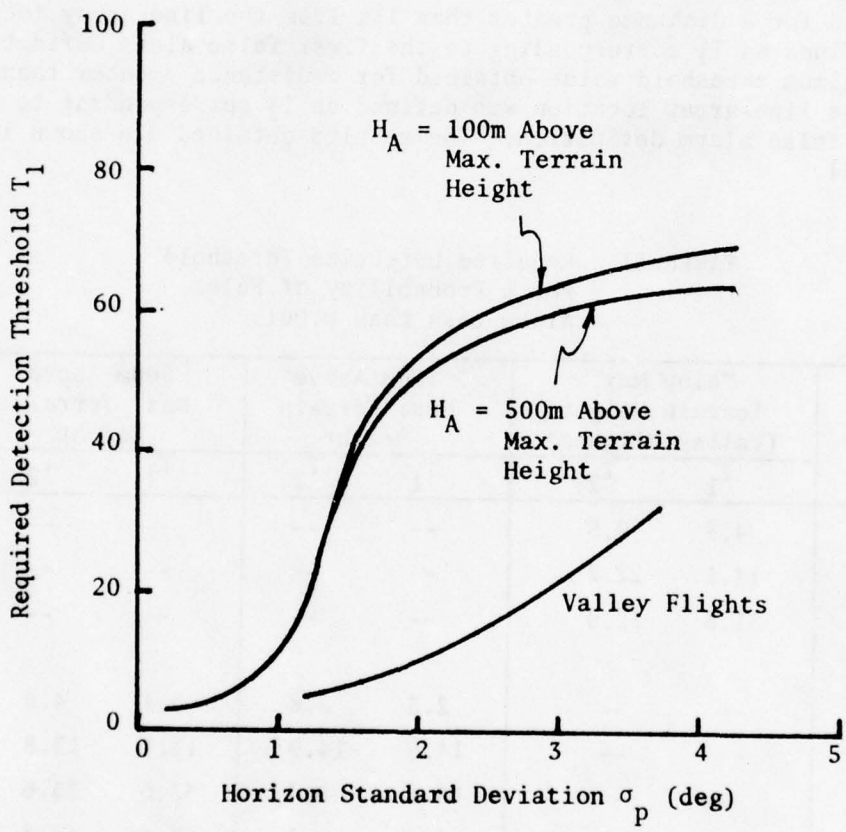


Fig. 28. Required Detection Threshold for $P_F < 0.001$ at Distances Greater than 1 Km from Line Array.

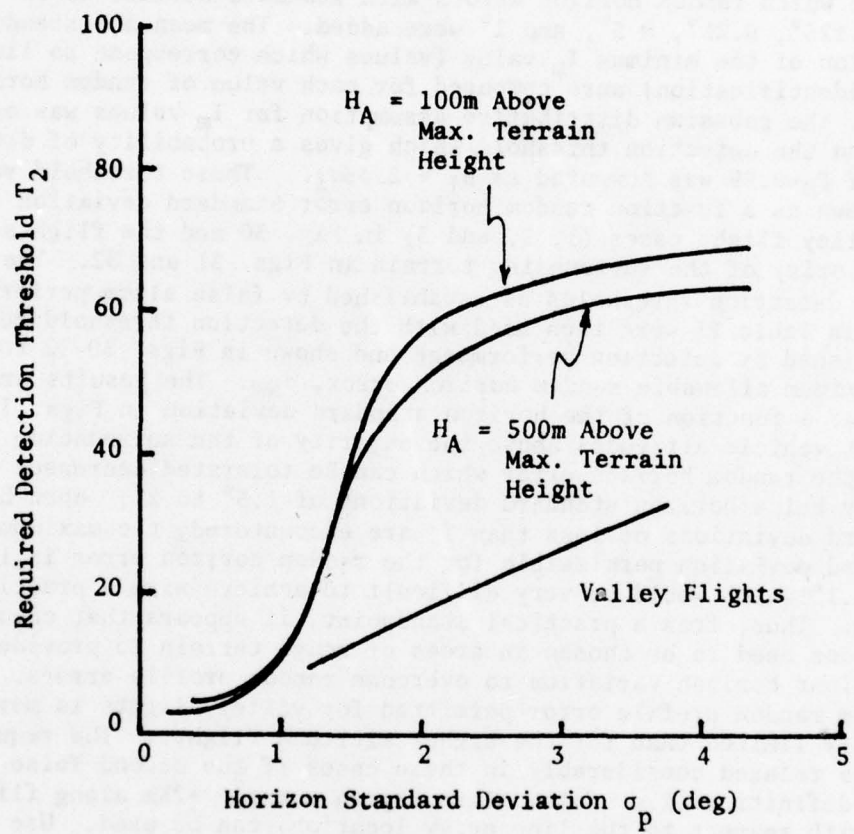


Fig. 29. Required Detection Threshold
for $P_F < 0.001$ at Distances
Greater than 2 Km from Line
Array.

detection threshold required for flights above the majority of the surrounding terrain is not very sensitive to altitude for the two altitudes considered. Also, as noted above, T_1 is similar to T_2 except for the valley flights.

Once the detection threshold was obtained, then the maximum allowable random horizon error was obtained for each of the analysis cases to determine the system sensitivity to random horizon errors. The following method was used to determine the maximum allowable random horizon error. First I_m data was obtained for the system using horizons to which random horizon errors with standard deviations of $\sigma_n = 0.125^\circ, 0.25^\circ, 0.5^\circ$, and 1° were added. The mean and standard deviation of the minimum I_m value (values which correspond to line array identification) were computed for each value of random horizon error. The gaussian distributive assumption for I_m values was again used and the detection threshold which gives a probability of detection of $P_D=0.99$ was computed as $\mu_I + 2.33\sigma_I$. These threshold values are shown as a function random horizon error standard deviation for the valley flight cases (1, 2, and 3) in Fig. 30 and the flights above the majority of the surrounding terrain in Figs. 31 and 32. The required detection thresholds as established by false alarm performance and shown in Table II were then used with the detection threshold curves as established by detection performance and shown in Figs. 30-32 to determine the maximum allowable random horizon error, σ_{NM} . The results are shown as a function of the horizon standard deviation in Figs. 33 and 34. At vehicle altitudes above the majority of the surrounding terrain, the random horizon error which can be tolerated decreases rapidly below horizon standard deviations of 1.5° to 2° . When horizon standard deviations of less than 1° are encountered, the maximum standard deviation permissible for the random horizon error is less than 0.1° which would be very difficult to achieve with a practical system. Thus, from a practical standpoint, it appears that checkpoint locations need to be chosen in areas of rough terrain to provide sufficient horizon variation to overcome random profile errors. The maximum random profile error permitted for valley flights is more severely limited than for the higher altitude flights. The requirement is relaxed considerably in these cases if the second false alarm definition (i.e. false alarm region outside $+2Km$ along flight path with respect to the line array location) can be used. Use of such a definition requires that a larger block of data be considered in making a decision as to whether a valid line array crossing has been detected and means that the minimum checkpoint spacing must be larger ($2Km$ instead of $1Km$) to avoid mismatch. Actually, the minimum checkpoint spacing is probably not too important practically since, in a practical case, checkpoints will usually be chosen much farther than $2Km$ apart.

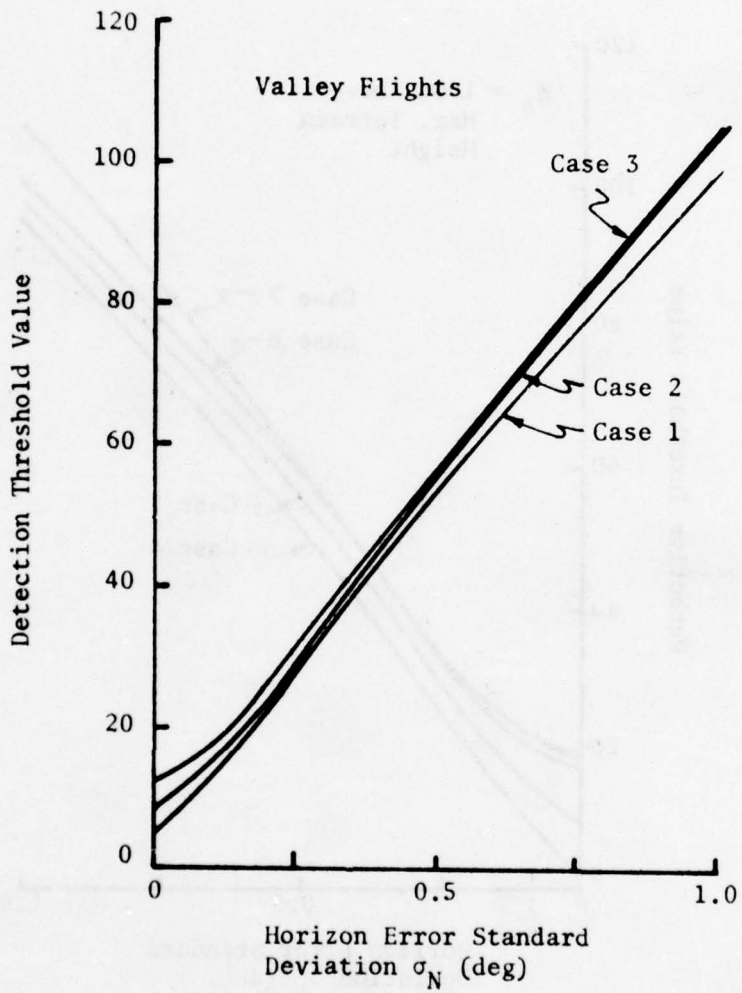


Fig. 30. Detection Threshold Needed to Give $P_D = 0.99$ (Valley Flights).

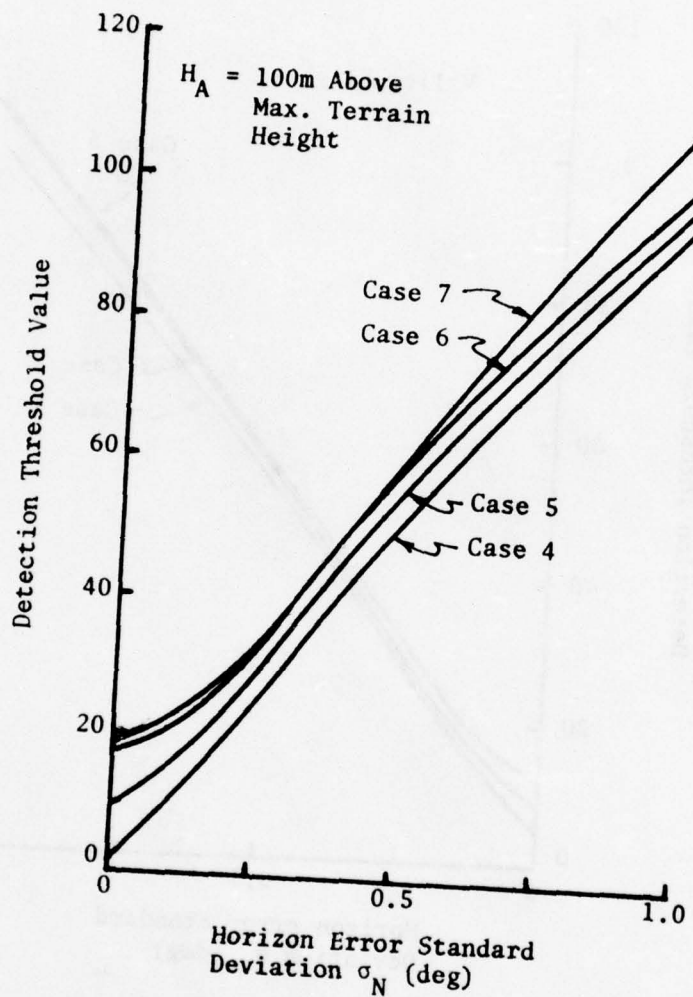


Fig. 31. Detection Threshold Needed to Give
 $P_D = 0.99$ (Flights at 100m Above
 Max. Terrain Height).

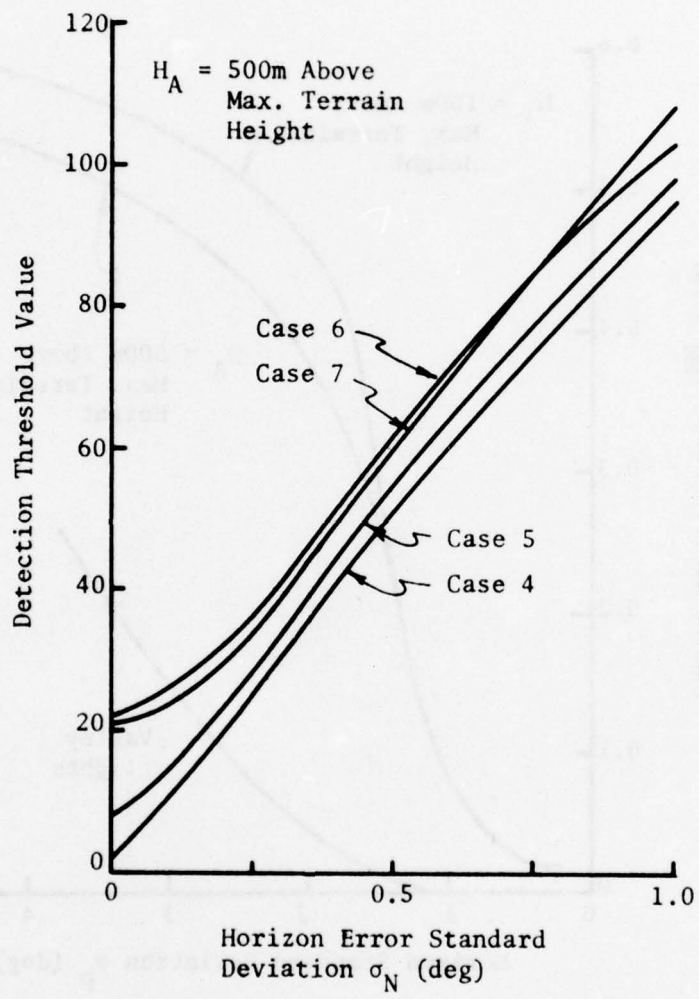


Fig. 32. Detection Threshold Needed to Give
 $P_D = 0.99$ (Flights at 500m Above
 Max. Terrain Height).

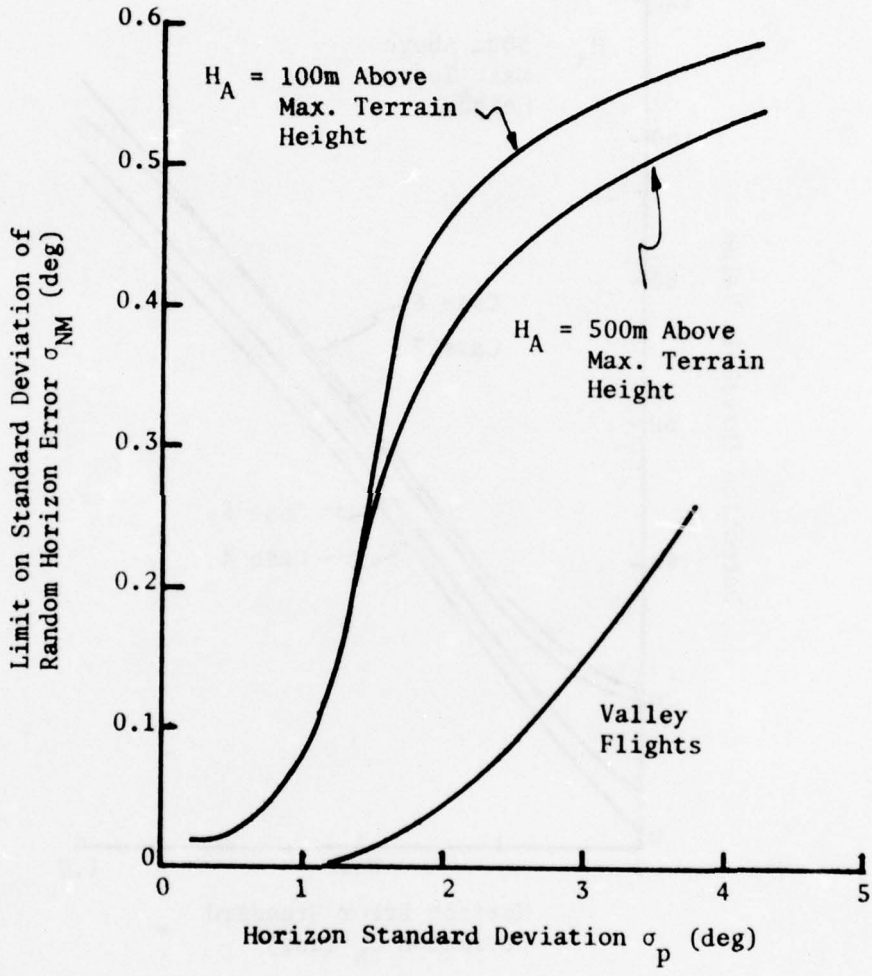


Fig. 33. Maximum Allowable Random Horizon Error with Threshold Set for $P_F < 0.001$ at Distances Greater than 1 Km from Line Array.

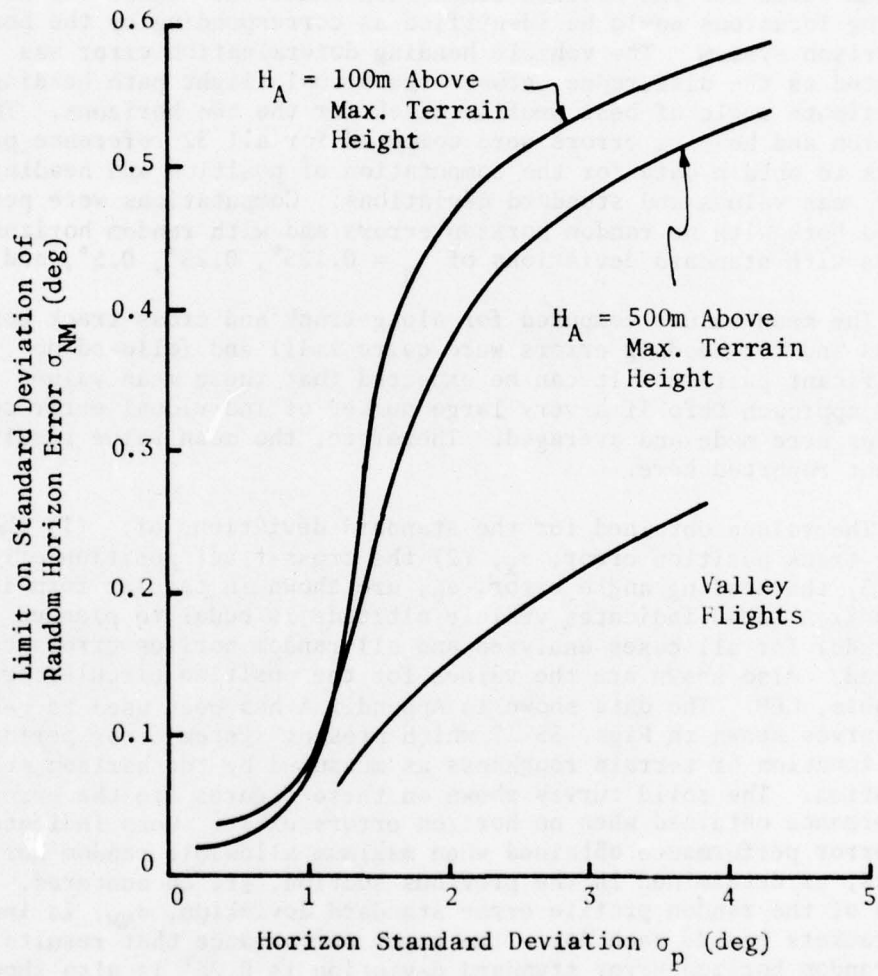


Fig. 34. Maximum Allowable Random Horizon Error with Threshold Set for $P_F < 0.001$ at Distances Greater than 2 Km from Line Array.

2. POSITION DETERMINATION ACCURACY

Vehicle position determination error at a line array crossing (checkpoint identification) was obtained by computing the along-track and cross-track distances between the viewing locations of the sensed horizon and the reference horizon which, when compared, gave the minimum value for the horizon comparison function. These two horizon viewing locations would be identified as corresponding by the horizon comparison system. The vehicle heading determination error was computed as the difference between the actual flight path heading and the azimuth angle of best profile match for the two horizons. The position and heading errors were computed for all 32 reference profile arrays to obtain data for the computation of position and heading error mean values and standard deviations. Computations were performed both with no random horizon errors and with random horizon errors with standard deviations of $N = 0.125^\circ, 0.25^\circ, 0.5^\circ$, and 1° .

The mean values computed for along-track and cross-track position errors and for heading errors were quite small and followed no significant pattern. It can be expected that these mean values would approach zero if a very large number of individual error computations were made and averaged. Therefore, the mean value results are not reported here.

The values obtained for the standard deviations of: (1) the along-track position error, σ_x , (2) the cross-track position error, σ_y , (3) the heading angle error, σ_θ , are shown in tabular form in Appendix A ($\Delta H=0$ indicates vehicle altitude is equal to planned flight altitude) for all cases analyzed and all random horizon errors considered. Also shown are the values for the position circular error probable, CEP. The data shown in Appendix A has been used to generate the curves shown in Figs. 35-37 which present system error performance as a function of terrain roughness as measured by the horizon standard deviation. The solid curves shown on these figures are the error performance obtained when no horizon errors exist. Dots indicate the error performance obtained when maximum allowable random horizon errors, as determined in the previous section, are encountered. The value of the random profile error standard deviation, σ_{NM} , is indicated in brackets beside each dot. The error performance that results when the random horizon error standard deviation is 0.25° is also shown by an x when this random horizon error standard deviation is less than the maximum allowable random horizon error. This has been included to indicate how the error performance varies when the random horizon error increases.

It should be noted than no interpolation is used between points of the horizon comparison function or between points of IAD curves obtained for individual reference horizons. Therefore, position and heading accuracy is limited because of the discrete spacing between viewing locations and heading angles which can be identified as vehicle positions and headings. The minimum position error standard

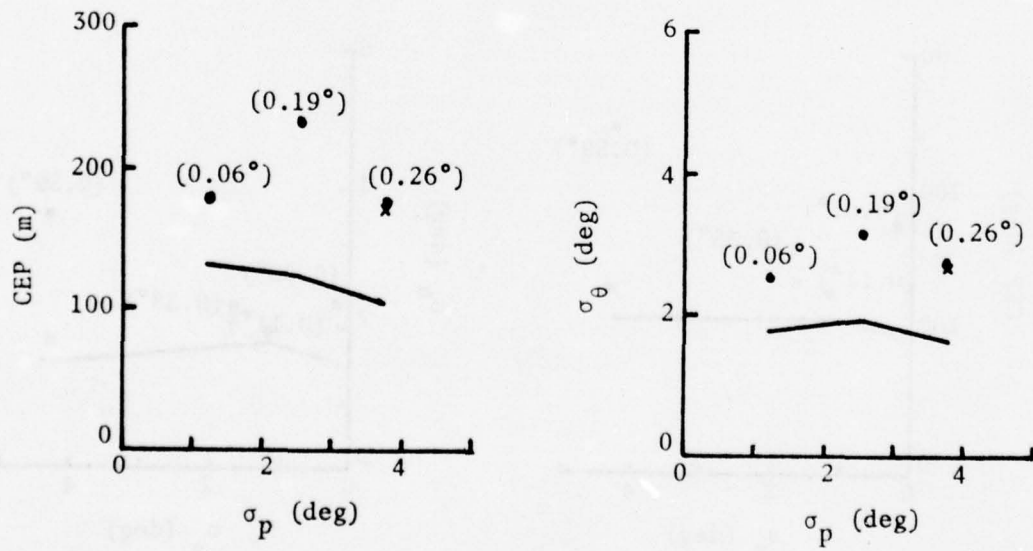
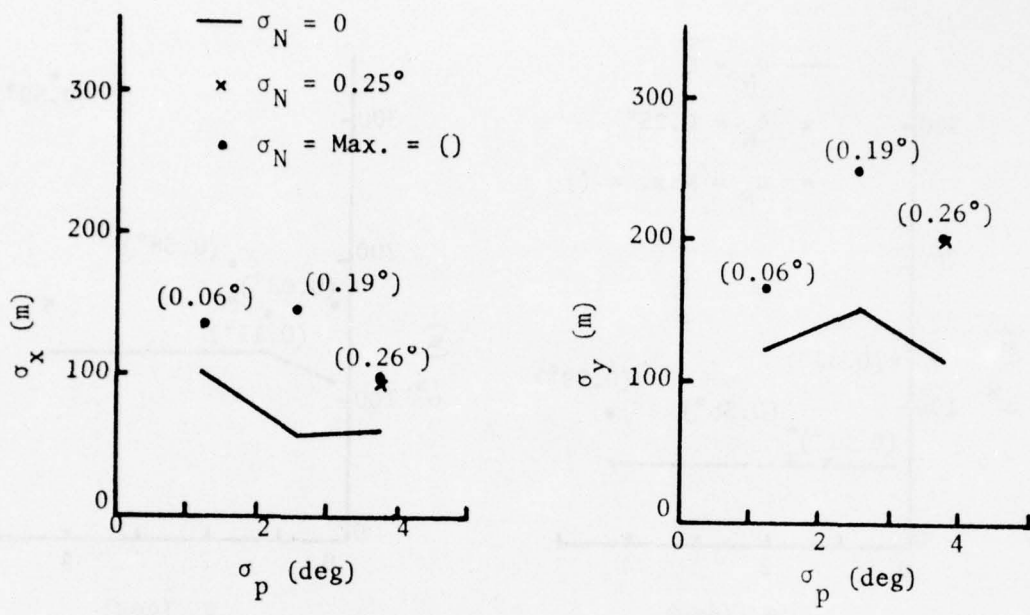


Fig. 35. Position and Heading Determination Accuracy (Valley Flights).

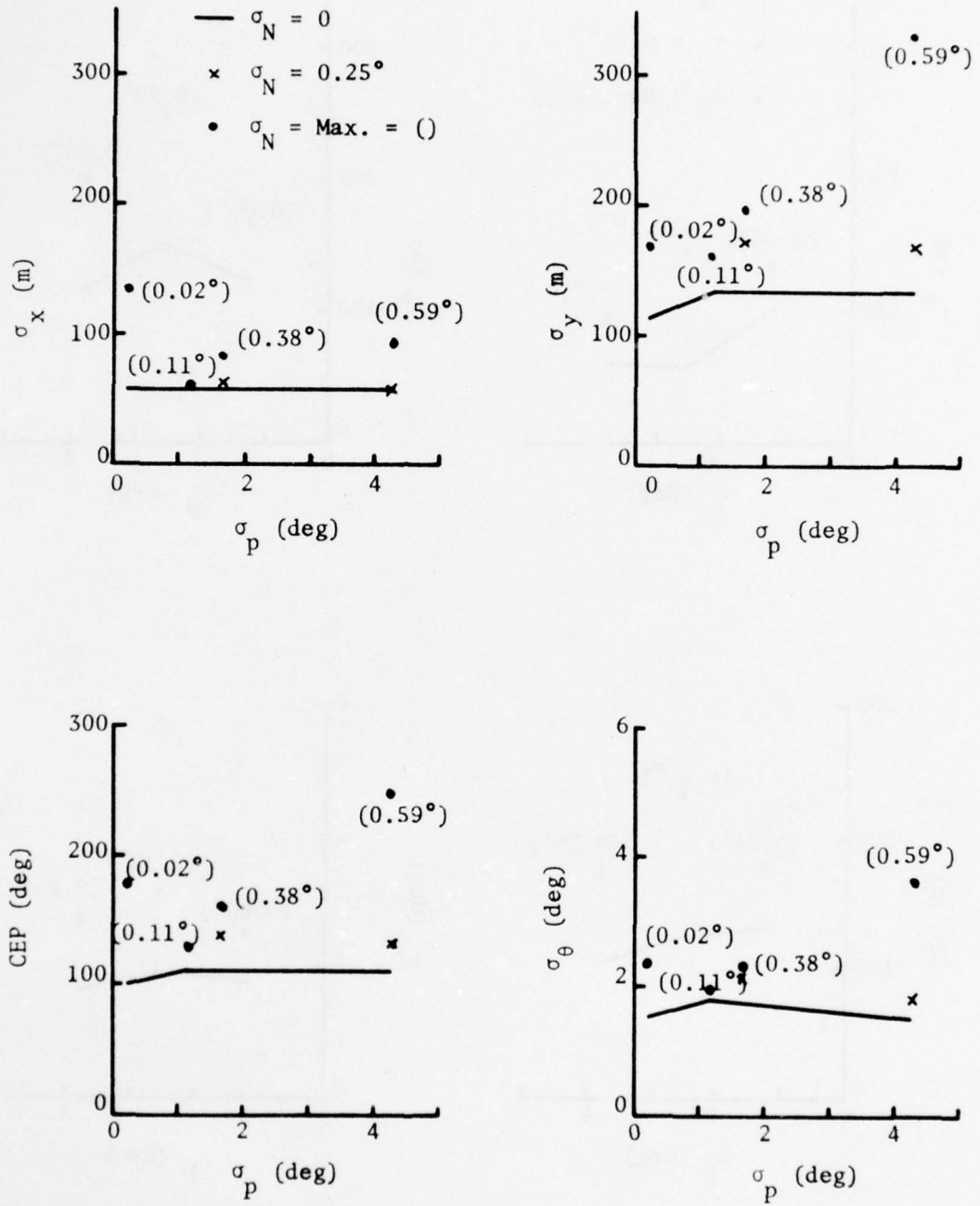


Fig. 36. Position and Heading Determination Accuracy (Flights at 100m Above Maximum Terrain Height).

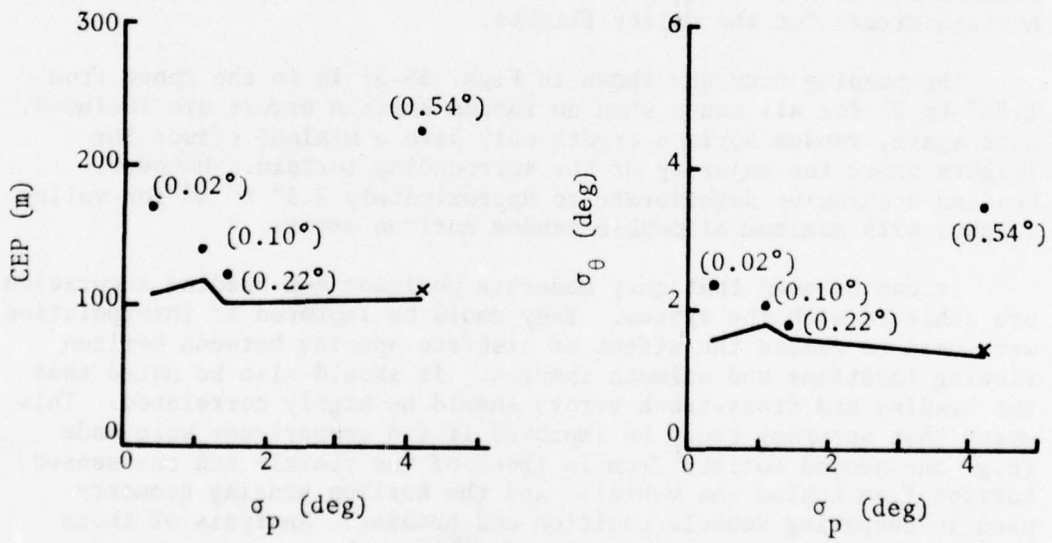
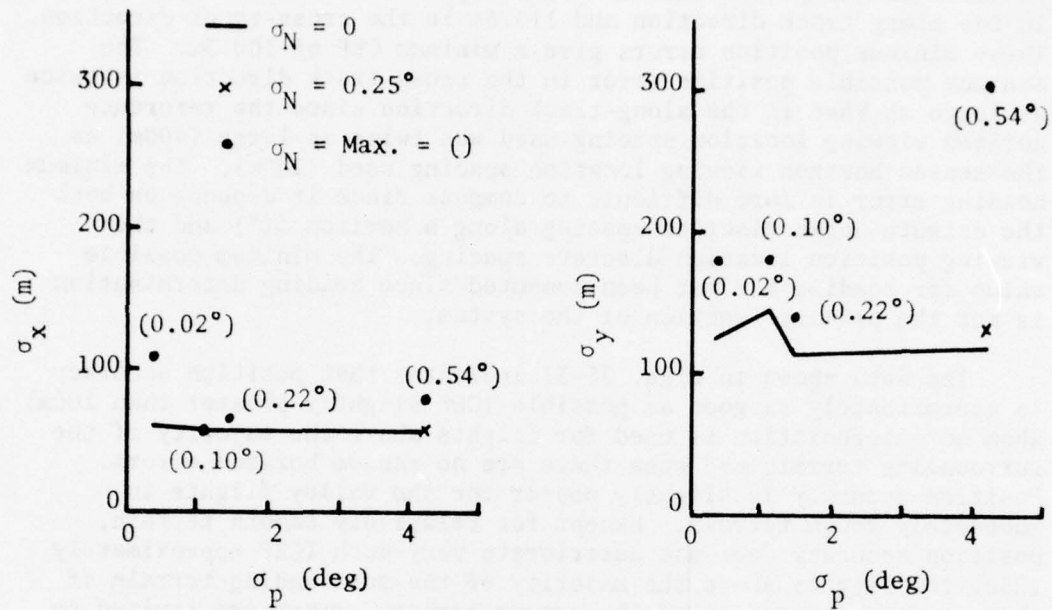


Fig. 37. Position and Heading Determination Accuracy (Flights at 500m Above Maximum Terrain Height).

deviations which can be obtained with a uniform distribution of possible flight path locations with respect to a line array are 56.8m in the along-track direction and 113.6m in the cross-track direction. These minimum position errors give a minimum CEP of 100.3m. The minimum possible position error in the cross-track direction is twice as large as that in the along-track direction since the reference horizon viewing location spacing used was twice as large (400m) as the sensed horizon viewing location spacing used (200m). The minimum heading error is more difficult to compute since it depends on both the azimuth angle discrete spacing along a horizon (1°) and the viewing position location discrete spacing. The minimum possible value for heading has not been computed since heading determination is not the primary function of the system.

The data shown in Figs. 35-37 indicates that position accuracy is approximately as good as possible (CEP slightly greater than 100m) when no interpolation is used for flights above the majority of the surrounding terrain and when there are no random horizon errors. Position accuracy is slightly poorer for the valley flights in moderately rough terrain. Except for relatively smooth terrain, position accuracy does not deteriorate very much (CEP approximately 125m) for flights above the majority of the surrounding terrain if the standard deviations of the random horizon errors are limited to the smaller of the maximum allowable error or 0.25° . The position errors for the valley flights are more sensitive to random profile errors giving a CEP of approximately 200m with the maximum allowable random horizon errors. This is expected since it was previously shown that the horizon comparison function is more sensitive to random horizon errors for the valley flights.

The heading accuracy shown in Figs. 35-37 is in the range from 1.75° to 2° for all cases when no random horizon errors are included. Once again, random horizon errors only have a minimal effect for flights above the majority of the surrounding terrain. However, heading accuracies deteriorate to approximately 2.5° to 3° for valley flights with maximum allowable random horizon errors.

It can be seen that only moderate position and heading accuracies are achieved with the system. They could be improved if interpolation were used to reduce the effect of discrete spacing between horizon viewing locations and azimuth samples. It should also be noted that the heading and cross-track errors should be highly correlated. This means that accuracy could be improved if two comparisons were made (e.g. one sensed horizon from in front of the vehicle and one sensed horizon from behind the vehicle) and the horizon sensing geometry used in computing vehicle position and heading. Analysis of these system refinements is desirable in further work.

3. PERFORMANCE COMPARISON OF RANGE-LIMITED HORIZON AND FIXED-RANGE PROFILE SYSTEMS.

It can be expected that the system utilizing range-limited horizons should have performance which is comparable with a system utilizing actual horizons for valley flights since the range-limited horizons and actual horizons should be nearly the same. Likewise, the system utilizing range-limited horizons should have performance which is comparable with a system using fixed-range profiles for flights which are at a sufficient altitude above the majority of the surrounding terrain since the range-limited horizons should be nearly the same as fixed-range profiles (i.e. few shadowed points on the fixed-range profiles).

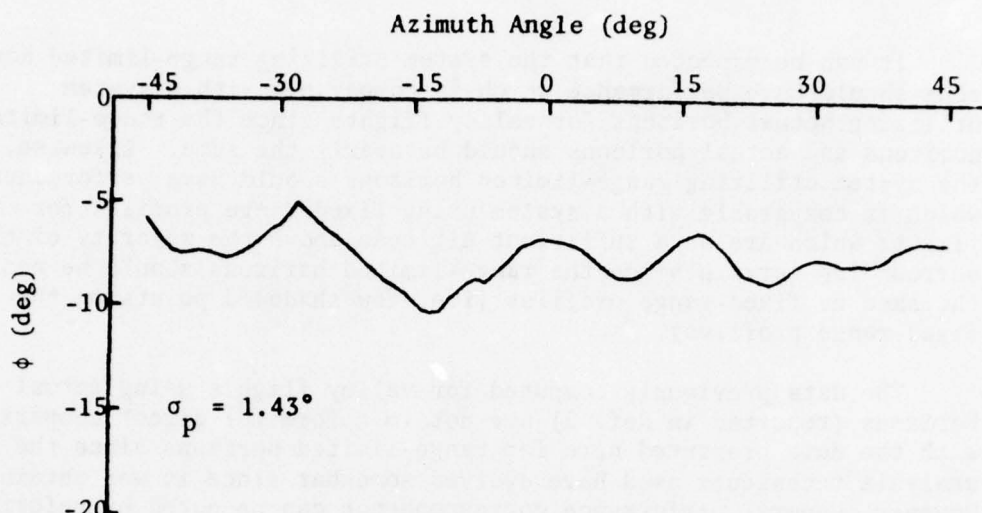
The data previously computed for valley flights using actual horizons (reported in Ref. 2) are not in a form for direct comparison with the data presented here for range-limited horizons since the analysis techniques used have evolved somewhat since it was obtained. However, general performance correspondence can be noted by referring to the summary of results in Ref. 2.

Direct comparison of performance results obtained for flights at an altitude of 500m above the maximum terrain height beneath the aircraft flight paths are possible for systems using range-limited horizons as reported here and systems using fixed-range profiles as reported in Ref. 1. Actually the performance data presented in Ref. 1 are for different fixed-ranges in some of the cases. However, they can be used for performance comparison since the comparisons presented here are presented as a function of profile standard deviation.

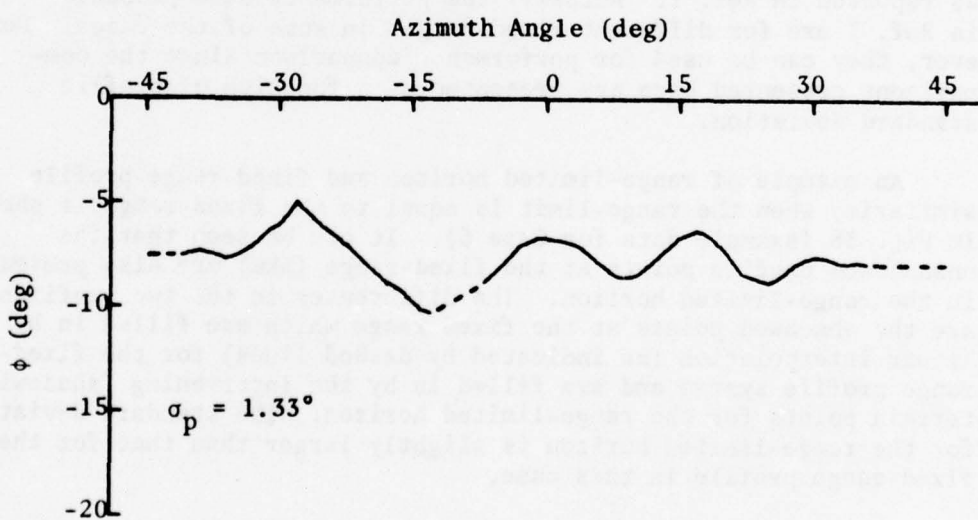
An example of range-limited horizon and fixed-range profile similarity when the range-limit is equal to the fixed-range is shown in Fig. 38 (example data for Case 6). It can be seen that the unshadowed profile points at the fixed-range (5Km) are also present in the range-limited horizon. The differences in the two profiles are the shadowed points at the fixed range which are filled in by linear interpolation (as indicated by dashed lines) for the fixed-range profile system and are filled in by the intervening (shadowing) terrain points for the range-limited horizon. The standard deviation for the range-limited horizon is slightly larger than that for the fixed-range profile in this case.

Fig. 39 shows the horizon comparison functions for Case 6 when range-limited horizons and fixed-range profiles are used. It can be seen that the horizon comparison functions are quite similar as expected.

The standard deviation of the maximum allowable random profile error, σ_{NM} , which gives $P_D \geq 0.99$ and $P_F \leq 0.001$ is shown in Fig. 40 as

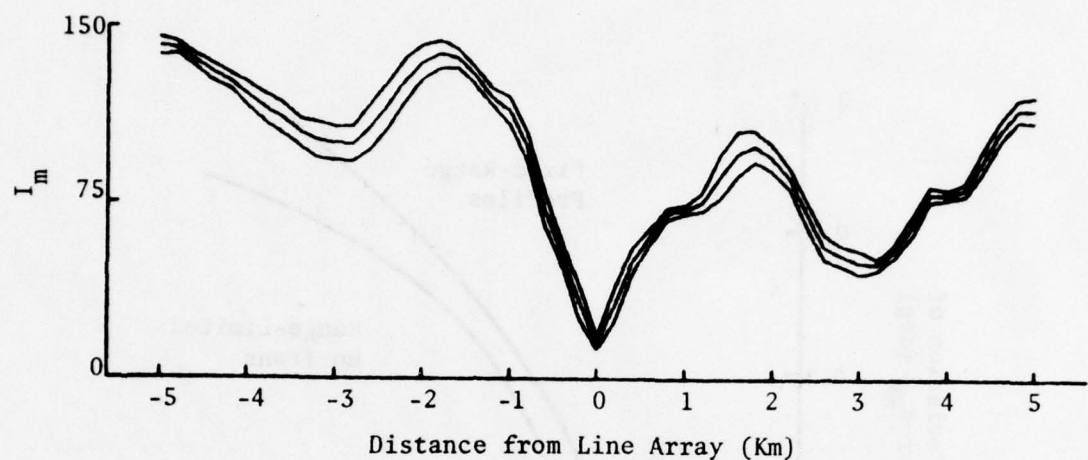


(a) Range-Limited Horizon

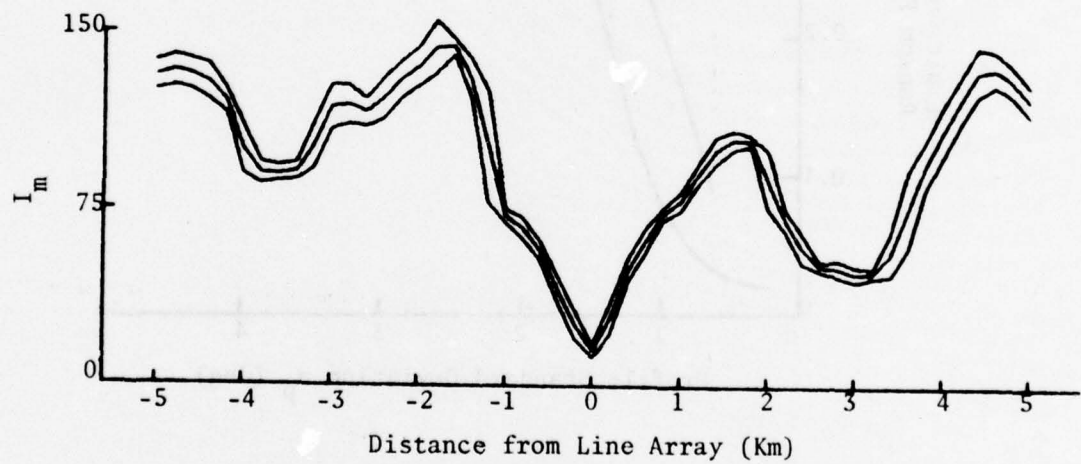


(b) Fixed-Range Profile

Fig. 38. Sensed Profiles for Case 6
 (Range-Limit = Fixed-Range = 5 Km,
 $H_A = 500\text{m}$ Above Max. Terrain Height).



(a) I_m for Range-Limited Horizon



(b) I_m for Fixed-Range Profile

Fig. 39. Horizon Comparison Functions for Case 6
 (Range-Limit = Fixed-Range = 5 Km,
 H_A = 500m Above Max. Terrain Height).

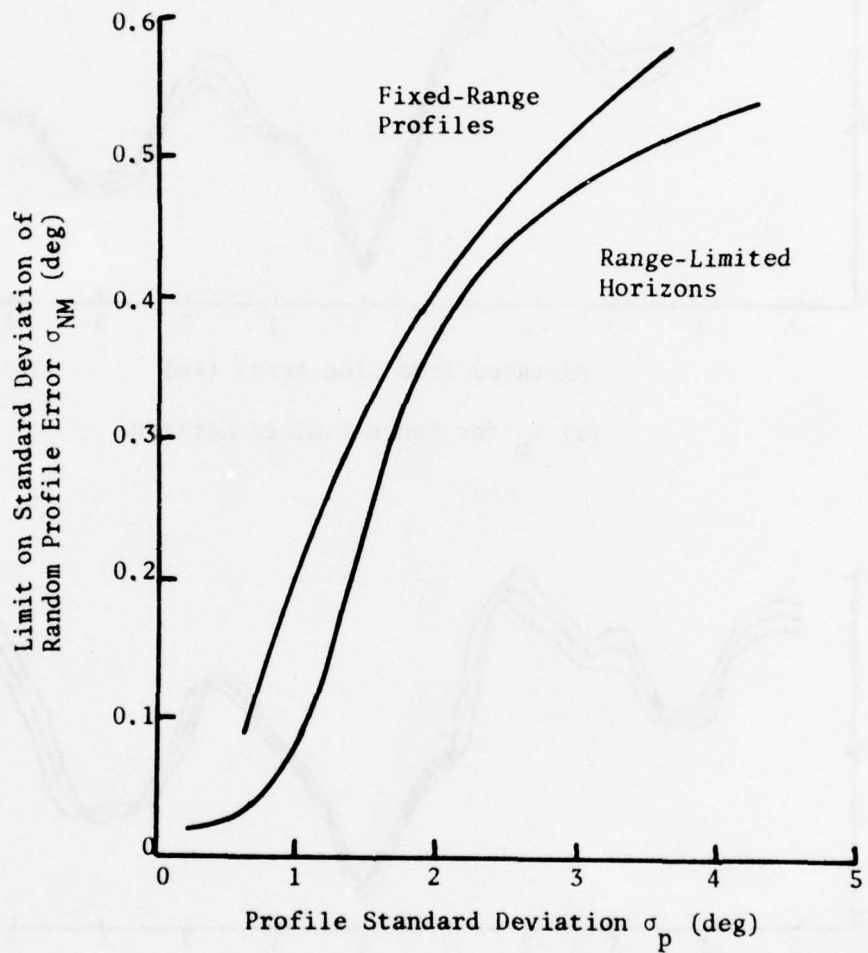


Fig. 40. Maximum Allowable Random Profile Error for Systems Using Range-Limited Horizons and Fixed-Range Profiles (Flights at 500m Above Max. Terrain Height).

a function of terrain roughness (as specified by profile standard deviation) for systems using range-limited horizons and fixed-range profiles. It can be seen that the limit on the allowable random profile error is similar for the two system concepts. The system which uses range-limited horizons appears to be somewhat more sensitive to random profile errors. This is particularly true for profiles with standard deviations less than 1.75° . The linear interpolation which is used to fill shadowed data point for the fixed-range profiles tends to smooth them somewhat which may contribute to the reduced random profile error sensitivity.

The position and heading accuracies obtained with a system using fixed-range profiles are shown in Fig. 41. This figure includes the data shown in Ref. 1 and additional data for $\sigma_N = 0^\circ$ and $\sigma_N = 0.25^\circ$ so the results are compatible with those previously presented (in Fig. 37) for a system using range-limited horizons. It can be seen that the position and heading accuracy is quite similar for systems using range-limited horizons and fixed-range profiles from this higher vehicle altitude. In fact, the data has not been plotted on a single set of curves for comparison since it would be difficult to distinguish the data for the two system concepts. The only points on the curves shown in Fig. 41 which are greatly different than those in Fig. 37 are those for the roughest terrain with the maximum allowable random profile error. These accuracies are poorer for the system using range-limited horizons. However, the performance is similar for random profile errors with a standard deviation of 0.25° and profiles of this accuracy are desirable anyway if the system is to be useful over a range of terrain roughness. Therefore, the position and heading accuracy achievable with the system which uses range-limited horizons can be considered to be comparable to that achievable with the system using fixed-range profiles.

In general it can be concluded, as expected, that range-limited horizons are as satisfactory as fixed-range profiles for comparison to determine vehicle position on flights at sufficient altitude above the majority of the surrounding terrain. In addition, as was mentioned earlier, a system which uses range-limited horizons can be used at all altitudes whereas a system which uses fixed-range profiles is limited to higher altitudes by the profile shadow constraint.

F. EFFECT OF ERRONEOUS VEHICLE ALTITUDE

On an actual flight, the vehicle altitude will differ somewhat from the planned flight path altitude. Therefore, the sensed horizon viewing locations will be at a different altitude than the viewing locations used to generate the reference horizons. This means that sensed and reference horizons will be slightly different even if they are taken from exactly the same horizontal position.

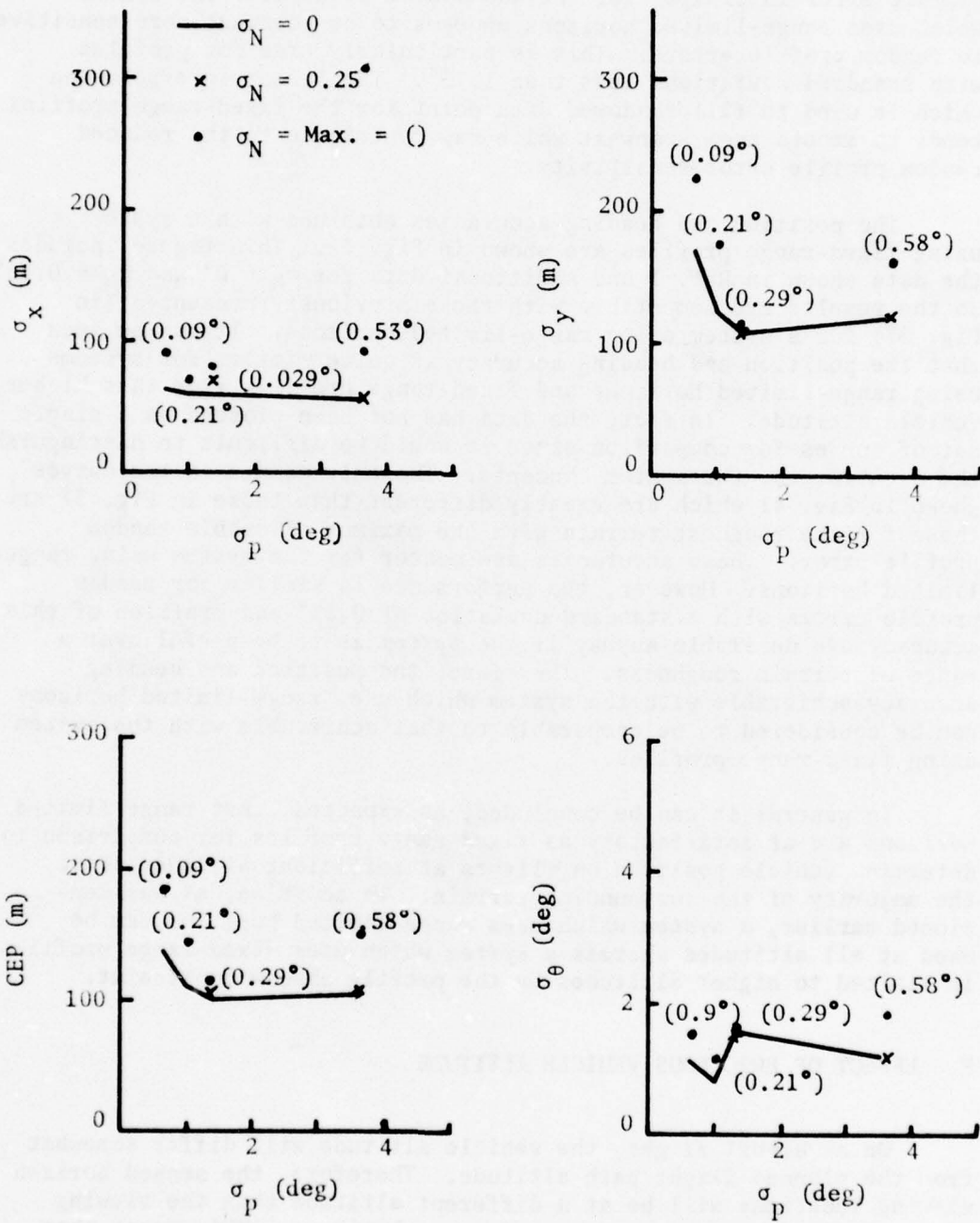


Fig. 41. Position and Heading Determination Accuracy for System Using Fixed-Range Profiles (Flights at 500m Above Max. Terrain Height).

The horizon comparison system has been analyzed with sensed horizons generated from a different altitude than the reference horizons to assess the effect of a difference (called altitude error) between the vehicle altitude and the planned flight path altitude. Case 4 (relatively smooth terrain) was not considered in this analysis since the analysis results presented in the previous section indicated that the maximum allowable random horizon error is too small to be practical in this case even if no altitude error is considered.

The analysis of the altitude error effect was performed by generating sensed horizons for flight paths at different altitudes than the altitude used to generate reference horizons. The analysis techniques previously outlined were used to obtain performance results like those shown in the previous section. The results are shown below plotted as a function of altitude error, ΔH . The range of altitude errors considered were: (1) +200m to -90m for Case 1 which is a valley flight at 100m above the valley floor, (2) $\pm 75m$ for Case 2 which is a valley flight at 200m above the valley floor, (3) $\pm 200m$ for Case 3 which is a valley flight at 300m above the valley floor, (4) +200m to -90m for flights at 100m above the maximum terrain height beneath the flight path, and (5) $\pm 200m$ for flights at 500m above the maximum terrain height. The performance results obtained were used to indicate maximum allowable vehicle altitude error, H_M , which does not severely affect system performance.

The first performance parameter determined as a function of altitude error was the maximum allowable random horizon error. The required detection thresholds for the various analysis cases were defined to be those which were established for vehicle flight at the planned altitude to give a false alarm probability which is less than 0.001 as shown in Table II. These values of required detection threshold are the proper ones to use since threshold values would be determined prior to a flight based on the planned vehicle flight path and the reference horizons used. As indicated earlier, it is desirable to use the threshold value T_1 for flights above the majority of the surrounding terrain and the threshold value T_2 for valley flights. Therefore, these are the detection threshold values which were used in the analysis of the effect of altitude error.

The next step in obtaining the maximum allowable random profile error is the determination of the detection threshold needed, as a function of random horizon error, to obtain a probability of detection of 0.99. An example of a plot of these needed thresholds is shown in Fig. 42 for Case 6 with a planned flight path altitude of 100m above the maximum terrain height beneath the flight path. Similar plots for the remainder of the analysis cases are shown in Appendix B.

The maximum allowable random horizon error which permits a maximum probability of false alarm of 0.001 and a minimum probability of detection of 0.99 was established as a function of altitude error by using the data in Table II and the curves in Appendix B. The results

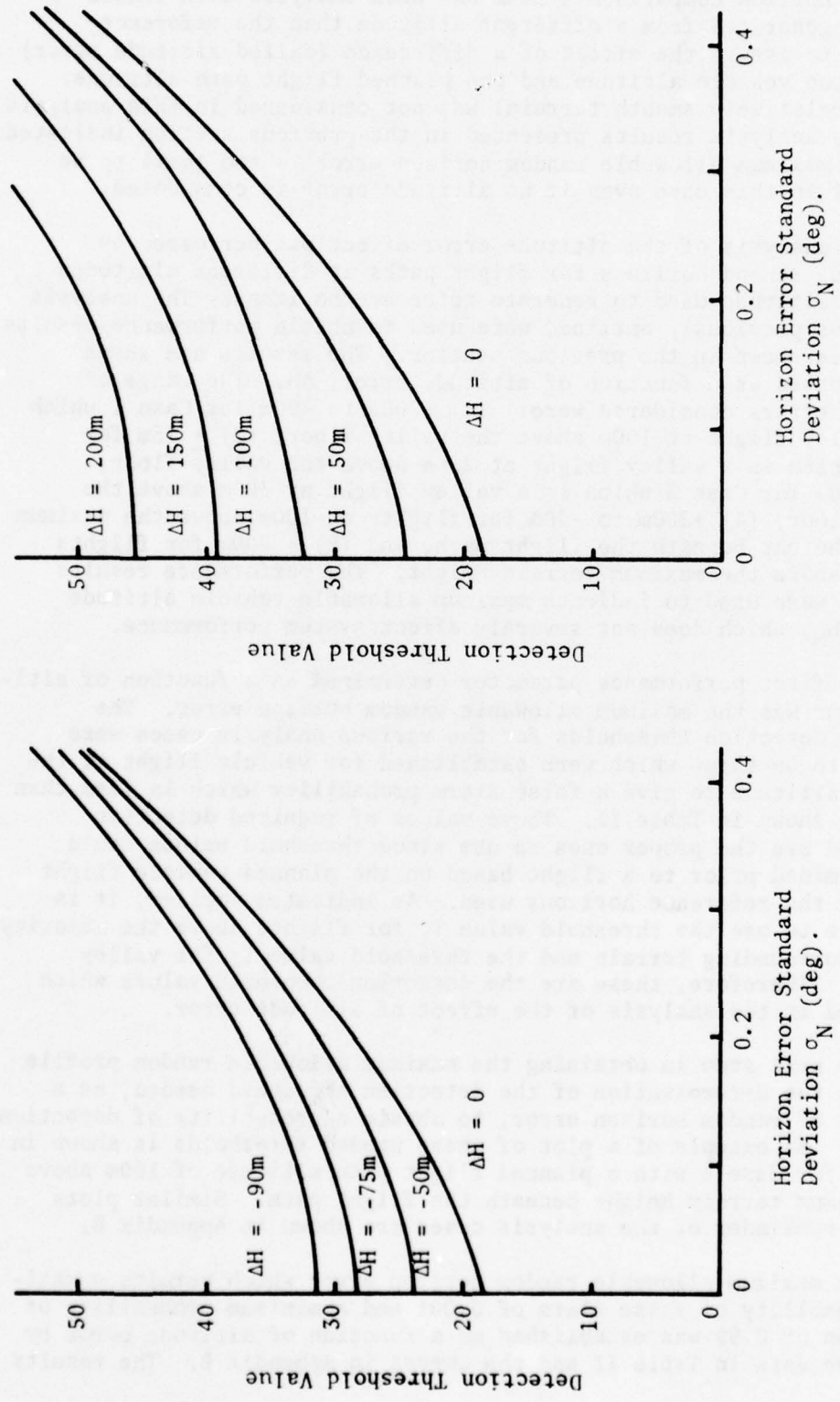


Fig. 42. Detection Threshold Needed to Give $P_D = 0.99$ (Case 6 Flight at 100m Above Max. Terrain Height).

are shown in Fig. 43 for the valley flight cases, in Fig. 44 for flights at 100m above the maximum terrain height beneath the flight path and in Fig. 45 for flights at 500m above the maximum terrain height beneath the flight path. It can be seen that, in general, the maximum allowable random horizon error decreases more rapidly with increasing altitude error for lower vehicle altitudes. Case 1 is an exception. For this case, the valley is very broad and flat (see horizon profile shown in Fig. 18) so the horizon profile is basically a fixed-range profile with little variation. Thus, it does not change much with changing viewing altitude.

It is apparent from Figs. 43-45 that the maximum allowable random horizon error must be decreased from the value determined in the last section (value at $\Delta H=0$ in Figs. 43-45) if the vehicle altitude is to be permitted to vary from the planned altitude. Reasonable selections of maximum allowable random horizon error standard deviations, σ_{NM} , with their approximate associated maximum allowable altitude errors, ΔH_M , have been obtained from Figs. 43-45 and are shown in Table III.

TABLE III. Maximum Allowable Random Horizon Error Standard Deviation and Associated Maximum Allowable Altitude Error.

Case	Valley Flight		100m Above Max. Terrain Height		500m Above Max. Terrain Height	
	σ_{NM} (deg)	ΔH_M (m)	σ_{NM} (deg)	ΔH_M (m)	σ_{NM} (deg)	ΔH_M (m)
1	0.065	+100 - 50	-	-	-	-
2	0.1	+ 55 - 40	-	-	-	-
3	0.2	+160 -135	-	-	-	-
5	-	-	0.075	+ 35 - 40	0.1	>+200 <-200
6	-	-	0.3	+115 -100	0.2	+100 -140
7	-	-	0.6	>+200 -100	0.5	>+200 <-200

Several of the maximum allowable altitude errors are shown as >+200m or <-200m. These were the largest altitude errors considered so true maximum allowable altitude errors were not determined in these cases. It was felt that altitude errors of more than 200m were not really of interest for a practical system.

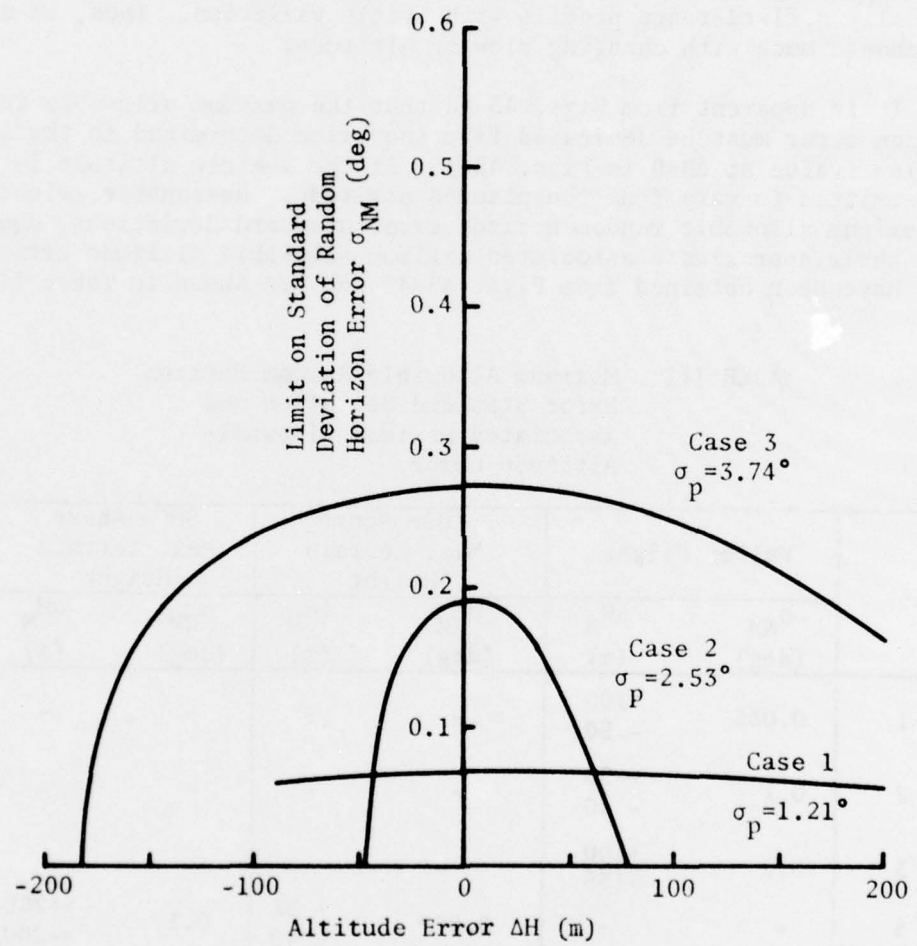


Fig. 43. Maximum Allowable Random Horizon Error as a Function of Altitude Error for Valley Flights.

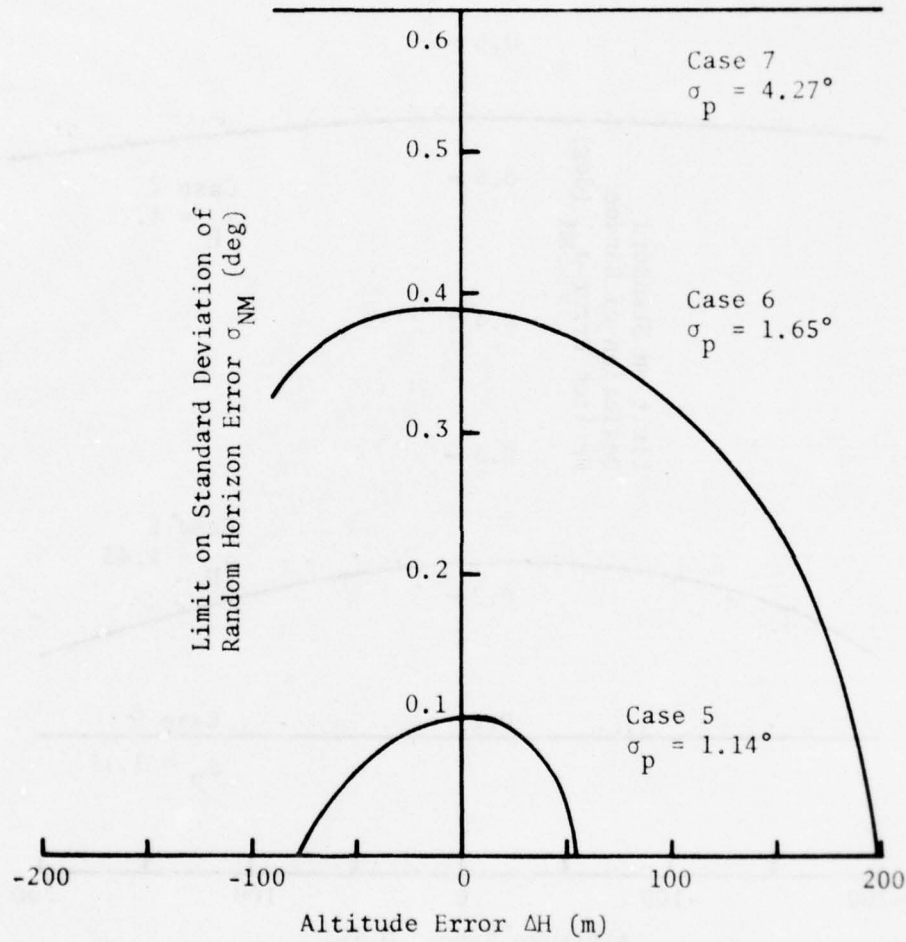


Fig. 44. Maximum Allowable Random Horizon Error as a Function of Altitude Error for Flights at 100m Above Max. Terrain Height.

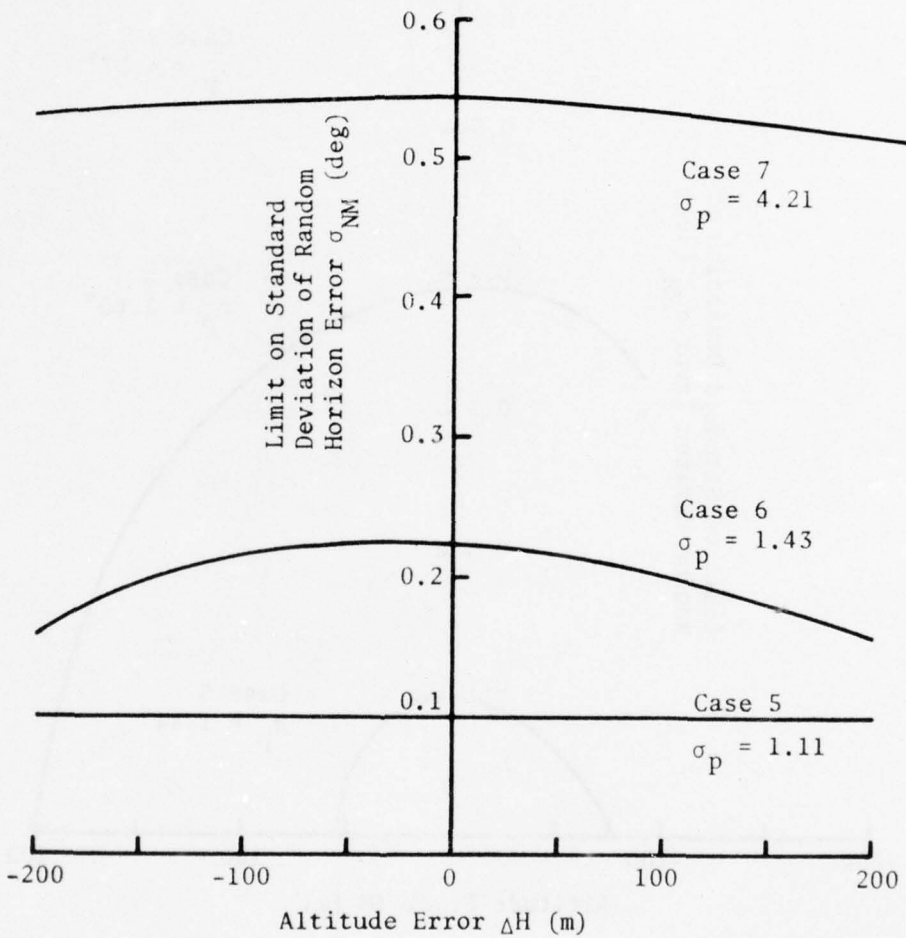


Fig. 45. Maximum Allowable Random Horizon Error as a Function of Altitude Error for Flights at 500m Above Max. Terrain Height.

Table III shows that, in general, considerable vehicle altitude variation is permissible with a moderate decrease in the maximum allowable random horizon error. Most cases analyzed permit more than ± 100 m variation in vehicle altitudes. One exception to this is the case which evaluates a flight through a narrow valley in moderately rough terrain (Case 2). In this case, the narrowness of the valley implies considerable change in the sensed horizon shape as vehicle altitude changes. Case 3 also is for a narrow valley. However, in this case, the valley structure is so dominant (as shown by the horizon profile in Fig. 18) that vehicle altitude changes are not as troublesome. A second exception is noted for the case which analyzes a flight over moderately rough terrain (Case 5) at an altitude of 100m above the maximum terrain height beneath the flight path. In this case, a significant position of the horizon is obtained from terrain contributors at a range which is significantly less than 5Km. The result is that the profile shape changes more rapidly with vehicle altitude changes.

The effect of altitude error on the other performance parameters (i.e. position and heading determination errors) was also computed. The computations were performed in the same manner used for the system when no altitude error was included as discussed in the previous section. Thus, values for along-track position determination error standard deviation, σ_x , cross-track position determination error standard deviation, σ_y , position circular error probable, CEP, and heading determination error standard deviation, σ_θ , were computed for system operation with random horizon errors of various standard deviations and altitude errors spanning a range of values.

The performance data obtained is shown in tabular form in Appendix C. The data shown in Appendix C and Appendix A (data for $H=0$) have been used to generate the smoothed curves shown in Figs. 46-49. These curves present system performance degradation (in terms of CEP and σ_θ) as a function of altitude error for each of the analysis cases and planned vehicle altitudes. Similar plots for σ_x and σ_y are shown in Appendix D. Each plot consists of two curves. The first curve shows the performance of a system operating with no random horizon errors (i.e. $\sigma_N=0$). The second curve shows the performance of a system operating with the maximum allowable random profile errors as previously defined in Table III. Also shown are dashed lines at the maximum allowable altitude error values, ΔH_M , which correspond to the maximum allowable random profile errors as also previously defined in Table III. It can be seen from the figures that little position or heading determination performance degradation is experienced over the maximum allowable altitude errors previously defined for flights above the majority of the surrounding terrain. More performance degradation is apparent for the valley flights. This is particularly true for the flight through a narrow valley in moderately rough terrain (Case 2) and, when maximum allowable random horizon errors are considered, for the flight through a wide valley in moderately rough terrain (Case 1).

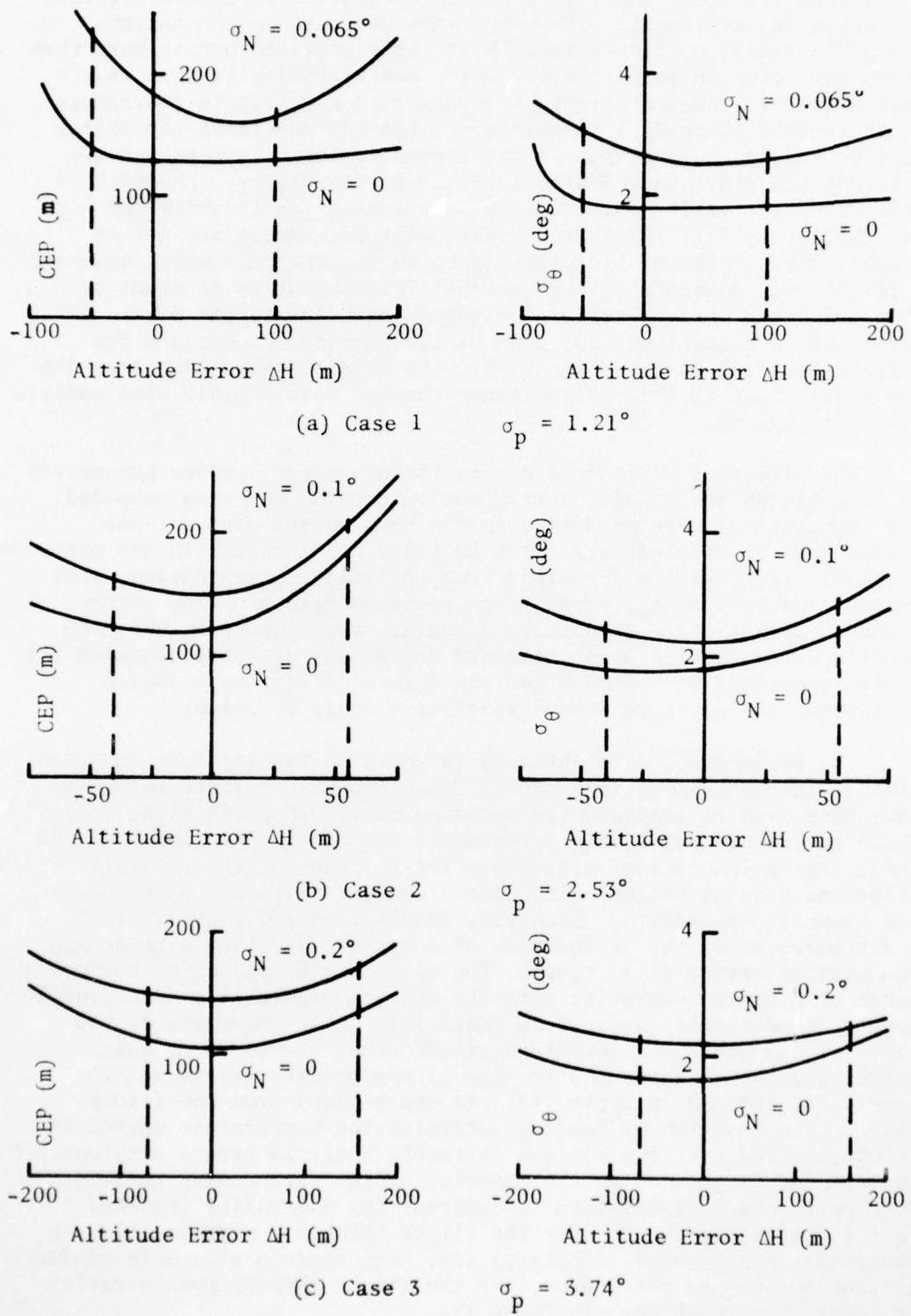
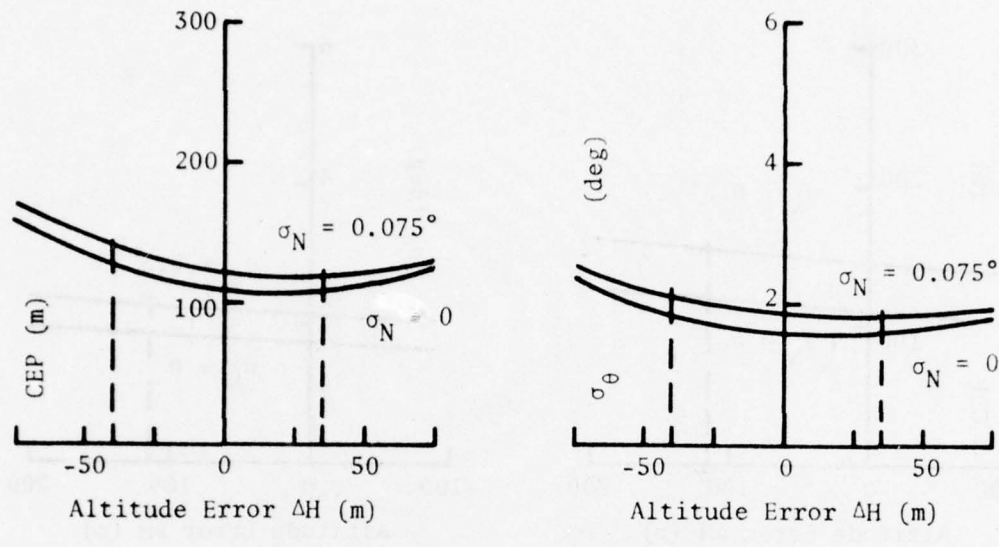
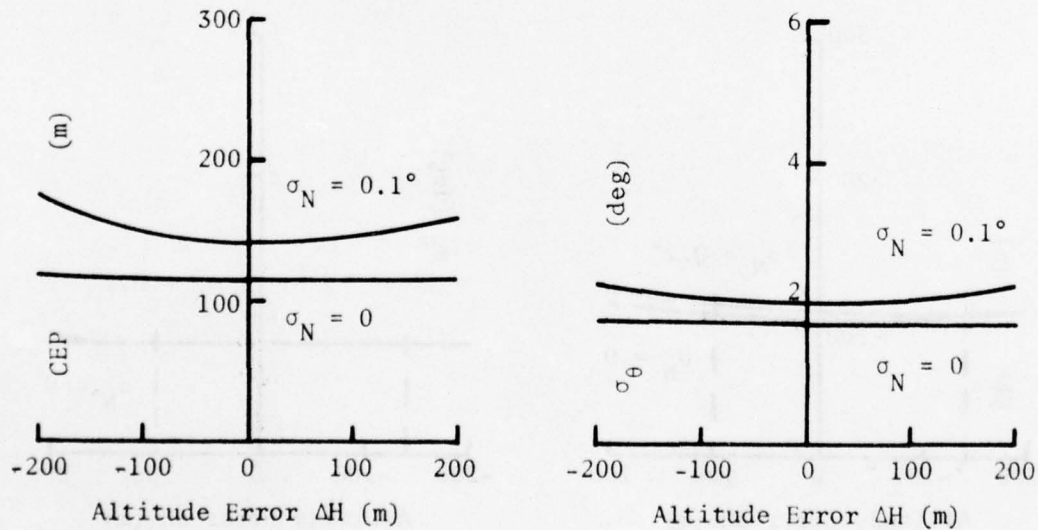


Fig. 46. Position and Heading Determination Accuracy as a Function of Altitude Error for Valley Flights.

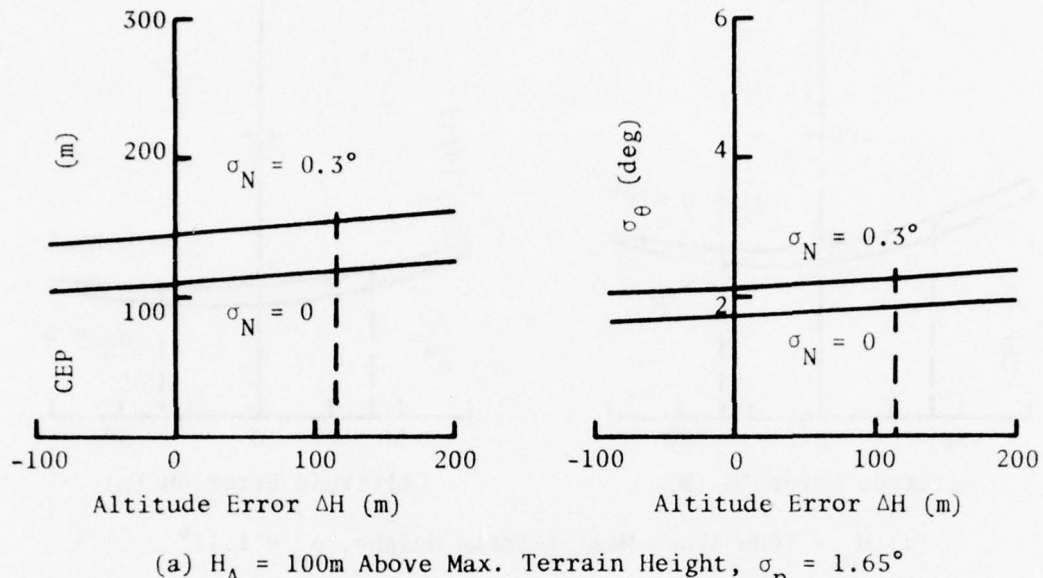


(a) $H_A = 100\text{m}$ Above Max. Terrain Height, $\sigma_p = 1.14^\circ$

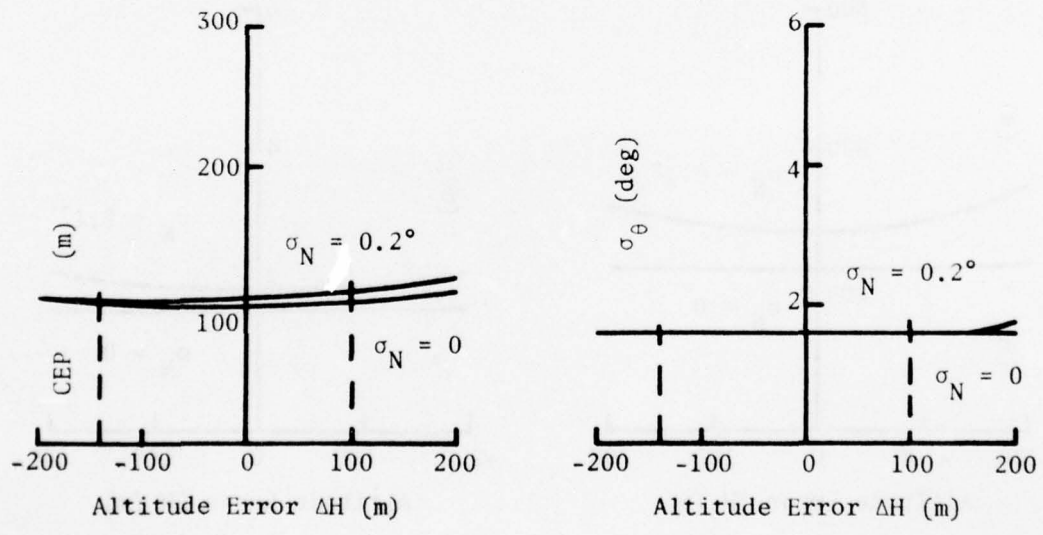


(b) $H_A = 500\text{m}$ Above Max. Terrain Height, $\sigma_p = 1.11^\circ$

Fig. 47. Position and Heading Determination Accuracy as a Function of Altitude Error for Case 5.



(a) $H_A = 100\text{m}$ Above Max. Terrain Height, $\sigma_p = 1.65^\circ$



(b) $H_A = 500\text{m}$ Above Max. Terrain Height, $\sigma_p = 1.43^\circ$

Fig. 48. Position and Heading Determination Accuracy as a Function of Altitude Error for Case 6.

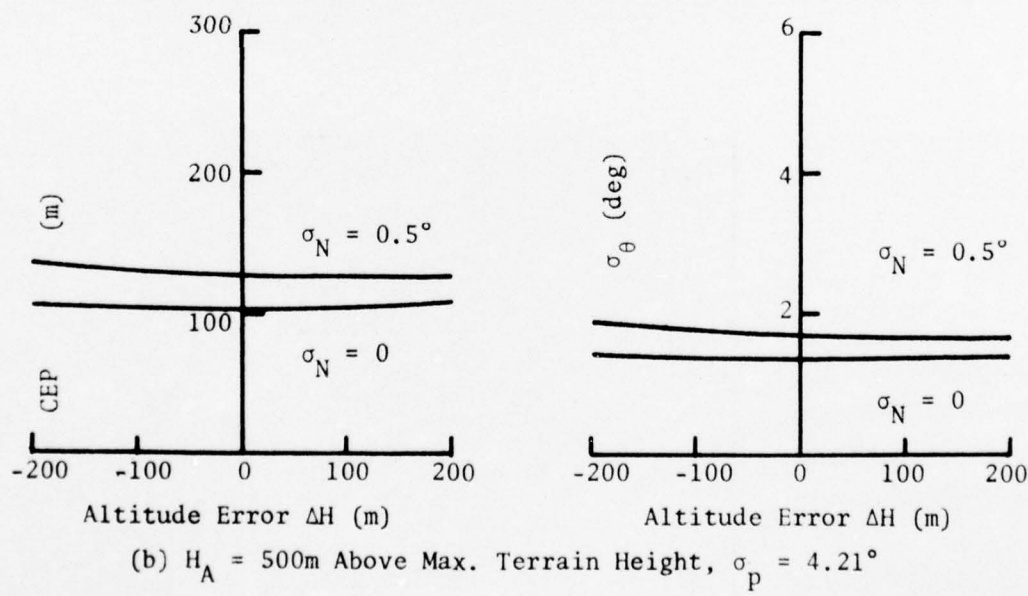
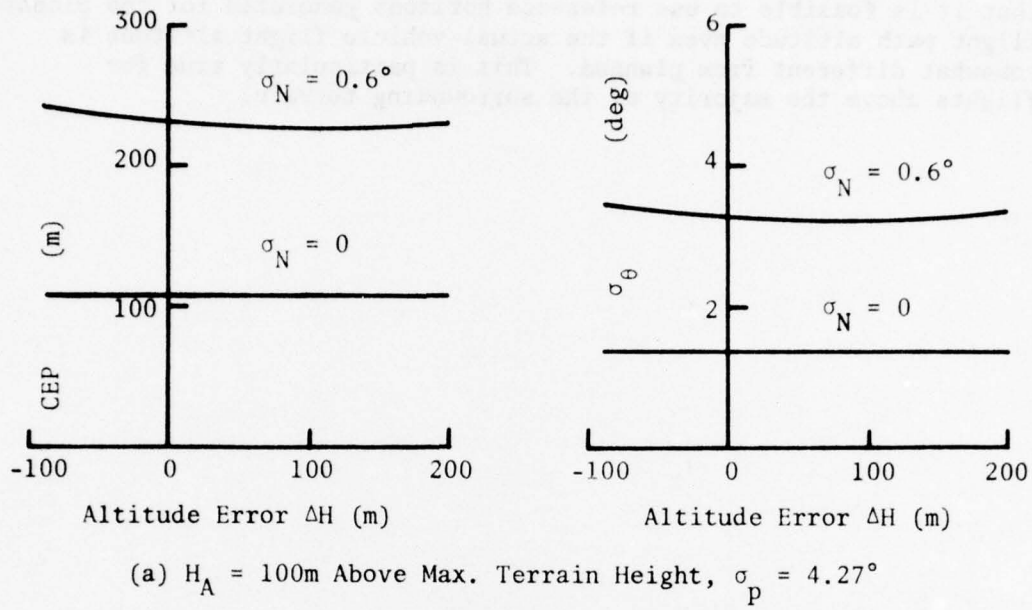


Fig. 49. Position and Heading Determination Accuracy as a Function of Altitude Error for Case 7.

In general, the analysis of altitude error effects has indicated that it is feasible to use reference horizons generated for the planned flight path altitude even if the actual vehicle flight altitude is somewhat different from planned. This is particularly true for flights above the majority of the surrounding terrain.

IV. EFFECT OF PRACTICAL SENSOR CHARACTERISTICS

Two radar sensor idealizations have been used to simplify and reduce the cost of the simulations used for system analysis. It was felt that these idealizations would not greatly affect the determination of system feasibility and basic performance.

The first idealization used was that each sensed horizon was obtained from a single vehicle position. On an actual flight, the vehicle moves an increment along the flight path during the period of time required for the sensor to scan the horizon. Thus, all sensed horizon points are not generated from the same viewing location.

The second idealization used was that the radar azimuth beamwidth was infinitesimal so individual terrain points could be sensed and the elevation angle to them measured. An actual radar has a finite beamwidth determined by its frequency and antenna aperture. Thus, the elevation angle data processed by the radar is actually a weighted average of the return from all terrain points in the azimuth beamwidth which are illuminated by a radar pulse at the same time (i.e. are at the same range). This section considers the effect of these idealizations by showing performance results obtained with simulations which model the practical radar characteristics.

A. VEHICLE MOTION DURING SENSOR SCAN

The first practical sensor characteristic considered was the vehicle motion during a sensor scan. The model required to analyze the effect of this characteristic, the analysis cases considered, and the analysis results obtained are discussed in this section.

1. SYSTEM MODEL AND ANALYSIS METHOD

Vehicle motion during the radar sensor scan period causes a change in the sensed horizon viewing location while the horizon is being obtained. This change and the resulting change in the location of the range limit are shown in exaggerated form in Fig. 50 (actual distance of vehicle motion is typically much less than the range limit). Points of the sensed horizon which are obtained at the range limit will come from slightly different terrain positions as shown in Fig. 50 and points of the sensed horizon which come from other than the range limit will be at slightly different azimuth angles and ranges. All of these effects cause the sensed horizon to change slightly.

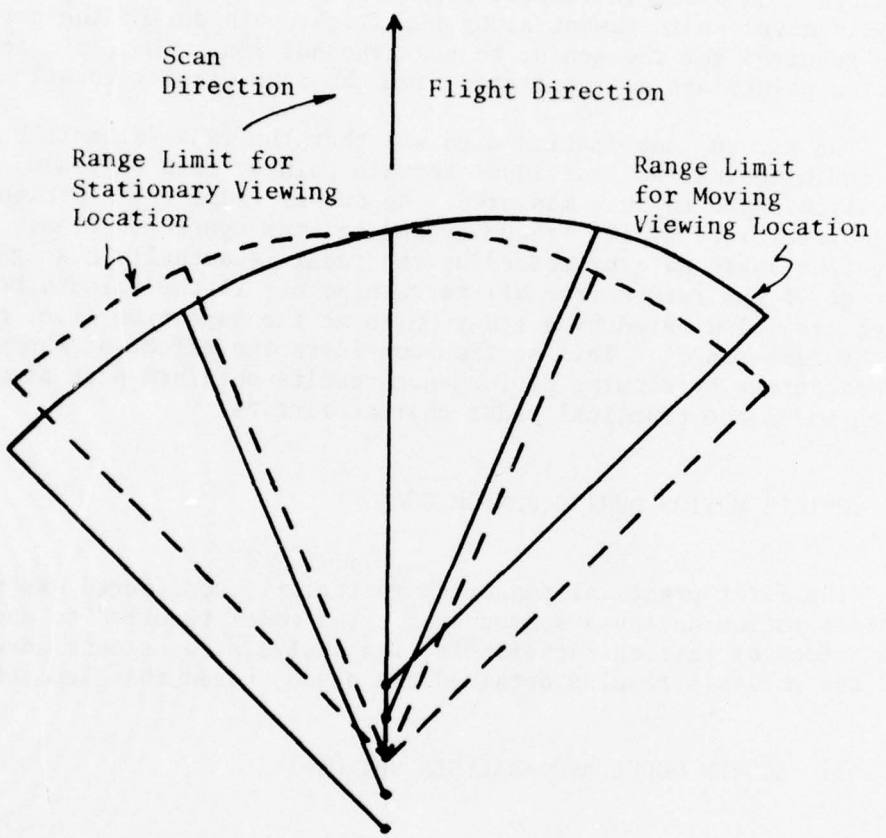


Fig. 50. Geometry for Stationary
and Moving Horizon
Viewing Locations.

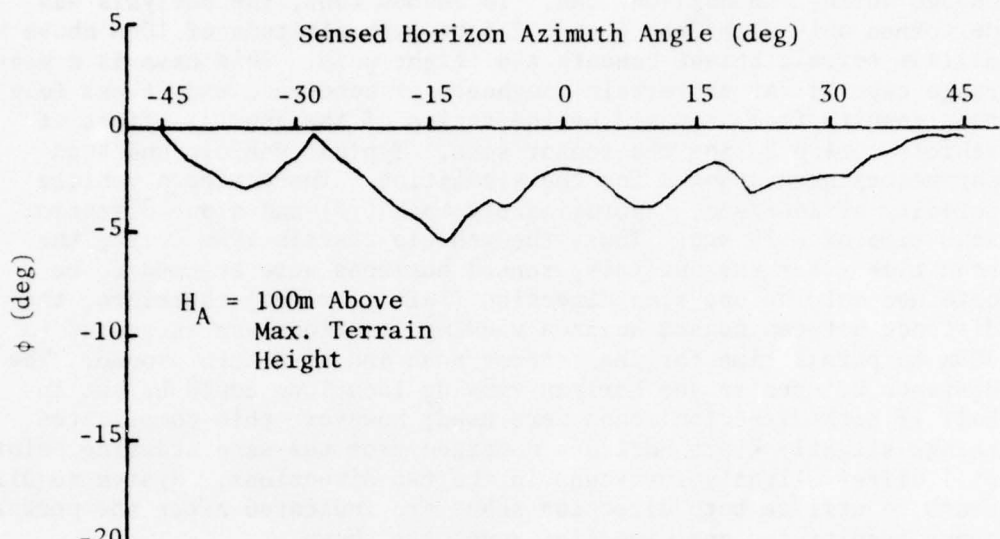
The effect of vehicle motion was analyzed by changing the simulation so horizons could be generated from viewing locations which change during the horizon scan. To reduce cost, the analysis was performed only with Case 6 at a flight path altitude of 100m above the maximum terrain height beneath the flight path. This case is a mid-range case as far as terrain roughness is concerned and it was felt that results from it would be indicative of the general effect of vehicle motion during the sensor scan. Typical vehicle and scan parameters were assumed for the simulation. These were a vehicle velocity of 260m/sec. (approximately Mach 0.8) and a one direction scan time of 0.75 sec. Thus, the vehicle travels 195m during the scan time. For the analysis, sensed horizons were assumed to be obtained only on one scan direction (left to right) therefore, the distance between sensed horizon viewing locations was increased to 400m to permit time for the reverse scan and scan turn around. The distance between sensed horizon viewing locations could be cut in half if both direction scans were used; however, this complicates things slightly since horizons obtained from the same starting point will differ slightly for scans in the two directions. System requirements to utilize both direction scans are indicated after the performance results for one direction scans are shown.

Since a larger sensed horizon spacing is used here, performance results will be different than those previously indicated for Case 6. This is primarily due to the increased discrete separation of sensed horizon viewing locations which: (1) increases the needed detection threshold for a detection probability of 0.99, and (2) increases the along-track position determination error since sensed horizons which should correspond to the reference horizon line array come from a larger distance increment in the along-track direction. Thus, Case 6 was simulated for stationary horizon viewing locations with a sensed horizon viewing location spacing of $\Delta S = 400m$ to obtain baseline data for comparison purposes.

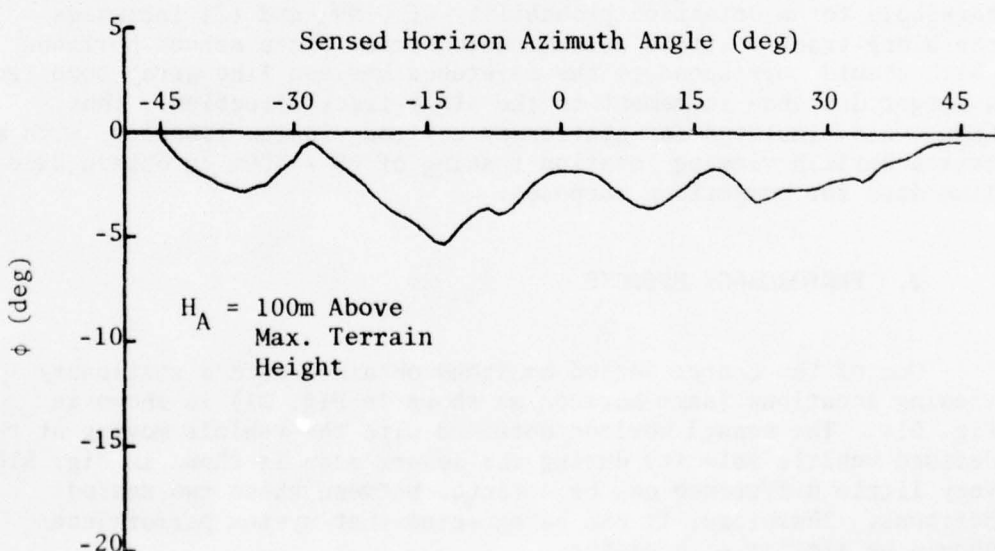
2. PERFORMANCE EFFECTS

One of the center sensed horizons obtained with a stationary viewing locations (same horizon as shown in Fig. 21) is shown in Fig. 51a. The sensed horizon obtained with the vehicle moving at the defined vehicle velocity during the sensor scan is shown in Fig. 51b. Very little difference can be detected between these two sensed horizons. Therefore, it can be expected that system performance should be similar with either.

Three different horizon comparison function plots (each consisting of the curves of the mean, μ_I , and the \pm one standard deviations from the mean, $\mu_I + \sigma_I$, $\mu_I - \sigma_I$) are shown in Fig. 52. The first plot is the baseline case for comparison which uses sensed and reference horizons generated from stationary viewing locations



(a) Stationary Viewing Location



(b) Moving Viewing Location

Fig. 51. Sensed Horizons for Case 6
with Stationary and Moving
Viewing Locations.

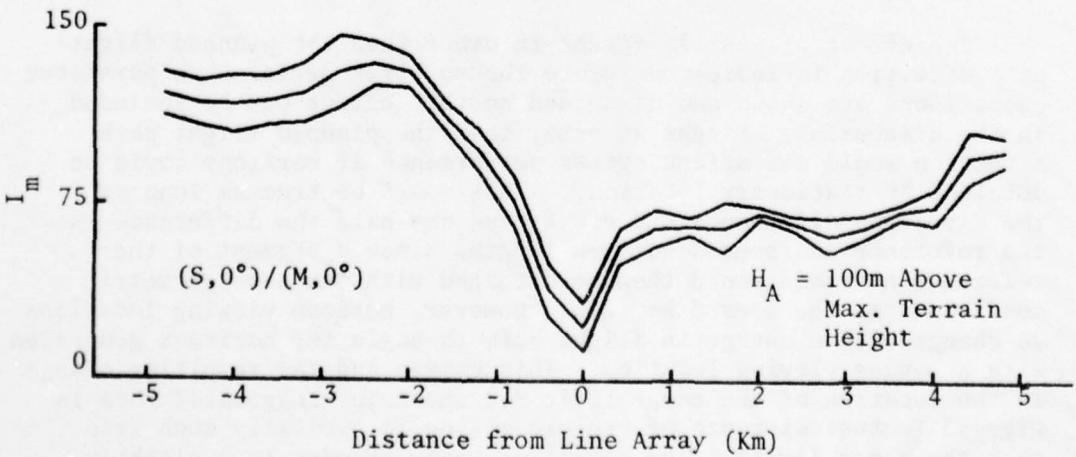
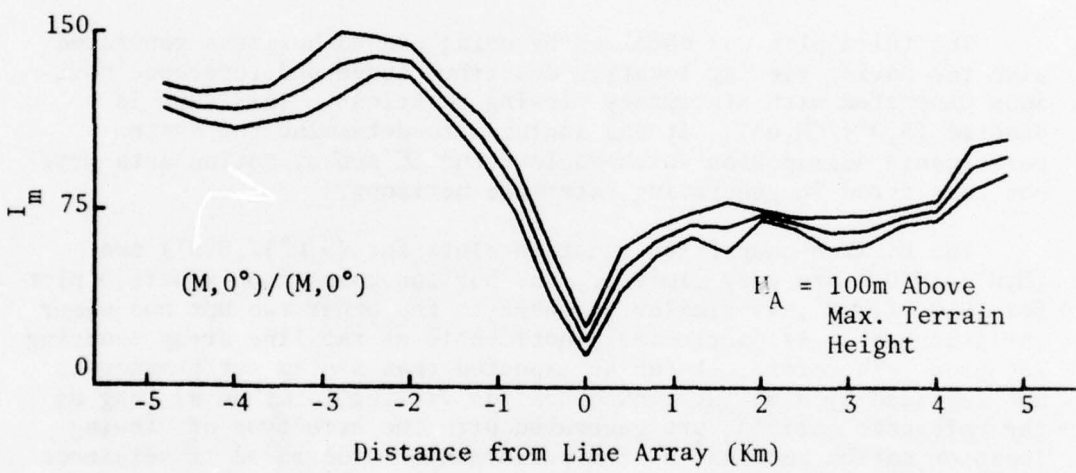
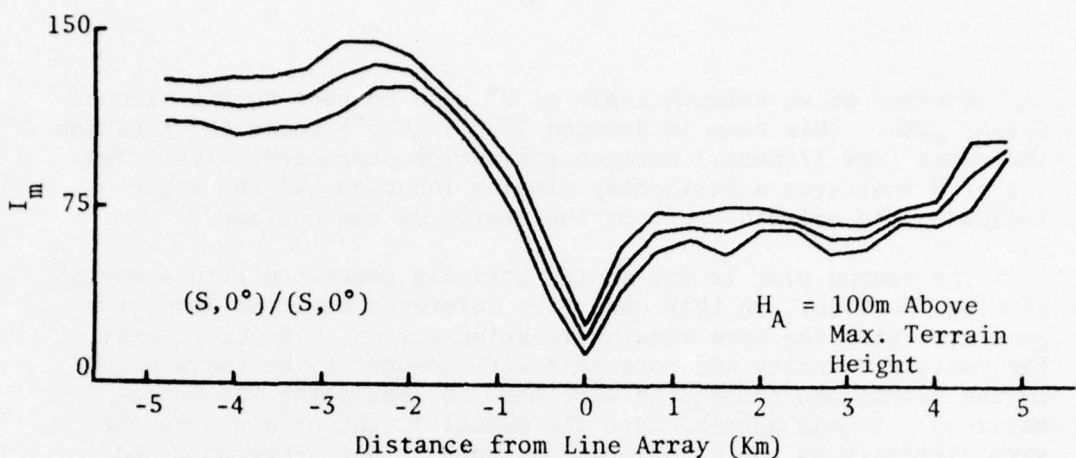


Fig. 52. Horizon Comparison Functions for Case 6
with Stationary and Moving Viewing Locations.

and centered on an azimuth angle of 0° with respect to the planned flight path. This case is denoted $(S, 0^\circ)/(S, 0^\circ)$ where the notation indicates (Ref.)/(Sens.) horizon generation characteristics. The letter S indicates a stationary viewing location and the angle indicates the azimuth angle of the center of the horizon.

The second plot is for sensed horizons generated with a moving viewing location. In this case, the reference horizons were also generated with the same viewing location motion. In other words, the vehicle velocity and scan rate were assumed to be known prior to the flight and these data were used in generating reference horizons. It was assumed that the actual flight path was in the same direction as the planned flight path so both reference and sensed profiles were centered on an azimuth angle of 0° with respect to the planned flight path. This case is denoted $(M, 0^\circ)/(M, 0^\circ)$.

The third plot was obtained by using sensed horizons generated with the moving viewing location described above and reference horizons generated with stationary viewing locations. This case is denoted $(S, 0^\circ)/(M, 0^\circ)$. It was included to determine the system performance degradation which would occur if sensor motion data were not considered in generating reference horizons.

The horizon comparison function plots for $(S, 0^\circ)/(S, 0^\circ)$ and $(M, 0^\circ)/(M, 0^\circ)$ are very similar. The horizon comparison function plot for $(S, 0^\circ)/(M, 0^\circ)$ is similar in shape to the other two but has wider variation which is particularly noticeable at the line array crossing location. Therefore, it can be expected that system performance is not degraded by a moving sensed horizon viewing location as long as the reference horizons are generated with the same type of viewing location motion but that system performance is degraded if reference horizons are generated from stationary locations. The specific performance parameter comparisons are shown later in this section.

The effect of vehicle flight in other than the planned flight path direction is indicated before the specific performance parameter comparisons are shown and discussed so this effect can be included in the discussion. Flight at other than the planned flight path direction would not affect system performance if horizons could be obtained at stationary locations. This would be true as long as the direction difference did not exceed one-half the difference in the reference and sensed horizon lengths since a segment of the reference horizons would then be obtained with the same geometric conditions as the sensed horizon. However, horizon viewing locations do change with a change in flight azimuth angle for horizons generated with a moving viewing location. This change and the resulting change in the location of the range limit are shown in exaggerated form in Fig. 53 (actual distance of vehicle motion is typically much less than the range limit). The result of these changes is a slightly changed horizon. Since reference horizons are generated for the

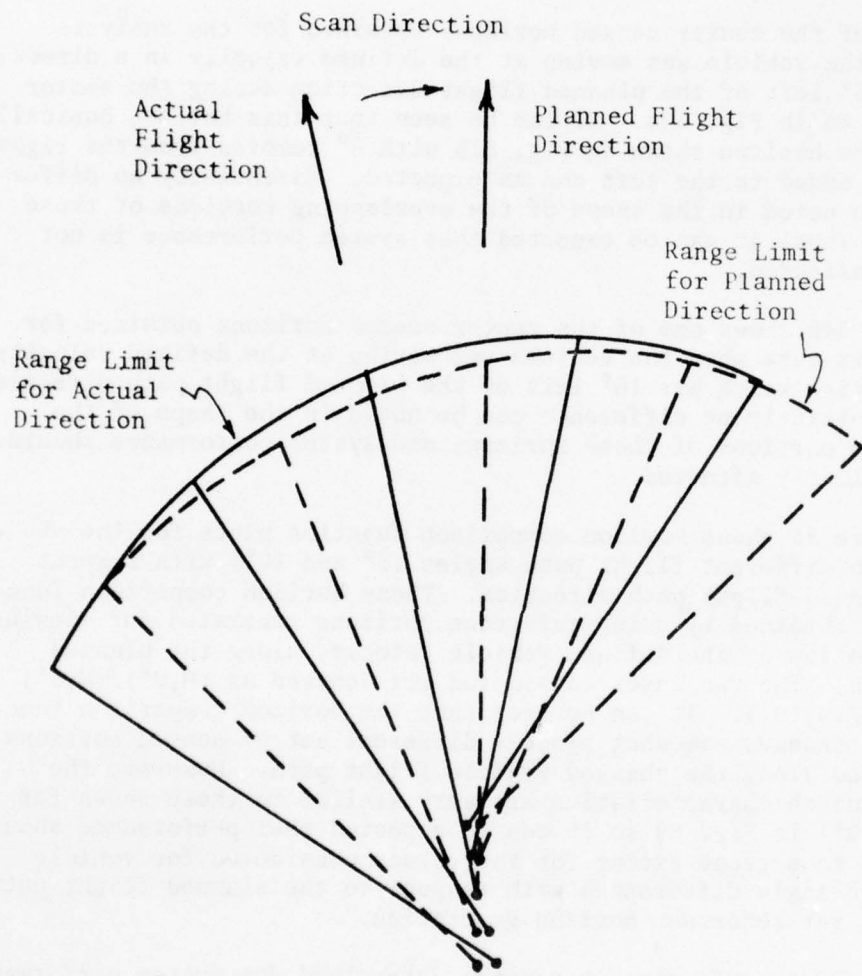


Fig. 53. Geometry for Moving
Horizon Viewing Locations
with Flight Direction
Mismatch.

AD-A038 247

MISSOURI UNIV-ROLLA DEPT OF ELECTRICAL ENGINEERING

F/G 17/7

RANGE-LIMITED HORIZON CORRELATION FOR NAVIGATION CHECKPOINTING.(U)

MAR 77 G E CARLSON, C M BENOIT, P W SAPP

N00014-75-C-0639

UNCLASSIFIED

CSR-77-1

NL

2 OF 2
AD-A038247



END

DATE
FILMED
5-77

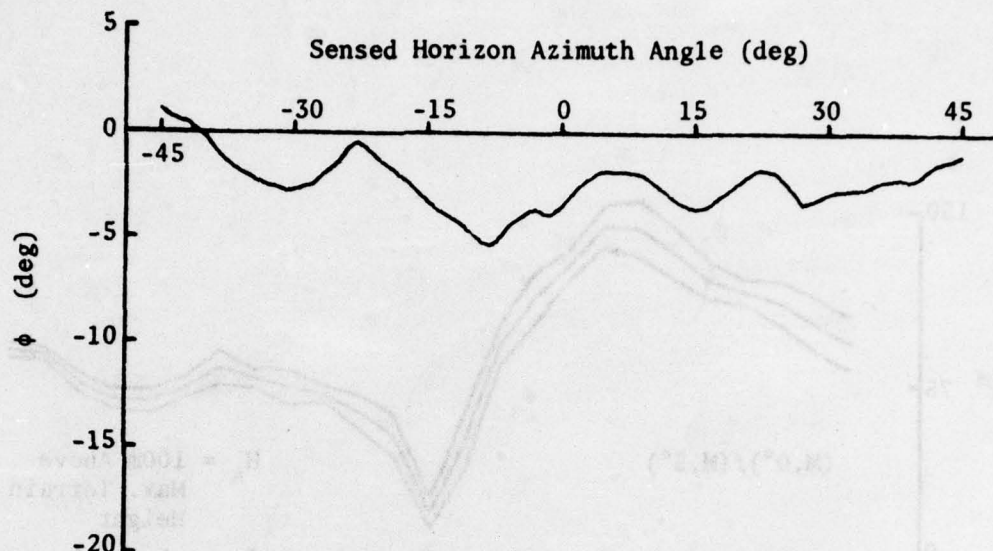
planned flight path direction, and sensed horizons are generated for the actual flight path direction, then the reference horizon segment and sensed horizon which should compare are not generated with the same geometric conditions. Performance degradation results if they are too dissimilar.

One of the center sensed horizons obtained for the analysis case when the vehicle was moving at the defined velocity in a direction which was 5° left of the planned flight direction during the sensor scan is shown in Fig. 54a. It can be seen that this horizon basically contains the horizon shown in Fig. 51b with 5° removed from the right end and 5° added to the left end as expected. Essentially no difference can be noted in the shape of the overlapping portions of these horizons. Thus, it can be expected that system performance is not seriously affected.

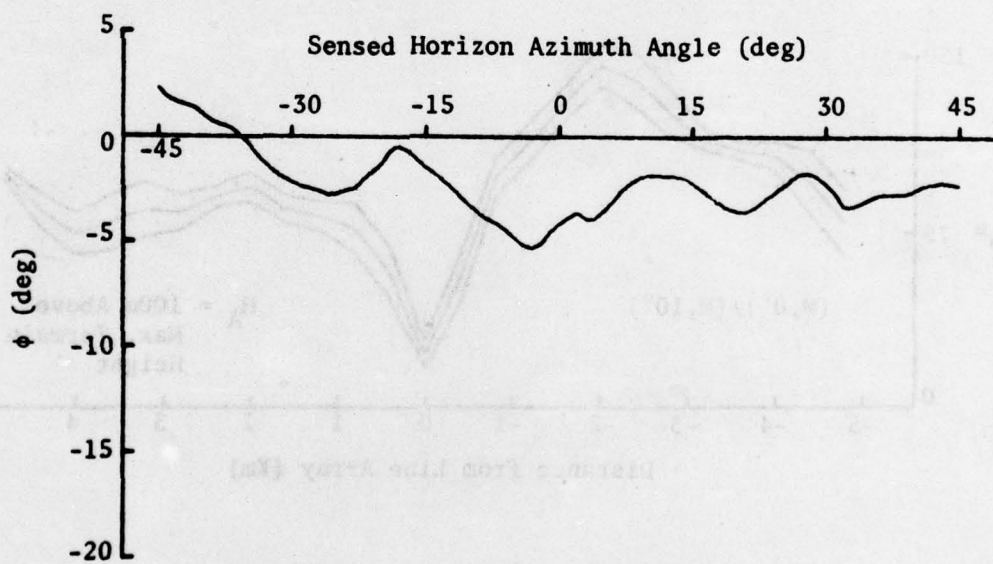
Fig. 54b shows one of the center sensed horizons obtained for the analysis case when the vehicle was moving at the defined velocity in a direction which was 10° left of the planned flight path direction. Again, essentially no difference can be noted in the shape of the overlapping portions of these horizons and system performance should not be seriously affected.

Figure 55 shows horizon comparison function plots for the above defined two different flight path angles (5° and 10°) with respect to the planned flight path direction. These horizon comparison functions were obtained by using reference horizons generated for viewing location motion at the defined vehicle velocity along the planned flight path. The two cases considered are denoted as $(M, 0^\circ)/(M, 5^\circ)$ and $(M, 0^\circ)/(M, 10^\circ)$. It can be seen that the horizon comparison function shape changes somewhat since a different set of sensed horizons are obtained along the changed vehicle flight path. However, the selection notch characteristics are very similar to those shown for $(M, 0^\circ)/(M, 0^\circ)$ in Fig. 52 so it can be expected that performance should not change to a great extent for the values considered for vehicle flight path angle differences with respect to the planned flight path angle used for reference horizon generation.

The first performance parameter determined for system performance comparison was the maximum allowable random horizon error. To obtain it, the required detection threshold, T_1 , for each of the analysis case variations indicated above was first determined to give a probability of false alarm of less than 0.001 for points along the flight path which are greater than 1Km from the line array location. These values are shown in Table IV. Then the detection threshold needed, as a function of random horizon error, to obtain a probability of detection of 0.99 was determined. The plots of these needed detection thresholds are shown in Fig. 56 for the various analysis case variations. The data from Table IV and Fig. 56 were used to determine the maximum allowable random profile errors which permit a maximum probability of false alarm of 0.001 and a minimum probability of detection of 0.99. The results are shown in Table V.



(a) Flight Path 5° Right of Planned



(b) Flight Path 10° Right of Planned

Fig. 54. Sensed Horizons for Case 6 with Moving Viewing Locations on Flight Path to Right of Planned.

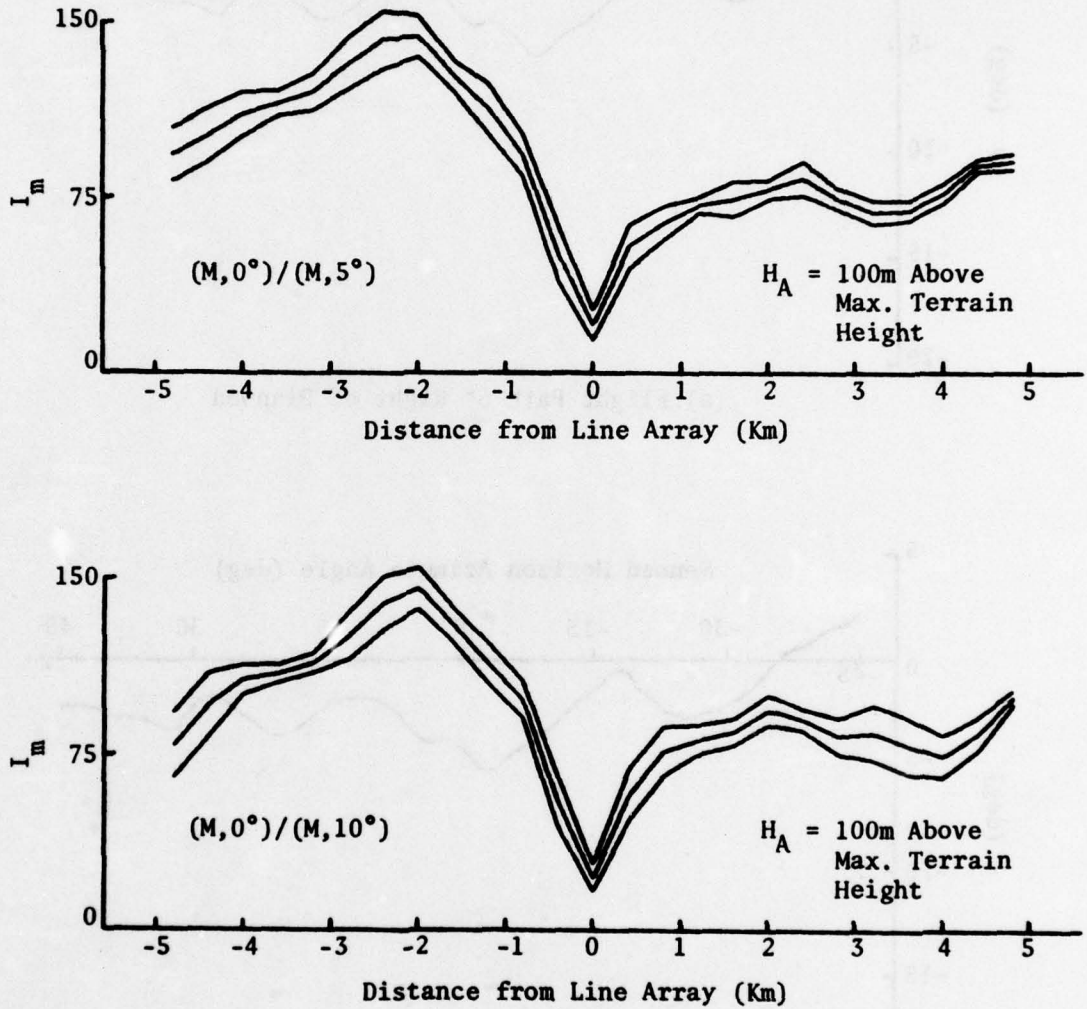


Fig. 55. Horizon Comparison Functions for Case 6 with Moving Viewing Locations on Flight Paths at Different Azimuth Angles.

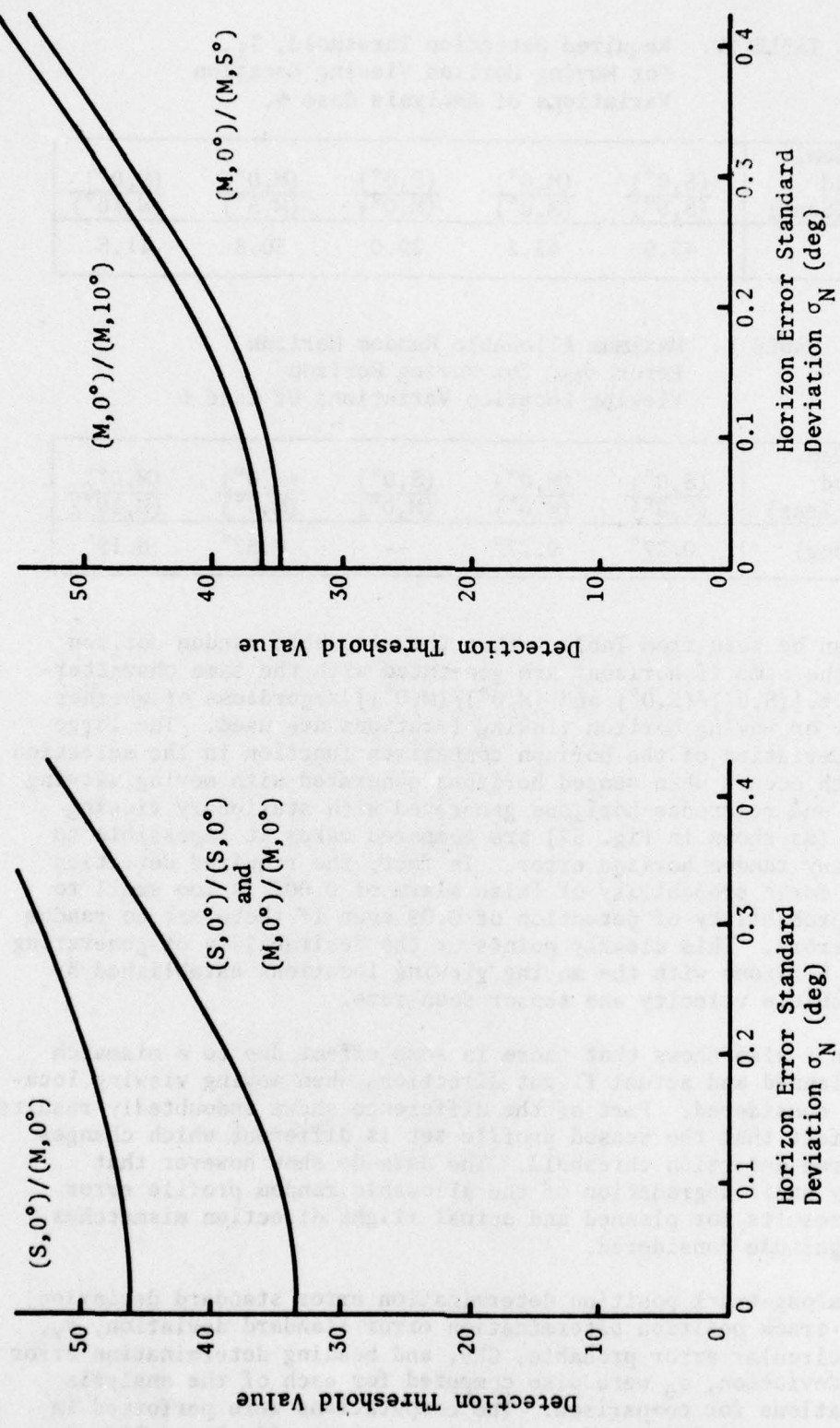


Fig. 56. Detection Threshold Needed to Give $P_D = 0.99$ for Moving Horizon Viewing Location Variations of Case 6.

TABLE IV. Required Detection Threshold, T_1 ,
For Moving Horizon Viewing Location
Variations of Analysis Case 6.

Hor. Gen. Method (Ref)/(Sens)	$\frac{(S, 0^\circ)}{(S, 0^\circ)}$	$\frac{(M, 0^\circ)}{(M, 0^\circ)}$	$\frac{(S, 0^\circ)}{(M, 0^\circ)}$	$\frac{(M, 0^\circ)}{(M, 5^\circ)}$	$\frac{(M, 0^\circ)}{(M, 10^\circ)}$
T_1	43.0	43.2	29.0	50.8	41.5

TABLE V. Maximum Allowable Random Horizon
Error, σ_{NM} , for Moving Horizon
Viewing Location Variations of Case 6.

Hor. Gen. Method (Ref)/(Sens)	$\frac{(S, 0^\circ)}{(S, 0^\circ)}$	$\frac{(M, 0^\circ)}{(M, 0^\circ)}$	$\frac{(S, 0^\circ)}{(M, 0^\circ)}$	$\frac{(M, 0^\circ)}{(M, 5^\circ)}$	$\frac{(M, 0^\circ)}{(M, 10^\circ)}$
σ_{NM} (deg)	0.27°	0.27°	--	0.37°	0.19°

It can be seen from Table V that the allowable random horizon error is the same if horizons are generated with the same characteristics i.e. $[(S, 0^\circ)/(S, 0^\circ)$ and $(M, 0^\circ)/(M, 0^\circ)$] regardless of whether stationary or moving horizon viewing locations are used. The large standard deviation of the horizon comparison function in the selection notch which occurs when sensed horizons generated with moving viewing locations and reference horizons generated with stationary viewing locations (as shown in Fig. 52) are compared makes it impossible to tolerate any random horizon error. In fact, the required detection threshold for a probability of false alarm of 0.001 is too small to permit a probability of detection of 0.99 even if there are no random horizon errors. This clearly points up the desirability of generating reference horizons with the moving viewing locations established by planned vehicle velocity and sensor scan rate.

Table V also shows that there is some effect due to a mismatch between planned and actual flight directions when moving viewing locations are considered. Part of the difference shown undoubtedly results from the fact that the sensed profile set is different which changes the required detection threshold. The data do show however that reasonably small degradation of the allowable random profile error probably results for planned and actual flight direction mismatches of the magnitude considered.

The along-track position determination error standard deviation, σ_x , cross-track position determination error standard deviation, σ_y , position circular error probable, CEP, and heading determination error standard deviation, σ_θ were also computed for each of the analysis case variations for comparison. The computations were performed in the same manner as indicated earlier in sections III. B and III. E

and the results are shown in tabular form in Table VI. In general, performance shown is similar for all cases. There is approximately a 12% increase in position CEP for smaller values of random horizon error when sensed horizons generated with moving viewing locations are compared with reference obtained with stationary viewing locations. This again points to the desirability of generating reference horizons with the moving viewing locations established by planned vehicle velocity and sensor scan rate. The decreasing along-track position error with increasing flight direction mismatch shown in the table results from the reduced (by the cosine of the angles) sensed horizon viewing location spacing in the planned flight direction (i.e. $113.2 = 113.6 \cos 5^\circ$ and $111.9 = 113.6 \cos 10^\circ$ are the smallest possible along-track error standard deviations as determined by the discrete sensed horizon spacing). This reduction occurs since the along-track and cross-track directions are defined with respect to the planned flight path direction. The reduced cross-track error evident for the $(M, 0^\circ)/(M, 10^\circ)$ analysis case variation is probably a result of increased horizon variation as shown in Fig. 54b.

In general, it can be concluded that analyses in previous sections using stationary horizon viewing locations present an adequate picture for system feasibility and theoretical performance determination. Also, it can be concluded that reference horizons should be generated with moving viewing locations corresponding to the planned vehicle flight to give best system performance. It should be noted that such reference horizon generation would only be correct for sensor scans in one direction. Sensor scans in the opposite direction are generated with slightly different geometry. Since it is desirable to use sensor scans in both directions to reduce the sensed horizon spacing, then it would be desirable to store two sets of reference horizons for each line array. The first set would be for a sensor scan from left to right and the second set would be for a sensor scan from right to left. Each sensed horizon could then be tagged with the scan direction used to obtain it so comparison could be made with the appropriate set. If reference storage is limited then it may be possible in some cases to generate reference horizons for stationary viewing locations so they would give compromise performance for the two directions of scan.

B. FINITE SENSOR BEAMWIDTH

The second practical sensor characteristic considered was a finite sensor beamwidth. The model required to analyze the effect of this characteristic, the analysis cases considered, and the analysis results obtained are discussed in this section.

TABLE VI. Position and Heading Determination Errors for Moving Viewing Location Variations of Analysis Case 6.

Hor. Gen. Method (Ref.)/(Sens.)	Parameter	σ_N (deg)			
		0.000	0.125	0.250	0.500
(S, 0°)/(S, 0°)	σ_x (m)	113.6	113.6	121.8	124.4
	σ_y (m)	141.4	156.1	253.7	264.0
	CEP(m)	150.1	158.8	221.1	228.7
	σ_θ (deg)	1.771	1.930	3.191	3.146
(M, 0°)/(M, 0°)	σ_x (m)	113.6	113.6	113.6	113.6
	σ_y (m)	160.1	160.1	138.5	264.0
	CEP(m)	161.1	161.1	148.4	222.3
	σ_θ (deg)	1.951	1.949	1.741	3.187
(S, 0°)/(M, 0°)	σ_x (m)	113.6	113.6	113.6	113.6
	σ_y (m)	195.1	195.1	278.2	236.9
	CEP(m)	181.7	181.7	230.7	206.3
	σ_θ (deg)	2.444	2.286	3.621	2.850
(M, 0°)/(M, 5°)	σ_x (m)	113.2	113.2	113.2	118.0
	σ_y (m)	160.6	160.6	147.6	199.0
	CEP(m)	161.2	161.2	153.5	186.6
	σ_θ (deg)	2.016	2.016	1.886	2.537
(M, 0°)/(M, 10°)	σ_x (m)	111.9	111.9	111.9	120.0
	σ_y (m)	132.0	133.8	123.8	215.9
	CEP(m)	143.6	144.6	138.8	197.7
	σ_θ (deg)	1.586	1.586	1.497	2.709

1. SYSTEM MODEL AND ANALYSIS METHOD

If a radar transmitter uniformly illuminates its antenna, then it transmits energy and receives return energy in a beamwidth of approximately

$$\theta_B = \lambda/D \text{ rad.} \quad (2)$$

where θ_B is the beamwidth between one-half power points, λ is the transmitted energy wavelength, and D is the antenna aperture dimension. Energy is received at the same time from all terrain points at the same range in the entire radar azimuth beamwidth. Thus, the return obtained to be used for elevation angle measurement is a composite of the return from all the illuminated terrain points. The measured elevation angle is therefore a weighted average of the elevation angles to the terrain within the radar azimuth beamwidth as illustrated in Fig. 57. The average is a weighted average since the antenna gain across the azimuth beamwidth is not constant and since the terrain reflectivity may not be constant over the illuminated area. Figure 57 is exaggerated in that the azimuth beamwidth shown is quite large with respect to the length of the terrain profile variations (terrain profile correlation length) shown. In an actual case, the beamwidth should be narrower so the average elevation angle measured would closely approximate the actual elevation angle to the terrain. The previous analyses assumed that the azimuth beamwidth was very small with respect to the terrain profile correlation length so the average elevation angle measured was essentially the actual elevation angle to the terrain. This section considers the effect of practical azimuth beamwidth by analyzing system performance with various azimuth beamwidths. Different terrain roughnesses are considered since terrain roughness affects the antenna beamwidth required.

The effect of finite sensor azimuth beamwidth was analyzed by changing the horizon generation computer routine used in the previously discussed analyses to model the effect of return from all points within the azimuth beamwidth. To do so, it was assumed that the radar antenna was uniformly illuminated so its two-way voltage gain pattern as a function of azimuth angle, θ , measured from the radar azimuth boresight was approximately given by

$$G(\theta) = \frac{\sin(2.78\theta/\theta_B)}{2.78\theta/\theta_B}^2 \quad (3)$$

where θ_B is the desired azimuth beamwidth between the one-half power points. It was assumed that the terrain reflectivity was constant. Therefore, the amplitude of the return from individual terrain points was assumed to be only a function of the two-way voltage gain to that point. No gain variations were assumed in the elevation direction since the elevation beamwidth is broad so essentially no gain variation will be apparent at the segment of horizon profile illuminated

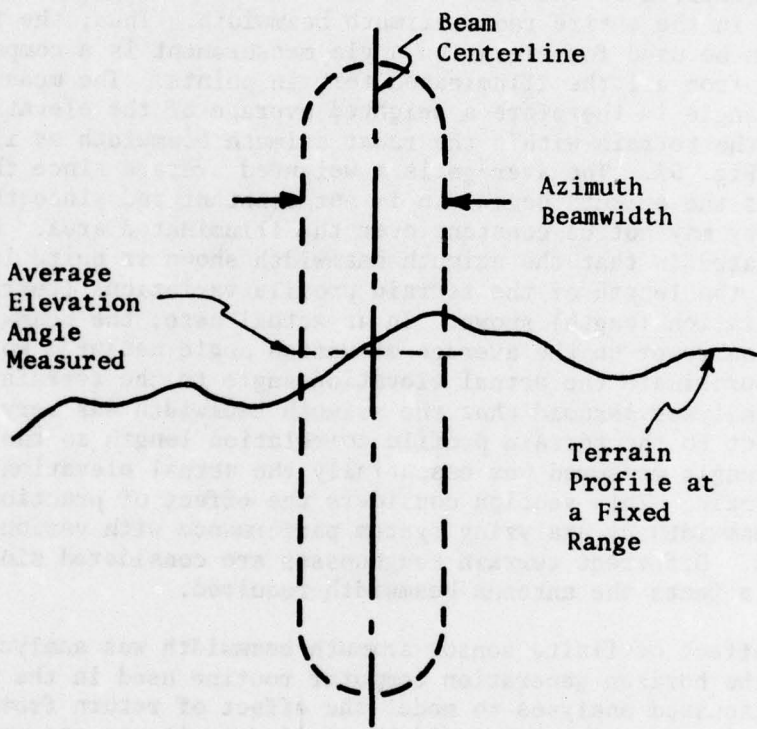


Fig. 57. Elevation Angle Measurement
with Finite Azimuth Beamwidth.

at one time. Horizon errors which result from nonconstant terrain reflectivity were assumed to be contained in random horizon errors added to the horizons during system analysis. It was assumed that the radar system used a frequency of 17.0 GHz. and elevation phase monopulse with the monopulse receiving antenna horns spaced by 1.0 cm. to obtain elevation angle measurements.

The amplitude and phase of terrain returns at each receiving antenna horn were computed for range positions separated by 30m along radial azimuth lines separated by $\Delta\theta_I$ and spanning the total azimuth scan angle. Radar shadowing was ignored since later peak detection essentially removed shadowed data. The spacing $\Delta\theta_I$ was chosen to give n radial lines within one azimuth beamwidth where the value of n used was different for different beamwidths. The geometry indicated above is illustrated in Fig. 58 for $\Delta\theta_I = \theta_B/4$ which gives $n = 5$.

Complex addition was used to combine the n returns within the azimuth beamwidth for each range at each possible azimuth location of the radar beam. This gave the total return at each antenna horn for each range and possible beam azimuth location. The phase difference between these two total returns was then used to determine the individual sensed elevation angles at each range as a function of the radar azimuth scan angle. The data obtained had an azimuth spacing of $\Delta\theta_I$ as shown diagrammatically in Fig. 59 for a single range and $\Delta\theta_I = \theta_B/4$.

An actual radar sensor averages several individual sensed elevation angle measurements to obtain a sufficient signal-to-noise ratio. Therefore, the individual elevation angles determined were averaged for an interval surrounding the desired data azimuth locations (desired data spacing equals $\Delta\theta$ deg.). The interval chosen was the azimuth beamwidth, θ_B since averaging will typically be done over a beamwidth in an actual system to obtain maximum return from the desired terrain point (i.e. maximum signal-to-noise ratio). This averaging is also illustrated diagrammatically in Fig. 59 for a single range and $\Delta\theta = \theta_B/2$. The resulting measured elevation angles were peak detected as a function of range for each desired azimuth data location to determine the measured elevation angle to the range-limited horizon as a function of azimuth angle.

It can be seen that many computations are required to generate one range-limited horizon with the finite sensor beamwidth model. Actually, computation time was considerably reduced by identifying the approximate range locations for the range-limited horizon and using a reduced search in range. The cost of using this model is still quite high so system analysis with this model was done with a bare minimum of cases.

After horizons had been generated by using the finite sensor beamwidth model, then system analysis was performed which was identical to that previously described. The only differences were that a flight path of 6Km instead of 10Km was used and 3 reference horizons

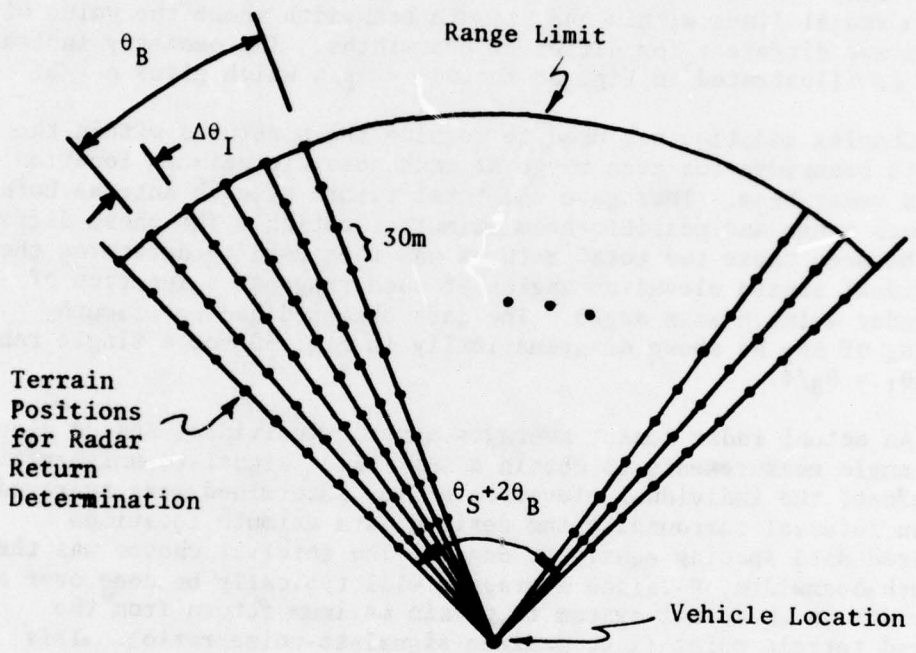


**Fig. 58. Geometry for Radar
Return Determination
for Finite Beamwidth
Analysis.**

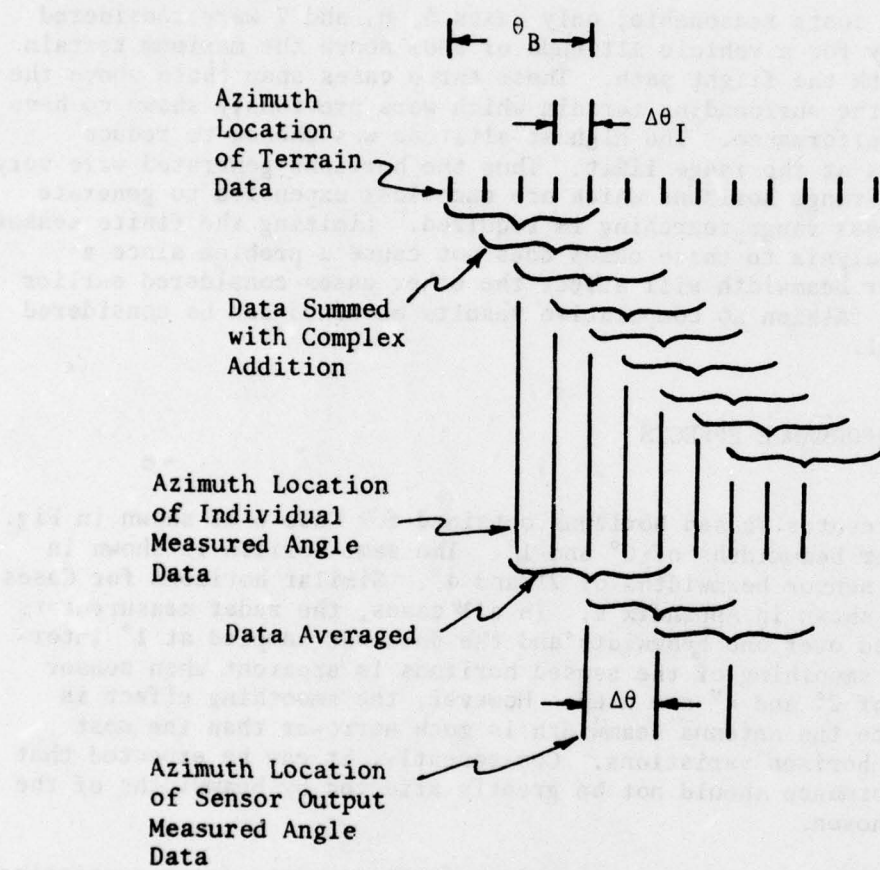


Fig. 59. Diagram Illustrating Terrain Return Data Processing for a Single Range.

instead of 5 were used in each reference line array. This significantly reduced the required computation cost since it required the generation of only 60% as many horizons. The previous analysis showed that the system performance data was generally obtained from this portion of the flight path and line array so negligible degradation of analysis results occurred due to the use of the reduced set of sensed and reference horizons.

To keep costs reasonable, only Cases 5, 6, and 7 were considered and then only for a vehicle altitude of 500m above the maximum terrain height beneath the flight path. These three cases span those above the majority of the surrounding terrain which were previously shown to have reasonable performance. The highest altitude was chosen to reduce radar shadows at the range limit. Thus the horizons generated were very nearly fixed-range horizons which are much less expensive to generate since much less range searching is required. Limiting the finite sensor beamwidth analysis to these cases does not cause a problem since a finite sensor beamwidth will affect the other cases considered earlier in a similar fashion so comparative results obtained can be considered to be general.

2. PERFORMANCE EFFECTS

One of center sensed horizons obtained for Case 6 is shown in Fig. 60 for sensor beamwidths of 0° and 1° . The same horizon is shown in Fig. 61 for sensor beamwidths of 2° and 4° . Similar horizons for Cases 5 and 7 are shown in Appendix E. In all cases, the radar measurements were averaged over one beamwidth and the data was sampled at 1° intervals. Some smoothing of the sensed horizons is apparent when sensor beamwidths of 2° and 4° are used. However, the smoothing effect is minimal since the antenna beamwidth is much narrower than the most significant horizon variations. Consequently, it can be expected that system performance should not be greatly affected by beamwidths of the magnitude chosen.

Three different horizon comparison function plots (each consisting of the mean, μ_I , and \pm one standard deviation from the mean) are shown in Fig. 62. Similar plots are shown for Cases 5 and 7 in Appendix E. The first plot in Fig. 62 is for the baseline case used for comparison which uses sensed and reference horizons which are both generated with beamwidths (θ_B and θ_{BR} respectively) of 0° . The second plot is for sensed and reference horizons which are generated with beamwidths of 4° (1° and 2° beamwidth cases are not shown since they are very similar). The third plot was obtained by using sensed horizons generated with a 4° beamwidth and reference horizons generated with a 0° beamwidth. This case was included to determine the effect on system performance if sensor beamwidth was not considered in generating reference horizons.

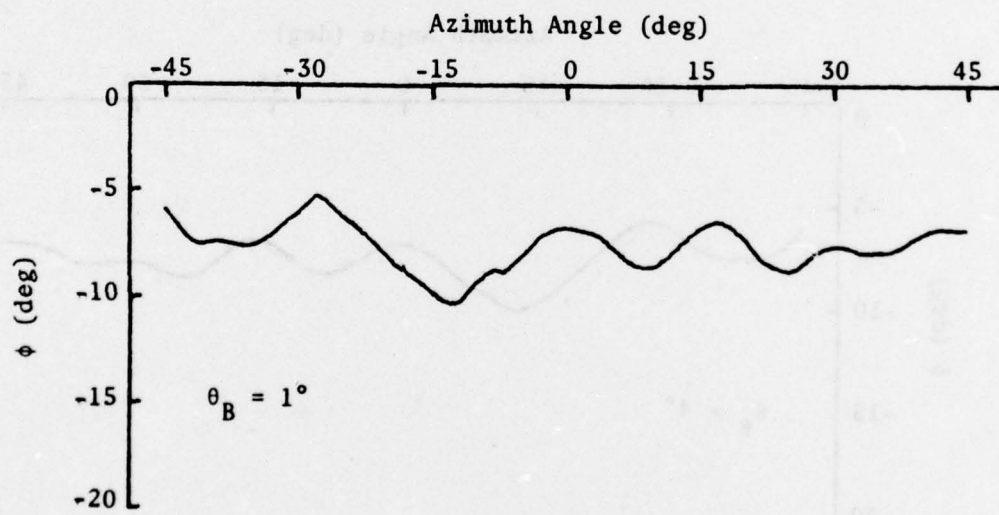
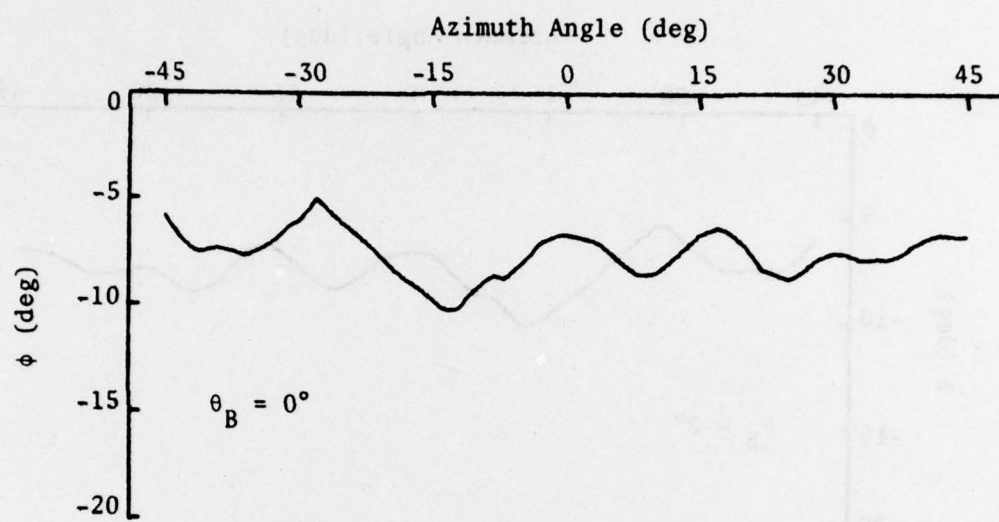


Fig. 60. Sensed Horizons for Case 6 with Sensor Beamwidths of 0° and 1° .

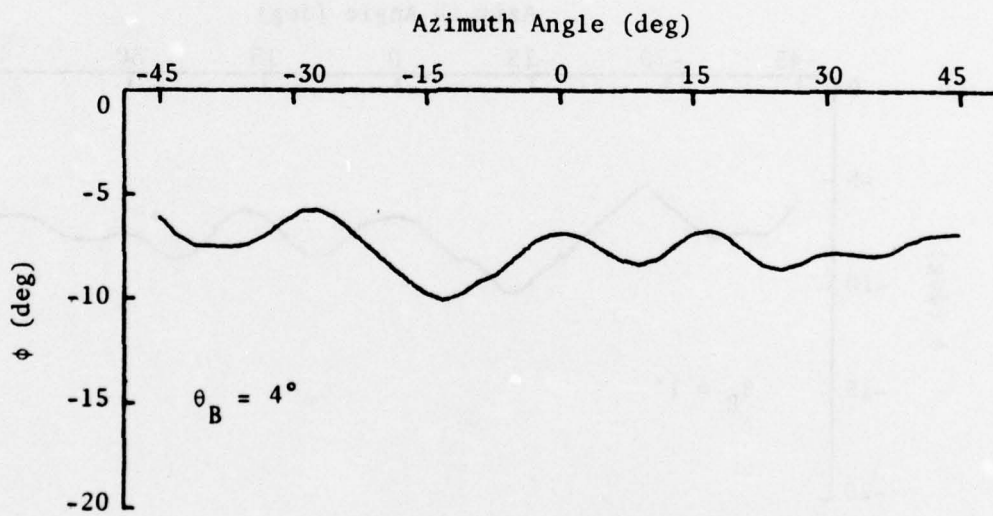
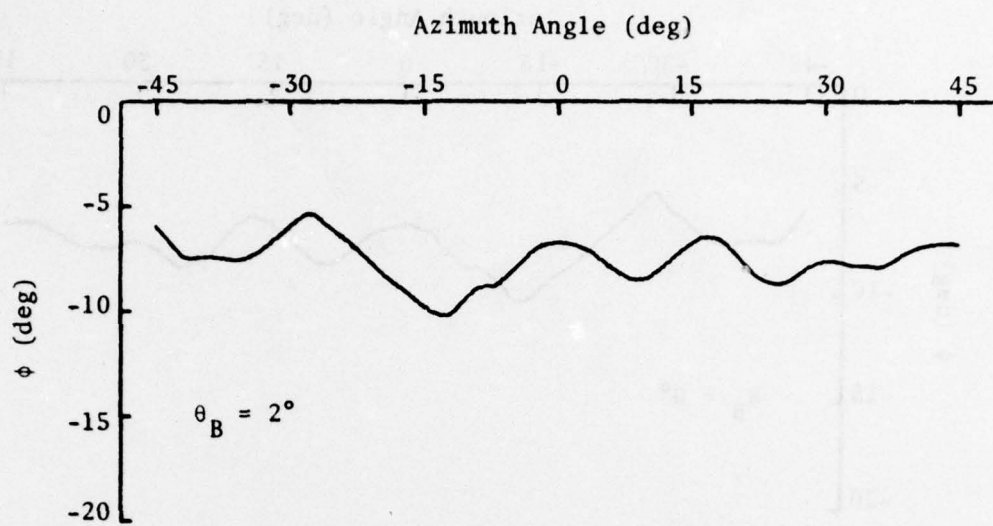


Fig. 61. Sensed Horizons for Case 6 with Sensor Beamwidths of 2° and 4° .

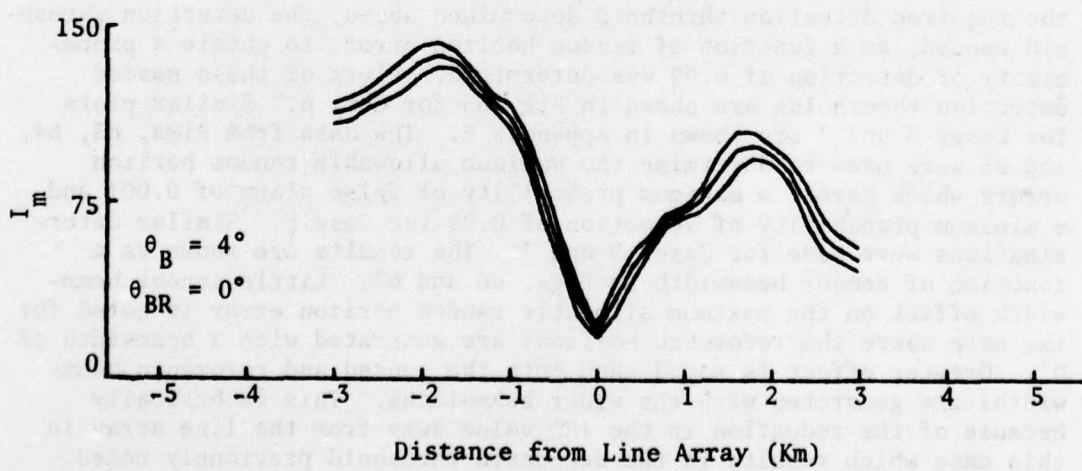
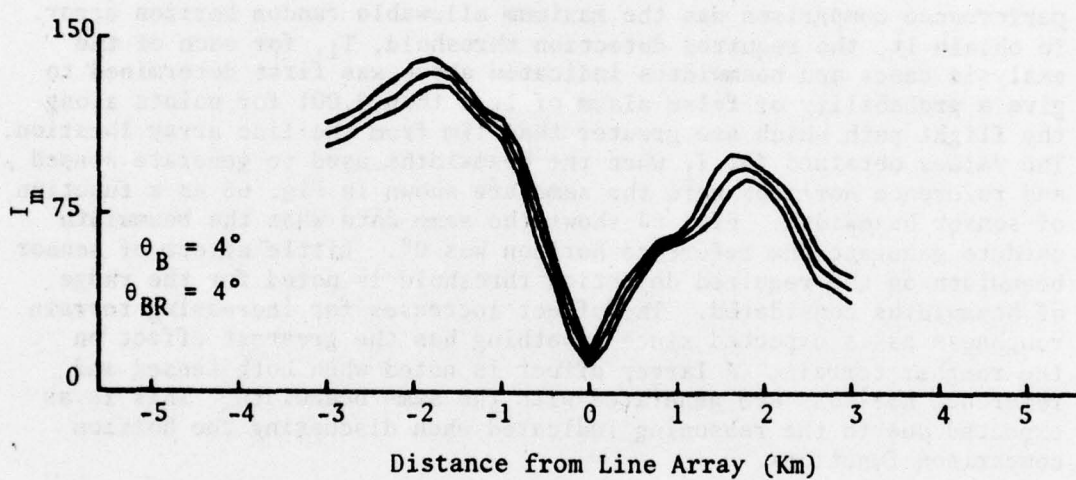
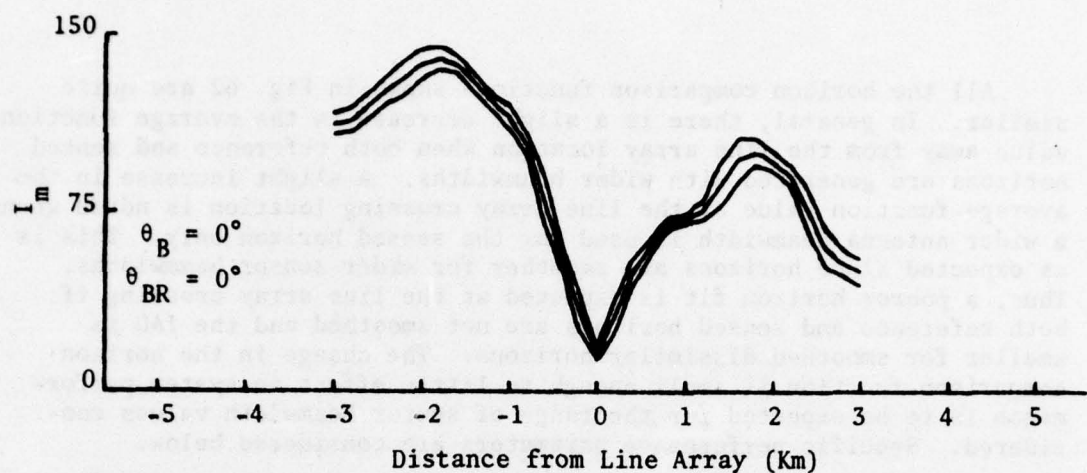


Fig. 62. Horizon Comparison Function for Case 6
with Various Sensor Beamwidths.

All the horizon comparison functions shown in Fig. 62 are quite similar. In general, there is a slight decrease in the average function value away from the line array location when both reference and sensed horizons are generated with wider beamwidths. A slight increase in the average function value at the line array crossing location is noted when a wider antenna beamwidth is used for the sensed horizon only. This is as expected since horizons are smoother for wider sensor beamwidths. Thus, a poorer horizon fit is expected at the line array crossing if both reference and sensed horizons are not smoothed and the IAD is smaller for smoothed dissimilar horizons. The change in the horizon comparison function is small enough so little effect on system performance is to be expected for the range of sensor beamwidth values considered. Specific performance parameters are considered below.

The first performance parameter determined to be used for system performance comparison was the maximum allowable random horizon error. To obtain it, the required detection threshold, T_1 , for each of the analysis cases and beamwidths indicated above was first determined to give a probability of false alarm of less than 0.001 for points along the flight path which are greater than 1Km from the line array location. The values obtained for T_1 when the beamwidths used to generate sensed and reference horizons were the same are shown in Fig. 63 as a function of sensor beamwidth. Fig. 64 shows the same data when the beamwidth used to generate the reference horizon was 0° . Little effect of sensor beamwidth on the required detection threshold is noted for the range of beamwidths considered. The effect increases for increasing terrain roughness as is expected since smoothing has the greatest effect on the rougher terrain. A larger effect is noted when both sensed and reference horizons are generated with the same beamwidth. This is as expected due to the reasoning indicated when discussing the horizon comparison functions.

To determine the maximum allowable random horizon error by using the required detection threshold determined above, the detection threshold needed, as a function of random horizon error, to obtain a probability of detection of 0.99 was determined. Plots of these needed detection thresholds are shown in Fig. 65 for Case 6. Similar plots for Cases 5 and 7 are shown in Appendix E. The data from Figs. 63, 64, and 65 were used to determine the maximum allowable random horizon errors which permit a maximum probability of false alarm of 0.001 and a minimum probability of detection of 0.99 for Case 6. Similar determinations were made for Cases 5 and 7. The results are shown as a function of sensor beamwidth in Figs. 66 and 67. Little sensor beamwidth effect on the maximum allowable random horizon error is noted for the case where the reference horizons are generated with a beamwidth of 0° . Greater effect is noted when both the sensed and reference beamwidths are generated with the wider beamwidths. This is basically because of the reduction in the IAD value away from the line array in this case which results in the decreased threshold previously noted. The data shown in Figs. 66 and 67 indicate that sensor beamwidths of up to 2° have negligible effect on the maximum random horizon error allowed. The effect becomes more noticeable with a beamwidth of 4° .

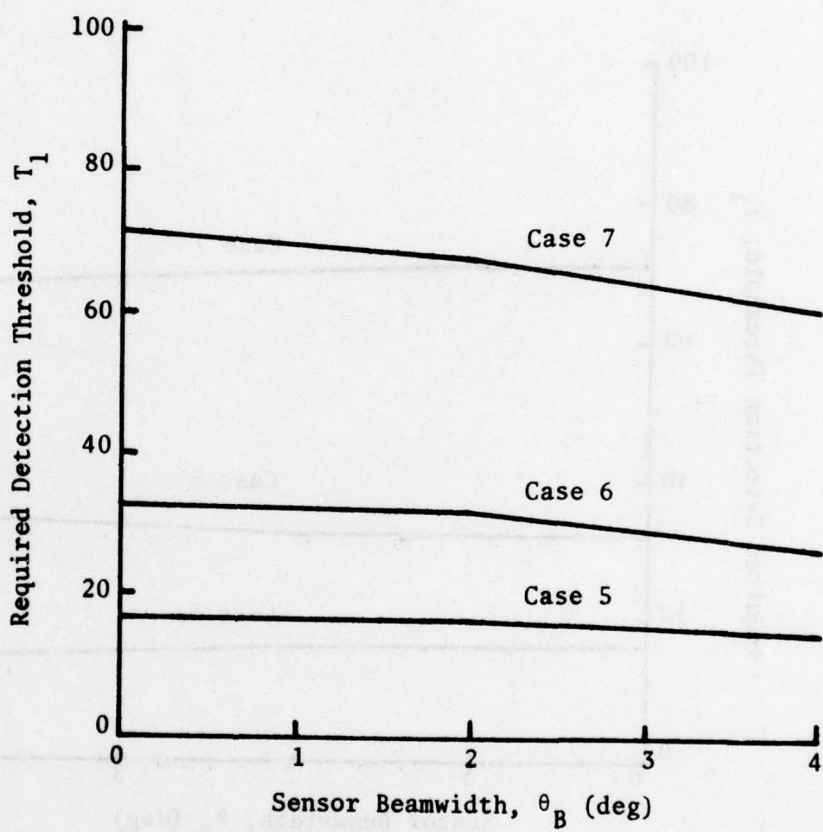


Fig. 63. Required Detection Threshold, T_1 , as a Function of Sensor Beamwidth when Sensed and Reference Horizons are Generated with the Same Beamwidth.

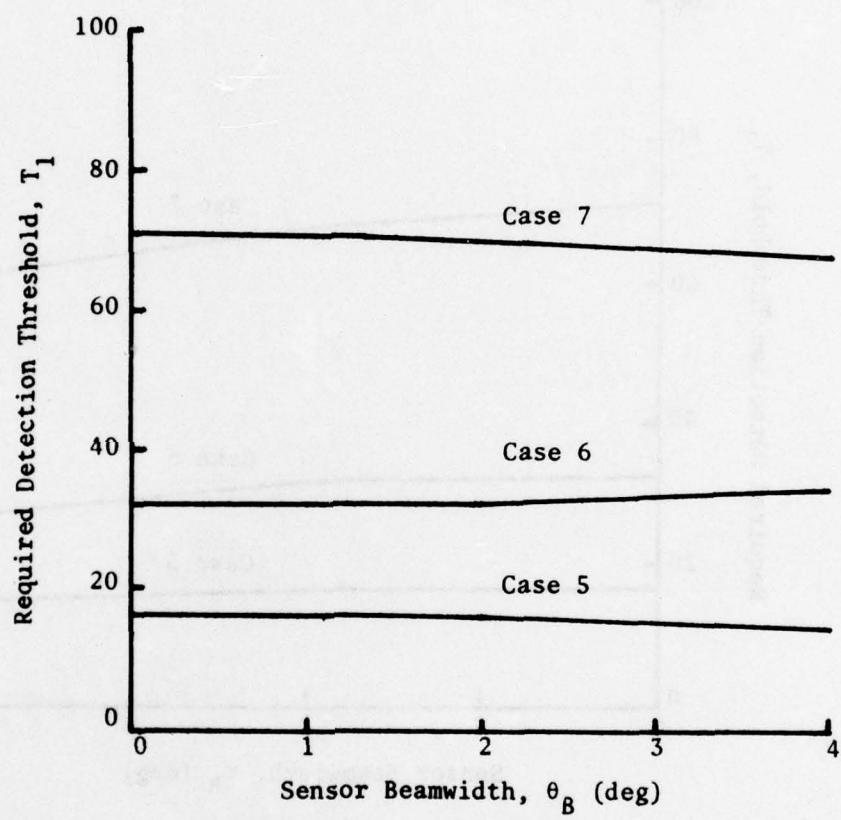


Fig. 64. Required Detection Threshold, T_1 , as a Function of Sensor Beamwidth when Reference Horizons are Generated with a 0° Beamwidth.

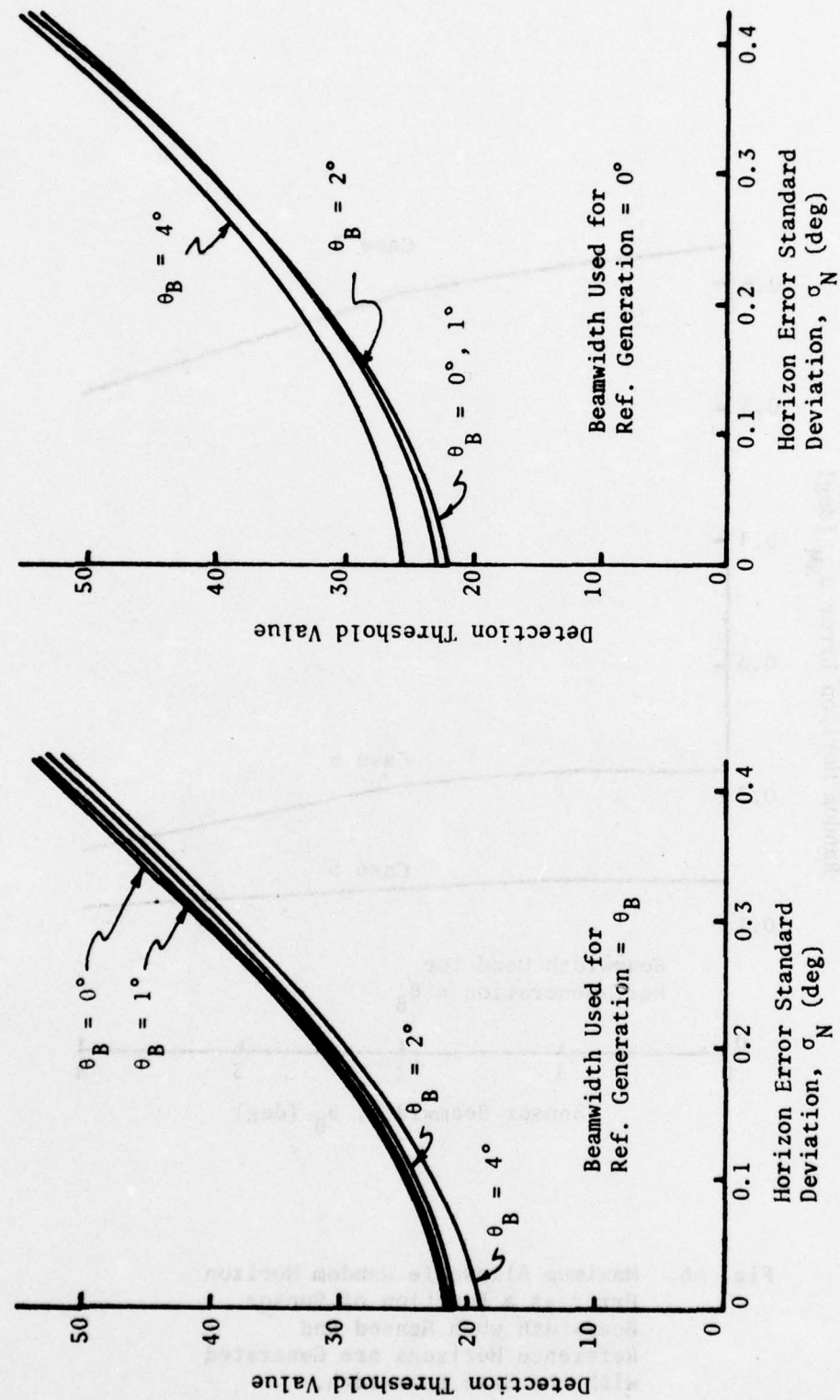


Fig. 65. Detection Threshold Needed to Give $P_D = 0.99$ for Various Sensor Beamwidths, θ_B , for Case 6.

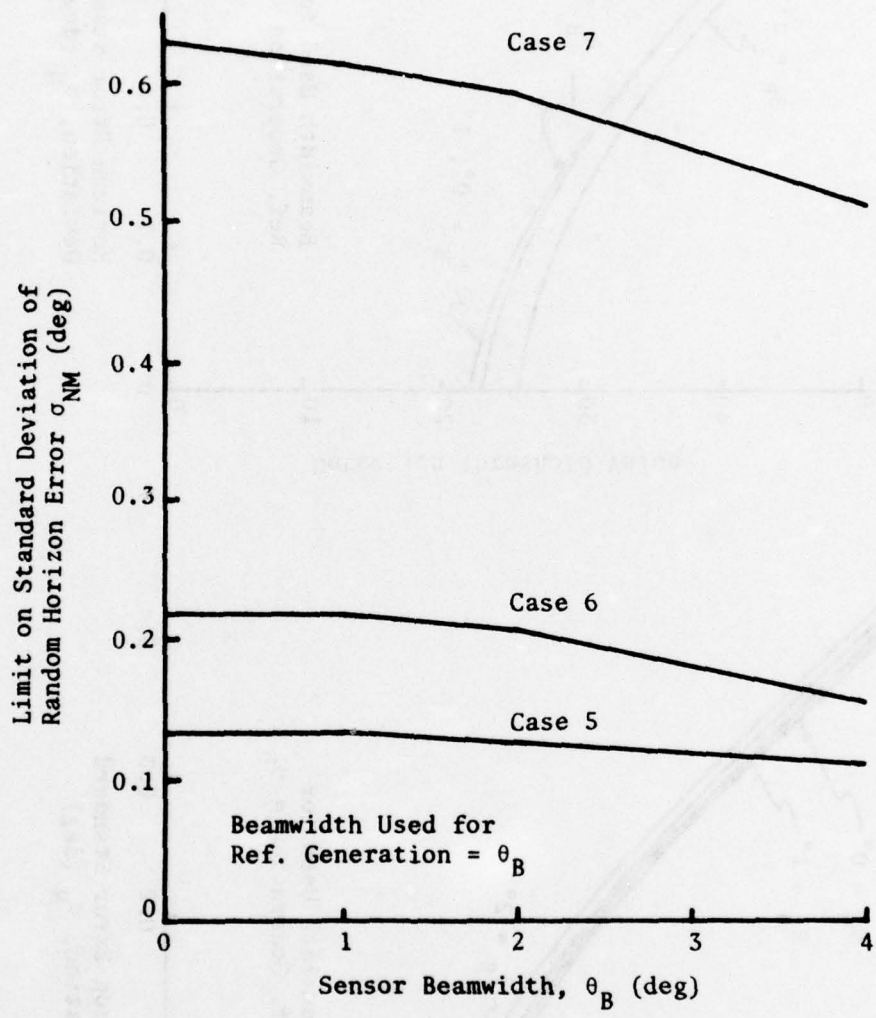


Fig. 66. Maximum Allowable Random Horizon Error as a Function of Sensor Beamwidth when Sensed and Reference Horizons are Generated with the Same Beamwidth.

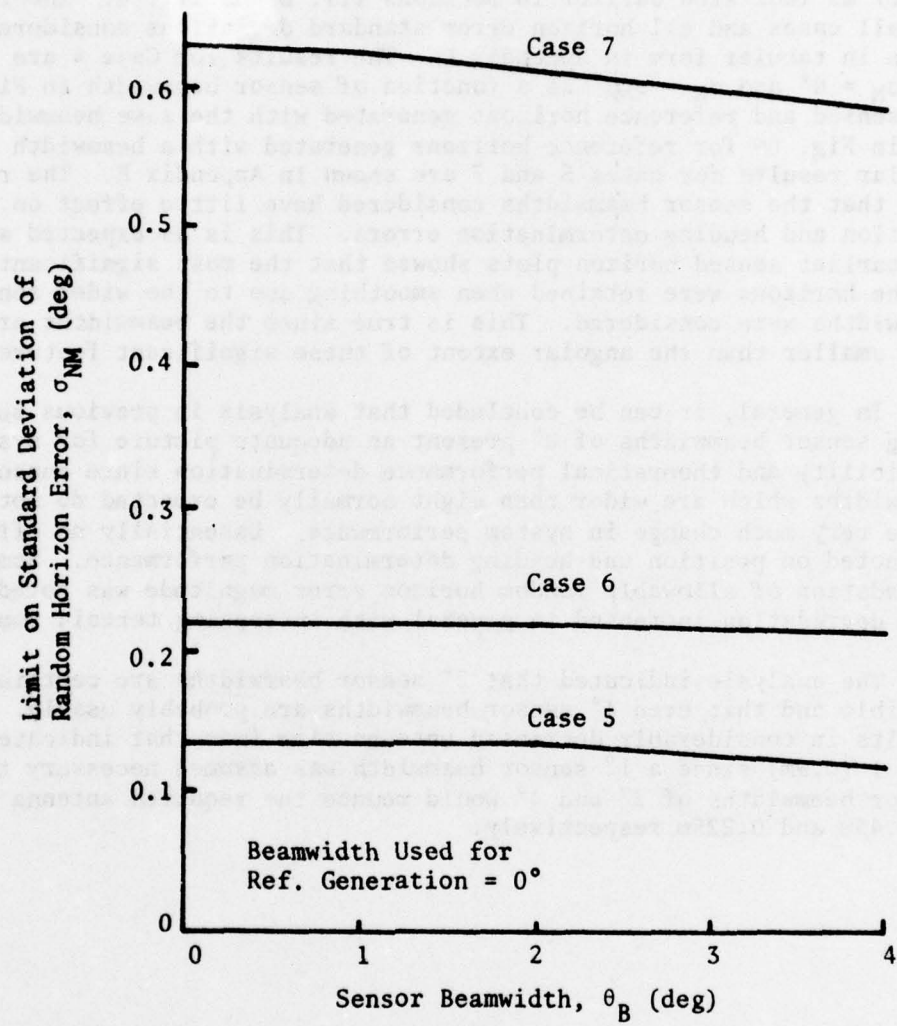


Fig. 67. Maximum Allowable Random Horizon Error as a Function of Sensor Beamwidth when Reference Horizons are Generated with a 0° Beamwidth.

The along-track position determination error standard deviation, σ_x , the cross-track position determination error standard deviation, σ_y , position circular error probable, CEP, and heading determination error standard deviation, σ_θ , were also computed for each analysis case and beamwidth considered. The computations were performed in the same manner as indicated earlier in sections III. B and III. E. The results for all cases and all horizon error standard deviations considered are shown in tabular form in Appendix E. The results for Case 4 are plotted for $\sigma_N = 0^\circ$ and $\sigma_N = \sigma_{NM}^\circ$ as a function of sensor beamwidth in Fig. 68 for sensed and reference horizons generated with the same beamwidth and in Fig. 69 for reference horizons generated with a beamwidth of 0° . Similar results for cases 5 and 7 are shown in Appendix E. The results show that the sensor beamwidths considered have little effect on the position and heading determination errors. This is as expected since the earlier sensed horizon plots showed that the most significant features of the horizons were retained when smoothing due to the wider sensor beamwidths were considered. This is true since the beamwidths are still much smaller than the angular extent of these significant features.

In general, it can be concluded that analysis in previous sections using sensor beamwidths of 0° present an adequate picture for system feasibility and theoretical performance determination since sensor beamwidths which are wider than might normally be expected do not cause very much change in system performance. Essentially no effect was noted on position and heading determination performance. Some degradation of allowable random horizon error magnitude was noted. This degradation increased in general with increasing terrain roughness.

The analysis indicated that 2° sensor beamwidths are certainly feasible and that even 4° sensor beamwidths are probably usable. This results in considerably decreased antenna size from that indicated in Ref. 1 (0.9m) since a 1° sensor beamwidth was assumed necessary there. Sensor beamwidths of 2° and 4° would reduce the required antenna length to 0.45m and 0.225m respectively.

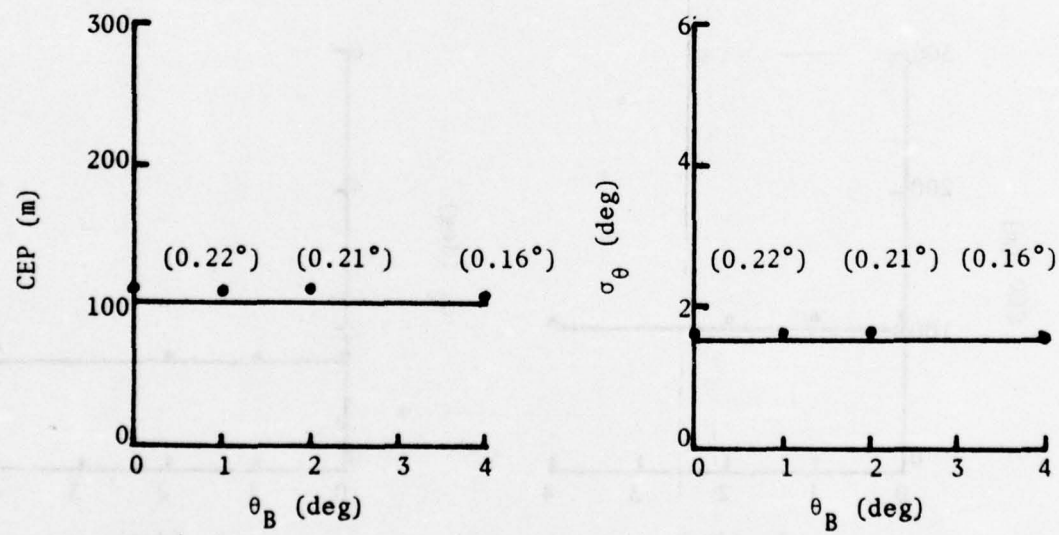
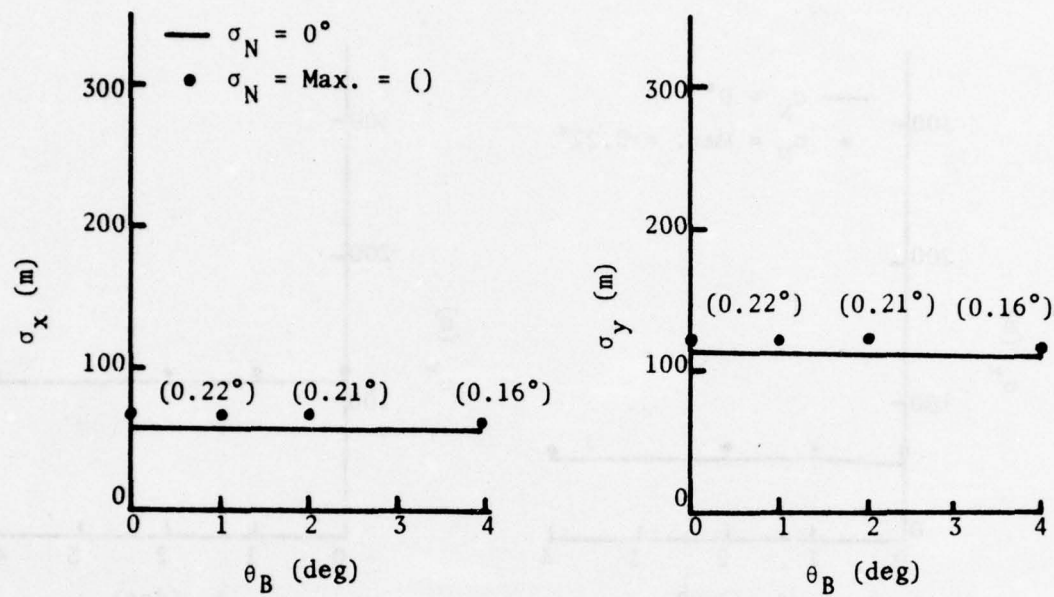


Fig. 68. Position and Heading Determination Accuracy when Sensed and Reference Horizons are Generated with the Same Beamwidth, θ_B (Case 6).

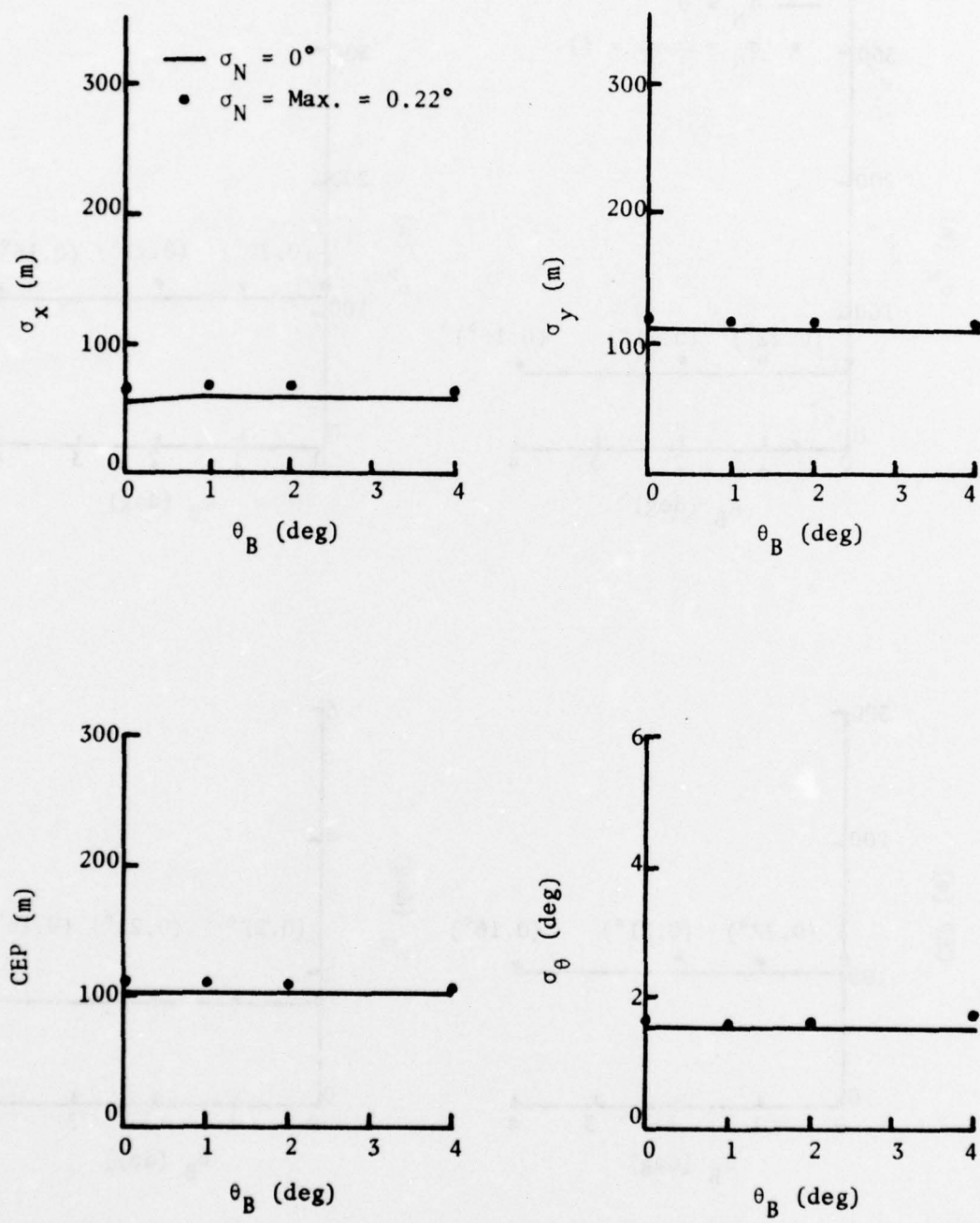


Fig. 69. Position and Heading Determination Accuracy when Reference Horizons are Generated with a 0° Beamwidth (Case 6).

V. SUMMARY AND CONCLUSIONS

The feasibility of utilizing horizon profiles as navigation checkpoints has been under investigation. Advantages of using horizons for checkpointing are: (1) the speed with which they can be obtained which provides flight path flexibility, (2) the simplicity of reference horizon generation which can be performed automatically in a computer with only topographic data, and (3) the fact that checkpoint identification is possible even if the vehicle heading is incorrectly known within limits.

Previous reports have documented the results obtained when actual horizons and fixed-range terrain profiles were used. Actual horizons proved to be satisfactory for very low-altitude flights between ridges (valley flights) but were not satisfactory for flights at higher altitudes above the majority of the surrounding terrain since they were obtained from too long a range. The long range gave horizons with reduced variation which gave system performance that was very susceptible to horizon errors. Fixed-range terrain profiles proved to be satisfactory for higher altitude flights but were not useful for very low altitude flights since too large a percentage of the profile at the fixed-range was shadowed.

The analysis reported here has considered a system which uses range-limited horizons. These are horizons generated only by terrain data within a fixed range limit. At very low vehicle altitudes, these range-limited horizons are essentially actual horizons. At vehicle altitudes sufficiently above the majority of the surrounding terrain, these range-limited horizons are essentially fixed-range terrain profiles. Thus, the system utilizing range-limited horizons gives performance similar to a system utilizing actual horizons at very low vehicle altitudes and to a system utilizing fixed-range terrain profiles at higher altitudes. This single system concept can be used for all flight altitudes.

The analyses reported were performed by using a computer simulation of horizon comparison for several flight paths over terrain of different roughness. Both the sensed and reference horizons used in the analysis were generated from digital topographic data obtained from the Defense Mapping Agency. The reference horizon viewing location spacing along a checkpoint line array; ΔR , and the sensed horizon scan width, θ_s , were selected to be those values previously chosen in the fixed-range terrain profile trade-off analyses (i.e. $\Delta R = 400m$, $\theta_s = 90^\circ$). The range limit was chosen to be 5Km to be compatible with the previous analysis of a system using fixed-range terrain profiles so comparisons could be made. Vehicle altitudes considered included 100m and 500m above the maximum terrain height beneath the flight path for flights above the majority of the terrain and reasonable heights above the valley floor for valley flights. Random horizon errors and vehicle

altitude errors were introduced to assess their impact on system performance and thus to determine their maximum allowable values. The analysis procedures used were identical to those previously used in analyzing a system using fixed-range terrain profiles. Some changes were made in the format used for the results to more clearly and concisely indicate system performance.

System performance was determined in terms of: (1) the maximum allowable random horizon error standard deviation, σ_{NM} , (2) the maximum allowable vehicle altitude error, σ_{HM} , (3) the along-track position determination error standard deviation, σ_x , (4) the cross-track position determination error standard deviation, σ_y , (5) the position determination circular error probable, CEP, and (6) the heading determination error standard deviation, σ_θ . Performance results were determined first for a system with no altitude error (i.e. no discrepancy between actual and planned vehicle altitude) and are summarized first.

The maximum allowable random horizon errors which give a probability of false alarm of less than 0.001 and a probability of detection of greater than 0.99 for flights above the majority of the surrounding terrain was determined to be greater than 0.1° for horizons with standard deviation, σ_p , greater than 1.1° . For relatively smooth terrain (σ_p approx. 0.2° or 0.3°) the maximum allowable random horizon error is quite small and precludes practical system operation. The maximum allowable random horizon error increases rapidly (from approx. 0.1° to approx. 0.4°) as the horizon standard deviation increases from 1° to 2° . It was considerably less for the valley flights (0.1° at $\sigma_p = 1.5^\circ$) and increases less rapidly with increasing horizon standard deviation.

The checkpoint position determination accuracy was analyzed and, except for relatively smooth terrain, gave a CEP of approximately 125m for flights above the majority of the surrounding terrain if the random horizon error was limited to be the smaller of the maximum allowable value or 0.25° . For the valley flights, the CEP is approximately 200m when the maximum allowable random horizon error is encountered. It should be noted that no interpolation between horizon comparison function points (200m spacing along-track and 400m spacing cross-track) was used so a large portion of the position error encountered is due to discrete match point quantization. Position performance could be improved by using interpolation.

The heading determination standard deviation obtained is approximately 1.75° to 2° for all cases without random horizon errors. Random horizon errors only have minimal effect on heading determination for flights above the majority of the surrounding terrain but increase the heading determination standard deviation to approximately 2.5° to 3° when maximum allowable values are considered for valley flights. Heading determination accuracy could be improved with interpolation and multiple measurements.

Comparisons of system performance with that previously obtained for a system using fixed-range terrain profiles were considered for a vehicle altitude of 500m above the maximum terrain height beneath the flight path. Results indicate little performance difference as expected.

If the vehicle is not flying at the planned altitude for which reference horizons were generated, then reference and sensed horizon differences result. The effect of such altitude errors was analyzed. They produce little position or heading determination performance degradation in most cases if held within practical limits. They do reduce the maximum allowable random horizon error. For reasonable maximum random horizon errors, it was determined that altitude errors of +100m or greater could be tolerated in most cases. A couple of cases were exceptions where the maximum altitude errors which could be tolerated were in the neighborhood of 40m to 50m.

The system analyses indicated above were performed with two radar sensor idealizations. These were: (1) horizons were obtained from a stationary viewing location, and (2) the radar azimuth beamwidth was infinitesimal. It was felt that these idealizations would not greatly affect the system feasibility and performance results. Analyses were performed with selected analysis cases to verify this conjecture and to provide a determination of radar azimuth beamwidth requirements.

The analysis of the effect of non-stationary horizon viewing locations was performed by using an assumed vehicle velocity of 260m/sec and a one direction radar scan time of 0.75 sec. Results indicate that system performance is basically the same as determined for horizons from stationary viewing locations as long as reference horizons are generated for moving viewing locations determined by the planned vehicle velocity and sensor scan rate.

The analysis of the effect of a finite sensor beamwidth was performed by developing a suitable system model and considering sensor beamwidths from 0° to 4° . Cases were considered for several terrain roughnesses and for reference horizons generated with either the sensor beamwidth or a beamwidth of 0° . Results indicate that system performance is basically the same as determined for horizons generated with sensor beamwidths of 0° . Performance results were not greatly different between cases where the reference horizons were generated with the sensor beamwidth and cases where the reference horizons were generated with a beamwidth of 0° . Therefore, reference horizon generation does not need to consider sensor beamwidth which provides generation simplification in a practical case. Sensor beamwidths of 2° are certainly feasible and 4° sensor beamwidths are probably usable. Sensor beamwidths of 2° or 4° would reduce the antenna length requirement defined in Ref. 1 (0.9m) to 0.45m or 0.225m respectively.

REFERENCES

1. G. E. Carlson, G. L. Bair, and C. M. Benoit, "Forward-Sensed Terrain Profile Comparison for Aircraft Geographic Orientation", University of Missouri-Rolla, Electrical Engineering Communication Sciences Report, CSR-76-3, March 1976.
2. G. E. Carlson, G. L. Bair, and C. M. Benoit, "Geographic Orientation for Low-Altitude Aircraft Using Horizon Matching", University of Missouri-Rolla, Electrical Engineering Communication Sciences Report, CSR-75-3, April 1975.
3. C. F. O'Donnell, Inertial Navigation, Analysis and Design. New York, N.Y.: McGraw-Hill Book Co. Inc., 1964.

PRECEDING PAGE BLANK NOT FILMED

APPENDIX A

TABULATED POSITION AND HEADING
ERROR RESULTS FOR ZERO
ALTITUDE ERROR

PRECEDING PAGE BLANK NOT FILMED

Case #	ΔH (m)	σ_N (deg)	σ_x (m)	σ_y (m)	CEP (m)	σ_θ (deg)
	H_A					
1 100m	0	0.000	100.8	121.8	131.0	1.80
		0.125	174.1	212.1	227.4	3.35
		0.250	415.6	380.2	468.5	5.97
		0.500	588.8	515.4	650.0	6.74
		1.000	539.4	389.4	546.8	5.86
2 200m	0	0.000	56.8	150.3	121.9	1.94
		0.125	91.4	174.1	156.3	2.29
		0.250	194.7	317.2	301.4	3.99
		0.500	394.7	374.8	453.0	4.88
		1.000	582.0	439.9	601.6	4.72
3 300m	0	0.000	60.9	113.6	102.7	1.61
		0.125	60.9	118.5	105.6	1.64
		0.250	93.1	199.6	172.3	2.69
		0.500	219.1	278.2	292.8	3.79
		1.000	284.5	415.6	412.1	5.43
4 100m	0	0.000	56.8	113.6	100.3	1.56
		0.125	538.7	450.8	582.5	6.40
		0.250	602.1	520.5	660.9	5.97
		0.500	599.5	577.0	692.6	6.42
		1.000	652.0	607.3	741.3	6.27
5 100m	0	0.000	56.8	134.4	112.6	1.80
		0.125	60.9	161.1	130.7	1.98
		0.250	98.2	309.0	239.7	3.63
		0.500	171.8	354.7	310.0	4.10
		1.000	450.1	396.6	498.5	5.44
6 100m	0	0.000	56.8	132.0	111.1	1.75
		0.125	56.8	134.4	112.6	1.76
		0.250	60.9	171.8	137.0	2.12
		0.500	91.6	220.0	183.4	2.49
		1.000	240.2	369.0	358.6	4.61
7 100m	0	0.000	56.8	132.0	111.1	1.50
		0.125	56.8	133.8	112.2	1.52
		0.250	56.8	168.0	132.3	1.82
		0.500	83.3	304.5	228.3	3.39
		1.000	132.0	447.9	341.4	4.67
4 500m	0	0.000	59.2	123.8	107.7	1.56
		0.125	364.5	476.4	495.0	6.24
		0.250	523.0	512.9	609.8	6.11
		0.500	575.8	561.1	669.3	6.22
		1.000	666.1	623.2	762.0	6.08

Case #	ΔH	σ_N	σ_x	σ_y	CEP	σ_θ
	(m)	(deg)	(m)	(m)	(m)	(deg)
5 500m	0	0.000	56.8	143.1	117.7	1.78
		0.125	56.8	189.7	145.1	2.09
		0.250	133.8	367.9	295.4	3.95
		0.500	332.9	554.0	522.1	5.67
		1.000	392.2	532.2	544.2	5.57
6 500m	0	0.000	56.8	118.5	103.2	1.64
		0.125	59.2	118.5	104.6	1.62
		0.250	60.9	123.8	108.7	1.61
		0.500	80.1	128.9	123.0	1.69
		1.000	174.9	359.0	314.3	4.07
7 500m	0	0.000	56.8	118.5	103.2	1.37
		0.125	56.8	124.4	106.7	1.44
		0.250	56.8	132.0	111.1	1.44
		0.500	73.8	291.8	215.2	3.37
		1.000	157.5	427.9	344.6	4.73

APPENDIX B

**DETECTION THRESHOLD NEEDED
TO GIVE $P_D=0.99$ FOR VARIOUS
VEHICLE ALTITUDE ERRORS**

PRECEDING PAGE BLANK NOT FILMED

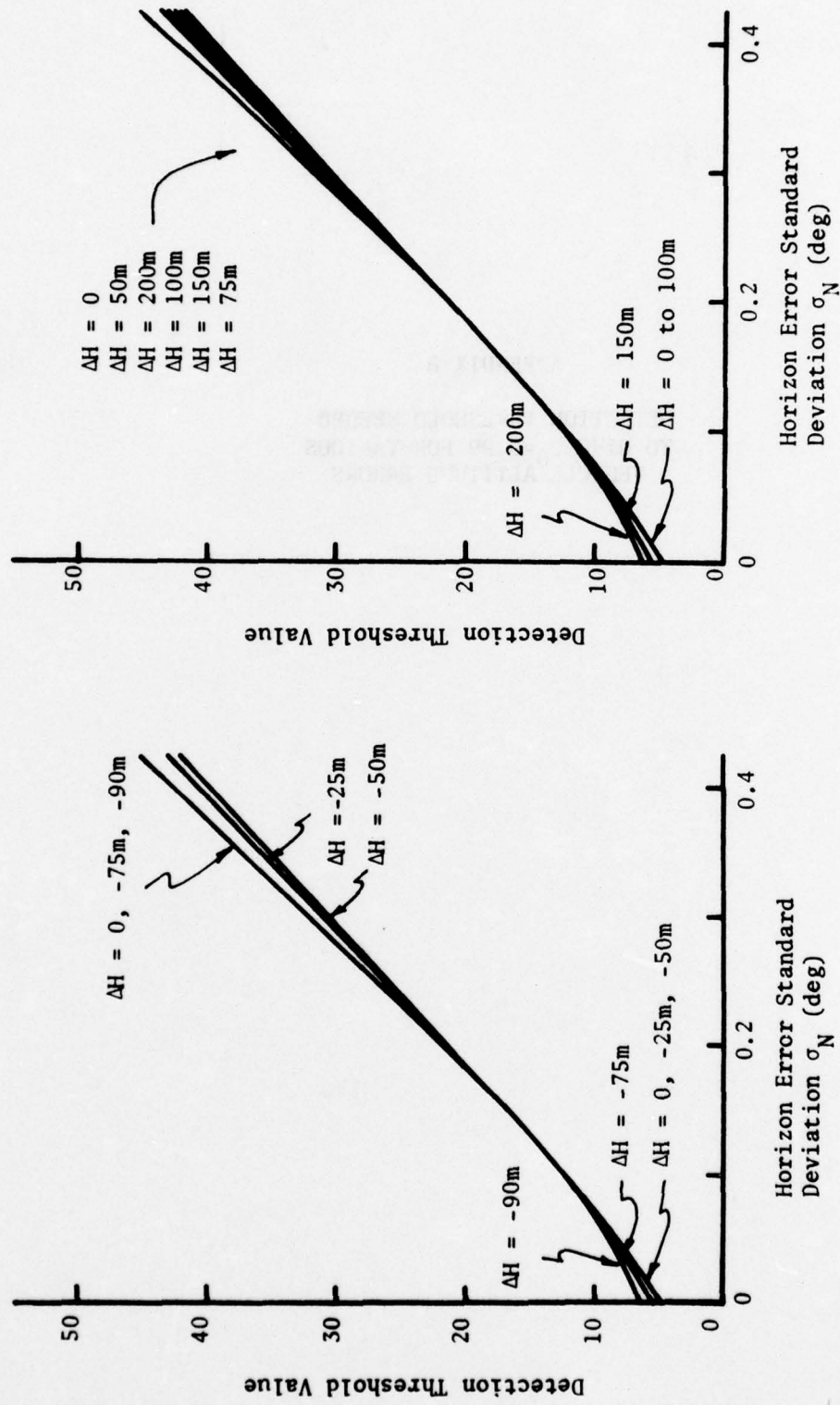


Fig. B1. Detection Threshold Needed to Give $P_D = 0.99$ (Case 1).

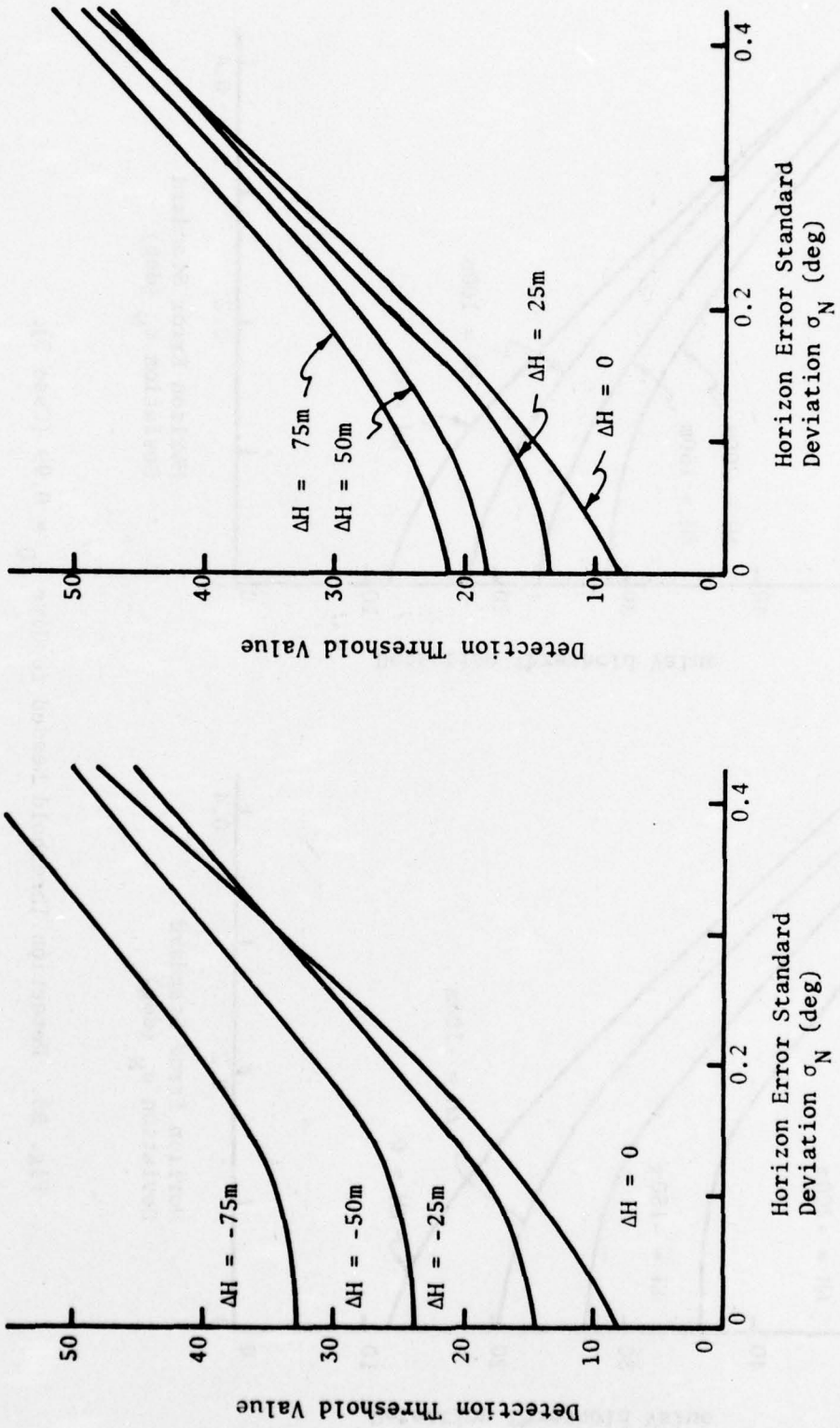


Fig. B2. Detection Threshold Needed to Give $P_D = 0.99$ (Case 2).

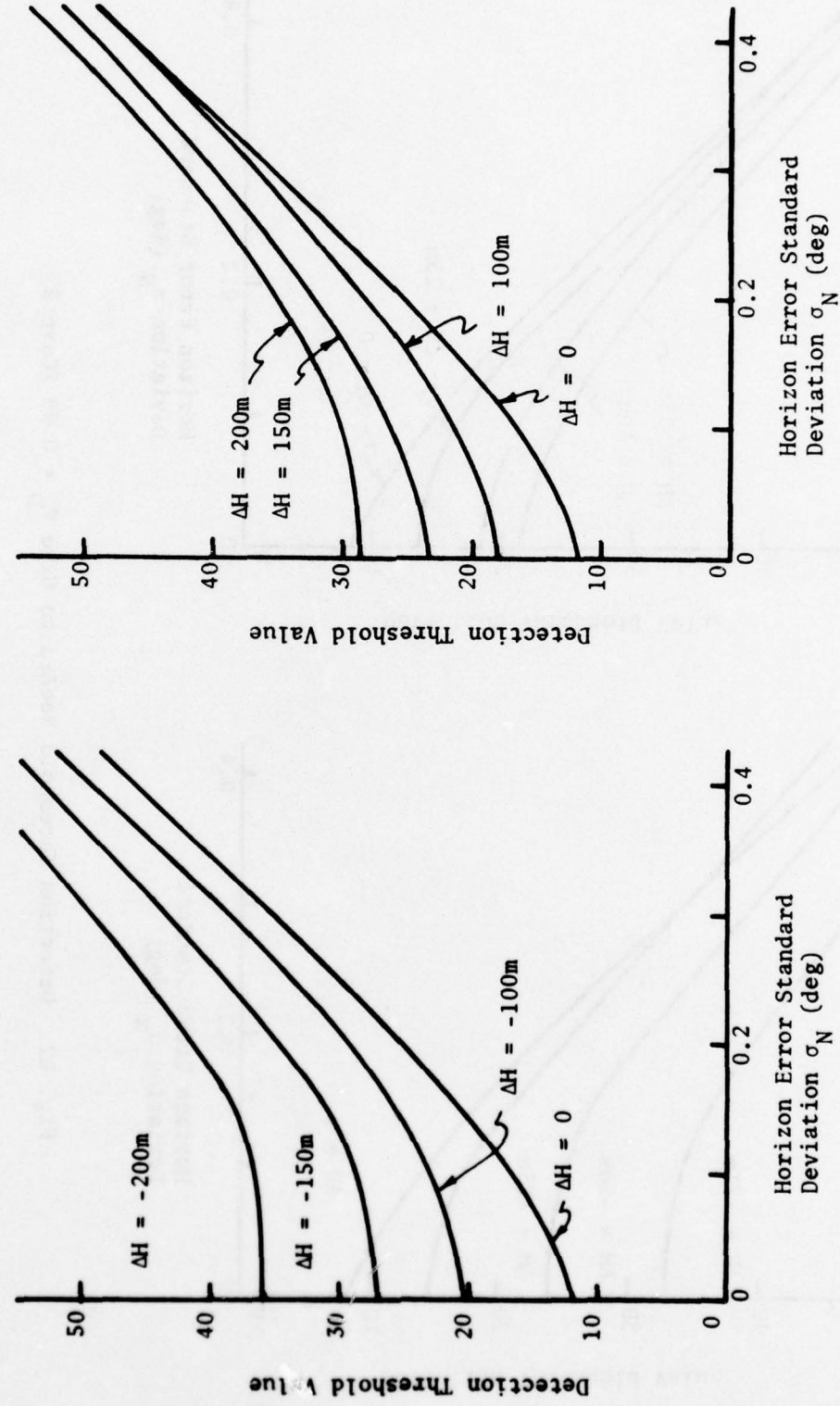


Fig. B3. Detection Threshold Needed to Give $P_D = 0.99$ (Case 3).

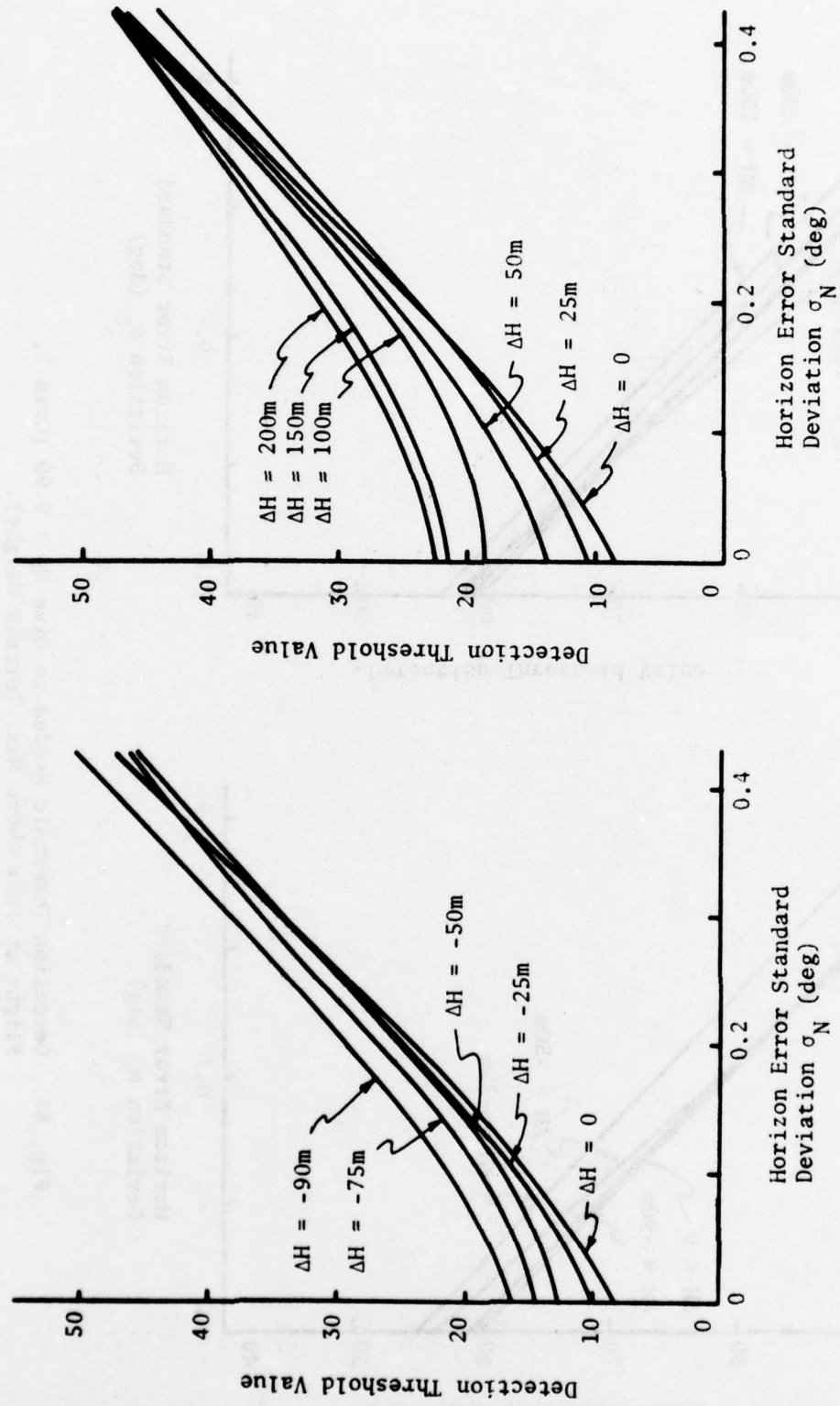


Fig. B4. Detection Threshold Needed to Give $P_D = 0.99$ (Case 5,
Flight at 100m Above Max. Terrain Height).

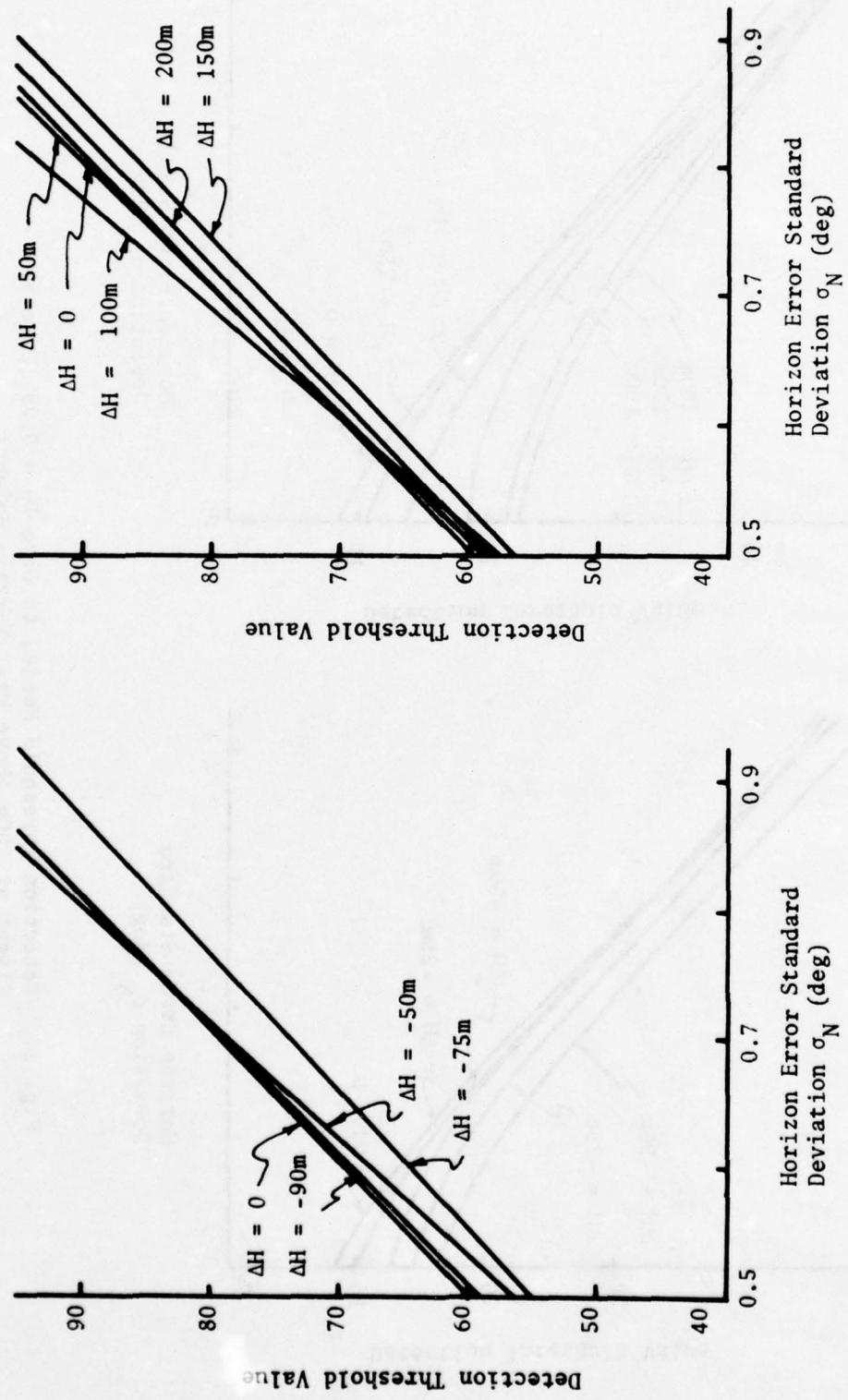


Fig. B5. Detection Threshold Needed to Give $P_D = 0.99$ (Case 7,
Flight at 100m Above Max. Terrain Height).

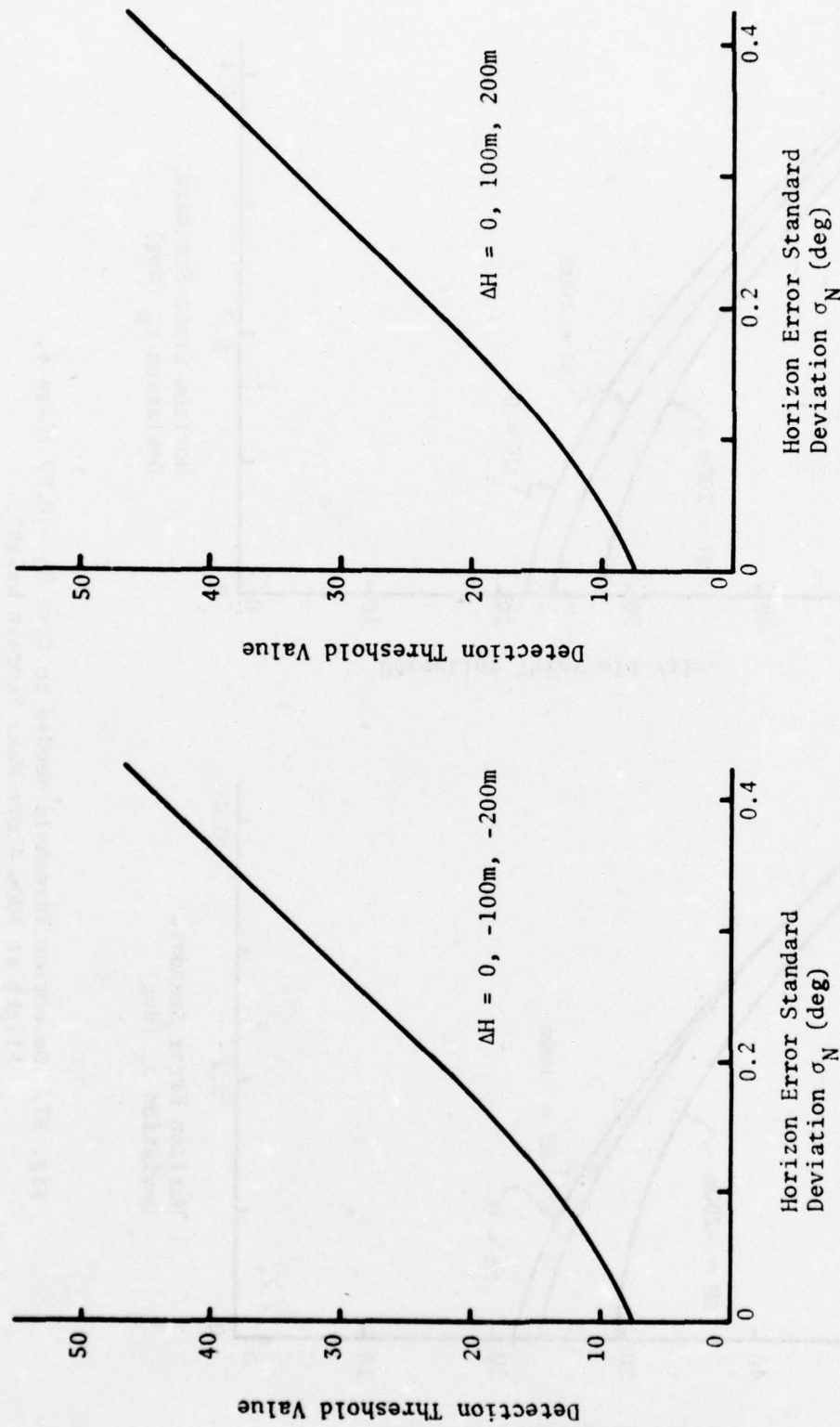


Fig. B6. Detection Threshold Needed to Give $P_D = 0.99$ (Case 5,
Flight at 500m Above Max. Terrain Height).

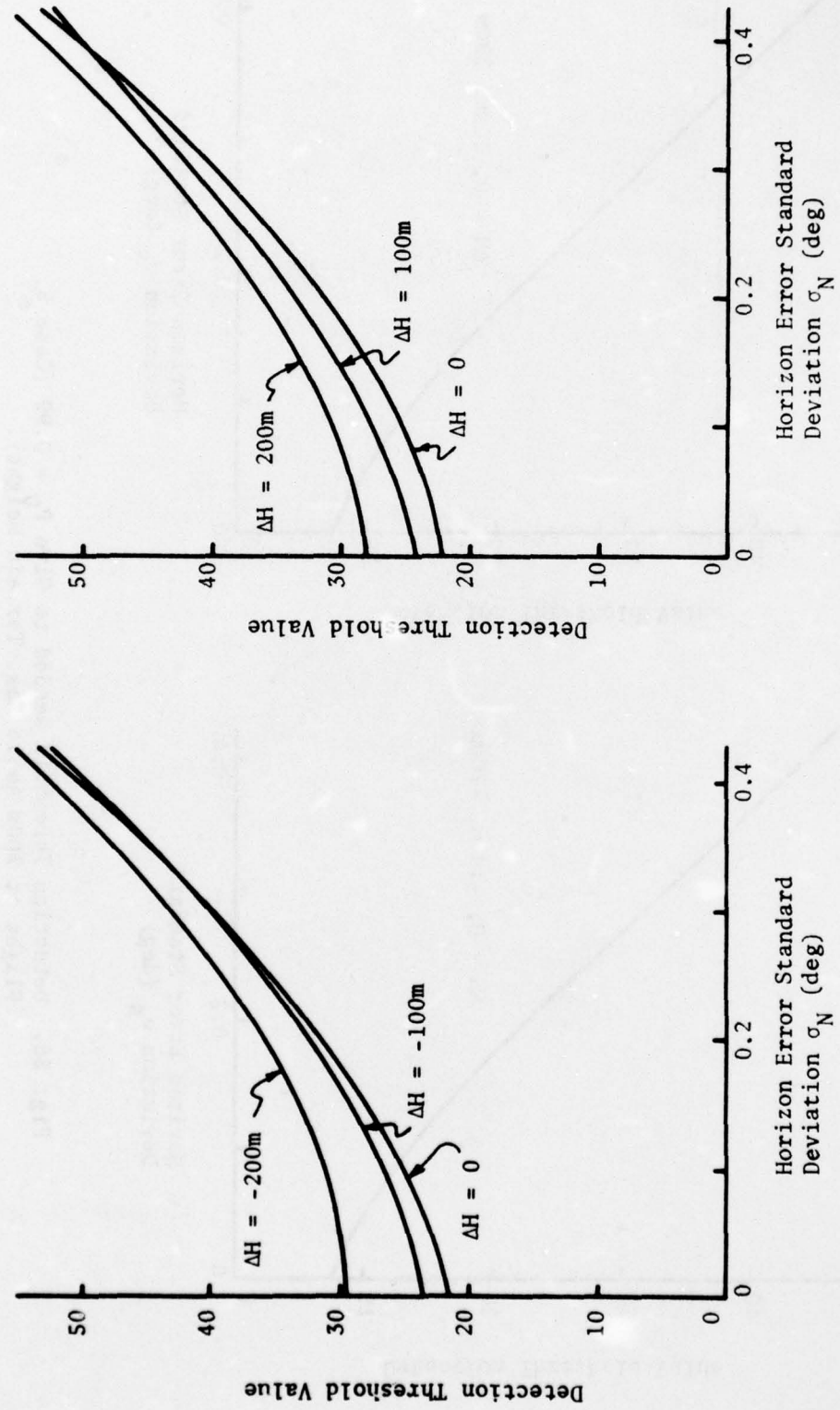


Fig. B7. Detection Threshold Needed to Give $P_D = 0.99$ (Case 6,
Flight at 500m Above Max. Terrain Height).

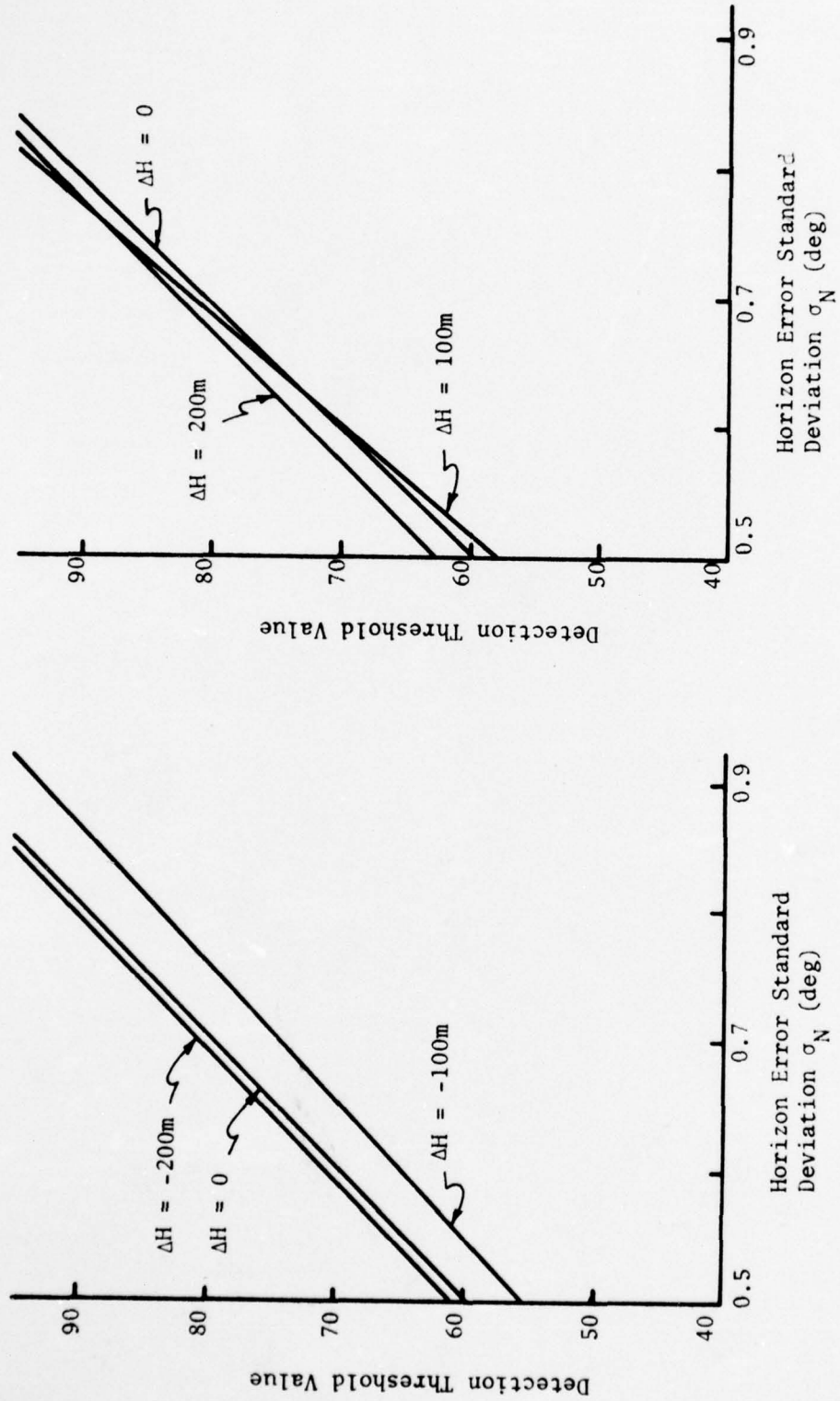
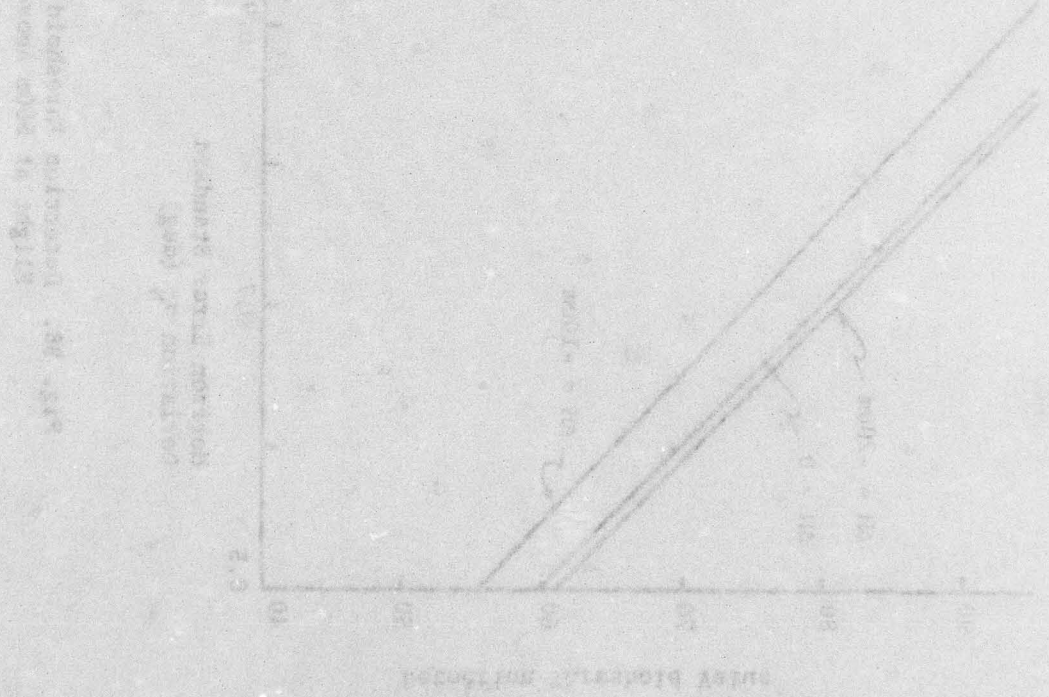
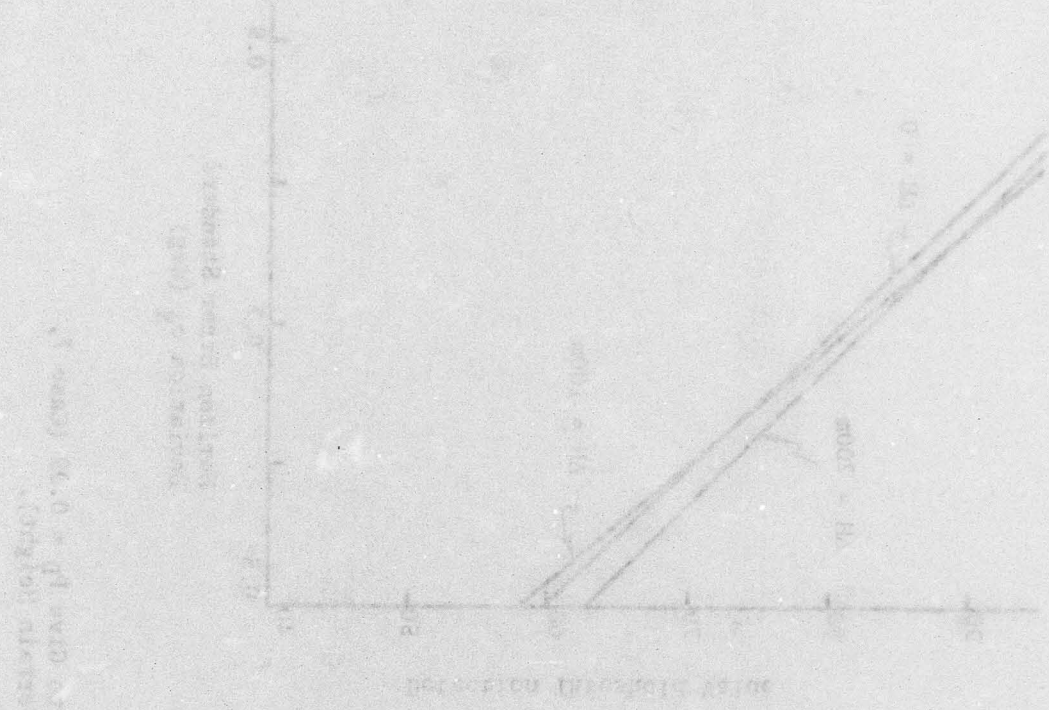


Fig. B8. Detection Threshold Needed to Give $P_D = 0.99$ (Case 7,
Flight at 500m Above Max. Terrain Height).



APPENDIX C

**TABULATED POSITION AND HEADING
ERROR RESULTS FOR NONZERO
ALTITUDE ERROR**

Case #	ΔH	σ_N (deg)	σ_x (m)	σ_y (m)	CEP (m)	σ_θ (deg)
H_A	(m)					
1 100m	-90	0.000	217.7	190.1	240.1	2.88
		0.125	255.8	280.3	315.6	4.35
		0.250	415.0	376.5	466.0	5.81
		0.500	718.2	483.1	707.2	6.53
		1.000	605.8	410.9	598.5	5.74
1 100m	-75	0.000	123.8	151.9	300.1	2.25
		0.125	241.5	259.0	294.6	3.95
		0.250	401.4	375.9	457.6	5.71
		0.500	745.5	453.7	706.1	6.10
		1.000	575.5	386.0	566.0	5.61
1 100m	-50	0.000	104.7	121.8	133.3	1.79
		0.125	379.9	323.0	413.8	4.70
		0.250	226.8	386.7	361.2	6.18
		0.500	507.2	352.0	505.8	5.79
		1.000	408.0	408.8	480.9	6.35
1 100m	-25	0.000	98.3	121.8	121.6	1.79
		0.125	251.4	261.2	301.8	4.13
		0.250	476.5	379.3	503.8	5.77
		0.500	471.8	351.0	484.4	5.86
		1.000	526.6	439.2	568.6	6.88
1 100m	25	0.000	91.3	121.8	125.5	1.79
		0.125	140.8	242.3	225.5	3.81
		0.250	376.7	325.3	413.3	4.98
		0.500	415.0	352.0	451.5	5.46
		1.000	511.1	510.5	601.4	6.94
1 100m	50	0.000	95.0	124.4	129.1	1.88
		0.125	119.1	160.6	164.7	2.34
		0.250	401.6	390.0	466.0	5.82
		0.500	482.2	392.7	515.1	5.86
		1.000	533.4	500.3	608.5	6.48
1 100m	75	0.000	95.0	124.4	129.2	1.88
		0.125	112.0	188.4	118.0	3.25
		0.250	354.6	375.9	430.0	5.76
		0.500	559.3	537.5	645.7	6.99
		1.000	606.4	466.8	631.8	6.59
1 100m	100	0.000	94.2	123.8	128.3	1.90
		0.125	129.4	206.0	197.4	3.38
		0.250	372.4	304.5	398.5	4.68
		0.500	353.6	347.3	412.6	5.74
		1.000	589.0	462.1	618.8	6.53

Case #	ΔH	σ_N (deg)	σ_x (m)	σ_y (m)	CEP	σ_θ (deg)
	H_A	(m)			(m)	
1 100m	150	0.000	98.2	121.8	121.5	1.90
		0.125	297.3	282.6	341.4	4.32
		0.250	214.7	403.2	363.8	6.28
		0.500	526.4	347.3	514.3	5.65
		1.000	386.0	390.2	456.9	6.47
1 100m	200	0.000	104.5	128.9	137.4	1.98
		0.125	146.9	202.8	205.9	3.37
		0.250	384.7	402.4	463.4	5.90
		0.500	363.2	362.8	427.4	6.05
		1.000	462.4	444.1	533.7	6.80
2 200m	-75	0.000	93.1	151.9	144.0	1.94
		0.125	94.2	267.6	213.0	3.35
		0.250	186.7	323.0	300.0	4.13
		0.500	207.0	371.0	340.3	4.80
		1.000	477.2	462.8	571.0	5.46
2 200m	-50	0.000	89.6	128.9	128.6	1.61
		0.125	117.6	124.4	142.5	1.70
		0.250	156.5	295.1	265.9	3.72
		0.500	303.5	355.6	388.0	4.70
		1.000	393.9	444.1	493.3	5.96
2 200m	-25	0.000	69.3	133.8	119.6	1.71
		0.125	87.8	182.7	159.2	2.46
		0.250	116.2	289.3	238.7	3.69
		0.500	250.1	375.9	368.5	4.75
		1.000	469.7	406.4	515.8	4.66
2 200m	25	0.000	56.8	196.7	149.2	2.43
		0.125	94.1	268.8	213.6	3.36
		0.250	221.1	280.3	295.2	3.57
		0.500	408.3	484.4	525.5	5.94
		1.000	554.1	395.9	559.3	5.40
2 200m	50	0.000	87.1	242.3	193.9	2.82
		0.125	110.5	238.3	205.3	2.77
		0.250	143.5	329.0	278.2	4.1
		0.500	281.7	386.7	393.5	4.77
		1.000	569.7	540.0	653.3	6.71
2 200m	75	0.000	162.6	212.1	220.6	2.44
		0.125	133.8	299.5	255.1	3.62
		0.250	408.7	596.2	591.6	7.25
		0.500	475.2	524.1	588.3	6.33
		1.000	492.3	514.9	592.9	6.09

Case #	ΔH	σ_N (deg)	σ_x (m)	σ_y (m)	CEP	σ_θ (deg)
H_A	(m)				(m)	
3 300m	-200	0.000	139.0	132.0	159.5	1.84
		0.125	116.4	133.8	147.3	2.03
		0.250	126.4	226.8	207.9	3.18
		0.500	450.0	398.2	499.3	5.75
		1.000	436.6	378.2		5.47
3 300m	-150	0.000	99.8	124.4	479.7	1.79
		0.125	116.2	133.8	147.2	1.85
		0.250	101.4	214.0	185.7	3.01
		0.500	484.6	344.3	488.0	5.13
		1.000	365.8	389.4	444.6	5.54
3 300m	-100	0.000	70.7	141.1	124.7	2.02
		0.125	70.7	123.8	124.9	1.73
		0.250	121.6	181.4	178.4	2.51
		0.500	290.6	336.0	368.9	4.75
		1.000	320.0	383.3	402.3	5.17
3 300m	100	0.000	61.9	160.6	75.8	2.24
		0.125	66.9	150.3	127.9	2.03
		0.250	87.1	160.6	145.8	2.22
		0.500	177.8	291.5	276.3	4.09
		1.000	154.4	369.0	308.1	4.79
3 200m	150	0.000	59.2	160.1	129.1	2.21
		0.125	75.1	160.6	138.8	2.19
		0.250	93.1	158.6	148.2	2.15
		0.500	160.5	306.6	275.0	4.24
		1.000	156.1	366.3	307.5	4.71
3 300m	200	0.000	60.9	168.5	135.0	2.29
		0.125	70.7	176.0	145.2	2.42
		0.250	190.1	207.9	234.3	2.85
		0.500	151.2	284.8	256.7	3.84
		1.000	379.1	376.5	444.8	4.98
5 100m	-90	0.000	71.8	236.9	181.7	2.63
		0.125	85.9	237.9	190.6	2.69
		0.250	143.7	312.9	268.8	3.45
		0.500	243.3	328.2	336.4	3.92
		1.000	308.7	426.3	432.7	5.33
5 100m	-75	0.000	62.2	218.1	165.0	2.41
		0.125	83.3	240.6	190.7	2.62
		0.250	128.1	278.2	239.2	3.04
		0.500	177.3	304.8	283.8	3.59
		1.000	193.0	497.7	406.6	6.04

Case #	ΔH	σ_N (deg)	σ_x (m)	σ_y (m)	CEP	σ_θ (deg)
H_A	(m)				(m)	
5 100m	-50	0.000	61.9	168.0	135.3	1.97
		0.125	73.8	196.7	159.2	2.47
		0.250	139.0	235.2	220.3	2.84
		0.500	294.0	390.2	402.8	4.77
		1.000	479.9	492.4	572.4	5.64
5 100m	-25	0.000	60.9	141.4	119.1	1.70
		0.125	60.9	189.7	147.5	2.41
		0.250	101.4	280.3	224.7	3.22
		0.500	195.0	347.3	319.3	4.06
		1.000	437.0	391.6	487.8	5.37
5 100m	25	0.000	59.2	121.8	106.6	1.59
		0.125	61.9	166.6	134.5	2.14
		0.250	94.8	327.0	248.3	3.79
		0.500	119.1	323.0	260.3	3.90
		1.000	180.9	473.7	385.4	5.49
5 100m	50	0.000	56.8	138.5	115.0	1.72
		0.125	61.9	141.4	119.7	1.72
		0.250	84.0	273.3	210.3	3.48
		0.500	453.5	389.4	496.2	3.73
		1.000	409.1	512.4	542.5	5.63
5 100m	100	0.000	66.9	171.8	140.5	2.24
		0.125	75.1	158.6	137.6	1.95
		0.250	87.8	257.8	203.5	3.33
		0.500	171.8	430.3	354.5	4.87
		1.000	244.2	517.9	448.6	5.71
5 100m	150	0.000	76.2	201.6	163.5	2.65
		0.125	67.2	221.4	169.9	2.56
		0.250	87.1	291.8	223.1	3.64
		0.500	191.3	369.8	330.3	4.04
		1.000	613.0	532.6	674.4	4.80
5 100m	200	0.000	70.7	221.4	172.0	2.89
		0.125	66.0	254.0	188.4	3.05
		0.250	79.3	365.4	261.8	4.09
		0.500	272.3	337.0	358.7	3.78
		1.000	614.6	640.4	738.8	5.40
6 100m	-90	0.000	62.2	124.4	109.9	1.69
		0.125	60.9	143.1	120.1	1.85
		0.250	60.9	143.1	120.1	1.84
		0.500	110.7	267.6	222.7	3.20
		1.000	146.9	351.0	293.1	4.41

Case #	ΔH (m)	σ_N (deg)	σ_x (m)	σ_y (m)	CEP (m)	σ_θ (deg)
H_A						
6 100m	-75	0.000	56.8	133.8	112.2	1.74
		0.125	60.9	121.8	107.6	1.63
		0.250	61.9	128.9	112.3	1.63
		0.500	70.7	248.9	188.1	2.99
		1.000	95.0	362.6	269.4	4.50
6 100m	-50	0.000	56.8	124.4	106.7	1.69
		0.125	59.2	147.6	129.4	1.90
		0.250	64.5	168.5	137.2	2.12
		0.500	84.0	220.0	179.0	2.80
		1.000	116.4	388.3	297.1	4.56
6 100m	50	0.000	56.8	147.6	120.3	1.91
		0.125	59.2	160.6	129.4	2.02
		0.250	62.2	168.5	135.8	2.09
		0.500	127.0	293.8	247.7	3.58
		1.000	140.8	386.0	310.0	4.95
6 100m	100	0.000	61.9	152.4	126.2	1.93
		0.125	59.2	152.4	124.6	1.95
		0.250	60.9	168.0	134.8	2.12
		0.500	88.0	284.8	219.5	3.48
		1.000	146.9	425.0	336.7	5.06
6 100m	150	0.000	60.9	143.7	120.4	1.83
		0.125	59.2	133.8	113.6	1.75
		0.250	66.9	175.5	142.7	2.20
		0.500	75.9	209.1	167.8	2.56
		1.000	115.7	428.0	320.1	5.05
6 100m	200	0.000	61.9	141.4	119.7	1.80
		0.125	62.2	156.1	128.5	1.94
		0.250	70.7	156.1	133.5	1.86
		0.500	119.1	308.7	251.8	3.89
		1.000	222.9	289.3	301.5	3.78
7 100m	-90	0.000	56.8	128.9	109.3	1.38
		0.125	56.8	128.9	109.3	1.52
		0.250	56.8	179.2	138.9	1.96
		0.500	71.6	336.7	240.4	3.65
		1.000	135.5	445.8	342.2	4.65
7 100m	-75	0.000	56.8	132.0	111.1	1.41
		0.125	56.8	141.4	116.7	1.59
		0.250	61.9	168.5	135.6	1.82
		0.500	71.8	238.3	182.6	2.60
		1.000	112.9	412.7	309.4	4.80

Case #	ΔH	σ_N	σ_x	σ_y	CEP	σ_θ
		(deg)	(m)	(m)	(m)	(deg)
7 100m	-50	0.000	56.8	132.0	111.1	1.41
		0.125	59.2	124.4	108.1	1.44
		0.250	64.5	143.7	122.6	1.59
		0.500	75.1	226.8	177.7	2.55
		1.000	132.0	479.1	359.8	5.13
7 100m	50	0.000	56.8	128.9	109.3	1.43
		0.125	56.8	138.5	115.0	1.53
		0.250	56.8	186.2	143.1	2.04
		0.500	93.1	282.8	221.3	3.00
		1.000	166.1	462.1	369.8	5.09
7 100m	100	0.000	56.8	118.5	103.2	1.27
		0.125	56.8	132.0	111.1	1.43
		0.250	56.8	168.0	132.3	1.80
		0.500	87.1	267.6	208.8	2.95
		1.000	135.4	473.1	358.2	5.09
7 100m	150	0.000	56.8	124.4	106.7	1.32
		0.125	56.8	124.4	106.7	1.38
		0.250	59.2	143.7	119.4	1.56
		0.500	66.0	215.2	165.5	2.21
		1.000	128.8	435.3	332.1	5.07
7 100m	200	0.000	56.8	128.9	109.3	1.37
		0.125	56.8	124.4	106.7	1.24
		0.250	60.9	193.0	149.5	2.04
		0.500	80.1	272.4	207.5	3.12
		1.000	147.6	293.9	259.9	3.55
5 500m	-200	0.000	56.8	143.7	118.0	1.74
		0.125	56.8	182.7	141.0	2.01
		0.250	131.8	357.2	287.9	3.94
		0.500	268.5	519.9	464.1	5.27
		1.000	355.6	501.4	504.5	5.47
5 500m	-100	0.000	58.8	138.5	115.0	1.77
		0.125	73.8	257.8	195.2	2.78
		0.250	227.1	391.6	364.2	3.75
		0.500	272.9	470.9	420.2	5.05
		1.000	244.9	505.5	441.8	5.17
5 500m	100	0.000	60.9	132.0	113.6	1.70
		0.125	66.0	189.7	150.5	2.08
		0.250	165.5	366.1	313.0	4.20
		0.500	335.0	495.0	488.6	5.64
		1.000	268.1	527.8	468.5	6.21

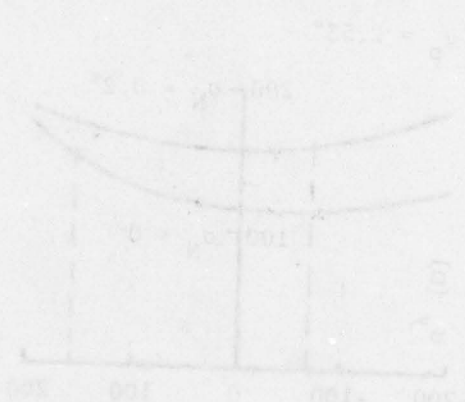
Case #	ΔH	σ_N (deg)	σ_x (m)	σ_y (m)	CEP	σ_θ (deg)
H_A	(m)				(m)	
5 500m	200	0.000	60.9	132.0	113.6	1.60
		0.125	66.0	226.8	172.4	2.42
		0.250	119.1	304.5	249.4	3.16
		0.500	278.2	487.1	450.5	5.52
		1.000	555.0	579.1	667.6	5.45
6 500m	-200	0.000	64.5	118.5	107.7	1.61
		0.125	59.2	121.8	106.6	1.65
		0.250	60.9	118.5	105.6	1.52
		0.500	98.4	206.0	179.2	2.54
		1.000	138.5	263.7	236.8	3.24
6 500m	-100	0.000	62.2	121.8	108.3	1.67
		0.125	61.9	113.6	103.3	1.56
		0.250	60.9	124.4	109.1	1.64
		0.500	61.9	168.5	109.7	1.98
		1.000	113.4	336.7	265.0	3.95
6 500m	100	0.000	61.9	118.5	106.2	1.64
		0.125	59.2	118.5	104.6	1.62
		0.250	60.9	123.8	108.7	1.61
		0.500	80.1	128.9	123.0	1.69
		1.000	174.9	359.0	314.3	4.07
6 500m	200	0.000	66.9	118.5	109.1	1.63
		0.125	67.2	133.8	118.3	1.78
		0.250	69.3	133.8	119.6	1.70
		0.500	145.4	124.4	158.8	1.77
		1.000	184.9	232.4	245.7	2.94
7 500m	-200	0.000	56.8	124.4	106.7	1.45
		0.125	56.8	121.8	105.1	1.44
		0.250	60.9	150.3	124.3	1.62
		0.500	73.8	258.7	195.7	2.82
		1.000	133.0	432.4	332.9	4.63
7 500m	-100	0.000	56.8	123.8	106.3	1.45
		0.125	56.8	133.8	112.2	1.52
		0.250	62.2	132.0	114.3	1.52
		0.500	64.5	266.1	194.6	2.81
		1.000	107.8	399.2	298.5	4.54
7 500m	100	0.000	56.8	118.5	103.2	1.35
		0.125	60.9	121.8	107.6	1.31
		0.250	59.2	138.5	116.4	1.58
		0.500	71.8	189.7	153.9	2.03
		1.000	158.1	447.0	356.2	4.61

Case #	ΔH	σ_N	σ_x	σ_y	CEP	σ_θ
	(m)	(deg)	(m)	(m)	(m)	(deg)
7 500m	200	0.000	62.2	121.8	108.3	1.42
		0.125	62.2	121.8	108.3	1.29
		0.250	62.2	134.4	115.7	1.39
		0.500	62.2	215.5	163.5	2.39
		1.000	153.3	465.4	364.2	5.39

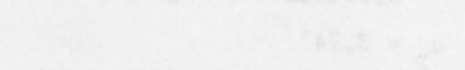
APPENDIX D

ALONG TRACK AND CROSS TRACK
POSITION ERRORS AS A
FUNCTION OF ALTITUDE ERROR

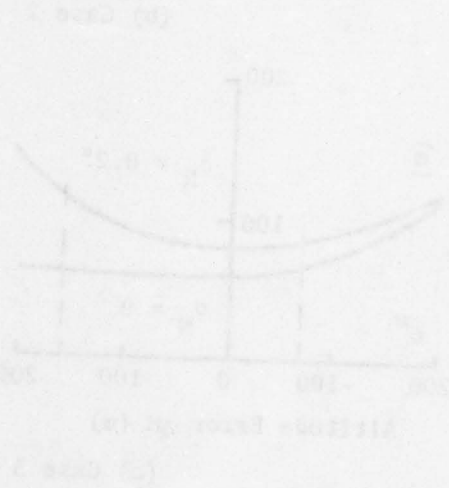
(a) 20 TOTAL ALTITUDE



(b) NO TOTAL ALTITUDE



(c) 10 TOTAL ALTITUDE



Y-axis: A transversal position correction has been applied to the along track velocity and result modified to match our error.

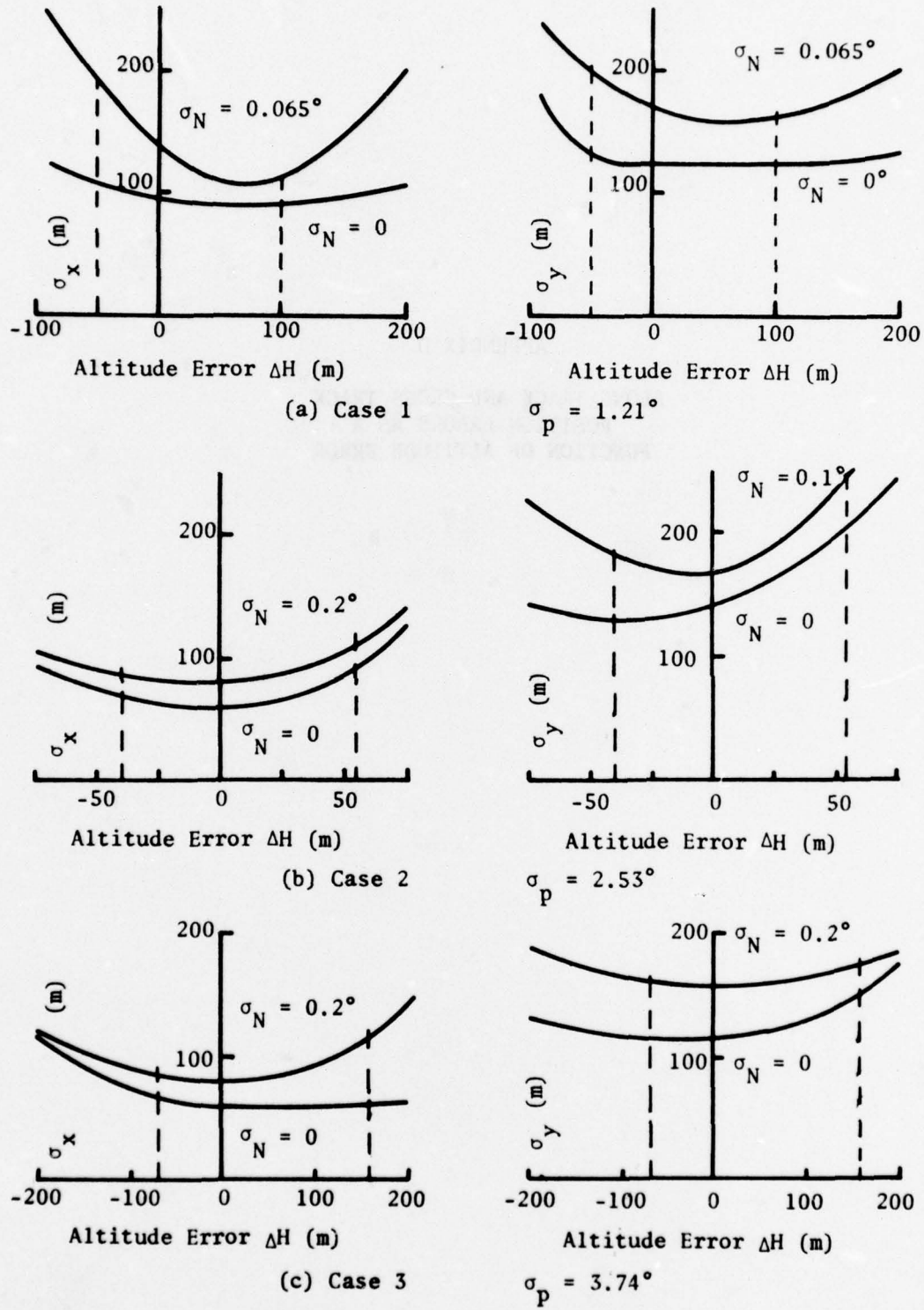


Fig. D1. Along-Track and Cross-Track Position Determination Accuracy as a Function of Altitude Error for Valley Flights.

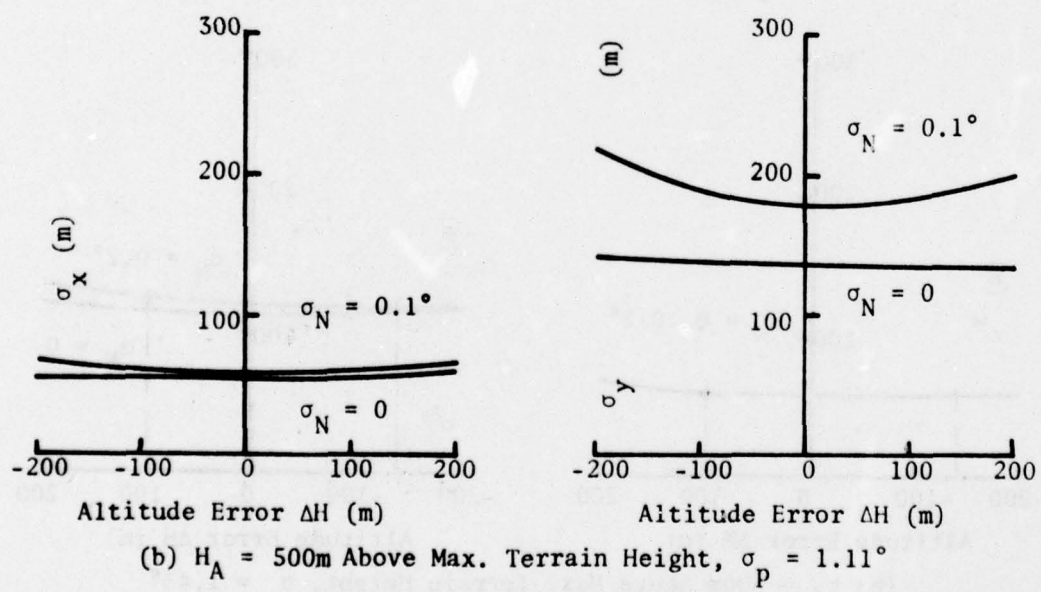
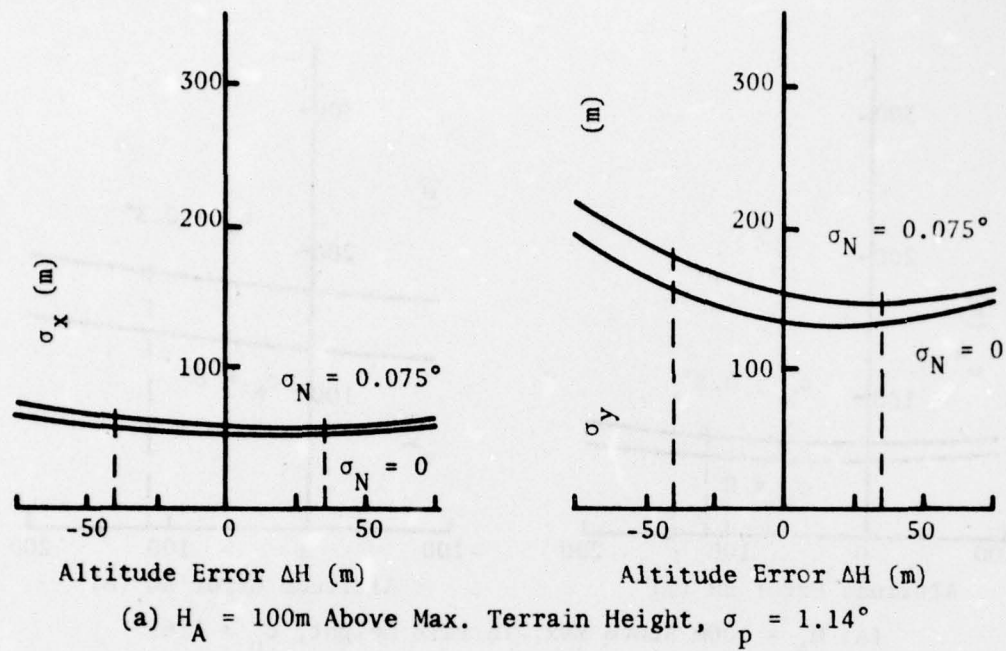


Fig. D2. Along-Track and Cross-Track Position Determination Accuracy as a Function of Altitude Error for Case 5.

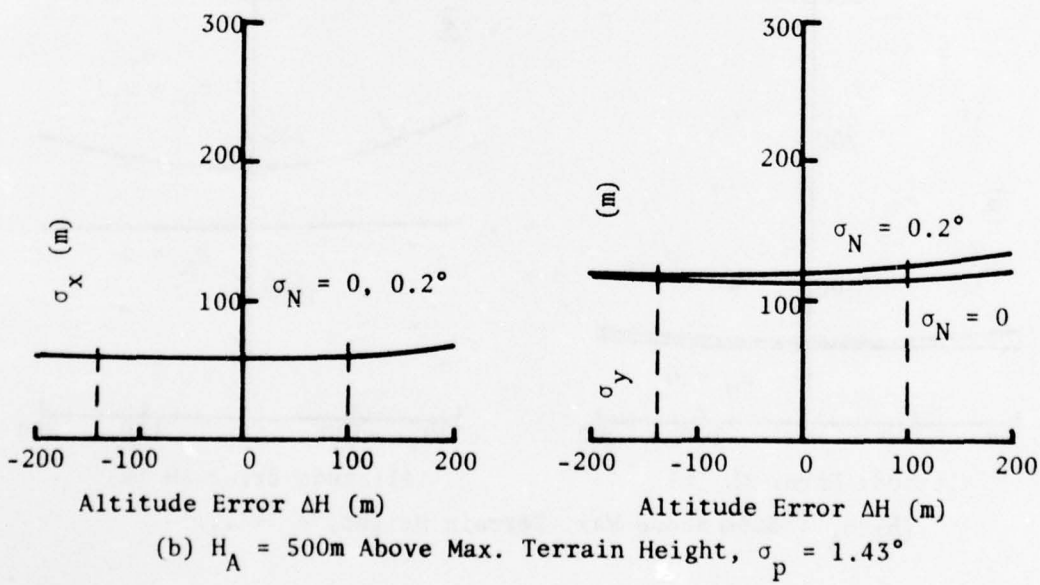
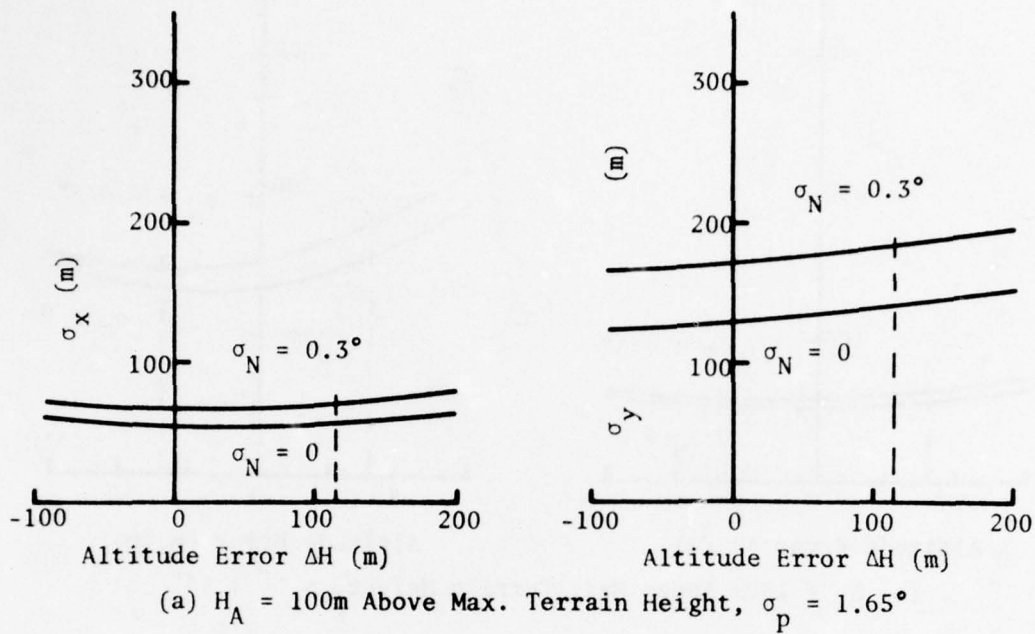


Fig. D3. Along-Track and Cross-Track Position Determination Accuracy as a Function of Altitude Error for Case 6.

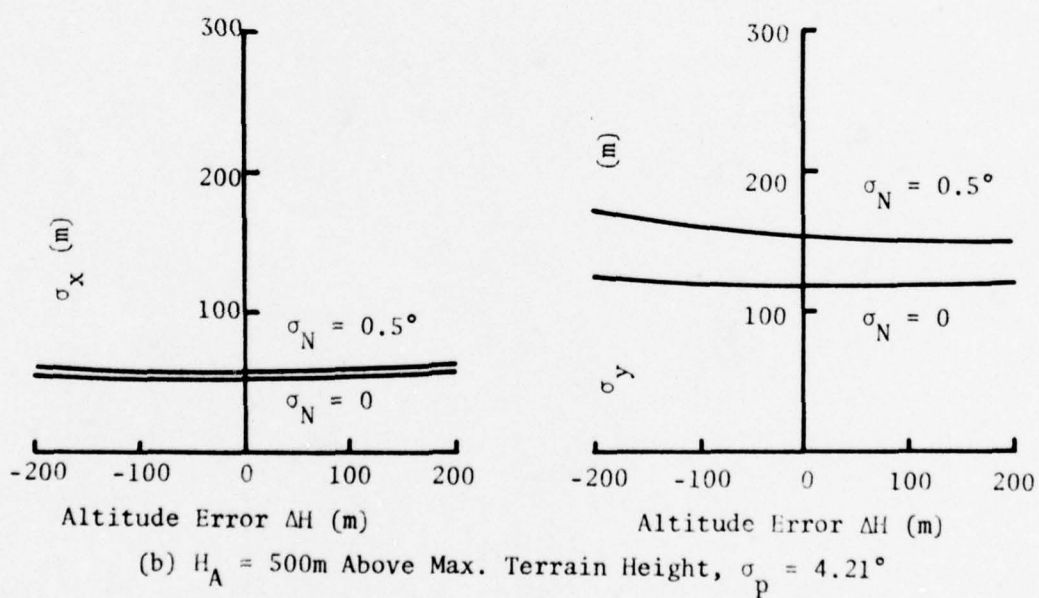
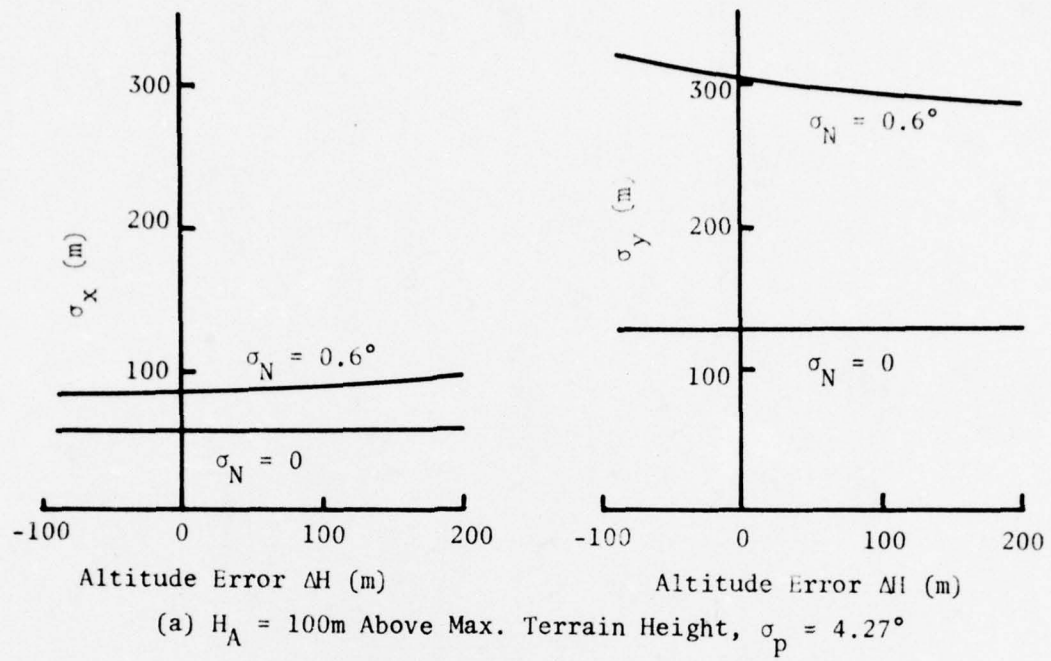


Fig. D4. Along-Track and Cross-Track Position Determination Accuracy as a Function of Altitude Error for Case 7.

(top) signal spectrum

APPENDIX E

ADDITIONAL DATA FOR FINITE
BEAMWIDTH ANALYSES

(top) signal spectrum

data 2 was 1st shown
1 has 50 to 60 more

PRECEDING PAGE BLANK-NOT FILMED

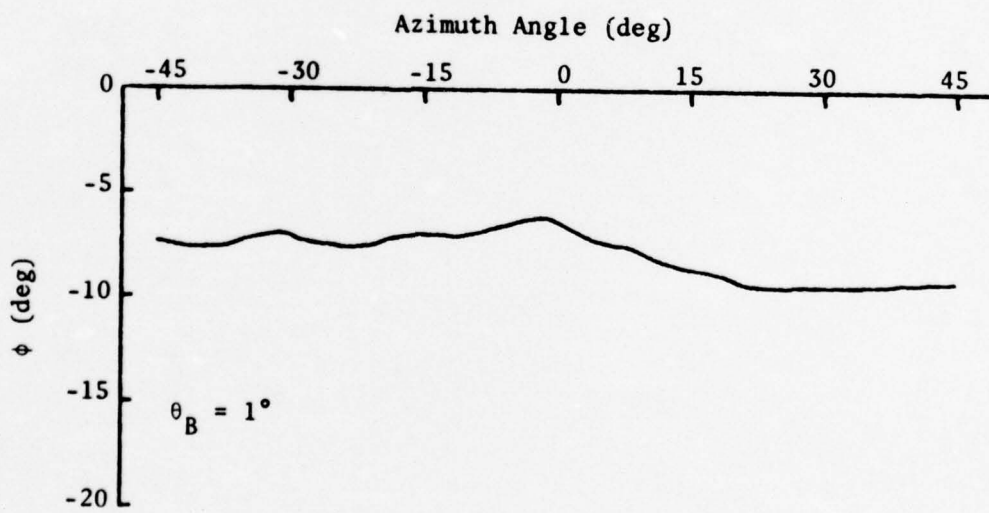
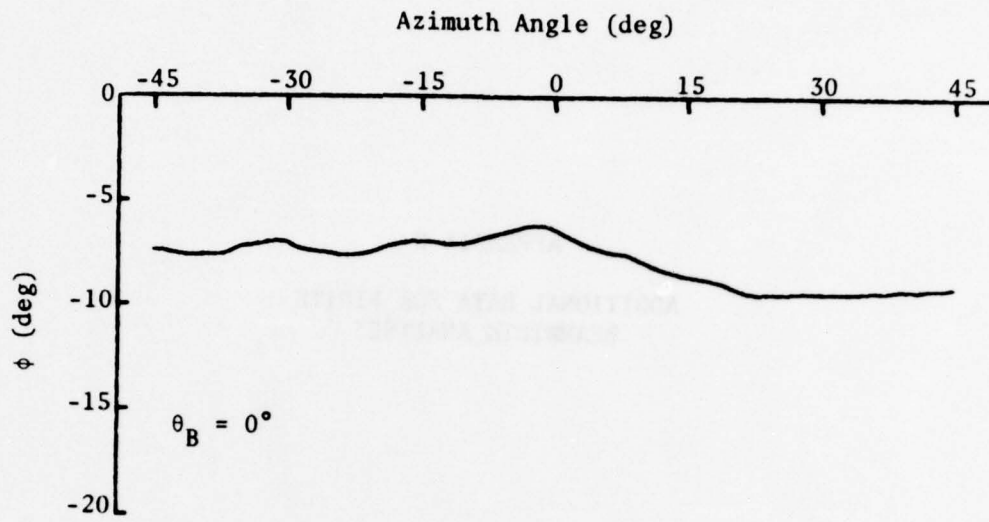


Fig. E1. Sensed Horizons for Case 5 with Sensor Beamwidths of 0° and 1° .

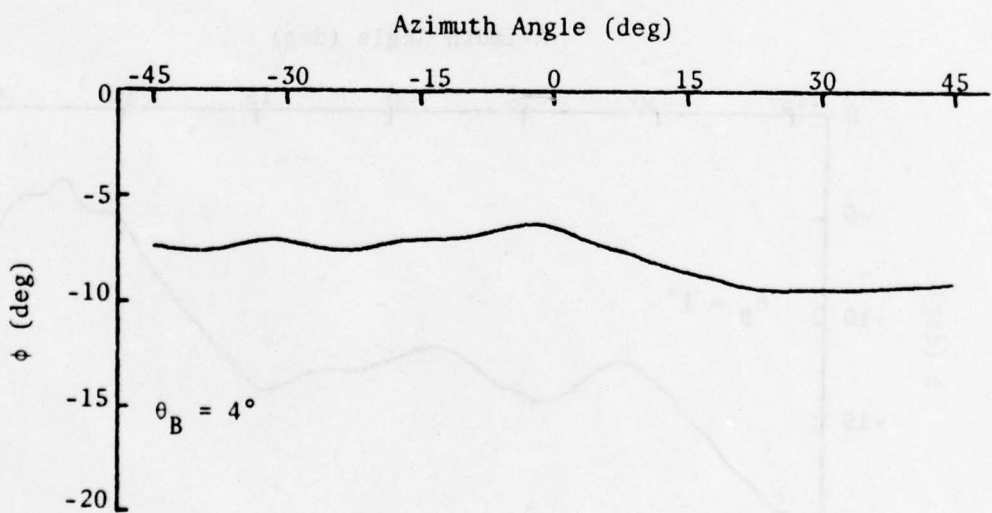
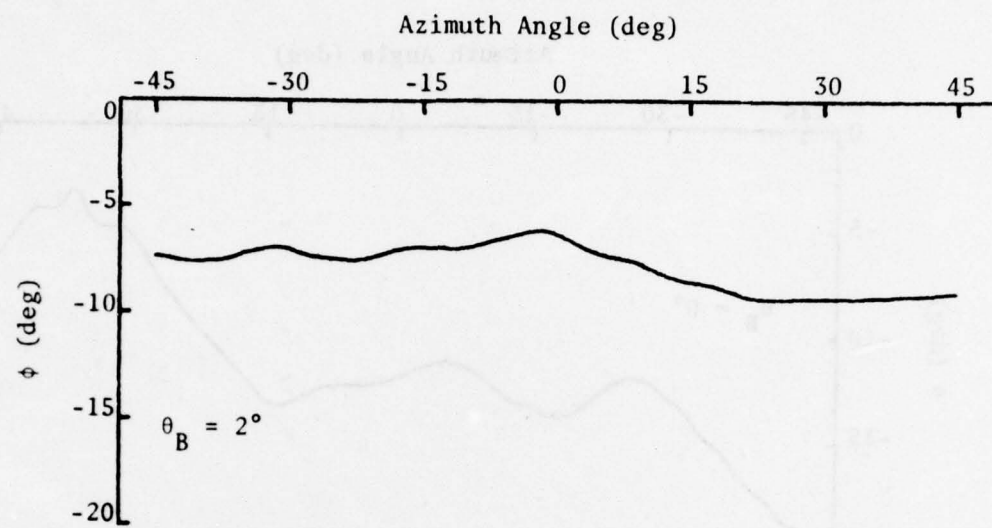


Fig. E2. Sensed Horizons for Case 5 with Sensor Beamwidths of 2° and 4° .

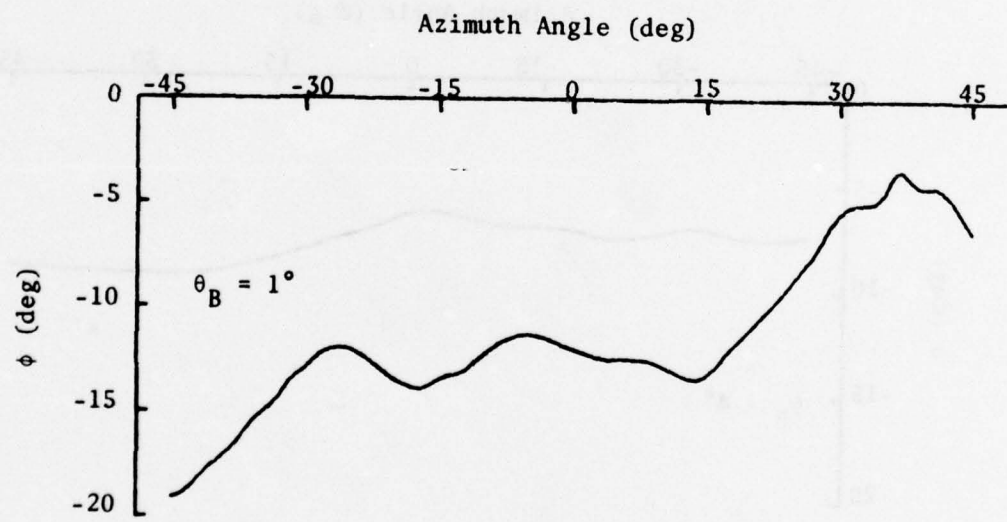
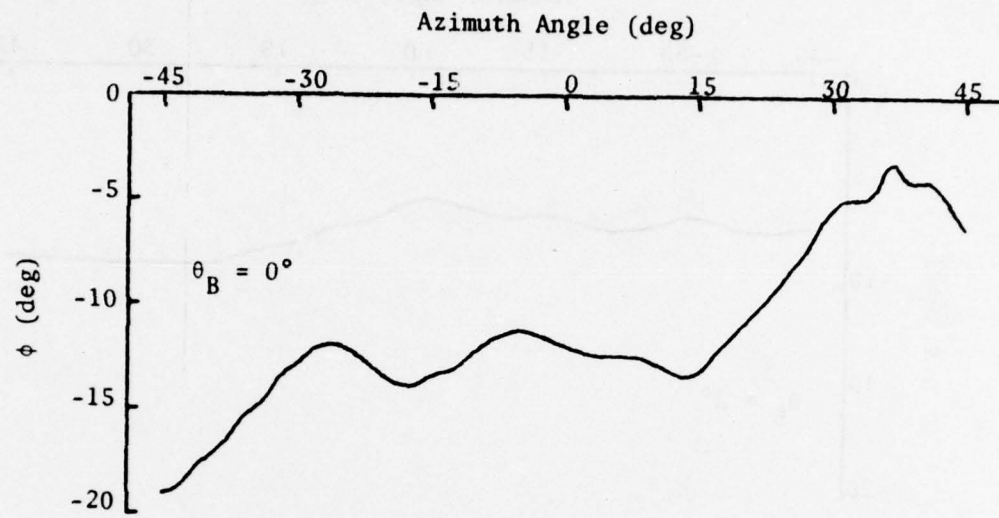


Fig. E3. Sensed Horizons for Case 7 with Sensor Beamwidths of 0° and 1° .

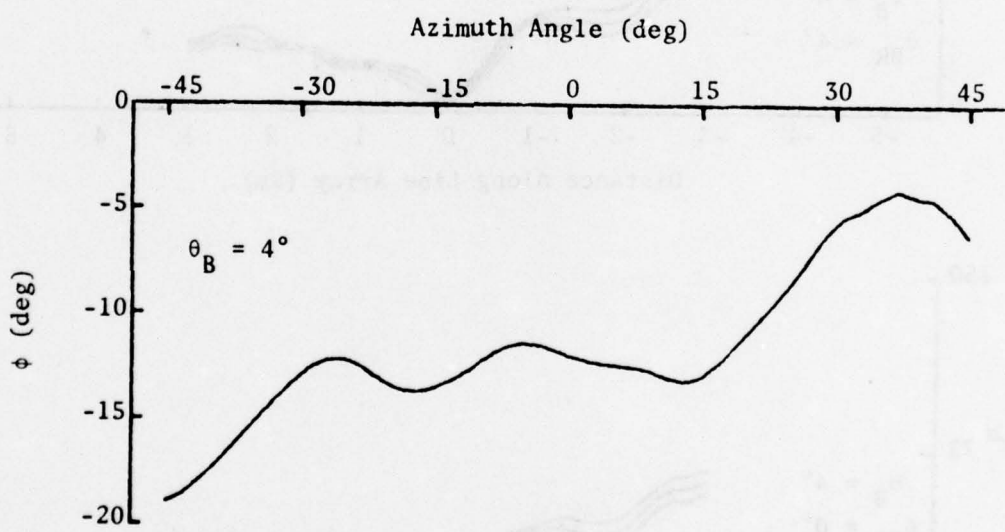
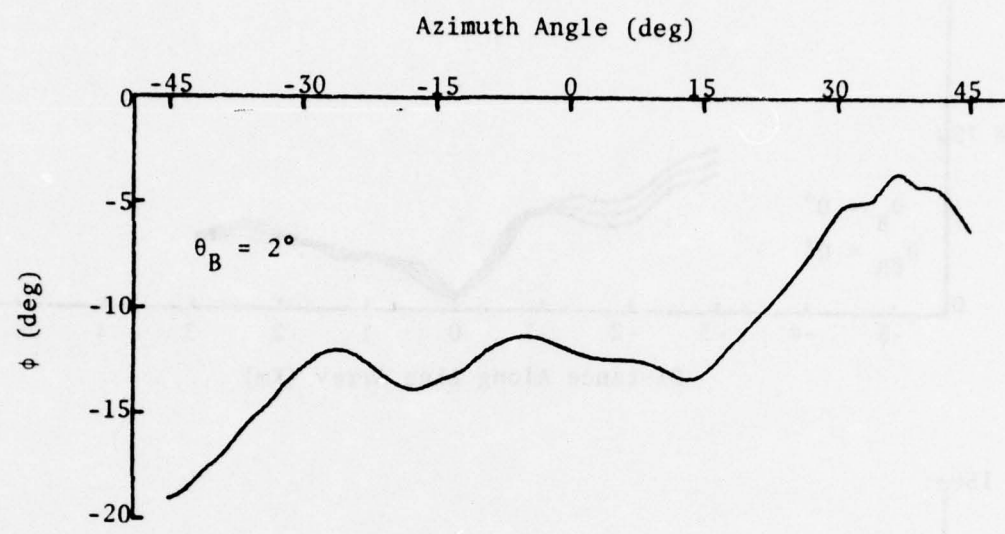


Fig. E4. Sensed Horizons for Case 7 with Sensor Beamwidths of 2° and 4° .

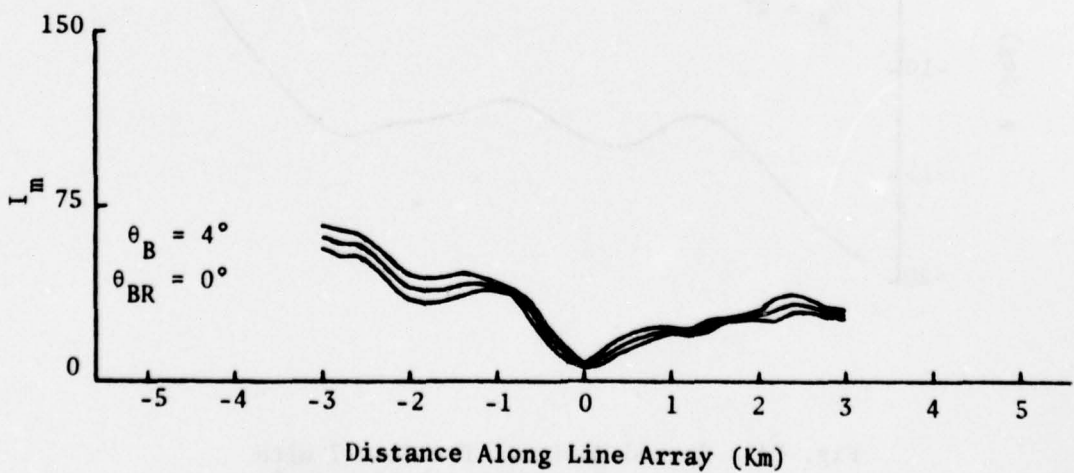
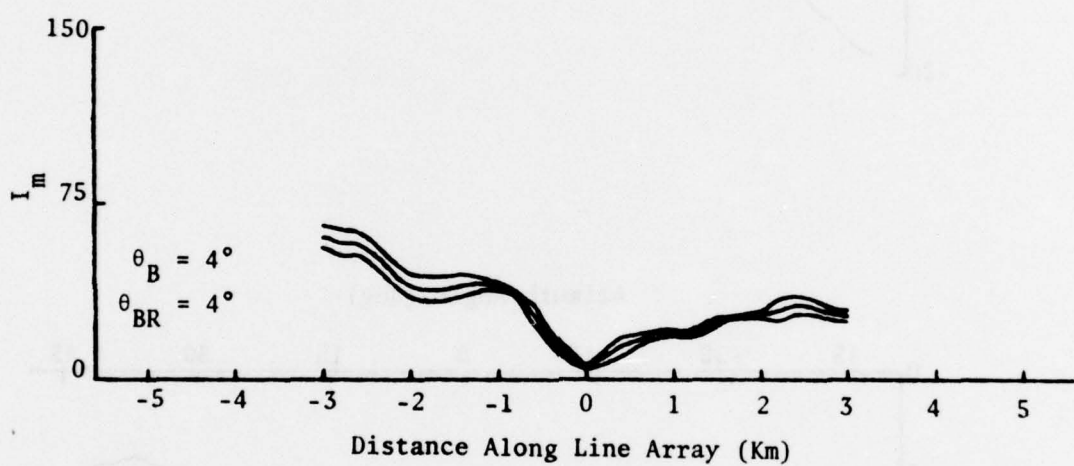
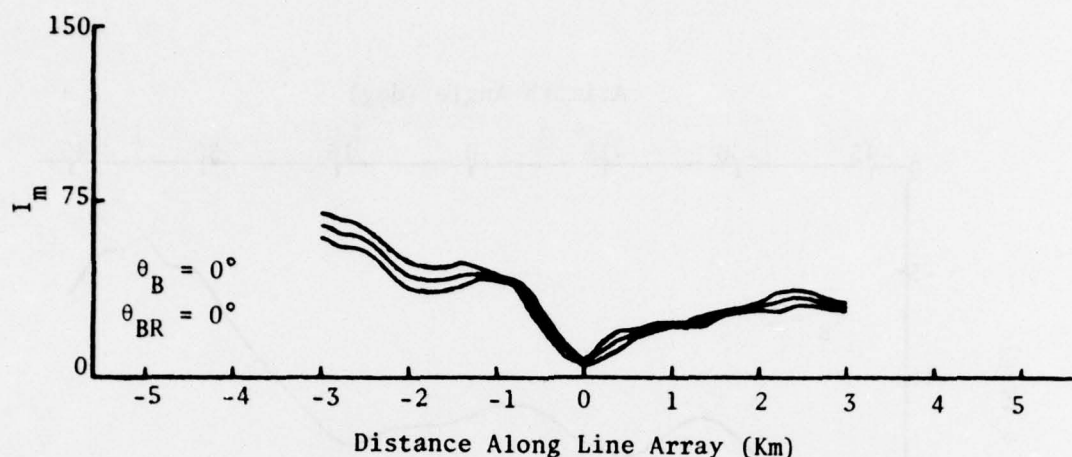


Fig. E5. Horizon Comparison Functions for Case 5
with Various Sensor Beamwidths.

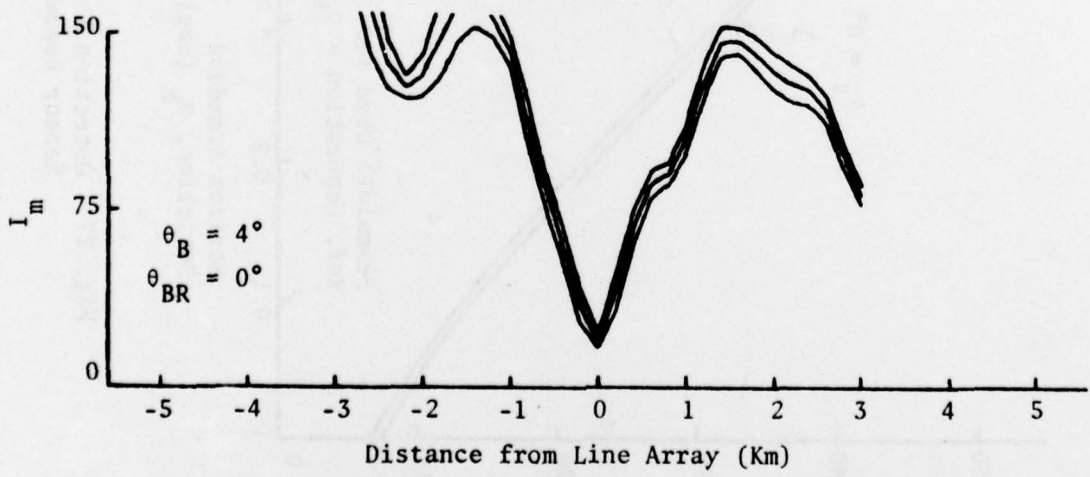
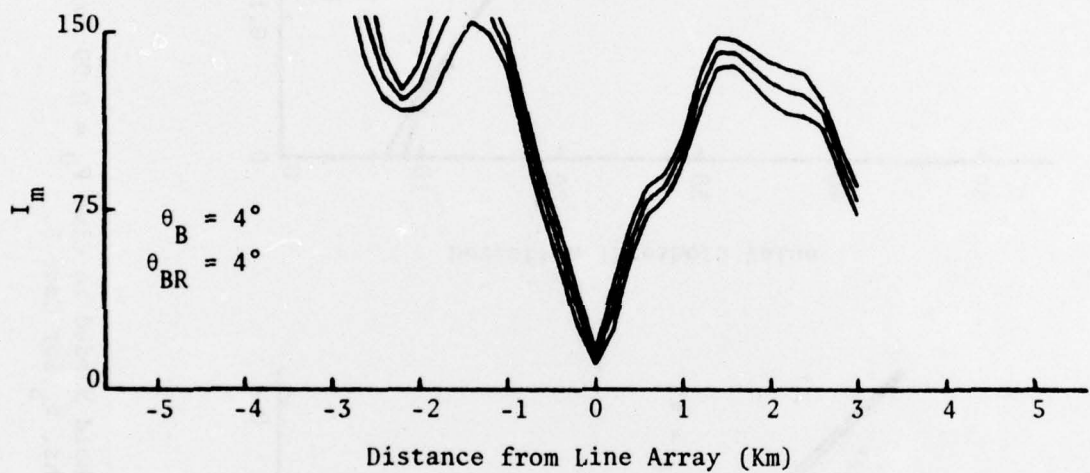
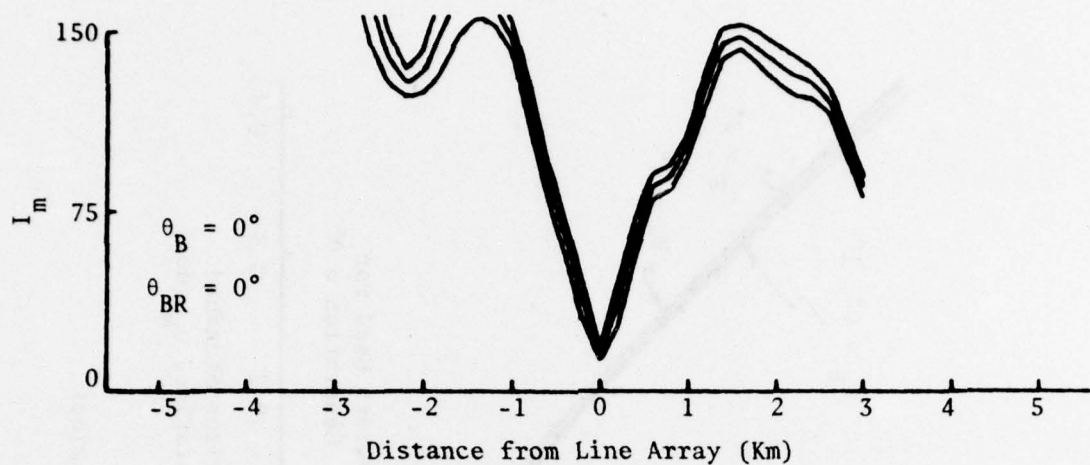


Fig. E6. Horizon Comparison Functions for Case 7
with Various Sensor Beamwidths.

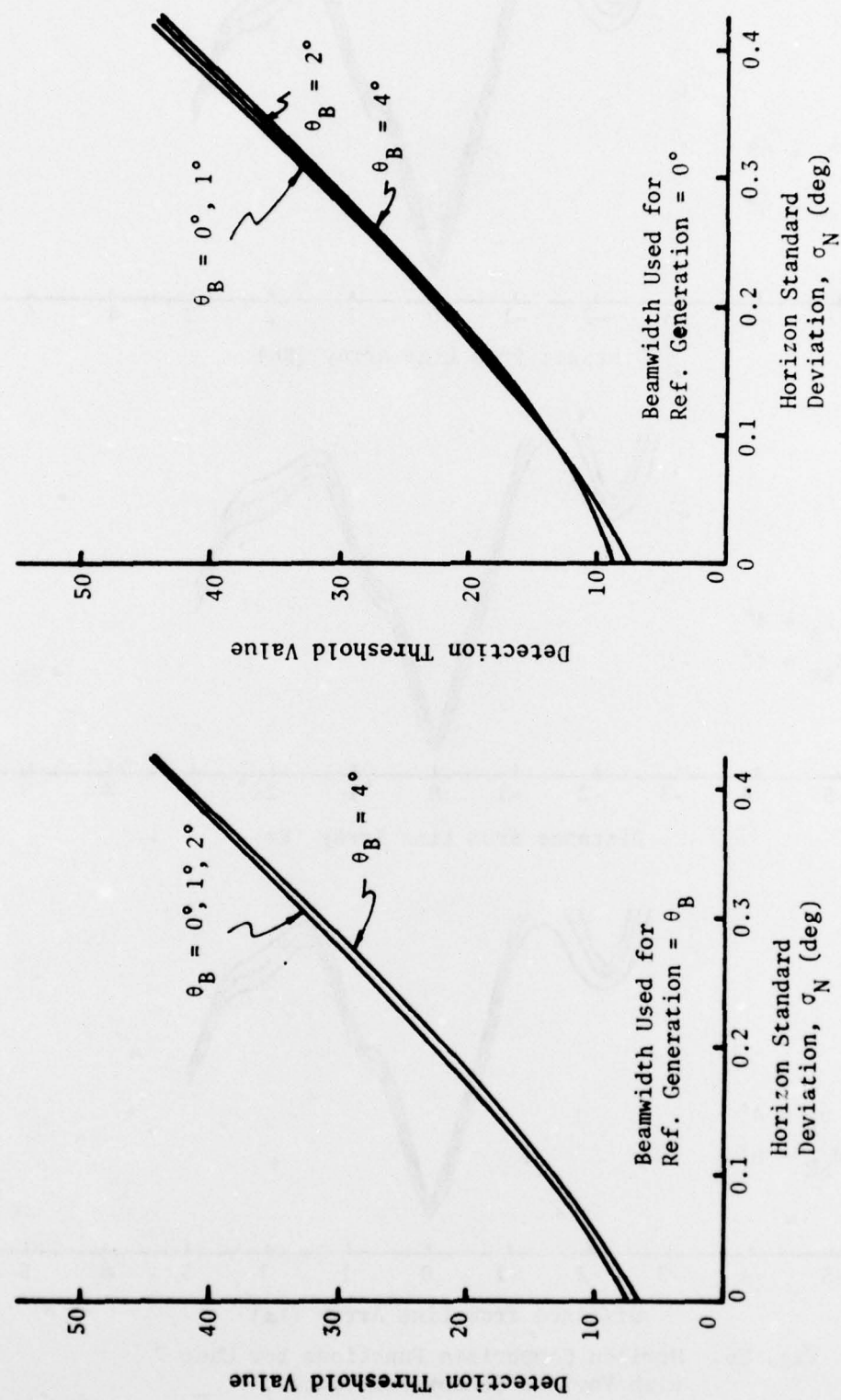


Fig. E7. Detection Threshold Needed to Give $P_D = 0.99$ for Various Sensor Beamwidths, θ_B for Case 5.

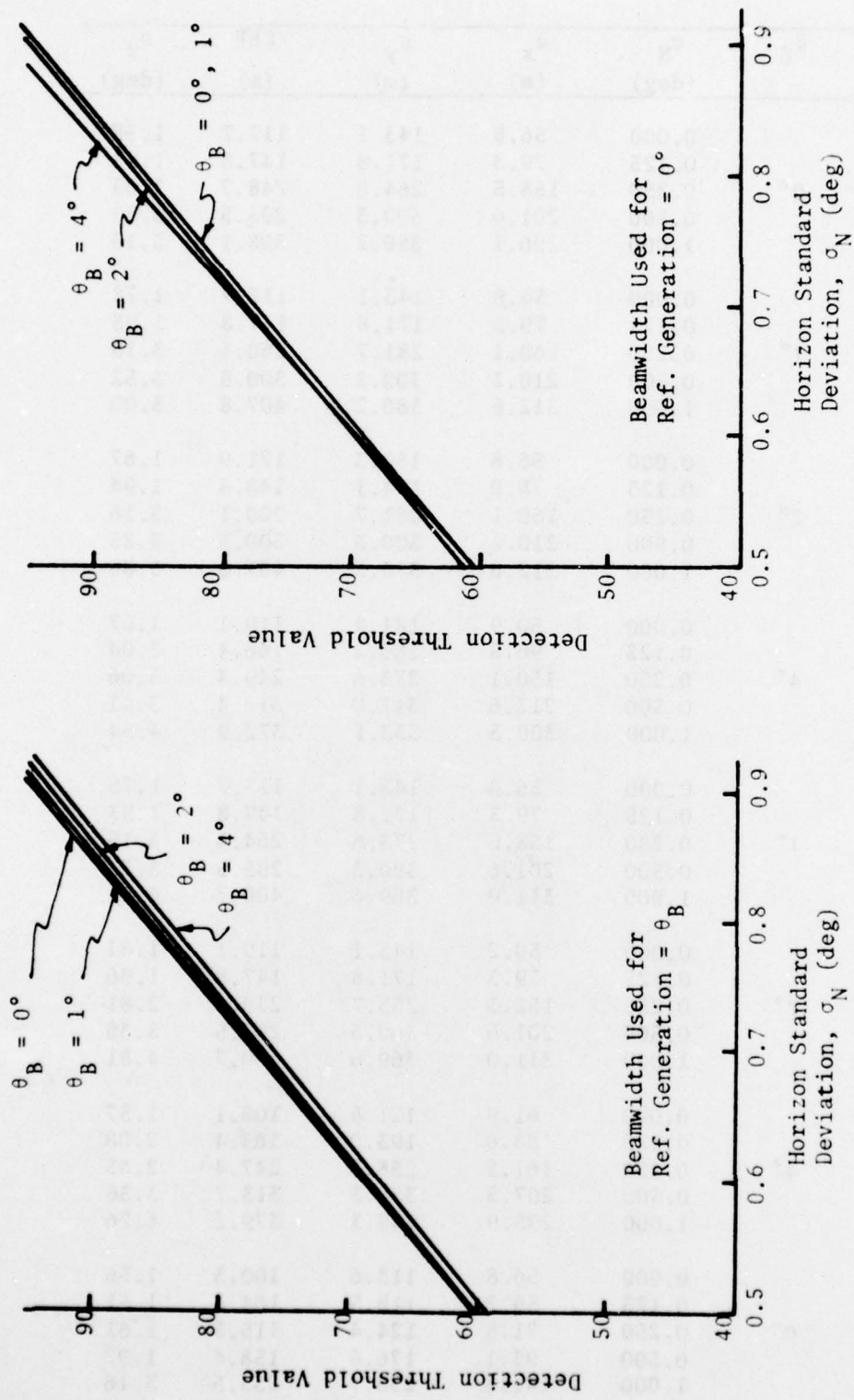


Fig. E8. Detection Threshold Needed to Give $P_D = 0.99$ for Various Sensor Beamwidths, θ_B for Case 7.

Case #	θ_B	σ_N (deg)	σ_x (m)	σ_y (m)	CEP (m)	σ_θ (deg)
Ref BW						
5 0°	0°	0.000	56.8	143.1	117.7	1.78
		0.125	79.3	171.8	147.8	1.91
		0.250	158.5	264.0	248.7	3.03
		0.500	201.6	300.3	295.5	3.53
		1.000	296.1	380.2	398.1	5.13
5 1°	1°	0.000	56.8	143.1	117.7	1.78
		0.125	79.3	171.8	147.8	1.93
		0.250	160.1	281.7	260.1	3.18
		0.500	210.1	300.3	300.5	3.52
		1.000	312.6	380.2	407.8	5.00
5 2°	2°	0.000	56.8	150.3	121.9	1.87
		0.125	78.0	174.1	148.4	1.94
		0.250	160.1	281.7	260.1	3.16
		0.500	210.1	300.3	300.5	3.23
		1.000	312.6	380.2	407.8	5.00
5 4°	4°	0.000	60.9	141.4	119.1	1.67
		0.125	96.5	186.2	166.4	2.04
		0.250	150.1	273.6	249.4	3.06
		0.500	213.6	317.0	312.4	3.41
		1.000	300.3	333.1	372.9	4.54
5 0°	1°	0.000	56.8	143.1	117.7	1.78
		0.125	79.3	171.8	147.8	1.93
		0.250	158.5	273.6	254.4	3.15
		0.500	201.6	300.3	295.5	3.53
		1.000	311.0	369.6	400.7	4.81
5 0°	2°	0.000	59.2	143.1	119.1	1.81
		0.125	79.3	171.8	147.8	1.96
		0.250	152.3	253.7	239.0	2.81
		0.500	201.6	300.3	295.5	3.30
		1.000	311.0	369.6	400.7	4.81
5 0°	4°	0.000	61.9	121.8	108.1	1.57
		0.125	88.0	193.0	165.4	2.08
		0.250	161.5	258.7	247.4	2.85
		0.500	207.5	325.3	313.7	3.36
		1.000	295.9	348.3	379.2	4.76
6 0°	0°	0.000	56.8	113.6	100.3	1.56
		0.125	59.2	118.5	104.6	1.61
		0.250	71.8	124.4	115.5	1.61
		0.500	93.1	176.0	158.4	1.97
		1.000	141.3	258.7	235.5	3.16

Case #	θ_B	σ_N (deg)	σ_x (m)	σ_y (m)	CEP (m)	σ_θ (deg)
Ref BW						
6 1°	1°	0.000	56.8	113.6	100.3	1.57
		0.125	59.2	118.5	104.6	1.59
		0.250	71.8	124.4	115.5	1.60
		0.500	91.6	171.8	155.1	1.98
		1.000	141.3	267.6	240.7	3.29
6 2°	2°	0.000	56.8	113.6	100.3	1.57
		0.125	59.2	118.5	104.6	1.60
		0.250	71.8	128.9	118.2	1.66
		0.500	91.6	171.8	155.1	2.03
		1.000	150.3	293.8	261.4	3.47
6 4°	4°	0.000	56.8	113.6	100.3	1.57
		0.125	59.2	113.6	101.7	1.54
		0.250	71.8	128.9	118.2	1.65
		0.500	83.3	156.1	140.9	1.93
		1.000	155.4	296.2	265.9	3.42
6 0°	1°	0.000	59.2	113.6	101.7	1.57
		0.125	59.2	118.5	104.6	1.59
		0.250	71.8	118.5	112.0	1.52
		0.500	93.1	176.0	158.4	2.06
		1.000	148.0	280.3	252.1	3.37
6 0°	2°	0.000	59.2	113.6	101.7	1.58
		0.125	60.9	118.5	105.6	1.59
		0.250	70.7	118.5	111.4	1.52
		0.500	91.6	171.8	155.1	2.12
		1.000	148.0	281.7	252.9	3.45
6 0°	4°	0.000	59.2	113.6	101.7	1.58
		0.125	60.9	113.6	102.7	1.49
		0.250	66.9	118.5	109.1	1.52
		0.500	99.8	193.0	172.4	2.33
		1.000	156.6	298.1	267.7	3.57
7 0°	0°	0.000	56.8	118.5	103.2	1.37
		0.125	56.8	121.8	105.1	1.39
		0.250	56.8	141.4	116.7	1.62
		0.500	75.9	175.5	148.0	1.76
		1.000	119.0	309.0	251.9	3.57
7 1°	1°	0.000	56.8	118.5	103.2	1.37
		0.125	56.8	121.8	105.1	1.39
		0.250	56.8	141.4	116.7	1.62
		0.500	76.2	183.2	152.7	1.81
		1.000	133.0	309.0	260.2	3.57

Case #	θ_B	σ_N (deg)	σ_x (m)	σ_y (m)	CEP (m)	σ_θ (deg)
Ref BW						
7 2°	2°	0.000	56.8	118.5	103.2	1.37
		0.125	56.8	123.8	106.3	1.36
		0.250	56.8	143.1	117.7	1.61
		0.500	80.1	183.2	155.0	1.90
		1.000	113.6	300.5	243.8	3.45
7 4°	4°	0.000	56.8	124.4	106.7	1.38
		0.125	56.8	123.8	106.3	1.34
		0.250	56.8	160.1	127.7	1.78
		0.500	83.3	232.4	185.9	2.51
		1.000	128.9	308.7	257.6	3.69
7 0°	1°	0.000	56.8	118.5	103.2	1.34
		0.125	56.8	121.8	105.1	1.39
		0.250	56.8	141.4	116.7	1.62
		0.500	75.9	175.5	148.0	1.77
		1.000	119.0	312.1	253.8	3.69
7 0°	2°	0.000	56.8	124.4	106.7	1.34
		0.125	56.8	123.8	106.3	1.34
		0.250	56.8	141.4	116.7	1.54
		0.500	76.2	189.7	156.5	1.78
		1.000	113.6	313.2	251.2	3.63
7 0°	4°	0.000	56.8	124.4	106.7	1.37
		0.125	56.8	133.8	112.2	1.34
		0.250	61.9	176.0	140.0	1.87
		0.500	82.1	214.0	174.3	2.02
		1.000	126.8	302.4	252.7	3.67

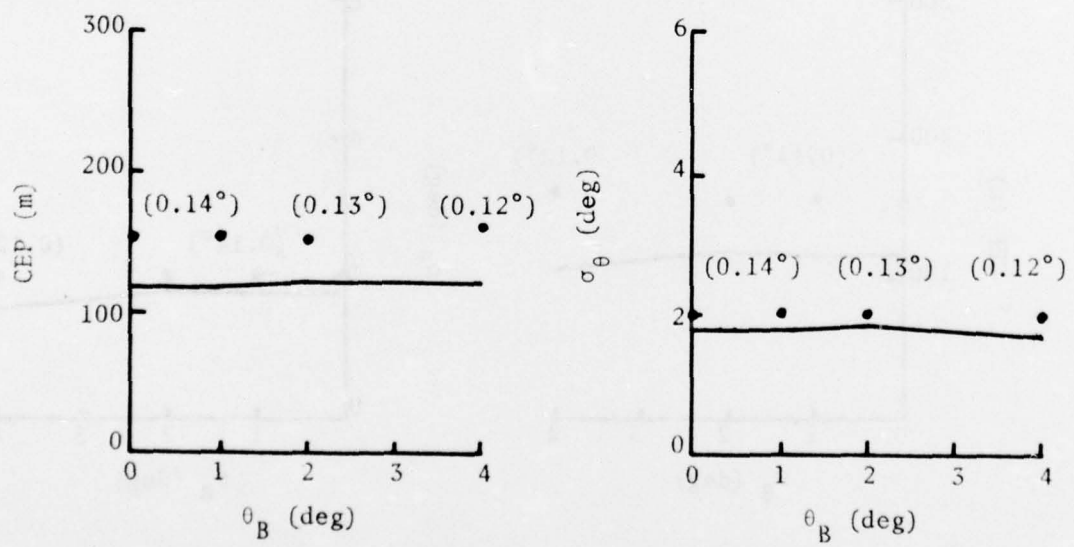
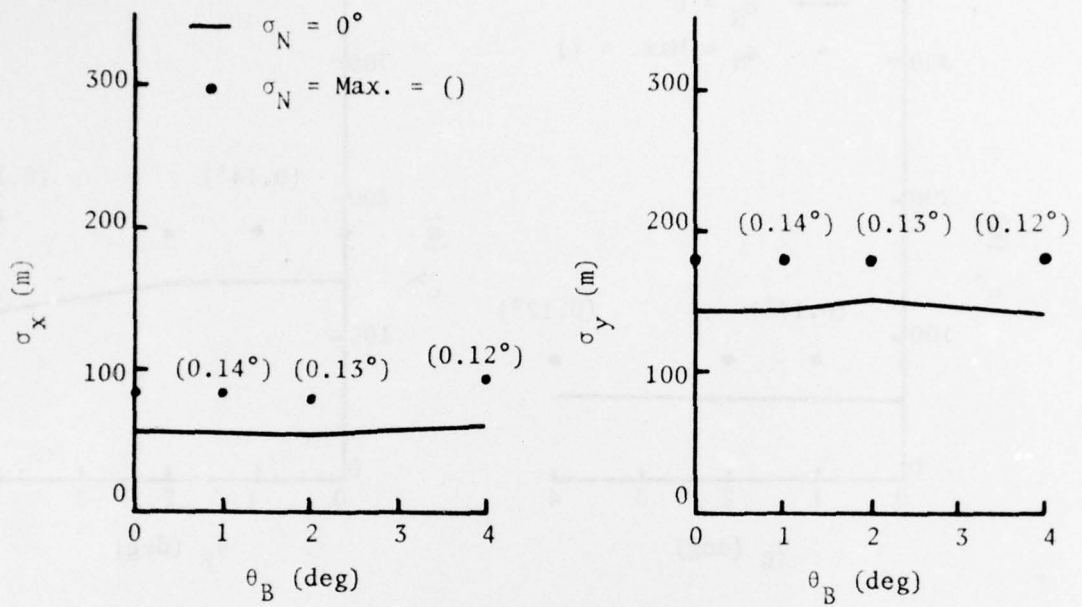


Fig. E9. Position and Heading Determination Accuracy when Sensed and Reference Horizons are Generated with the Same Beamwidth, θ_B (Case 5).

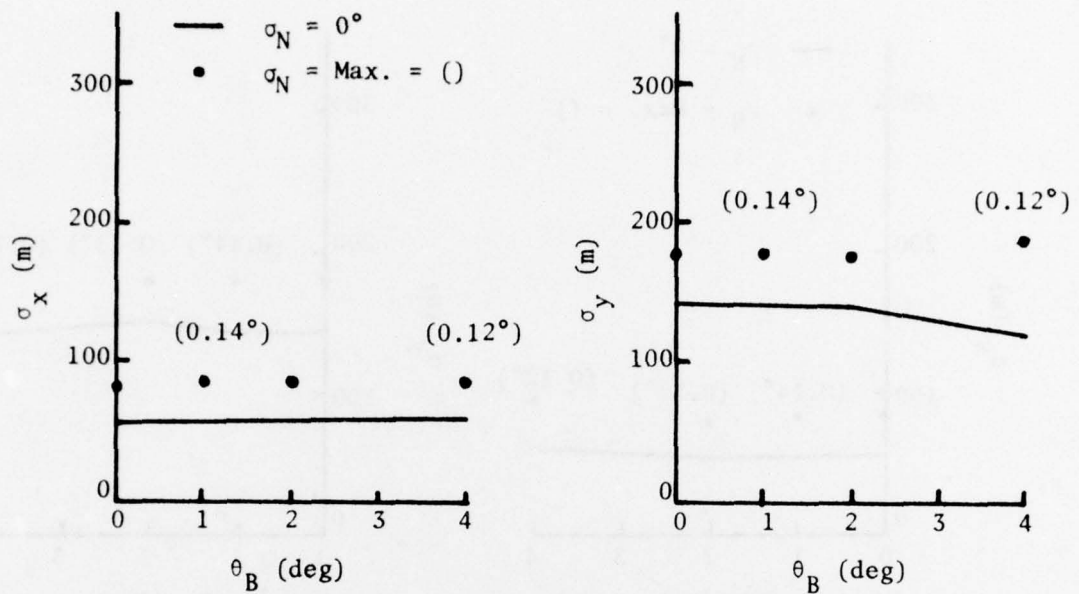


Fig. E10. Position and Heading Determination Accuracy when Reference Horizons are Generated with a 0° Beamwidth (Case 5).

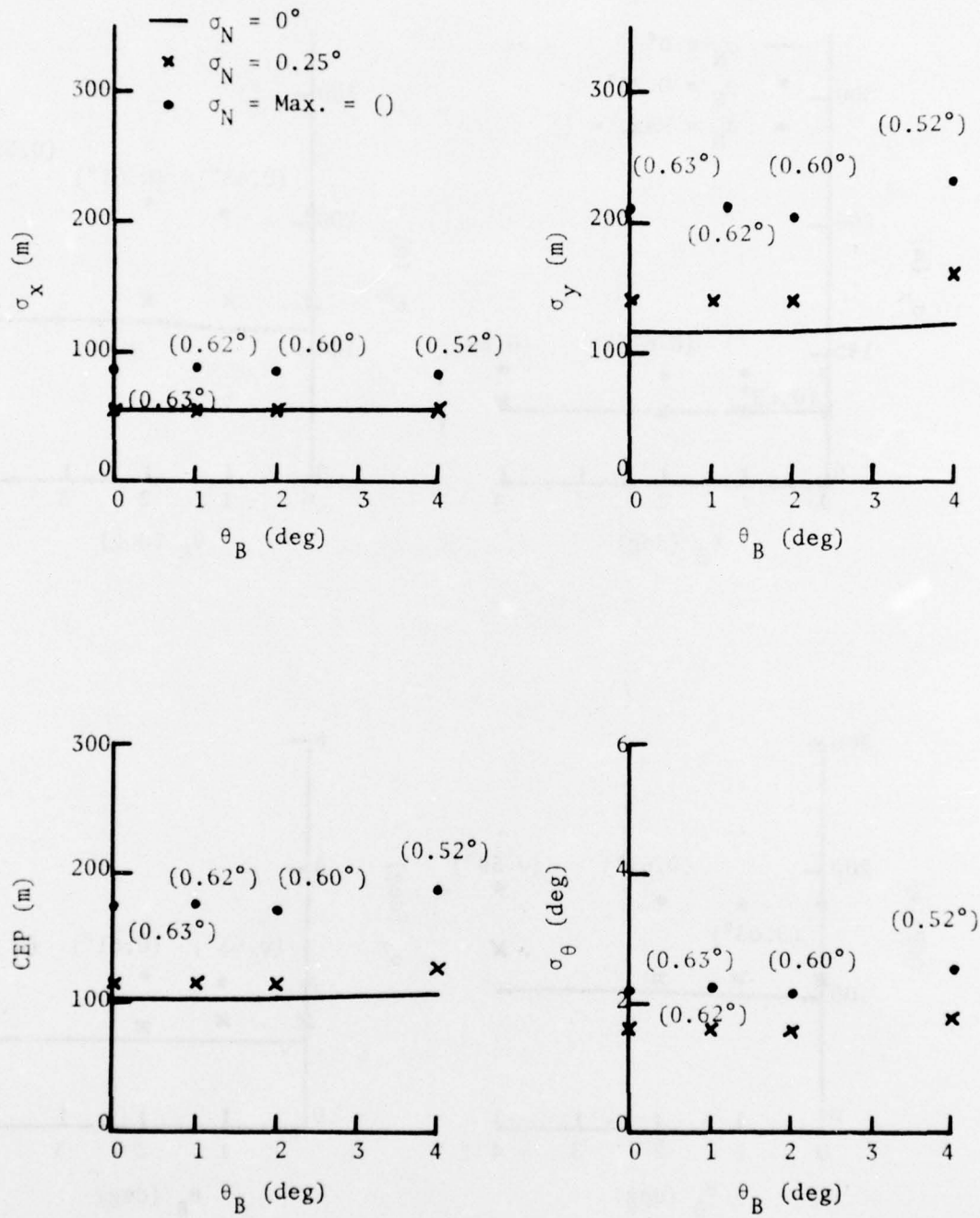


Fig. E11. Position and Heading Determination Accuracy when Sensed and Reference Horizons are Generated with the Same Beamwidth, θ_B (Case 7).

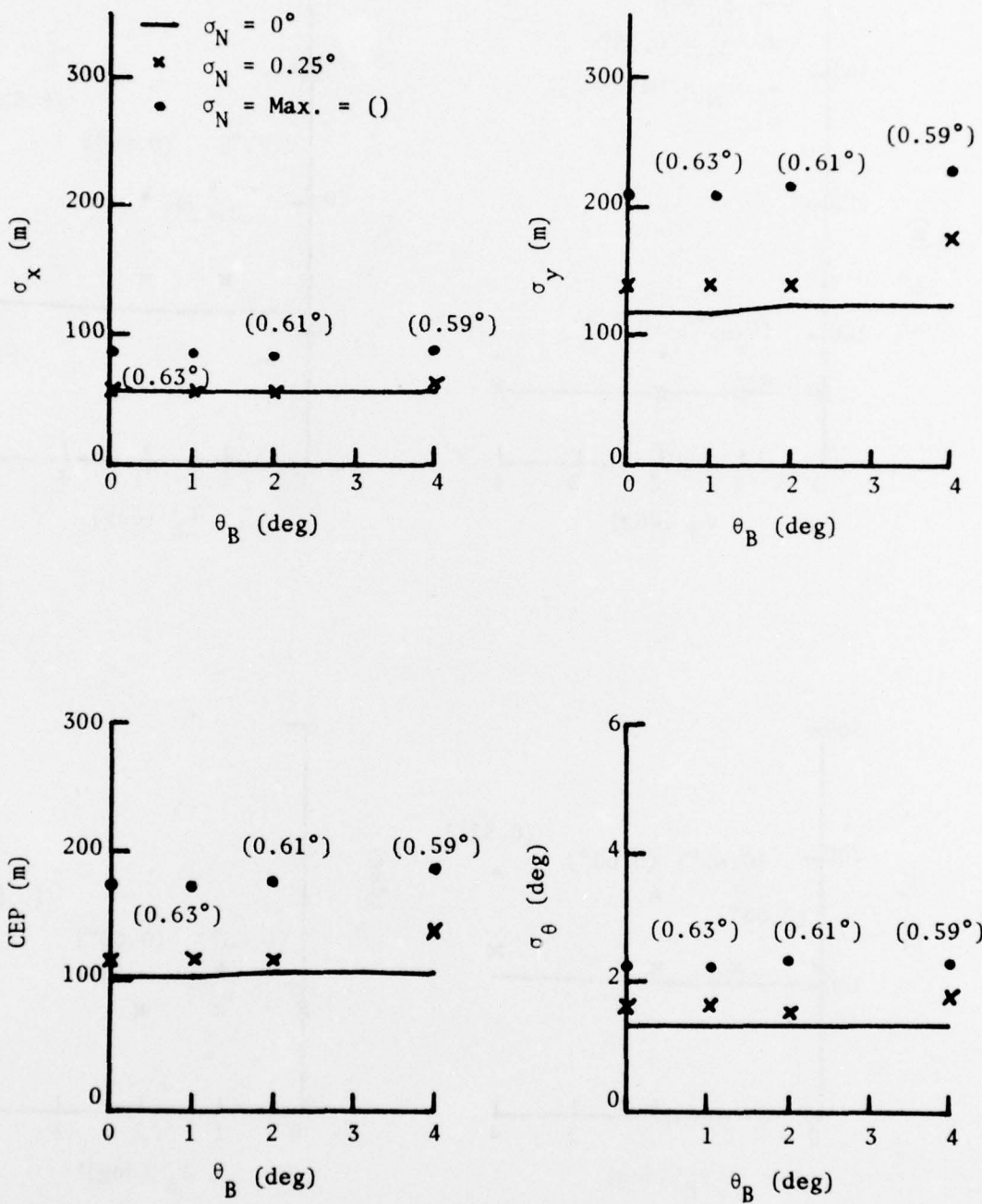


Fig. E12. Position and Heading Determination Accuracy when Reference Horizons are Generated with a 0° Beamwidth (Case 7).

DISTRIBUTION

Office of Naval Research (2) Geography Programs Code 462 Arlington, VA 22217	NORDA Code 400 National Space Technology Laboratories Bay St. Louis, MS 39520
Defense Documentation Center Cameron Station (12) Alexandria, VA 22314	Office of Naval Research Operational Applications Division Code 200 Arlington, VA 22217
Director, Naval Research Lab Attention Technical Information Officer (6) Washington, D.C. 20375	Office of Naval Research Scientific Liaison Officer Scripps Institution of Oceanography La Jolla, CA 92093
Director Office of Naval Research Branch Office 1030 East Green Street Pasadena, CA 91101	Director, Naval Research Laboratory Attn. Library, CODE 2628 Washington, D.C. 20375
Director Office of Naval Research Branch Office 536 South Clark Street Chicago, IL 60605	ONR Scientific Liaison Group American Embassy - Room A-407 APO San Francisco 96503
Director Office of Naval Research Branch Office 495 Summer Street Boston, MA 02210	Commander Naval Oceanographic Office Attn. Library Code 1600 Washington, D.C. 20374
Commanding Officer Office of Naval Research Branch Office Box 39 FPO New York 09510	Naval Oceanographic Office Code 3001 Washington, D.C. 20374
Chief of Naval Research Asst. for Marine Corps Matters Code 100M Office of Naval Research Arlington, VA 22217	Chief of Naval Operations OP 987P1 Department of the Navy Washington, D.C. 20350
	Oceanographer of the Navy Hoffman II Building 200 Stovall Street Alexandria, VA 22322

DISTRIBUTION (cont.)

Naval Academy Library
U.S. Naval Academy
Annapolis, MD 21402

Commanding Officer
Naval Coastal Systems
Laboratory
Panama City, FL 32401

Librarian
Naval Intelligence Support
Center
4301 Suitland Road
Washington, D.C. 20390

Commanding Officer
Naval Air Development Center
Warminster, Johnsville
PA 18974

Naval Ordnance Laboratory
White Oak
Silver Spring, MD 20910

Director
Amphibious Warfare Board
U.S. Atlantic Fleet
Naval Amphibious Base
Norfolk, Little Creek, VA 23520

Commander, Amphibious Force
U.S. Pacific Fleet
Force Meteorologist
Comphibpac Code 25 5
San Diego, CA 92155

Commanding General
Marine Corps Development and
Educational Command
Quantico, VA 22134

Dr. A. L. Slafkosky
Scientific Advisor
Commandant of the Marine Corps
Code MC-RD-1
Washington, D.C. 20380

Defense Intelligence Agency
Central Reference Division
Code RDS-3
Washington, D.C. 20301

Director
Defense Mapping Topographic Center
Attn. Code 50200
Washington, D.C. 20315

Commanding Officer
U.S. Army Engineering
Topographic Laboratory
Attn. ETL-ST
Fort Belvoir, VA 22060

Chief, Wave Dynamics Division
USAE-WES
P. O. Box 631
Vicksburg, MS 39180

Commandant
U.S. Coast Guard
Attn. GECV/61
Washington, D.C. 20591

Office of Research and Development
%DS/62
U.S. Coast Guard
Washington, D.C. 20591

National Oceanographic Data Center
%D764
Environmental Data Services
NOAA
Washington, D.C. 20235

Assistant Director for Research
and Development
National Ocean Survey
6001 Executive Boulevard
Rockville, MD 20852

Central Intelligence Agency
Attention OCR/DD-Publications
Washington, D.C. 20505

DISTRIBUTION (cont.)

Dr. Mark M. Macomber
Advanced Technology Division
Defense Mapping Agency
Naval Observatory
Washington, D.C. 20390

Ministerialdirektor Dr. F. Wever
RUE/FO
Bundesministerium der Verteidigung
Hardthoehe
D-5300 Bonn, West Germany

Oberregierungsrat Dr. Ullrich
RUE/FO
Bundesministerium der Verteidigung
Hardthoehe
D-5300 Bonn, West Germany

Mr. Tage Strarup
Defence Research Establishment
Osterbrogades Kaserne
DK-2100 Kobenhavn O, Denmark

Prof. Dr. Rer. Nat.
H. G. Gierloff-Emden
Institut F. Geographie
Universitaet Muenchen
Luisenstrasse 37/III
D-800 Muenchen 2, West Germany

Prof. Dr. Klaus Hasselmann
Institut F. Geophysik
Universitaet Hamburg
Schlueterstrasse 22
D-2000 Hamburg 13, West Germany

Prof. Dr. Nils Jerlov
Institute for Physical Oceanography
Kobenhavns Universitet
Haraldsgade 6
DK-2200 Kobenhavn, Denmark

IR. M. W. Van Batenberg
Physisch Laboratorium TNO
Oude Waalsdorper Weg 63
Den Haag, Netherlands

Dr. Gordon E. Carlson
University of Missouri
Department of Electrical Engineering
Rolla, MO 65401

Mr. H. G. Tornatore
ITT Avionics
9140 Old Annapolis Road
Columbia, MD 21043

Prof. John D. Isaacs
University of California A-207
Institute of Marine Resources
La Jolla, CA 92093

Mr. Donald A. Leonard
Computer Genetics Corporation
4 Lakeside Office Park
Wakefield, MA 01880

Dr. G. D. Hickman
Applied Science Technology, Inc.
19212 Plummer Drive
Germantown, MD 20767

Coastal Studies Institute
Louisiana State University
Baton Rouge, LA 70803

Dr. Bernard Le Mehaute
Tetra Tech, Inc.
630 North Rosemead Boulevard
Pasadena, CA 91107

Dr. William S. Gaither
Dean, College of Marine Studies
Robinson Hall
University of Delaware
Newark, DE 19711

Prof. C. A. M. King
Department of Geography
University of Nottingham
Nottingham, England NG7 2RD

DISTRIBUTION (cont.)

Dr. Omar Shemdin
Jet Propulsion Laboratory
183-501
4800 Oak Grove Drive
Pasadena, CA 91103

Dr. Alan W. Niedoroda
Director, Coastal Research Center
University of Massachusetts
Amherst, MA 01002

Dr. Lester A. Gerhardt
Rensselaer Polytechnic Institute
Troy, NY 12181

Mr. Fred Thomson
Environmental Research Institute
P. O. Box 618
Ann Arbor, MI 48107

Dr. J. A. Dracup
Environmental Dynamics, Inc.
1609 Westwood Boulevard, Suite 202
Los Angeles, CA 90024

Dr. Bruce Hayden
Department of Environmental
Sciences
University of Virginia
Charlottesville, VA 22903